Volume I, 1957

TRANSACTIONS of the SOCIETY OF RHEOLOGY

Editor:
BRYCE MAXWELL
Princeton University

Assistant Editor:
R. D. ANDREWS
The Dow Chemical Co.

CONTENTS

HUGH S. TAYLOR: Presentation of the Bingham Medal to Arthur V. Tobolsky 1
J. J. BIKERMAN: The Tackiness of Liquid Adhesives 3
JAMES V. ROBINSON: The Viscosity of Suspensions of Spheres. III. Sediment Volume as a Determining Parameter 15
HERSHEL MARKOVITZ and R. BRADY WILLIAMSON: Normal Stress Effect in Polyisobutylene Solutions. I. Measurements in a Cone and Plate Instrument 25
HERSHEL MARKOVITZ: Normal Stress Effect in Polyisobutylene Solutions. II. Classification and Application of Rheological Theories 37
STEPHEN PRAGER: Stress–Strain Relations in a Suspension of Dumbbells 53
M. MOONEY: A Theory of the Viscosity of a Maxwellian Elastic Liquid 63
W. PHILIPPOFF: On Normal Stresses, Flow Curves, Flow Birefringence, and Normal Stresses of Polyisobutylene Solutions. Part I. Fundamental Principles 95
JOHN G. BRODNYAN, F. H. GASKINS, and W. PHILIPPOFF: On Normal Stresses, Flow Curves, Flow Birefringence, and Normal Stresses of Polyisobutylene Solutions. Part II. Experimental 109
HARRIS M. BURTE: Strain Aging Hydrogen Embrittlement in Alpha-Beta Titanium Alloys 119
BERNARD D. COLEMAN: A Stochastic Process Model for Mechanical Breakdown 153
WILLIAM PRAGER: On Ideal Locking Materials 169
H. L. TOOR: Heat Generation and Conduction in the Flow of a Viscous Compressible Liquid 177
E. T. SEVERS and J. M. AUSTIN: The Thermal Incline: A Means of Measuring Viscosities of Plastisols at Elevated Temperatures 191
J. P. TORDELLA: Capillary Flow of Molten Polyethylene—A Photographic Study of Melt Fracture 203
HERBERT LEADERMAN: Proposed Nomenclature for Linear Viscoelastic Behavior 213

INTERSCIENCE PUBLISHERS NEW YORK • LONDON

TRANSACTIONS of the SOCIETY OF RHEOLOGY

VOLUME I · 1957

INTERSCIENCE PUBLISHERS · NEW YORK · LONDON

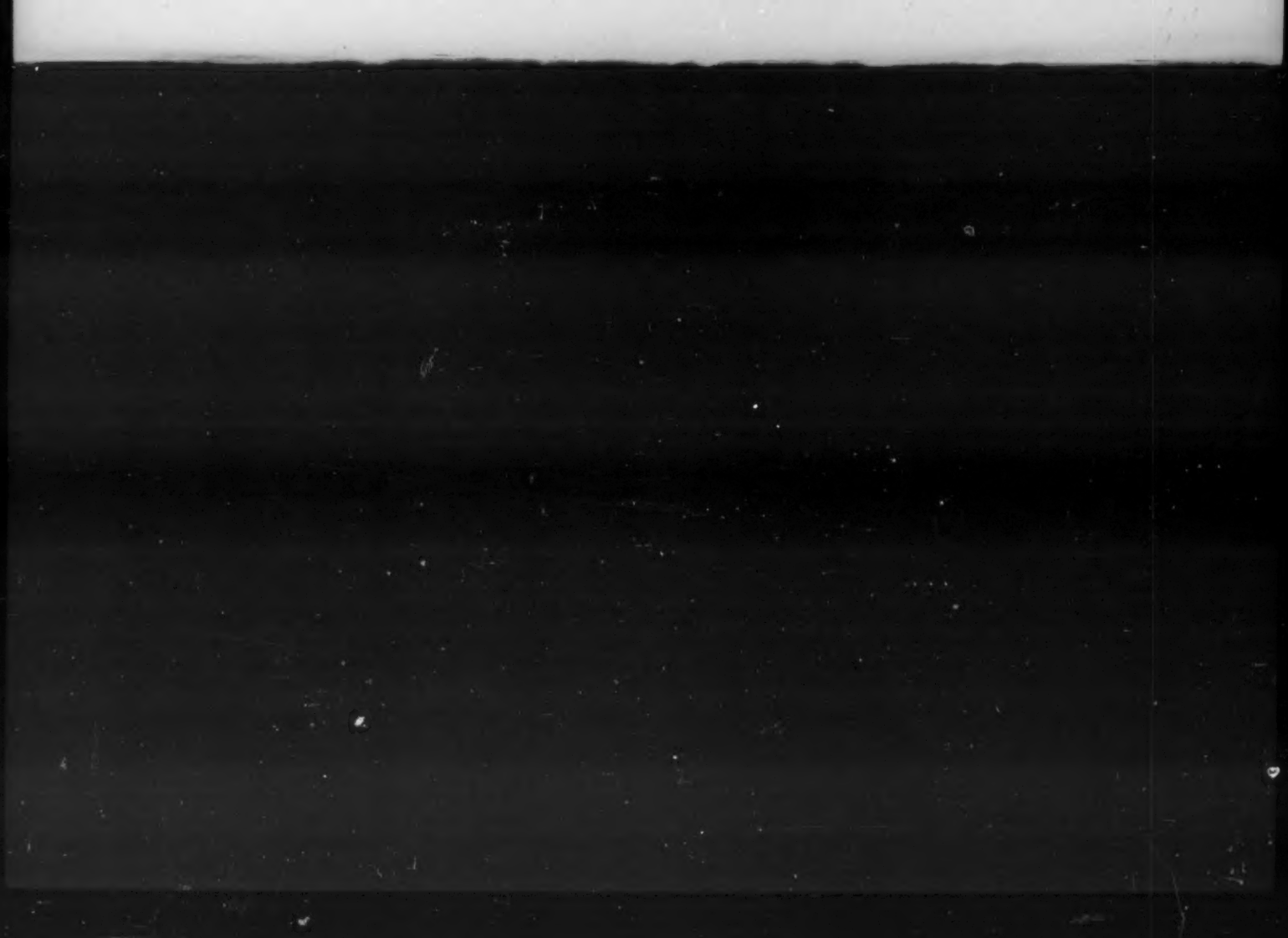

Volume I, 1957

TRANSACTIONS of the SOCIETY OF RHEOLOGY

Editor:
BRYCE MAXWELL
Princeton University

Assistant Editor:
R. D. ANDREWS
The Dow Chemical Co.

CONTENTS

HUGH S. TAYLOR: Presentation of the Bingham Medal to Arthur V. Tobolsky 1
J. J. BIKERMAN: The Tackiness of Liquid Adhesives 3
JAMES V. ROBINSON: The Viscosity of Suspensions of Spheres. III. Sediment Volume as a Determining Parameter 15
HERSHEL MARKOVITZ and R. BRADY WILLIAMSON: Normal Stress Effect in Polyisobutylene Solutions. I. Measurements in a Cone and Plate Instrument 25
HERSHEL MARKOVITZ: Normal Stress Effect in Polyisobutylene Solutions. II. Classification and Application of Rheological Theories 37
STEPHEN PRAGER: Stress–Strain Relations in a Suspension of Dumbbells 53
M. MOONEY: A Theory of the Viscosity of a Maxwellian Elastic Liquid 63
W. PHILIPPOFF: On Normal Stresses, Flow Curves, Flow Birefringence, and Normal Stresses of Polyisobutylene Solutions. Part I. Fundamental Principles 95
JOHN G. BRODNYAN, F. H. GASKINS, and W. PHILIPPOFF: On Normal Stresses, Flow Curves, Flow Birefringence, and Normal Stresses of Polyisobutylene Solutions. Part II. Experimental 109
HARRIS M. BURTE: Strain Aging Hydrogen Embrittlement in Alpha-Beta Titanium Alloys 119
BERNARD D. COLEMAN: A Stochastic Process Model for Mechanical Breakdown 153
WILLIAM PRAGER: On Ideal Locking Materials 169
H. L. TOOR: Heat Generation and Conduction in the Flow of a Viscous Compressible Liquid 177
E. T. SEVERS and J. M. AUSTIN: The Thermal Incline: A Means of Measuring Viscosities of Plastisols at Elevated Temperatures 191
J. P. TORDELLA: Capillary Flow of Molten Polyethylene—A Photographic Study of Melt Fracture 203
HERBERT LEADERMAN: Proposed Nomenclature for Linear Viscoelastic Behavior 213

INTERSCIENCE PUBLISHERS NEW YORK • LONDON

Copyright © 1957 by
INTERSCIENCE PUBLISHERS, INC.

Library of Congress Catalog
Card Number 57-11926

INTERSCIENCE PUBLISHERS, INC.
250 Fifth Avenue, New York 1, N.Y.

For Great Britain and Northern Ireland:
INTERSCIENCE PUBLISHERS LTD.
88/90 Chancery Lane, London, W. C. 2

PRINTED IN THE UNITED STATES OF AMERICA BY MACK PRINTING CO., EASTON, PA.

TRANSACTIONS OF THE SOCIETY OF RHEOLOGY VOL. I, 1–2 (1957)

Presentation of the Bingham Medal to Arthur V. Tobolsky

HUGH S. TAYLOR,* *Professor of Chemistry and Dean of the Graduate School, Princeton University, N. J.*

Princeton University fell heir to the medalist through the insistence of Professor Harold C. Urey that a student born in New York City in 1919 and attaining his A. B. degree in Columbia University at the age of 21, with triple honors in Chemistry, Mathematics, and Physics, was entitled to graduate training in the residential Graduate School of Princeton University. It is not surprising that, two years later, he qualified for the A. M. degree in 1942 and became the Jacobus Fellow, the highest distinction among graduate students in Princeton. One year later he proceeded to the degree of Ph.D., as with the A.M. degree in Physics and Physical Chemistry.

His training under Henry Eyring set the stage for his own first major achievement, an analysis of the factors operative in the viscoelastic behavior of natural and synthetic rubber stocks. Out of that analysis emerged the conviction that stress relaxation at constant extension was intrinsically easier to analyze theoretically than extension of elastomers at constant load. It was fortunate that Drs. John H. Dillon and I. B. Prettyman of Firestone Tire and Rubber Company were able immediately to translate the theoretical prediction into experimental measurements, which abundantly confirmed the theoretical analysis. It was possible to describe the relaxation of stress with time among a wide variety of polymers. The influences of chain scission and crosslinking were revealed in the net relaxation observed. He introduced the concept of multiplication of stress by $298/T$ to obtain reduced values. His contributions to this field have been extensive. He has worked out a rationale with an elegance entirely superior to anything previously expressed. The

* Read by J. H. Dillon.

extreme generality of the phenomena has been exhibited by the medalist and his co-workers with vinyl and diene polymers, polysulfide rubbers, polyisobutylene, polyethylene, silicones, amorphous and crystalline polymers, and natural fibers such as wool. Quite recently he reviewed the results of more than a decade of work in this field and gave a general formulation of the elastoviscous properties for amorphous, crystalline, and certain natural polymers as well as for polyelectrolytes. It is evident that, in his chosen field, the medalist blazed new pathways, years ahead of his contemporaries.

Toward midnight one night during World War II, in a discussion arising from queries addressed to the writer, there emerged a formulation of what now seems so obvious, namely, that the steps in a depolymerization process were the entire reverse of the chain processes in polymerization, resulting in the dropping of monomer units from a depolymerizing radical. This observation led to studies of simultaneous polymerization-depolymerization reactions and to oxidation effects in aging and degradation of polymers. The concept of simultaneous scission and crosslinking originally introduced to explain the physical changes in polymers produced by high temperatures and oxygen now plays a vital role in the interpretation of changes produced in polymers by high-energy radiation.

In the development of these polymer studies, the medalist worked for a number of years in close association with Dr. Herman Mark, collaborating with him in the writing of the second edition of the standard text, *Physical Chemistry of High Polymeric Systems*. In the period 1948–50 he served as Assistant Director of Research at Textile Research Institute, while continuing his teaching and research at Princeton University. For a year he acted as Assistant Director to Dr. Mark in the Brooklyn Polytechnic Institute and was for that year, 1950–51, Professor of Chemistry there. He returned to Princeton in 1951 and became a Higgins Associate Professor of Chemistry in the spring of 1953. Since his return the tempo of his research activity has notably increased and he has become a leader in research output among the younger generation in chemistry at Princeton. There are some three decades of useful life ahead which Princeton hopes to share with him. The Society of Rheology has earned the thanks of Princeton University and his colleagues in selecting for the award of the Bingham Medal a worthy successor to Henry Eyring, its earlier Princeton choice, this time Arthur Victor Tobolsky.

TRANSACTIONS OF THE SOCIETY OF RHEOLOGY VOL. I, 3–14 (1957)

The Tackiness of Liquid Adhesives

J. J. BIKERMAN, *Department of Civil and Sanitary Engineering, Massachusetts Institute of Technology, Cambridge 39, Mass.*

I. INTRODUCTION

The existence of a close relationship between tackiness and Stefan's "apparent adhesion"[1] was suggested earlier.[2] In particular, for Newtonian liquids these two quantities should be equal in a wide range of the applied stresses. However, the experimental confirmation of the proposed equality was not satisfactory. Thus, Green[3] (who did not know Stefan's work) empirically found an equation which, it is true, was similar to Stefan's formula but not identical with it; Heidebroek[4] claimed that, contrary to the theory, the results were affected by the nature of the solid adherends and by liquid properties other than viscosity; Banks and Mill[5] published observations supposed to show that bubble formation was more important for tackiness than viscosity was; and so on. In view of these disagreements another experimental study of the tackiness of Newtonian liquids seemed indicated.

II. THEORY

Consider two plane and parallel solid plates, as in Figure 1, immersed in a Newtonian liquid. When a force is applied to the plates, pulling them apart (indicated by the vertical arrows in the figure), a pressure difference is established between the periphery and the center of the liquid film, and the liquid flows toward the axis of the plates as illustrated by the horizontal arrows. The rate of this centripetal flow is governed by the geometry of the system and the viscosity of the liquid; and, in its turn, that rate governs the rate of separation of the plates. If f is the applied stress (= pull), r the radius of the plates, and η the viscosity, then the distance between the

plates increases from δ to δ_1 in t seconds, and t is given by Stefan's equation:

$$t = \frac{3\eta r^2}{4f}\left(\frac{1}{\delta^2} - \frac{1}{\delta_1{}^2}\right) \tag{1}$$

As δ_1 in all experiments was much greater than δ, equation (2):

$$ft = 3\eta r^2/4\delta^2 \tag{2}$$

may be used instead of (1).

In some of our experiments the plates were not immersed in a liquid; the liquid filled only the clearance between the plates and formed a meniscus around the clearance. As only wetting liquids were used, the meniscus was concave toward the atmosphere and, consequently, the pressure in the liquid was smaller than the atmospheric pressure. The difference was (Laplace's formula):

$$\Delta P = 2\gamma/\delta \tag{3}$$

if γ denotes surface tension. This value has to be subtracted from the experimental magnitude of f, whence the equation:

$$\left(f - \frac{2\gamma}{\delta}\right) t = \frac{3\eta r^2}{4\delta^2} \tag{4}$$

results as a counterpart of (2).

III. EXPERIMENTATION

(a) Apparatus

In principle, the apparatus reproduced the system shown in Figure 1; the upper plate was rigidly fixed and the lower plate was pulled downward by a weight.

The actual instrument is illustrated in Figures 2 and 3. The three vertical columns support the top plate (1) (steel), 2.54 cm. thick and 20.3 cm. in diameter; the base plate (2) whose function is only to keep the columns in place, rests on 3 leveling screws. The top plate is symmetrically perforated by 3 threaded holes 4.1 cm. from the axis. The upper working plate (3) (hereinafter designated as *disc*) also carries 3 threaded holes 4.1 cm. from the center so that it can be screwed to the lower surface of the top plate.

The lower "plate" (4) has a stem (5), as indicated in Figure 1;

hence, this part is called *mushroom* in the following. The mushrooms had diameters of 5.08 cm.; their plates were about 1.3 cm. thick, and their stems were threaded both inside and outside so that the load could be applied either through a large universal joint surrounding the stem or to a chain (as in Figs. 2 and 3) attached to a male screw in the body of the stem.

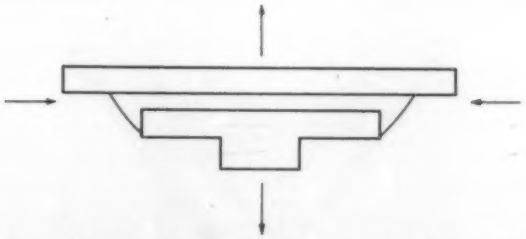

Fig. 1. Scheme of the experiment. When pull is applied in the direction of the verticle arrows, the liquid moves toward the axis, as indicated by the horizontal arrows.

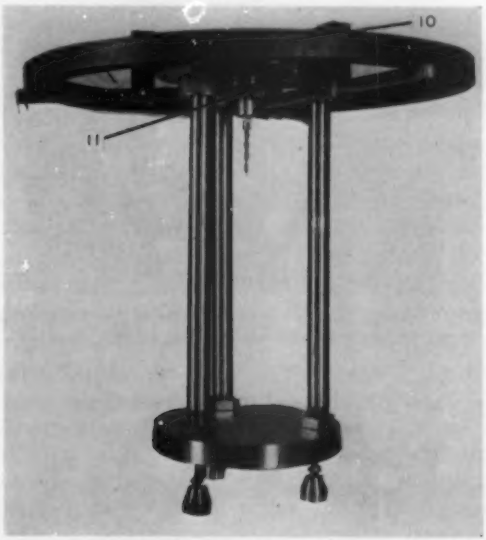

Fig. 2. The instrument during the first stage of the experiment. See text for the meaning of the numbers.

Each experiment consisted of two steps: first the mushroom, with a drop of liquid on it, was pressed against the disc; and then it was pulled away from the disc. Figure 2 illustrates the first, and Figure 3 the second step, but the arrangement for pressing is more easily seen on Figure 3. It consisted of a 3-ray steel star (6) resting on the upper plate; three vertical holders (7) welded to the external ends of the rays and each carrying two ball bearings (8); three steel bars (9)

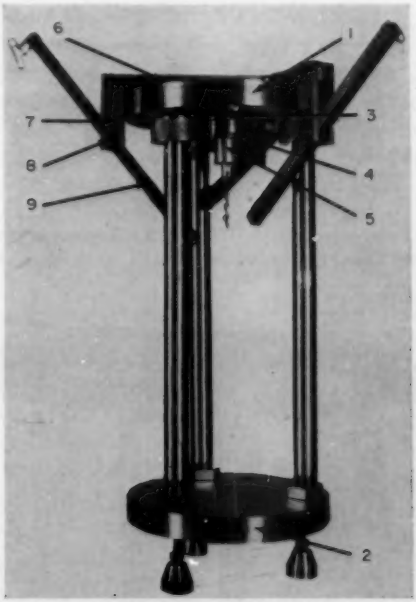

Fig. 3. The instrument during the second stage of the experiment. See text for the meaning of the numbers.

freely movable in a vertical plane about the shafts of the 3 pairs of ball bearings; and a steel ring (10) which could be placed on and removed from the bars; Figure 2 shows it in place, while Figure 3 shows the bars freely hanging after the removal of the ring.

When the ring was pressing on the exterior ends of the bars, their interior ends pressed the mushroom against the disc; the screws (11) passing through the bars served to place the mushroom in a position in which each of the bars transmitted one-third the total force.

In the experiments on which Tables II to V are based, 0.023 cm.^{3}

medicinal paraffin oil was placed on the central area of the mushroom, and the mushroom pressed with a force of 2.70×10^6 g. cm./sec.^{2} ($\pm 1\%$) against the bottom of the disc for a time equal to 200η seconds, if η is the viscosity of the oil in g./cm. sec.; see Section *b* below.

(b) Suitability of the Apparatus

The instrument shown in Figures 2 and 3 was built to test equation (2), and it is necessary to examine whether the assumptions implied in this equation are fulfilled by the actual apparatus.

Quantity f in equation (2) is calculated as $f = W/\pi r^2$, W being the load and πr^2 the area of the mushroom plate. This equation is correct only if the working metal surfaces are horizontal. The horizontality was checked with a spiritus level sensitive to about 0.02°. Fortunately, deviation from horizontal position was noticeable in the experiment itself; as the disc (3 in Fig. 3) was larger than the mushroom, the latter slid toward an edge of the disc as soon as there was a tilt. The tilt required to cause sliding was not determined but a deliberate tilt of 0.12° gave rise to a much quicker sliding than was ever observed in the regular experiments. The time of fall, *i.e.*, t in equation (2), usually was long when the mushroom slid, and all experiments in which sliding was noticed were disregarded.

Strictly speaking, equation $W = \pi r^2 f$ implies that the weight was uniformly distributed over the whole area of the mushroom. In reality it was concentrated near its axis. Obviously, a nonaxial loading would introduce a peeling component. To examine this possibility, the system was deliberately made asymmetrical by sticking small pieces of solder to various parts of the mushroom; as no effect on ft was discerned, it is believed that the casual asymmetry of the system was insignificant.

Equation (2) assumes that the liquid flows between two plane and parallel walls. The two working surfaces of steel and copper were machined, lapped, and then hand-polished on silicon carbide paper and with alumina suspension until the major part of them showed only one interference color when an optical flat was placed on the surface; the one-color field usually was surrounded by about two interference fringes. Thus the surfaces were flat within about 0.3 micron over the central part and within about 1 micron elsewhere.

When a disc or mushroom showed many (say, over 10) interference fringes in contact with the optical flat, the measured ft was significantly smaller than when the number of fringes was, *e.g.*, four.

When a spacer (a 23 micron thick piece of cellophane foil) was placed at one spot between the rim of the mushroom and the disc, the product ft was approximately one-third its usual value. The effect seems unexpectedly large if it is remembered that the insertion of cellophane raised the angle between the two metal surfaces from zero to 0.03° only, but its magnitude is readily understood if, instead of the angle, the dimensions of the clearance are considered: in the regular experiments (without spacer) of this type the clearance was 5 microns; thus the liquid film in the presence of spacer was 5 microns thick at one end of the capillary slit and 23 microns at the opposite end; no wonder that Stefan's equation was not applicable.

Additional curvature undoubtedly was caused by the axial loading of the mushroom, which made its upper surface concave toward the liquid film; but the depth of this "cup" was shown, by calculation, to be insignificant.

The thickness δ, see equation (2), depended on the magnitude and duration of the pressure tending first to spread the drop (see Section IIIa above) and then to squeeze out the liquid. Unless specifically noted, the mushroom face was completely covered by the liquid before a pull was applied.

The duration of the application of pressure was varied according to temperature so as to maintain the ratio of duration to the viscosity of the liquid constant; that would give a value of δ independent of temperature.

(c) Materials

The copper discs were made from "electrolytic tough pitch copper" donated by Chase Brass & Copper Company and stress-relieved here at 371°C. for 100 minutes. The copper mushrooms were machined from round, hard-drawn rods.

The stainless-steel discs were donated by U. S. Steel Corporation; they were Type 302. The steel mushrooms were supplied by Lord Manufacturing Company; their type was 304.

The International Nickel Company, Inc. supplied nickel discs of various degrees of roughness; the material was low-carbon nickel containing about 0.5% other elements. The nickel mushrooms were made in the shop of Lord Manufacturing Company.

The vacuum oil was of the type used for vacuum pumps; its viscosity was 7.40 and 9.35 g./cm. sec. at 25 and 21°, respectively. The viscosity of the medicinal paraffin oil was determined at 1° intervals with the results collected in Table I.

TABLE I
Viscosity of Medicinal Paraffin Oil (Nujol)

Temp., °C.	Viscosity, g./cm. sec.	Temp., °C.	Viscosity, g./cm. sec.
21	1.91	27	1.29
22	1.79	28	1.21
23	1.68	29	1.14
24	1.57	30	1.07
25	1.47	31	1.00
26	1.38		

IV. RESULTS

(a) *ft* Is Independent of *f*

According to equation (2), the product (ft) of the stress f and time t should be independent of stress. Tables II and III confirm this prediction within the whole range of stresses convenient for the experiment; at smaller stresses, t was too long, and for too large stresses the apparatus was not sturdy enough. Because the stainless-steel discs often developed cracks of about 1 cm. length and about 20 microns deep after the application of the highest stress (0.383 bar, see Table II), the product ft obtained in these experiments was disregarded when calculating the value listed in Table IV. h_{rms} is the root-mean-square average of the hill heights on the solid surface, as measured with a stylus instrument.

TABLE II
Stress f and Product of Stress and Time, ft
Polished stainless-steel plates (h_{rms} near 0.08 micron). Paraffin oil, 0.023 cm.^{2}. Averages of 12–24 measurements. Average temperature 28.1°.

f, g./cm. sec.^{2} × 10^3	ft, g./cm. sec. × 10^6	f, g./cm. sec.^{2} × 10^3	ft, g./cm. sec. × 10^6
135	23	1060	20
246	23	1715	21
472	20	3830	18
736	19		

(b) *ft* Is Independent of the Solid

As the movement occurs in the liquid phase only, the material of mushroom and disc should not affect the results. This conclusion is confirmed by Table IV, although the value for stainless steel seems

to be a little low. The copper surfaces were a little rougher (0.12 micron) than those of steel (0.03 micron) and nickel (0.05–0.10 micron).

TABLE III

Stress f and Product of Stress and Time, ft

Polished nickel mushroom (h_{rms} = 0.05–0.1 micron) and nickel disc of h_{rms} = 0.22 micron. Paraffin oil, 0.023 cm.^{3}. Average of 9 measurements. Average temperature 27.2°.

f, g./cm. sec.^{2} × 10^2	ft, g./cm. sec. × 10^6	f, g./cm. sec.^{2} × 10^2	ft, g./cm. sec. × 10^6
144	11	745	13
255	14	1070	14
480	14		

TABLE IV

Stress f and Product of Stress and Time, ft

Polished metals. Paraffin oil, 0.023 cm.^{3}.

Metal	Average of	ft	Temp., °C.
Stainless steel.....	4–6 series	21.0 × 10^6	28.1
Nickel.....	4 series	22.5	27.5
Copper.....	4 series	23.4	28.7

(c) ft Depends on Surface Roughness

The movement of the liquid outward during the application of pressure and inward during the pull may be expected to be influenced by rugosity.[6] The effect of rugosity on tackiness deserves study also because some earlier discrepancies between the experiment and Stefan's theory were attributed to roughness.[7]

This effect was tested on two series of samples. In one, a stainless-steel plate of h_{rms} = 0.03 micron was compared with the same plate which was roughened to h_{rms} = 0.08 micron by 96 strokes of a Carborundum paper No. 180. The product ft was about 10% less after than before coarsening, which is hardly significant.

In the other series, discs of nickel finished to 7 different degrees of roughness were paired with polished nickel mushrooms. The results are collected in Table V. The disc having h_{rms} = 0.675 was not flat, as seen with a "straight edge"; this presumably accounts for its low ft value.

The pronounced effect of surface roughness confirms the view that the apparent failure of Stefan's equation might be due to the disregard of rugosity.

TABLE V

Product of Stress and Time, ft, and Surface Roughness

Polished nickel against nickel of varying rugosities. Paraffin oil, 0.023 cm.³.

Surface roughness, h_{rms}, microns	ft, g./cm. sec. $\times 10^6$	Temp., °C.
0.05–0.10	22.5	27.4
0.05–0.10	24.5	26.3
0.225	13.3	28.5
0.675	3.2	27.6
2.0	3.8	27.8
6.0	0.8	27.5
18.0	0.1 (?)	27.2

The reproducibility of the ft values was better for rough than for smooth surfaces. For instance, for $h_{rms} = 6$ microns and $f = 255 \times 10^2$ baryes, time t in three determinations on one day varied in the ratio 1:1.13, while for $h_{rms} = 0.1$ micron the variation was 1:1.28 and 1:1.95 on two consecutive days. Apparently, the movement of oil along the deep valleys of a rough surface is less subject to chance than that between two surfaces whose profile is significantly affected by every dust particle. An approximate calculation may show what fraction of the oil applied was present in the grooves. The geometric contact area of mushroom and disc was 20 cm.²; assume that the valleys occupied half the area, *i.e.*, 10 cm.²; let the average depth be 6 microns; the volume then was 0.006 cm.³. Thus, a large fraction of the oil (whose total volume was 0.023 cm.³) was spent on filling the grooves.

(d) Temperature Coefficient of ft

The temperature coefficient of ft should be equal to that of viscosity η. The range of room temperatures at which ft was measured permits an approximate confirmation of this expectation. Thus (for polished steel), ft was 18×10^6 when the average room temperature (on 2 days) was 29.9 and 30.0°, while it was 23×10^6 when this temperature (again on 2 days) was 26.2°. The ratio 23:18 is equal to that of the viscosities at 26.2 and 30.0° (see Table I).

(e) ft and Wetting

Stefan's equation presupposes perfect wetting. When a steel surface was polished with an aqueous suspension of alumina and then washed first with soap and water and then with distilled water, paraffin oil did not properly spread on it, and after a measurement of ft the oil could be seen gathered in minute droplets. In all these in-

stances the value of ft was only a fraction (*e.g.*, one quarter) of the usual value. In the regular experiments the surfaces were rinsed with freshly distilled carbon tetrachloride or trichloroethylene before each application of oil.

(f) Film Thickness

The thickness δ of the liquid film can be calculated from ft and viscosity η by the equation:

$$\delta = (3\eta/ft)^{1/2} (r/2) \tag{5}$$

which is equation (2), rewritten. The radius r was 2.54 cm. in all experiments. In the major part of the experiments, when the paraffin oil volume was 0.023 cm.^{3} and the duration of pressure was 200η sec. (as mentioned in section IIIa above), the film thickness was approximately 5 microns. Thus, for the experiment referred to in IVd above, $ft = 23 \times 10^6$ and $\eta = 1.36$ (at 26.2°) afford $\delta = 5.3 \times 10^{-4}$ cm. The volume of oil was sufficient to cover the mushroom with a layer 11 microns thick; thus, half the oil was squeezed out before pull was applied.

The effect of oil volume and pressure time is illustrated by Table VI, in which some experiments carried out at near temperatures are compared; the ft are for polished stainless steel except the first line, which includes also a test on polished nickel. It is seen that increase of oil volume has little effect, while δ is markedly smaller when the volume is less at a constant duration of pressure; when this duration is small, less oil is squeezed out, and δ is considerably greater.

TABLE VI

Effect of Oil Volume and Pressure Duration on ft and δ (Paraffin Oil)

Oil vol., cm.^{3}	Pressure duration, sec.	ft	Temp., °C.	δ, microns
0.046	200η	25×10^6	25.5	5.2
0.023	200η	23	26.2	5.3
0.011	200η	31	26.4	4.6
0.011	67η	17	26.2	6.3

Table VII is analogous to Table VI but reproduces values for a more viscous liquid (a vacuum oil); it is seen that high η causes large t values even though δ is large.

TABLE VII

Effect of Oil Volume and Pressure Duration on ft and δ (Vacuum Oil)

Oil vol., cm.³	Pressure duration, sec.	ft	Temp., °C.	δ, microns
0.033	13η	19×10^6	26.9	12.8
0.017	40η	47	27.3	8.1

The values of δ calculated from ft were compared with those obtained by electric means. The determination of the thickness of thin insulator films from their electrical conductance or capacitance is difficult—for a recent statement to this effect see reference 8—because their resistance is not proportional to thickness and is often so small that only a negligible fraction of the current is used to charge and discharge the parallel condenser whence the capacitance of the latter cannot be determined.

When medicinal paraffin oil was the insulator, its capacitance could be estimated only when the measurements were carried out as rapidly as possible, before ionization of the oil too much lowered its resistance. In this manner capacitances of about 0.009 to 0.010 microfarad were observed, corresponding to δ of about 3 to 4 microns, for the conditions giving δ of about 5 microns.

The measurements were less troublesome when the more viscous oil was employed. When 0.033 cm.³ of vacuum oil was squeezed for 13η seconds between mushroom and disc and the load taken off, the capacitance at 26.9° was 0.00378 a few seconds later and then stabilized at the value 0.00310–0.00330 microfarad, which remained from the 6th to the 16th minute. Obviously, capillary attraction maintained the mushroom suspended at an invariable distance from the disc. To calculate δ from the capacitance, the dielectric constant of the oil would be needed. Instead, the capacitance of a vacuum oil film between mushroom and disc was measured, when these were spaced apart by 3 fragments of a cellophane foil, 24 microns thick. The 24 microns thick oil film had a capacitance of 0.00182 microfarad at 25.7°. Hence, neglecting the difference between the dielectric constants at 25.7 and 26.9°, capacitances of 0.00378 and 0.00320 microfarad corresponded to thicknesses of 11.6 and 13.6 microns, respectively. The δ value calculated from ft was 12.8 microns (see Table VII). Thus, equation (2) was quantitatively confirmed.

Equation (4) twice contains δ. Thus, determinations of ft in the presence of a meniscus would give two values of δ, and their identity would prove equation (4) and, naturally, also equation (2). Unfortunately, it proved impossible to adjust the oil volume and the duration of pressure in such a manner that the meniscus remained in the clearance but the whole mushroom surface was covered with oil; usually, the meniscus was outside the capillary slit and its radius of curvature was greater than $\delta/2$; thus, in one series of tests, this radius, from equation (4), was 10 microns when δ was about 6.5 microns.

The author wishes to thank Lord Manufacturing Company of Erie, Pennsylvania, for sponsorship and assistance in the execution of the research described in this paper. The companies which kindly supplied some of the materials used are mentioned in the text of the paper. Mr. William Yap helped to perform the experiments. The assistance afforded by several members of the M. I. T. faculty either as an advice or as loan of an instrument is gratefully recorded here.

References

1. J. Stefan, *Sitzber. Akad. Wiss. Wien, Math.-naturw. Klasse*, **69**, 713 (1874).
2. J. J. Bikerman, *J. Colloid Sci.*, **2**, 163 (1947).
3. H. Green, *Ind. Eng. Chem., Anal. Ed.*, **13**, 632 (1941).
4. E. Heidebroek, *Ber. Verh. Sächsischen Akad. Wiss., Math.-naturw. Klasse*, **97**, No. 6, 20 (1952).
5. W. H. Banks and C. C. Mill, *J. Colloid Sci.*, **8**, 137 (1953).
6. J. J. Bikerman, *J. Colloid Sci.*, **11**, 299 (1956).
7. J. J. Bikerman, *J. Soc. Chem. Ind.*, **62**, 41 (1943).
8. C. F. Bruce and B. S. Thornton, *J. Appl. Phys.*, **27**, 853 (1956).

Synopsis

Tackiness, *i.e.*, the resistance of adhesive joints to separation as long as the adhesive is liquid, is determined by the rheology of the adhesive and is not affected by molecular adhesion. If the adhesive is a Newtonian liquid, tackiness is governed by Stefan's equation $4ft\delta^2 = 3\eta\pi^2$; f is the applied stress, t time of separation, δ initial thickness of the liquid film, η its viscosity, and r radius of the adherend plates. This equation was confirmed for two hydrocarbon oils between surfaces of copper, nickel, or stainless steel; the oil film thickness calculated from the experimental values of ft was in accord with the thickness determined from the electrostatic capacity. The degree of flatness aud smoothness of the metal surfaces greatly affected the value of ft; the deviations from the theory recorded in earlier papers may have been due to disregard of waviness and rugosity. In the conditions of this work, the product ft was, at a first approximation, inversely proportional to the average height of hills on the metal surface.

TRANSACTIONS OF THE SOCIETY OF RHEOLOGY VOL. I, 15–24 (1957)

The Viscosity of Suspensions of Spheres. III. Sediment Volume as a Determining Parameter

JAMES V. ROBINSON, *The Mead Corporation, Chillicothe, Ohio*

INTRODUCTION

The subject of the dependence of the viscosity of suspensions of spheres upon the volume concentration has received attention in recent years, and a number of investigators have proposed equations of the form:

$$f(\eta) = kV/(1 - S'V)$$

as follows:

Vand:[1]

$$f(\eta) = \ln \eta_r$$

where k = a shape factor which for single spheres has the value 2.5, and S' = a hydrodynamic interaction constant with the value 0.609 for single spheres.

Robinson:[2]

$$f(\eta) = \eta_{sp}$$

where k = a constant characteristic of the particular suspension and S' = relative sediment volume.

Mooney:[3]

$$f(\eta) = \ln \eta_r$$

where k = the Einstein constant = 2.5 and S' = a self-crowding factor.

Maron *et al.*:[4]

$$f(\eta) = \log \eta_r$$

where $k = 2.303b\alpha$, $S' = \alpha$, and $1/\alpha$ is the volume fraction at which the viscosity becomes infinite.

Maron and Belner:[5]

$$f(\eta) = (\eta_r^{1/2} - 1)$$

where k and S' are not specifically characterized.

Vand and Mooney, respectively, stated that the proportionality constant, k, is equal to 2.5, as in the Einstein equation derived for extremely low concentrations, $\eta_{sp} = 2.5$ v. Robinson and Maron, respectively, stated that the proportionality constant may be different for different suspensions of spheres, and it is considered to be a parameter characteristic of the suspension. This view of the changeability of the proportionality constant is supported by the data of Williams,[6] who found that the constant, S', of the Mooney equation progressively decreased as the concentration of glass spheres in glycerol–water increased. Mooney[7] thought that the aberration might be due to adsorbed layers of liquid on the spheres, but Maron and Fok[8] demonstrated that, with a proper value for the proportionality constant, the denominator parameter, S', is very nearly a constant.

Robinson[2] and Maron[4] have pointed out that the reciprocal of the denominator parameter is the volume fraction at which the viscosity becomes infinite. Both authors have recognized that this limit is determined by the volume of space into which the particles can pack, Robinson by the generalized concept of relative sediment volume, and Maron by relation of results to the theoretical packing of uniformly sized spheres. There is disagreement about the function of viscosity in this general equation. Robinson chose specific viscosity, $\eta_{sp} = (\eta - \eta_0)/\eta_0$, on empirical grounds, others derived equations, in logarithm of relative viscosity, $\log (\eta/\eta_0)$ or $\ln (\eta/\eta_0)$, on theoretical grounds, and Maron and Belner introduced another function, $(\eta_r^{1/2} - 1)$, for both theoretical and empirical reasons. The previous data of Robinson,[9] the data of Williams,[6] and the new data of this paper were used to demonstrate that the denominator parameter S' from the equation in η_{sp} fits the independently measured relative sediment volume, for the case of suspended glass spheres, better than if an equation in logarithm of relative viscosity is used. The data of Maron *et al.*[4,10] were recalculated to demonstrate that the denominator parameter from the equation in $\log \eta_r$ is more reasonable in the case of synthetic latices. Possibly, this case is the one to which Ward[11] referred when he stated that other workers have found wide discrepancies at high volume concentration, in attempting to apply the equation in η_{sp}. The function $(\eta_r^{1/2} - 1)$ is successfully applicable to existing data, for both latices and glass spheres.

New data have been obtained for viscosity and relative sediment volume of glass spheres, in sucrose solution, and in white mineral oil, respectively, and the relative sediment volumes and the denominator parameters are compared.

EXPERIMENTAL

Viscosity measurements were made by essentially the same method as described previously,[2] but with the important difference that a small, unpredictable variability in the speed of rotation of the Sun Chemical Company viscometer was found and compensated for by the use of an accurate, continuously indicating tachometer. Another instrumental change was made, by substituting a cup and bob of three-fold greater radius (1.6675 and 1.6180 cm., respectively), thereby increasing the maximum rate of shear to 1860 sec.$^{-1}$. A new collection of glass spheres was used, obtained from Cataphote Corporation (Toledo 10, Ohio). An inspection of the spheres under the microscope indicated a high degree of perfection, with a particle size distribution between 5 and 45 microns diameter, and with the great preponderance of spheres being between 20 and 30 microns diameter. A certain deviation from Newtonian behavior was observed, namely, that the viscosities of all of the suspensions decreased slightly as the speed of rotation was increased, as shown in Table IV. Viscosities were measured at 7 equally spaced rates of shear. The values at the maximum rate of shear, 1860 sec.$^{-1}$, were used in the calculations.

The Vand[12] corrections were not applied. The correction for concentration increase due to crowding the outermost spheres into the center was negligible. Correction for slip along the wall, due to a layer having the viscosity of the suspension medium, was not reasonable by the formula given: for small spheres, the factor for correcting the viscosity function ($\eta_0/\eta - 1$) reduces to the clearance between the cup and bob, in centimeters. With Vand's instrument, the clearance ($R_2 - R_1$) was 1.175 cm., and the "correction" was reasonably near to unity. The instrument used in this work has a clearance of 0.05 cm. Such a correction is not consistent with the data obtained in calibrating the instrument.

The sediment volumes were measured on the same suspensions used for the viscosity measurements, by allowing the glass spheres to settle, in graduated cylinders, first under gravity, then in a centrifuge (700 $\times$ gravity). Densities of the suspensions were measured to obtain the density of the glass spheres for use in calculating volume concentrations.

TABLE I

Viscosity of Suspensions of Glass Spheres

% by wt.	% by vol., 100 V	Viscosity, η, poise	Rel. sediment vol. Gravity	Rel. sediment vol. Centrifuged	Density of suspension, g./cm.^{3}
		In Sucrose Solution No. 1			
0.0	0.0	1.135 (η_0)	—	—	1.323
10.0	6.15	1.235	1.65	1.63	1.376
20.0	12.86	1.653	1.71	1.67	1.439
30.0	20.2	1.949	1.70	1.63	1.511
35.0	24.2	2.38	—	—	—
40.0	28.2	2.89	1.68	1.61	1.590
50.0	37.1	5.58	1.70	1.66	1.671
55.0	41.9	7.39	1.69	1.65	1.731
60.0	47.0	16.11	1.67	1.59	1.783
		In Sucrose Solution No. 2			
0.0	0.0	1.721 (η_0)	—	—	1.345
10.0	6.23	2.10	1.92	1.67	1.387
20.0	13.02	2.60	1.81	1.72	1.447
30.0	20.4	3.30	1.77	1.68	1.519
35.0	24.3	3.83	1.73	1.55	1.559
40.0	28.5	4.67	1.83	1.62	1.606
45.0	32.9	6.10	1.98	1.64	1.648
50.0	37.4	7.98	1.71	1.64	1.690
55.0	42.2	12.09	1.78	1.67	1.736
		In White Mineral Oil			
0.0	0.0	0.725 (η_0)	—	—	0.866
10.0	4.14	0.811	—	—	0.923
20.0	8.85	0.948	—	—	1.000
30.0	14.27	1.102	2.79	1.87	1.066
35.0	17.29	1.236	—	—	1.121
40.0	20.6	1.382	3.14	1.76	1.171
45.0	24.7	1.635	2.93	1.75	1.208
50.0	28.0	2.02	2.77	1.81	1.257
55.0	32.2	2.54	2.89	1.77	1.312
60.0	36.8	3.58	2.66	1.73	1.372
62.0	38.5	4.14	—	—	1.405
64.0	40.8	5.03	—	—	1.438
66.0	43.0	6.54	—	—	—
68.0	45.2	7.84	—	—	—

The viscosity and relative sediment volume data are summarized in Table I. In order to derive from them the parameters of the respective equations, graphs were made, plotting, respectively:

(*1*) $V/\ln \eta_r$ *versus* V.
(*2*) V/η_{sp} *versus* V.
(*3*) $V/(\eta^{1/3} - 1)$ *versus* V.

TABLE II. Comparison of S' Parameters from Equations (1), (2), and (3) with Relative Sediment Volume

Reference	Diameter (microns)	Description	S' parameter, from $\log_e \eta_r$ (eq. 1)	η_{sp} (eq. 2)	$\eta_r^{1/2} - 1$ (eq. 3)	Rel. sediment vol. (av.) Gravity	Centrifuged
Table I	5-45	Spheres in sucrose soln. No. 1	1.42	1.96	1.65	1.69	1.63
Table I	5-45	Spheres in sucrose soln. No. 2	1.15	1.92	1.62	1.85	1.65
Table I	5-45	Spheres in white mineral oil	1.31	2.05	1.74	2.86	1.78
Robinson[9]	3-4	Spheres in glucose soln.	1.83	2.44	2.22	3.17	1.97
Robinson[9]	4-10	Spheres in glucose soln.	1.46	2.22	1.94	2.57	1.81
Robinson[9]	10-30	Spheres in glucose soln.	.81	1.96	1.49	1.92	1.70
Williams[6]	4	Spheres in glycerol–water	1.38	2.08	1.77	—	2.07
Williams[6]	8	Spheres in glycerol–water	1.27	2.15	1.77	—	—
Williams[6]	12	Spheres in glycerol–water	1.50	2.35	1.97	—	2.31

TABLE III. Comparison of Proportionality Constants, k, from Equations (1), (2), and (3)

Reference	Diameter (microns)	Description	Constant, k, from $\ln \eta_r$ (eq. 1)	η_{sp} (eq. 2)	$\eta_r^{1/2} - 1$ (eq. 3)
Table I	5-45	Spheres in sucrose soln. No. 1	1.94	2.38	1.18
Table I	5-45	Spheres in sucrose soln. No. 2	2.38	2.70	1.24
Table I	5-45	Spheres in white mineral oil	2.25	2.60	1.18
Robinson[9]	3-4	Spheres in glucose soln.	2.06	2.32	1.08
Robinson[9]	4-10	Spheres in glucose soln.	2.33	2.94	1.28
Robinson[9]	10-30	Spheres in glucose soln.	3.33	3.51	1.68
Williams[6]	4	Spheres in glycerol–water	2.70	3.77	1.68
Williams[6]	8	Spheres in glycerol–water	3.22	4.26	1.85
Williams[6]	12	Spheres in glycerol–water	3.08	3.85	1.66

TABLE IV

Viscosity of Suspensions of Glass Spheres (poises)
Variation with Rate of Shear (Sec.$^{-1}$).

% by wt.	Rate of shear (approx.) 296	555	800	1042	1305	1565	1860
			In Sucrose Solution No. 1				
0	1.153	1.167	1.163	1.147	1.145	1.145	1.135
10	1.349	1.367	1.306	1.304	1.277	1.258	1.235
20	1.689	1.667	1.653	1.647	1.647	1.636	1.653
30	2.05	2.03	2.02	2.01	2.01	2.01	1.949
35	2.51	2.50	2.44	2.47	2.43	2.43	2.38
40	2.98	2.94	2.91	2.91	2.91	2.96	2.89
50	6.05	5.77	5.63	5.58	5.60	5.66	5.58
55	8.08	7.75	7.56	7.55	7.56	7.63	7.39
60	20.9	19.54	18.73	18.00	17.45	17.27	16.11
			In Sucrose Solution No. 2				
0	1.882	1.798	1.775	1.766	1.757	1.759	1.721
10	2.33	2.22	2.18	2.17	2.16	2.16	2.10
20	2.77	2.68	2.67	2.66	2.65	2.66	2.60
30	3.53	3.47	3.46	3.42	3.40	3.36	3.30
35	4.09	3.96	3.92	3.88	3.88	3.89	3.83
40	4.91	4.80	4.85	4.80	4.76	4.76	4.67
45	6.19	6.19	6.19	6.21	6.20	6.22	6.10
50	9.00	8.58	8.47	8.38	8.22	8.19	7.98
55	14.18	13.40	13.18	12.90	12.49	12.30	12.09
			In White Mineral Oil				
0	0.745	0.741	0.750	0.745	0.750	0.763	0.725
10	0.845	0.836	0.829	0.830	0.830	0.833	0.811
20	0.952	0.946	0.939	0.948	0.950	0.958	0.948
30	1.092	1.102	1.107	1.106	1.113	1.120	1.102
35	1.287	1.242	1.256	1.248	1.258	1.266	1.236
40	1.442	1.407	1.404	1.395	1.394	1.398	1.387
45	1.729	1.671	1.669	1.678	1.662	1.669	1.635
50	2.11	2.06	2.04	2.00	1.98	2.03	2.02
55	2.75	2.59	2.55	2.55	2.57	2.61	2.54
60	3.98	3.80	3.73	3.68	3.70	3.68	3.58
62	4.54	4.28	4.22	4.11	4.10	4.13	4.14
64	6.39	5.87	5.62	5.41	5.23	5.12	5.03
66	8.04	7.51	7.29	7.05	6.86	6.70	6.54
68	10.74	9.79	9.32	8.98	8.60	8.34	7.84

The graphs are all substantially linear. The intercepts of the linear graphs are the reciprocals of the proportionality constants and of the denominator parameters, for equations having the form:

$$f(\eta) = kV/(1 - S'V)$$

The parameters and constants, so derived, are listed in Tables II and III, and in addition, the average values of relative sediment volume, from direct measurement. For comparison, older data were similarly plotted, and the reciprocals of the intercepts included in Tables II and III.

DISCUSSION

In Table II are collected all of the comparisons known to this author between relative sediment volume and the parameter S' calculated from viscosity measurements. Whether the equation in η_{sp} or in $(\eta_r^{1/3} - 1)$ is used, there is approximate agreement between relative sediment volume and the parameter S'. Because the data of this paper were obtained with especial care, for the purpose of making this comparison, the good agreement between relative sediment volume and the S' parameter obtained from the equation in $(\eta_r^{1/3} - 1)$ is believed to be more than coincidence. The earlier data of Robinson[9] were recalculated, using viscosities at the maximum rate of shear (640 sec.$^{-1}$), instead of using averaged viscosities. However, the values of the S' parameter, and also of k, were changed only slightly by the recalculation. These data likewise show a somewhat better agreement between relative sediment volume and S' when the function $(\eta_r^{1/3} - 1)$ is used. The data of Williams,[6] on the other hand, are better suited by the function η_{sp}. The assumption is being made that there is a single function of viscosity which is applicable to all suspensions of spheres, and this is substantiated by the empirical finding that the function $(\eta_r^{1/3} - 1)$ is equally appropriate for latices (Maron) and glass spheres.

The identity of the parameter S' and the relative sediment volume is a matter of definition. In the expression $kV/(1 - S'V)$, a limit is defined by $S'V = 1$, since the expression becomes infinite when $(1 - S'V) = 0$. At this limit, $V = 1/S'$, and the limit expresses the fact that there is a concentration above which the volume of suspending medium will not be sufficient to fill the space between the suspended particles. The volume which unit volume of solid occupies, in a sediment, is the relative sediment volume. The volume which a solid volume V will occupy in a packed sediment is the product V (relative sediment volume). Since the packed sediment is the upper limit of concentration of a suspension:

$$V \text{ (relative sediment volume)} = S'V$$

and S' = relative sediment volume. The relationship is shown schematically in Figure 1. Since one parameter, S', expresses the behavior of the suspension at all concentrations, the implication is that the packed volume of the suspended solid determines the rheological behavior of the suspension.

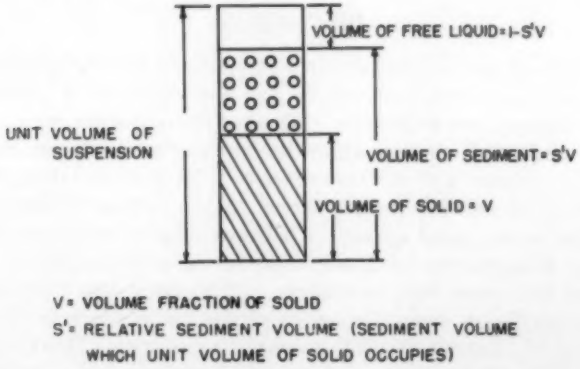
VOLUME OF FREE LIQUID = 1-S'V
UNIT VOLUME OF SUSPENSION
VOLUME OF SEDIMENT = S'V
VOLUME OF SOLID = V
V = VOLUME FRACTION OF SOLID
S' = RELATIVE SEDIMENT VOLUME (SEDIMENT VOLUME WHICH UNIT VOLUME OF SOLID OCCUPIES)

Fig. 1. Schematic representation of volumes.

There are important qualifications to this concept. The situation is as outlined above for a suspension, in which the particles do not interact with the suspending medium, as they might by forming adsorbed layers on their surfaces, nor do they stick to each other. If the particles are increased in effective size by forming layers on their surfaces, or if they stick together so that they fail to slide into the positions of close packing, then the relative sediment volume is increased. However, both of these phenomena, *i.e.*, the formation of surface layers or the sticking together of particles, may be dependent upon the mechanical forces, such as shearing, to which the particles are subjected. Therefore, the same suspension may be characterized by different values of S', at different concentrations and under different rates of shear. It is to achieve freedom from the complicating effects that attention is concentrated upon suspensions of spheres. In this work, the spheres apparently had some tendency to stick together: the relative sediment volume decreased under centrifugal force, and the suspensions showed a slight decrease in viscosity with increasing rate of shear. These phenomena may be due to interaction with the

suspending medium, as demonstrated previously,[9] with suspensions of glass spheres which when in water showed a small relative sediment volume, unaffected by centrifuging, and which when in glucose solution showed a larger relative sediment volume, decreased by centrifuging.

The values of the proportionality constant, k, are shown in Table III. The k derived from the equation in $(\eta_r^{1/2} - 1)$ is related to the k derived from the equation in η_{sp} by a factor of 2. This may be shown by reducing the equations to their approximate forms at very small values of V. The equation in $(\eta_r^{1/2} - 1)$ may be written in the form:

$$\left[\eta_r = 1 + \frac{kV}{1 - S'V}\right]^2$$

Considering that $(1 - S'V)$ approximates 1 when V is small:

$$\eta_r = 1 + 2kV + (kV)^2$$

The $(kV)^2$ term may be neglected also when V is small, and the equation reduces to $\eta_r - 1 = 2kV$. When V is small, the equation in η_{sp} reduces directly to:

$$\eta_{sp} = \eta_r - 1 = kV$$

What has been said about the dependence of S' upon the formation of surface layers on the spheres and upon their sticking together, applies to some degree also to the proportionality constant k. The value of 2.5 appears to be well established for spheres which do not interact with the solvent nor stick together. However, several authors, some of them cited by Ward,[11] have found values of k deviating from 2.5, both larger and smaller. Robinson[2] noted a dependence of k upon the suspension medium used for glass spheres. Maron and Belner[6] showed that the value of k calculated from viscosity measurements upon latices could be brought to the value of 2.5 by taking into account the monolayer of dispersant around the latex particles.

The ultimate purpose of this work was to permit analysis of the rheology of complex suspension systems such as are encountered in paper coating. A method of treating practical systems, with concepts analogous to those presented above, is described by Asbeck Scherer, and Van Loo.[13]

The author is indebted to The Mead Corporation for permission to publish this work. Thanks are due to Mr. D. Karl Landstrom for his painstaking work in making the viscosity, density, and sediment volume measurements.

References

1. V. Vand, *J. Phys. & Colloid Chem.*, **52**, 277–299 (1948).
2. J. V. Robinson, *J. Phys. & Colloid Chem.*, **53**, 1042–1056 (1949).
3. M. Mooney, *J. Colloid Sci.*, **6**, 162–170 (1951).
4. S. H. Maron, B. P. Madow, and I. M. Krieger, *J. Colloid Sci.*, **6**, 584–591 (1951).
5. S. H. Maron and R. J. Belner, *J. Colloid Sci.*, **10**, 523–535 (1955).
6. P. S. Williams, *J. Appl. Chem.*, **3**, 120–128 (1953).
7. M. Mooney and W. A. Hermonat, *J. Colloid Sci.*, **10**, 121–122 (1955).
8. S. H. Maron and Shin-Ming Fok, *J. Colloid Sci.*, **8**, 540–542 (1953).
9. J. V. Robinson, *J. Phys. & Colloid Chem.*, **55**, 455–464 (1951).
10. S. H. Maron and B. P. Madow, *J. Colloid Sci.*, **8**, 130–136 (1953).
11. S. G. Ward, *J. Oil Colour Chemists' Assoc.*, **38**, 9–31 (1955).
12. V. Vand, *J. Phys. & Colloid Chem.*, **52**, 300–313 (1948).
13. W. K. Asbeck, G. A. Scherer, and M. Van Loo, *Ind. Eng. Chem.*, **47**, 1472–1476 (1955).

Synopsis

The upper limit of volume concentration for a suspension is the reciprocal of the relative sediment volume. The dependence of viscosity upon the volume concentration of a suspension is expressed by an equation of the form:

$$f(\text{viscosity}) = kV/(1 - S'V)$$

in which the parameter, S', is identified as the relative sediment volume. For suspensions of glass spheres, the parameter S', calculated from measured viscosities, is most nearly equal to directly measured relative sediment volume when:

$$(\text{viscosity}) = (\eta_r^{1/2} - 1)$$

TRANSACTIONS OF THE SOCIETY OF RHEOLOGY VOL. I, 25–36 (1957)

Normal Stress Effect in Polyisobutylene Solutions. I. Measurements in a Cone and Plate Instrument*

HERSHEL MARKOVITZ and R. BRADY WILLIAMSON,†
Mellon Institute, Pittsburgh 13, Pa.

I. INTRODUCTION

When polymer solutions are subjected to continuous shear, stresses are required not only parallel but also normal to the shearing surfaces. Various manifestations of this effect have been described in the literature although quantitative data are still scarce. A number of phenomenological theories of deformation have also appeared. In this paper results of experiments on the shearing of solutions of polyisobutylene in decalin between a rotating cone and a stationary plate are reported. Padden and DeWitt[1] have suggested that normal stress data should be related to the dynamic rigidity and that the concentration and temperature dependence should be expressible in terms of reduced variables which are so successful in the case of the dynamic mechanical properties. These suggestions are subjected to further tests with the data herein reported. The results are discussed in relation to some recent rheological theories.

II. EXPERIMENTAL

The polyisobutylene solutions were made from commercial Vistanex B-100 obtained from Enjay Company and decalin as obtained

* This work was supported by the Rubber Research Group of the National Science Foundation under Government Contract NSF/RR-C 11, and by a grant from the National Science Foundation.

† Present address: Department of Physics, Carnegie Institute of Technology, Pittsburgh 13, Pa.

from Eastman Kodak Company. Data were taken on 3, 5, 8, and 13% solutions.

The instrument used for these measurements was a modified version of an apparatus that has been alluded to in a previous paper,[1] and has some strong resemblances to that described by Greensmith and Rivlin.[2]

The solutions were sheared between a conical surface rotating beneath a stationary plane (see Fig. 1). Such a geometry gives prac-

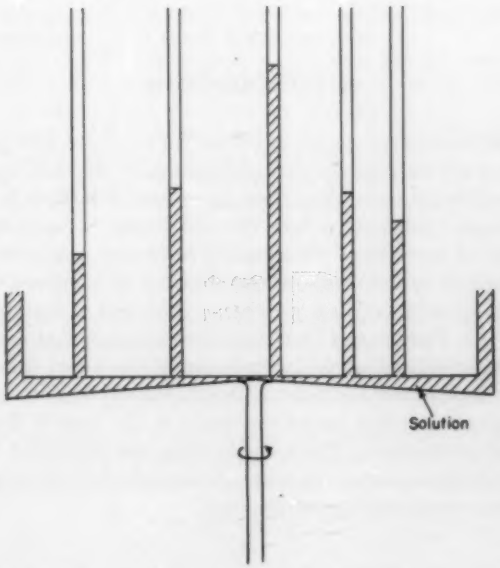

Fig. 1. A schematic diagram of cone and plate instrument for normal stress measurements.

tically a uniform rate of shear throughout the material. The angle between the plane and the generator of the cone was about 4° (0.075 radian). The plane was the bottom of a shallow hollow aluminum cylinder (15 cm. in diameter, 4 cm. high) which was rigidly attached to three symmetrically disposed arms which were supported on three

posts that rose from the base of the instrument. The orientation of the plane could be adjusted by nuts on the supporting posts. The conical surface was machined from brass and was placed on the flat bottom of a shallow outer cylinder of greater diameter (18 cm.) than the inner.

One set of experiments was performed on the 8% solution without the conical surface in place. The results of these runs are included in the following paper together with other work on torsional shearing between two circular discs.

The temperature was controlled by circulating water from a thermostat through a coil, one in the inside of the inner cylinder and one in a jacket surrounding the outer cylinder. These experiments were performed at 33°C.

To decrease loss of solvent from the solution, an annular cover was made which rested on the inner cylinder and formed a loose fit over the outer cylinder. The underside of this cover had a trough in which solvent could be put to further reduce the rate of evaporation.

A Graham variable speed drive was used to cover the range of 0.3 to 50 r.p.m. Rates of shear from 0.5 to 70 sec.$^{-1}$ were thus attainable.

The total stress developed normal to the plane surface was measured at various distances (1.69, 3.35, 4.15, 5.01, 5.77, and 6.64 cm.) from the axis of rotation of the cone. These stresses were determined by observing the height of rise of the solution in glass tubes which were placed over small holes (about 1 mm. diameter) in the flat plate. Three of the eight holes were placed at the same distance from the axis to serve as a check on the alignment of the instrument. The rise due to the normal stress was determined by averaging the heights of rise found by rotating the cone in the clockwise and counterclockwise directions. This procedure is followed because, if the plate is tilted even slightly from its correct position, a significant Pitot effect will be added to the normal stress effect. Greensmith and Rivlin[2] have shown that the Pitot contribution can be cancelled by the averaging procedure. It is this average which is called the height of rise in the discussion of experimental results.

The height of rise in the glass tubes was measured with a cathetometer. To avoid interference with the observation by the contain-

ing walls, a small negative pressure (a few centimeters of water) was applied uniformly to all the tubes. This was accomplished by attaching flexible tubing from the tops of all the tubes to a large suction flask. The pressure was controlled by the use of a vertically supported 100-cc. hypodermic syringe, the piston of which was counterbalanced with a weight sufficient to give the desired vacuum. The piston moved freely enough to give good pressure control but was still sufficiently gastight so that much less than 100 cc. of air leaked into the whole system in a period of a day.

Because of the high viscosity of the solutions used and the small size of the holes in the top plate, a long time was necessary to attain the equilibrium height of liquid in the tubes. To shorten this time, three-way metal stopcocks of the type used with medical syringes were inserted above each tube. The level of the liquid in each tube could thus be adjusted individually with a syringe.

III. RESULTS AND DISCUSSION

As has been reported previously by Roberts[3] and Pilpel,[4] who have used instruments of the same geometry, the height of rise of liquid in the tube is a logarithmic function of the distance from the axis of rotation. This is illustrated in Figure 2, which shows the data for one of our runs. Because of edge effects the absolute value of the heights of rise is not significant. They are just values obtained from cathetometer readings. To characterize the normal stress effect we use the quantity $dH/d(\ln r')$, which we designate -3ν. Here H is the normal pressure in dynes per square centimeter at a distance r' cm. from the axis of rotation when the liquid is being deformed at a rate of shear equal to $\dot{\gamma}$. The quantity ν has the same units as elasticity.

A reduced quantity, ν_r, can be defined in the same way as the reduced dynamic rigidity G_r' was defined for these solutions previously.[5] Such a procedure has been suggested in the previous work of Padden and DeWitt.[1] In this case, $\nu_r = \nu T_0/Tf(c)$, $f(c) = c/c_0$ for $c \leq c_0$, $f(c) = c^2/c_0^2$ for $c \geq c_0$, $c_0 = 0.08$, T is the absolute temperature, and $T_0 = 298°\text{K}$. The reduced rate of shear, $\dot{\gamma}_r$, is defined as before[5] for solutions of Vistanex B-100 in decalin as $\dot{\gamma}\eta T_0/Tf(c)$, where η is the zero shear viscosity of the solution. A logarithmic plot of ν_r *versus* $\dot{\gamma}_r$ is shown in Figure 3.

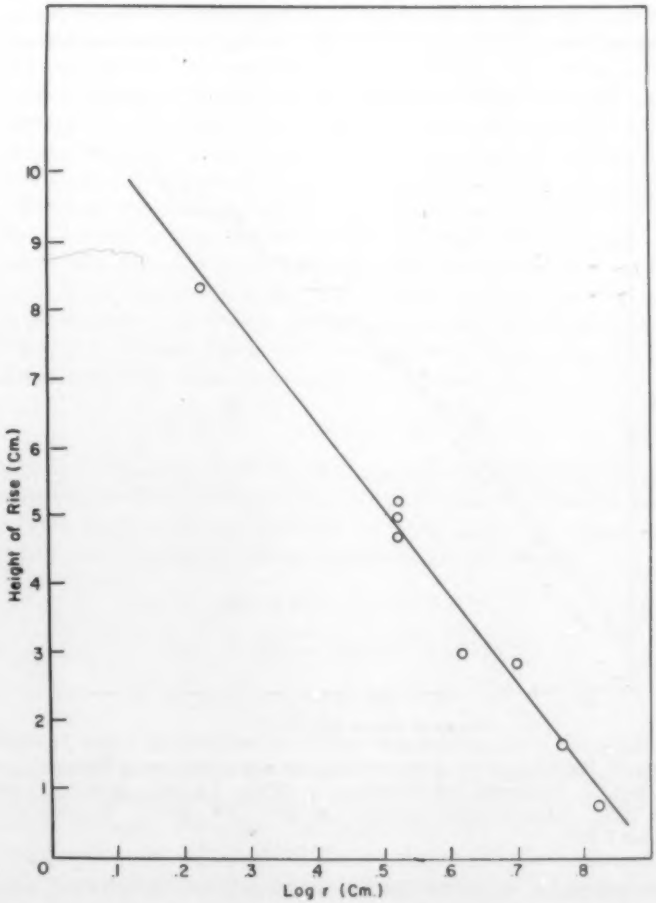

Fig. 2. Variation of normal stress with logarithm of distance from the axis of rotation for 8% solution of polyisobutylene (Vistanex B-100) in Decalin at 0.430 rev./sec. Each point is the average of a clockwise and counterclockwise reading.

Philippoff[6] has recently reported normal stress measurements at 30 and 50°C. for a 15% solution of Vistanex B-100 in Decalin prepared by us. He used a Weissenberg rheogoniometer where the total normal force (F_n) is measured while the liquid is sheared between a

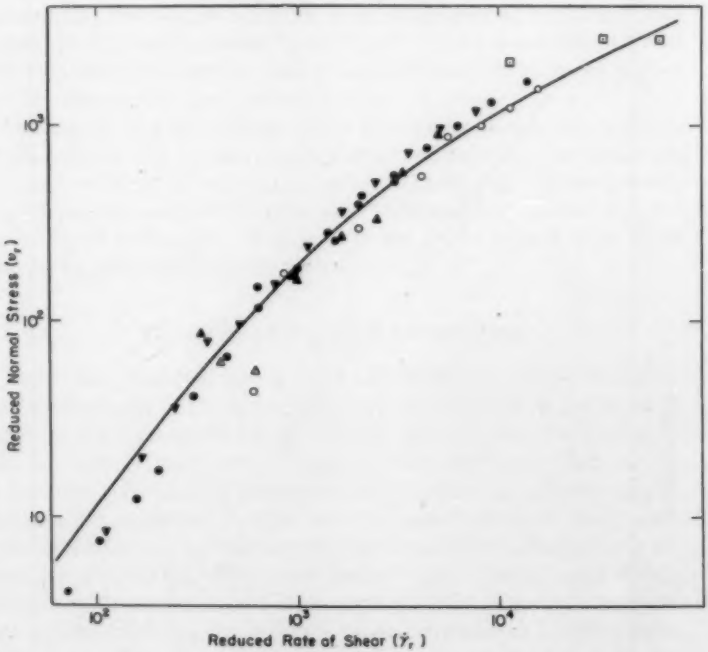

Fig. 3. Reduced normal stress plot for cone and plate data on Vistanex B-100 in Decalin. Markovitz and Williamson at 33°C.: (△) 3%, (▲) 5%, (○) 8%, (⊡) 13%. Philippoff, 15% solution: (●) 30°C., (▼) 50° C. (—) Plot of G'_r against $1.4\omega^*_r$.

cone and plate. Since $dH/d(\ln r') = -3\nu$, $H = -3\nu \ln (r'/a)$, where H is taken as zero at the edge of the plate, $r' = a$. The total normal force is then:

$$F_n = \int_0^a H(2\pi r')\, dr' = 3\pi a^2 \nu/2$$

or

$$\nu = 2F_n/3\pi a^2 \qquad (1)$$

This equation can be used to obtain ν from his data as 1/3 the quantity which he labels $(P_{11}-P_{22})$. Using the temperature and concentration dependence of the zero shear viscosity as found in this laboratory these data are also plotted in Figure 3. The validity of temperature and concentration superposition thus finds further support here.

DeWitt Theory. DeWitt[7] has proposed a rheological theory which relates to dynamic mechanical properties, and both the shearing and normal stresses in steady state flow. He has applied the theory to capillary flow, shearing between rotating coaxial cylinders, and shearing between two rotating parallel plates (torsional shearing).

To solve his equation for the case of shearing between a cone and plate it is convenient to use the spherical coordinates r, θ, and φ, where r is the distance from the origin, θ is the angle of colatitude, and ϕ is the azimuth (longitude). Assuming laminar flow with the conical surfaces θ = constant being surfaces of constant velocity, the physical components of the velocity can then be expressed as:

$$v_r = 0, \qquad v_\theta = 0, \qquad v_\phi = r\omega' \tag{2}$$

where ω' is a function of θ but not of r or ϕ. The subscripts indicate the directions of the components. If the velocity distribution given by (2) is substituted into DeWitt's tensor equation, the theory then predicts the following deviatoric components of the stress:

$$\langle\theta\phi\rangle = \eta^* S/(1 + \tau^2 S^2) \tag{3}$$

$$-\langle\phi\phi\rangle = \langle\theta\theta\rangle = -\eta^*\tau S^2/(1 + \tau^2 S^2) \tag{4}$$

$$\langle rr\rangle = \langle r\phi\rangle = \langle r\theta\rangle = 0 \tag{5}$$

where η^* and τ are parameters in the Maxwell element, the symbols[8] $\langle rr\rangle$, $\langle\theta\theta\rangle$, etc. represent the deviatoric physical components of the stresses in the direction indicated, and $S = (\partial\omega'/\partial\theta) - \cot\theta$, which is the rate of shear. Note that S is independent of r.

If equations (3), (4), and (5) are substituted in the equations of equilibrium as expressed in spherical coordinates,[8] it is found that:

$$\partial p/\partial r = 0 \tag{6}$$

where p is the isotropic pressure:

$$p = -{}^1/_3(\langle RR\rangle + \langle\Theta\Theta\rangle + \langle\Phi\Phi\rangle)$$

where $\langle RR \rangle$, etc. are the physical components of the total stress. The total normal stress as measured is:

$$\langle \Theta\Theta \rangle = \langle \theta\theta \rangle - p$$

which is independent of r by virtue of (6) and (4) and the fact that S is independent of r. This is contrary to the experimental results obtained by Pilpel,[4] Roberts,[9] and the present work, where H has been found to vary like log r as shown in Figure 2.

The derivation of the theory of DeWitt[7] from the Maxwell model suggested to him a possible connection between dynamic mechanical properties as a function of frequency and the steady state flow properties as a function of the rate of shear. A test of this conjecture for the viscosity of polyisobutylene solutions has been reported.[5] The theory had predicted that, if we write $\eta_a(\dot{\gamma}) = g(\dot{\gamma})$, then $\eta'(\omega^*) = g(\omega^*)$, where $\eta_a(\dot{\gamma})$ is the viscosity as a function of rate of shear and $\eta'(\omega^*)$ is the dynamic viscosity as a function of frequency. Experimentally it turned out that, for these solutions over the range studied, if $\eta_a(\dot{\gamma}) = g(\dot{\gamma})$ then $\eta'(\omega^*) = g(1.4\omega^*)$. Here ω^*, the pulsatance, is equal to 2π times the frequency.

It remains to see if a connection can be found between the dynamic rigidity and the normal stress effect. From the above data and those of Padden and DeWitt[1] it is clear that this connection is not of the form expected on the basis of the DeWitt theory. However, if we plot, on our graph of ν_r against $\dot{\gamma}_r$, curves of G'_r *versus* $1.4\,\omega_r{}^*$, we find somewhat better coincidence. Indeed the curve which has been drawn in Figure 3 is this dynamic rigidity curve from data which has been published previously.[5] From Figure 3 it appears that if we write $\nu(\dot{\gamma}) = h(\dot{\gamma})$, then $G'(\omega^*) = h(1.4\omega^*)$.

The factor of 1.4 used to multiply the reduced frequency was, of course, obtained empirically. One could point out that $\dot{\gamma}$ as defined in this paper is the rate of shear as used by Lamb,[10] for example. Many workers define their rate of shear, $\dot{\gamma}'$, as $\dot{\gamma}/2$. Had we used this measure, the connection between steady flow properties could have been expressed as: if $\eta_a(\dot{\gamma}') = g'(\dot{\gamma}')$, then $\eta'(\omega^*) = g'(\omega^*/1.4)$ and if $\nu(\dot{\gamma}') = h(\dot{\gamma}')$, then $G'(\omega^*) = h(\omega^*/1.4)$. It is possible that the 1.4 involves only the definition of rate of shear and may be an aid in arriving at a "natural" rate of shear. Experiments with other materials are necessary to determine whether the 1.4 is a universal constant or a property of the material.

Weissenberg Theory. A result of this theory, as given in the work of Roberts[3] and Pilpel,[4] in the case of shearing between a cone and plate is that:

$$\langle RR \rangle = \langle \Theta\Theta \rangle \tag{7}$$

When inserted in the equation of equilibrium this leads to the result:

$$\partial\langle RR \rangle / \partial(\ln r) = \langle \Phi\Phi \rangle - \langle \Theta\Theta \rangle \tag{8}$$

On the basis of their experiments they concluded that:

$$\partial\langle \Theta\Theta \rangle / \partial(\ln r) = K \tag{9}$$

at $\theta = \pi/2$, where K is independent of r, and that the validity of equations (7) and (8) was demonstrated. The experimental result expressed in equation (9) was found to be valid in the case of our polyisobutylene solutions where K corresponds to 3ν as used above.

Other deductions can be made from this theory which can be checked with their data. From (7), (8), and (9) one can compute the deviatoric components of the stresses:

$$\langle \varphi\varphi \rangle = \langle \Phi\Phi \rangle + p = 2K/3 \tag{10}$$

$$\langle rr \rangle = \langle RR \rangle + p = -K/3 \tag{11}$$

$$\langle \theta\theta \rangle = \langle \Theta\Theta \rangle + p = -K/3 \tag{12}$$

These results imply that these deviatoric components are independent of the distance from the axis. This deduction as well as the numerical relationship among these components and the relationship between them and the value of $\partial\langle \Theta\Theta \rangle / \partial(\ln r)$ appear to be substantiated by their data.[4,9] Also equation (1), which involves the Weissenberg theory in the assumption that $\langle \Theta\Theta \rangle = H = 0$ at $r' = a$, together with Figure 3, can be used as evidence for this theory.

Rivlin Theory. Rivlin[11] has recently presented an "exact theory of viscoelasticity." If the velocity distribution as expressed in (2) is inserted in this theory, one obtains the results that $\mathbf{A}_r = 0$ for $r > 2$ and that the matrix of total stress $\mathbf{T}$ is given by

$$\mathbf{T} = -P\mathbf{1} + f_1\mathbf{A}_1 + f_2\mathbf{A}_2 + f_3\mathbf{A}_1^2 \tag{13}$$

where P is a hydrostatic pressure, $f_1 = \alpha_1 + 2\mu^2\alpha_5 + 4\mu^4\alpha_7$, $f_2 = \alpha_2 + 2u^2\alpha_6 + 4u^4\alpha_8$, $f_3 = \alpha_3$, the α_i are polynomials in certain scalar

invariants all of which are functions of μ^2, $\mu = (r/r')(\partial\omega/\partial\xi) = \sin\theta(\partial\omega/\partial\theta)$ = rate of shear, $(r')^2 = x_1^2 + x_2^2$, $\xi = x_3/r'$, $\omega = r\omega'/r$,

$$\mathbf{A}_1 = \frac{1}{(r')^4}\frac{\partial\omega'}{\partial\xi} \begin{Vmatrix} 2x_1x_2x_3 & (x_2^2 - x_1^2)x_3 & -x_2(r')^2 \\ (x_2^2 - x_1^2)x_3 & -2x_1x_2x_3 & x_1(r')^2 \\ -x_2(r')^2 & x_1(r')^2 & 0 \end{Vmatrix}$$

$$\mathbf{A}_2 = \frac{2\xi^2}{(r')^2x_3^2}\left(\frac{\partial\omega'}{\partial\xi}\right) \begin{Vmatrix} x_1x_2^2 & x_1x_2x_3^2 & -x_1x_3(r')^2 \\ x_1x_2x_3^2 & x_2x_3^2 & -x_2x_3(r')^2 \\ -x_1x_3(r')^2 & -x_2x_3(r')^2 & (r')^4 \end{Vmatrix}$$

and x_1, x_2, x_3 are a set of Cartesian coordinates where the positive x_3 axis corresponds to the line $\theta = 0$. It is to be noted that the rate of shear, μ, is not a function of r.

This result can be translated into spherical coordinates by the tensor transformation rules to give:

$$\langle RR\rangle = -P \tag{14}$$

$$\langle\Theta\Theta\rangle = -P + \mu^2[(2\alpha_2 + \alpha_3) + 4\mu^2(\alpha_4 + \alpha_5) + 8\mu^4\alpha_6] \tag{15}$$

$$\langle\Phi\Phi\rangle = -P + \alpha_3\mu^2 \tag{16}$$

$$\langle R\Theta\rangle = \langle R\Phi\rangle = 0 \tag{17}$$

$$\langle\Theta\Phi\rangle = \mu[\alpha_2 + 2(\alpha_4 + \alpha_5)\mu^2 + 4\alpha_6\mu^2] \tag{18}$$

It is to be noted that here $\langle RR\rangle + \langle\Theta\Theta\rangle + \langle\Phi\Phi\rangle \neq -3P$ and therefore $\langle RR\rangle + P$, etc. are not deviatoric components of the stress.

Equations (14) to (18) can be inserted into the equations of equilibrium[8] to obtain the following results for cone and plate shearing:

$$\langle\theta\phi\rangle = C/\sin^2\theta \tag{19}$$

$$\partial P/\partial(\ln r) = -\mu^2[2\alpha_2 + 2\alpha_3 + 4\mu^2(\alpha_4 + \alpha_5) + 8\mu^4\alpha_6] \tag{20}$$

where C is an integration constant. In the types of apparatus described in this paper, measurements are made of $\langle\Theta\Theta\rangle$ as a function of r at $\theta = \pi/2$. It is therefore of interest to note that, from (15), one obtains:

$$\partial\langle\Theta\Theta\rangle/\partial(\ln r) = -\partial p/\partial(\ln r) \tag{21}$$

since the α_i are functions of μ, and μ does not vary with r. It is then seen from (20) that the Rivlin theory leads us to expect a logarithmic

dependence of the normal stress with distance from the axis of rotation. It can also be shown on calculating the deviatoric components of the stress that

$$\partial\langle\Theta\Theta\rangle/\partial(\ln r) = -3\langle rr\rangle \tag{22}$$

From (14), (15), and (16) one can also see that $\langle rr\rangle$, $\langle\theta\theta\rangle$, and $\langle\phi\phi\rangle$ are functions of μ and are independent of r.

The correct dependence of the normal stress on the distance from the axis of rotation is found in other theories also. Further discussion is deferred to the following paper.

IV. CONCLUSIONS

1. Normal stress data on concentrated polyisobutylene solutions can be superposed by using reduced variables similar to those used for dynamic mechanical properties.

2. It is found empirically that, over the range of variables studied, a relationship exists between the normal stress effect and the dynamic rigidity.

3. The dependence of the normal stress on the distance from the axis of rotation is predicted correctly by the Rivlin theory of viscoelasticity but incorrectly by the DeWitt theory. Some evidence for the Weissenberg theory is also cited.

References

1. F. J. Padden and T. W. DeWitt, *J. Appl. Phys.*, **25**, 1086 (1954).

2. H. W. Greensmith and R. S. Rivlin, *Trans. Roy. Soc. (London)*, **A245**, 399 (1953).

3. J. E. Roberts, in V. G. W. Harrison, ed., *Proceedings of the Second International Congress on Rheology*, Academic Press, London, 1954, p. 91 ff.

4. N. Pilpel, *Trans. Faraday Soc.*, **50**, 1369 (1954).

5. T. W. DeWitt, H. Markovitz, F. J. Padden, Jr., and L. J. Zapas, *J. Colloid Sci.*, **10**, 174 (1955).

6. W. Philippoff, *J. Appl. Phys.*, **27**, 984 (1956).

7. T. W. DeWitt, *J. Appl. Phys.*, **26**, 889 (1955).

8. See for example: A. E. H. Love, *A Treatise on the Mathematical Theory of Elasticity*, 4th ed., Cambridge Univ. Press, London, 1952, p. 91.

9. J. E. Roberts, "The pressure distribution in liquids in laminar shearing motion and comparison with predictions from various theories," August, 1952. Unpublished British Ministry of Supply Report.

10. H. Lamb, *Hydrodynamics*, 6th ed., Dover Publications, New York, 1945.

11. R. S. Rivlin, *J. Rational Mech. Anal.*, **5**, 179 (1956).

Synopsis

Normal stress measurements have been made on concentrated solutions of an unfractionated polyisobutylene in Decalin in an apparatus with a cone and plate geometry. Data taken at various concentrations and temperatures can be superposed in a way similar to that used for the dynamic rigidity. The functional relationship between the normal stress and rate of shear is related to that between the dynamic rigidity and the frequency. The results are discussed in terms of the recent rheological theories of DeWitt and Rivlin.

TRANSACTIONS OF THE SOCIETY OF RHEOLOGY VOL. I, 37–52 (1957)

Normal Stress Effect in Polyisobutylene Solutions. II. Classification and Application of Rheological Theories*

HERSHEL MARKOVITZ, *Mellon Institute, Pittsburgh 13, Pa.*

I. CLASSIFICATION OF RHEOLOGICAL THEORIES

A considerable number of phenomenological theories of deformation have already been proposed. They differ in their basic assumptions, the method of development, the type of rheological equation resulting, and their predictions of experimental results. In several of these theories an extended mathematical analysis is necessary for each type of shearing to be investigated. However, if these results are examined, they may be summarized in a simple form with respect to the shearing of an infinitesimal cube of the material. Let us set up an orthogonal set of coordinates x_1, x_2, x_3 (see Fig. 1), where x_2 is the direction of motion of a particle, and x_3 = constant is a surface of constant velocity. In torsional shearing between rotating parallel plates, x_1, x_2, and x_3 would refer to the cylindrical coordinates r', θ', and z, respectively; in the coaxial cylinder (Couette) shearing, to the cylindrical coordinates z, θ', and r'; in the cone and plate case, to the spherical polar coordinates r, ϕ, and θ as defined in the preceding paper.[1]

In terms of the coordinates of Figure 1, the results of the DeWitt[2] theory can be summarized as follows:

$$\langle x_2x_2\rangle = -\langle x_3x_3\rangle = \eta^*\tau\dot{\gamma}^2/(1+\tau^2\dot{\gamma}^2) \quad (1)$$

$$\langle x_2x_3\rangle = \eta^*\dot{\gamma}/(1+\tau^2\dot{\gamma}^2) \quad (2)$$

$$\langle x_1x_1\rangle = \langle x_1x_2\rangle = \langle x_1x_3\rangle = 0 \quad (3)$$

* This work was supported by a grant from the National Science Foundation.

where η^* and τ are parameters of the Maxwell element, $\dot{\gamma}$ is the rate of shear, and the symbols $\langle x_1 x_1 \rangle$, etc. are the physical components corresponding to the deviatoric stress tensor. The validity of this summary can be seen by comparing equations (1), (2), and (3) with the results previously obtained in the cases of shearing between rotating parallel discs[2] ($\dot{\gamma} = r'\omega/l$), between coaxial cylinders[2] ($\dot{\gamma} = r'\partial\omega/\partial r'$), between a cone and plate[1] ($\dot{\gamma} = \partial\omega'/\partial\theta - \cot\theta$), and in capillary flow[2] ($\dot{\gamma} = \partial v_z/\partial r'$). Here ω is the angular velocity about the axis of rotation at a distance r' from the axis, $\omega' = r'\omega/r$, l is the distance between the discs, and v_z is the velocity of motion in the capillary.

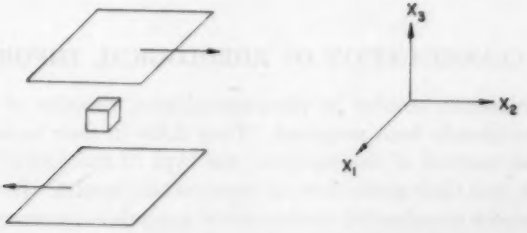

Fig. 1. General coordinate axes for description of flow.

Rivlin's[3] general theory of viscoelasticity can be summarized in terms of the coordinates of Figure 1 as follows:

$$\langle X_1 X_1 \rangle = -P \tag{4}$$

$$\langle X_2 X_2 \rangle = -P + \alpha_3 \dot{\gamma}^2 \tag{5}$$

$$\langle X_3 X_3 \rangle = -P + \dot{\gamma}^2[(2\alpha_2 + \alpha_3) + 4(\alpha_4 + \alpha_6)\dot{\gamma}^2 + 8\alpha_3\dot{\gamma}^4] \tag{6}$$

$$\langle X_2 X_3 \rangle = \dot{\gamma}[\alpha_1 + 2\alpha_5\dot{\gamma}^2 + 4\alpha_7\dot{\gamma}^4] \tag{7}$$

$$\langle X_1 X_2 \rangle = \langle X_1 X_3 \rangle = 0 \tag{8}$$

where $\langle X_1 X_1 \rangle$, etc. are the components of the total stress. The α_i's are polynomials in $\dot{\gamma}^2$ and P is a hydrostatic pressure. Equations (4) to (8) can be compared to results obtained previously for various types of shearing.[1,3] Apparently if one calculates a complex shearing which can be considered a superposition of two simple types of shear[3] characterized by $\dot{\gamma}_1$ and $\dot{\gamma}_2$, α_i is a function of $\dot{\gamma}_1^2 + \dot{\gamma}_2^2$ and $\dot{\gamma}^2$ is replaced by $\dot{\gamma}_1^2 + \dot{\gamma}_2^2$ in the above formulas. From equations (4) to (6) one can obtain the corresponding deviatoric components of the normal stresses:

$$\langle x_1x_1\rangle = \langle X_1X_1\rangle + p = -(1/3)\,\dot\gamma^2 A \tag{9}$$

$$\langle x_2x_2\rangle = \langle X_2X_2\rangle + p = -(1/3)\,\dot\gamma^2(A - 3\alpha_3) \tag{10}$$

$$\langle x_3x_3\rangle = \langle X_3X_3\rangle + p = (1/3)\,\dot\gamma^2(2A - 3\alpha_3) \tag{11}$$

where $A = 2\alpha_2 + 2\alpha_3 + 4(\alpha_4 + \alpha_6)\,\dot\gamma^2 + 8\alpha_3\dot\gamma^4$ and p, the isotropic pressure, is $-(1/3)\,(\langle X_1X_1\rangle + \langle X_2X_2\rangle + \langle X_3X_3\rangle)$.

In the above theories the fundamental tensor equations involve space derivatives of the velocity. These derivatives do not occur simply as the rate of shear but also in other combinations. Yet, when these theories are used for any particular type of shearing, it turns out that the deviatoric components are just functions of the rate of shear as can be seen from equations (1) to (3) and (7) to (11). Thus it seems plausible to write:

$$\langle x_1x_1\rangle = \langle X_1X_1\rangle + p = -\nu_1 \tag{12}$$

$$\langle x_2x_2\rangle = \langle X_2X_2\rangle + p = -\nu_2 \tag{13}$$

$$\langle x_3x_3\rangle = \langle X_3X_3\rangle + p = -\nu_3 \tag{14}$$

$$\langle x_2x_3\rangle = \langle X_2X_3\rangle = \dot\gamma\nu_4 \tag{15}$$

$$\langle x_1x_2\rangle = \langle x_1x_3\rangle = 0 \tag{16}$$

where the ν_i are functions of $\dot\gamma^2$ and p is the isotropic pressure as defined above so that:

$$\nu_1 + \nu_2 + \nu_3 = 0 \tag{17}$$

Not only are the above-mentioned theories of DeWitt[2] and Rivlin[3] of the type indicated by equations (12) to (16), but also others which will be mentioned below. However, the explanation of Garner, Nissan, and Wood[4] is not of this type. The dependence of the ν_i on $\dot\gamma^2$ is expected since the normal tensions are not affected when the direction of shearing is reversed.

Thus if we know the functions ν_i for a given material we could determine the components of the stress by using equations (12) to (16) in conjunction with the appropriate equilibrium equations. Actually by virtue of (17) only three of the ν_i are necessary, one of which (ν_4) is the apparent viscosity as a function of rate of shear.

An examination of some of the theories further shows that they are characterized by particularly simple connections among the ν_i. These results are summarized in Table I. The first column is a letter for convenience in referring to these classes of theories, the

TABLE I
Classification of Rheological Theories

A.....	$\nu_1 = \nu_2 = 0$	$\nu_3 = 0$	Classical hydrodynamics[5]
B.....	$\nu_1 = 0$	$\nu_2 = -\nu_3$	DeWitt[2]
C.....	$\nu_2 = 0$	$\nu_1 = -\nu_3$	
D.....	$\nu_3 = 0$	$\nu_1 = -\nu_2$	
E.....	$\nu_1 = \nu_2$	$\nu_3 = -2\nu_1$	Oldroyd[6] A
F.....	$\nu_1 = \nu_3$	$\nu_2 = -2\nu_1$	Weissenberg,[7-9] Oldroyd[6] B
G.....	$\nu_2 = \nu_3$	$\nu_1 = -2\nu_2$	Rivlin,[10] Reiner[11,12]
H.....	$\nu_1 \neq \nu_2 \neq \nu_3$		Rivlin,[3] Mooney[13,14] Oldroyd[6]

second, a characterizing relationship between the ν_i, the third, a result which can be deduced from column 2 with the use of (17), and the fourth, examples of theories in the particular classes. No allusion to theories in classes C and D have been found in the literature by the author. In class H are lumped all theories of a more complicated nature. Presumably some other recent theories are of this class also. These could, in some cases, include some of the simpler

TABLE II
Application of Theories

Class of theory	Cone and plate $\frac{\partial\langle\Theta\Theta\rangle}{\partial \ln r}$	Torsion of cylinder $\partial\langle ZZ\rangle/\partial r'$	Coaxial cylinder $\partial\langle R'R'\rangle/\partial r'$
A.....	0	0	0
B.....	0	$(\partial\nu_2/\partial r') - \nu_2/r'$	$-2\nu_2/r'$
C.....	$3\nu_1$	$2(\partial\nu_1/\partial r') + \nu_1/r'$	$-\nu_1/r'$
D.....	$3\nu_1$	$\partial\nu_1/\partial r' + 2\nu_1/r'$	ν_1/r'
E.....	$3\nu_1$	$3(\partial\nu_1/\partial r')$	$-3\nu_1/r'$
F.....	$3\nu_1$	$3\nu_1/r'$	$3\nu_1/r'$
G.....	$3\nu_1$	$(3\partial\nu_1/\partial r' + 3\nu_1/r')/2$	0
H.....	$3\nu_1$	$\partial(2\nu_1 + \nu_2/\partial r' + (\nu_1 - \nu_2)/r'$	$-(\nu_1 + 2\nu_2)r'$

theories as special cases, *e.g.*, Mooney's[13,14] theory becomes class F if, in his notation, $G = H$, a special case which he considers in his work. Also that particular case of Rivlin's theory[3] where:

$$2\alpha_2 + \alpha_3 + 4(\alpha_4 + \alpha_6)\,\dot\gamma^2 + 8\alpha_3\dot\gamma^4 = 0$$

is in class F.

Although this classification, of course, says nothing about the functional dependence of ν_i, it can be conveniently used to determine how to characterize a given material rheologically so that, for example, if the normal stress has been measured in one or two instruments, the value in another type of shearing could be deduced. This is illustrated in Table II. All of the examples are given in terms of ν_1 and ν_2. Equation (17) can be used if it is desired to express the results in terms of ν_3. The results are given here for three experimental setups. They were obtained by using equations (12) to (16) in the appropriate equations of equilibrium.[15] The effect of inertia of the liquid has been ignored.

Under "*cone and plate*" are given the predictions for the value of the slope in a plot of total stress $\langle\Theta\Theta\rangle$ against the logarithm of the distance from the axis r in the type of experiment discussed in the preceding paper.[1] It is to be noticed that the result is the same for all cases except class A and B theories, which predict no variation of $\langle\Theta\Theta\rangle$ with r. Thus these types of theories cannot represent the behavior of those polymer solutions, emulsions, or solutions of soaps and aluminum soaps which give rise to a linear behavior of $\langle\Theta\Theta\rangle$ with $\ln r$.[7-9] This type of dependence is predicted by all other theories since ν_1 is a function of $\dot{\gamma}$ which is independent of r. The cone and plate technique is thus a very useful method for determining ν_1 as a function of rate of shear.

In column 3 of Table II are the predicted results for *torsional shearing of a cylinder* of the liquid. Such a deformation occurs if the liquid is placed between two circular plates one of which is rotated. Data obtained with this type of instrument have been reported.[4,16,17] The traction $\langle ZZ\rangle$ produced normal to one of the plates is measured as a function of the distance r' from the axis of rotation by using the same method as reported above. The predicted value of the slope of the plot of this traction against the distance from the axis is listed.

The fourth column of Table II refers to a type of experiment which has been reported by Padden and DeWitt[17] where a liquid is sheared between two *coaxial cylinders*, one of which is rotating. The difference between the stresses $\langle R'R'\rangle$ normal to the two cylindrical walls is measured. The expressions in column four must be integrated over the gap to obtain results for quantitative comparison with experiment. It is interesting, however, to make some qualitative observations. Class G, and of course class A, theories predict no nor-

mal stress effect in this type of shearing. For those materials where ν_1 is positive, as for example polyisobutylene solutions, class C and E theories predict that the liquid would rise higher in the outer than in the inner tube of the Padden and DeWitt[17] apparatus. Class D and F theories indicate the reverse, which is what has been reported.[17] In the other classes of theories, the qualitative result will depend on the value of ν_2.

Evaluation of ν_i. If equations (12) to (16) do describe the rheological behavior of a material, Table II is a convenient summary which can be used to suggest methods for the evaluation of ν_1 and ν_2. One could presumably determine ν_1 and ν_2 by the use of any two types of flow. It is clear, however, that even in the general case (class H), ν_1 could be evaluated from cone and plate experiments.

II. POLYISOBUTYLENE SOLUTIONS

If data were available over a large range of rates of shear in each of several types of instruments for a given solution, one could use the above results to determine which, if any, of the above classes of theories described its rheological behavior. Unfortunately such a set of data is not available to us. However, a not inconsiderable number of results on polyisobutylene solutions have been reported. Padden and DeWitt[17] have suggested that reduced variables can be used for steady flow measurements as well as linear viscoelasticity. As the following discussion indicates, an examination of the available data appears to validate a reduced variable treatment for ν_1 and ν_2 similar to that for the dynamic rigidity where $\nu_{i_r} = \nu_i T_0/Tf(c)$ and $\dot{\gamma}_r = \dot{\gamma}\eta T_0/Tf(c)$, where η is the zero-shear viscosity, T is the absolute temperature, and T_0 is 298°K. Ferry's[18] proposal that $f(c) = c$ has been found to be valid for many systems. However, for the more concentrated solutions of Vistanex B — 100, the behavior is more complicated and a c^2 dependence occurs.[19] For these solutions we use $f(c)$ as determined by previous experiments on dynamic mechanical properties.[1,19] These reduced variables are not only applicable to solutions of various concentrations at various temperatures but also to a good approximation include the effect of changing solvent[20] and molecular weight.[21]

Cone and Plate Experiments. Figure 3 of the preceding paper is a test of the validity of superposition for solutions of varying concentrations and temperatures. The ν defined there is found to be ν_1 by comparison with Table II. This figure thus gives a reduced plot for ν_1 for these solutions.

Cylindrical Torsion. Having determined ν_1, it appears that shearing between rotating discs should serve to establish ν_2 and perhaps to determine the applicability of one of the classes of theories in view of the volume of data on this method in the literature and the variety of expressions for the various classes of theories. It is convenient to rearrange the expression:

$$\partial\langle ZZ\rangle/\partial \ln r' = \partial(2\nu_1 + \nu_2)/\partial(\ln r') + \nu_1 - \nu_2$$

obtained from Table II, class H, to:

$$\frac{\partial \langle ZZ\rangle}{\partial \ln r'} = 3\nu_1\left[1 + \frac{1}{3}\left(2 + \frac{\nu_2}{\nu_1}\right)\left(\frac{\partial \ln (2\nu_1 + \nu_2)}{\partial \ln r'} - 1\right)\right] \quad (18)$$

If, furthermore:

$$\nu_2 = k\nu_1 \quad (19)$$

as it is in theories of classes C, D, E, F, and G where k takes the values 0, -1, 1, -2, and $-1/2$, respectively:

$$\frac{\partial \langle ZZ\rangle}{\partial \ln r'} = 3\nu_1\left[1 + \frac{1}{3}(2 + k)\left\{\frac{\partial \ln \nu_1}{\partial \ln r'} - 1\right\}\right] \quad (20)$$

Greensmith and Rivlin[16] have reported results on a series of polyisobutylene solutions taken with a cylindrical torsion apparatus. There is an extensive range of rates of shear for many solutions where the normal stress is found to be a linear function of the distance from the axis. In these cases the results are expressed in terms of Ψ' where:

$$d\langle ZZ\rangle/d(\ln r') = 2\Omega r'\Psi'/l$$

where Ω is the angular velocity of the rotating disc and l is the gap between the two plates. From (18) it is seen that a reduced variable treatment of ν_1 implies that it should also be valid for $\partial\langle ZZ\rangle/\partial(\ln r')$ so that one should be able to write:

$$(\partial \langle ZZ\rangle/\partial \ln r')(T_0/Tf(c)) = 2\dot{\gamma}_r(\Psi'/\eta) \quad (21)$$

where $\dot{\gamma}$ in this case is $\Omega r'/l$ and the left-hand side can be considered as $(\partial\langle ZZ\rangle/\partial \ln r')_r$. Equation (21) implies that Ψ'/η is a dimensionless constant over a series of solutions of various concentrations. This result was first noted empirically in this laboratory[22] as quoted by Mooney[13] and by Greensmith and Rivlin,[16] who also observed this

to be true in their work. For a 6% solution[16] of polyisobutylene B-120 in Tetralin, Ψ' varies from 15 to 27 dyne sec. cm.$^{-2}$ over the temperature range 19 to 46° while Ψ'/η varies only from 0.37 to 0.43.

At low values of the velocity gradient, Greensmith and Rivlin[2] represent their results in terms of Ψ_0 and Ψ_1, which can be evaluated from the equation:

$$\partial\langle ZZ\rangle/\partial \ln r' = \dot{\gamma}^2(3\Psi_0/2 + 5\dot{\gamma}^2\Psi_1/8) \tag{22}$$

which when expressed in terms of reduced variables predicts the constancy of $\Psi_0 f(c)T/\eta^2 T_0$ and $\Psi_1(Tf(c))^3/\eta^4 T_0^3$. For B-120 solutions, they note that Ψ_0 increases like the eighth power of the concentration, which is what one would expect from the fact that the η is proportional to c^5 in this region and that $f(c)$ is proportional to c^2. The c^{11} dependence of Ψ_0 and the variation of Ψ_1 as c^{21} found for solutions of polyisobutylene B-15 can be explained if the viscosity varies as c^6 and $f(c)$ with c in the range of high concentrations used for this low molecular weight material. For the 6% B-120 solution at low rates of shear, Ψ_0 varied from 6 to 19 dyne sec.^{2} cm.$^{-2}$ for temperatures from 21 to 46°C. while $\Psi_0 T/\eta^2 T_0$ varied only from 3.9 to 5.1 $\times$ 10^{-3} cm.^{2}/dyne. For a 30% solution of B-15, Ψ_0 went from 0.10 to 0.22 dyne sec.^{2} cm.$^{-2}$ from 30 to 18°C. while $\Psi_0 T/\eta^2 T_0$ varied only from 7.9 to 8.5 $\times$ 10^{-6} cm.^{2}/dyne. In these calculations it was assumed that the temperature coefficient of η for the Greensmith and Rivlin solution was the same as for the B-100 solutions used in our laboratory.

Further evidence for the validity of superposition can be seen in Figure 2. The Greensmith and Rivlin points are for a 6% B-120 solution in Tetralin as obtained from data given in detail in Tables 15 and 17 of the dissertation.[23] There is a set of points obtained on an 8% Vistanex B-100 in Decalin as mentioned in the preceding paper. The other points represent data obtained some years ago in this laboratory.[22] Almost all of it was summarized in the paper by Padden and DeWitt.[17] It includes data on 6.7, 7.7, 10.0, and 12.3% solutions of Vistanex B-140 in Tetralin. The points on this graph thus represent 4 molecular weights, two solvents, three sets of workers, and many concentrations. The ordinate we have used here is $(\partial\langle ZZ\rangle/\partial \ln r')$ $(0.08/3c)$ while the abscissa is $0.08\ \Omega\ r'\eta/lc$. We have used the c dependence rather than c^2 since, for solutions other than B-100, we do not know whether or at what concentration the c^2 dependence begins. Furthermore we would not be able to discern whether the c or the c^2 dependence is more appropriate from the pres-

ent data, since a change to c^2 would shift the points somewhat along a line of unit slope on this logarithmic plot which very nearly has that slope. The reason for using $(\partial\langle ZZ\rangle/\partial \ln r')/3$ for ν_1 can be seen from equation (20). Since $\partial \ln \nu_1/\partial \ln r$ takes on values from about 0.6 to 1.3 over the range included in this figure, the factor in square brackets in (20) is equal to 1 within about 10% for the theories of

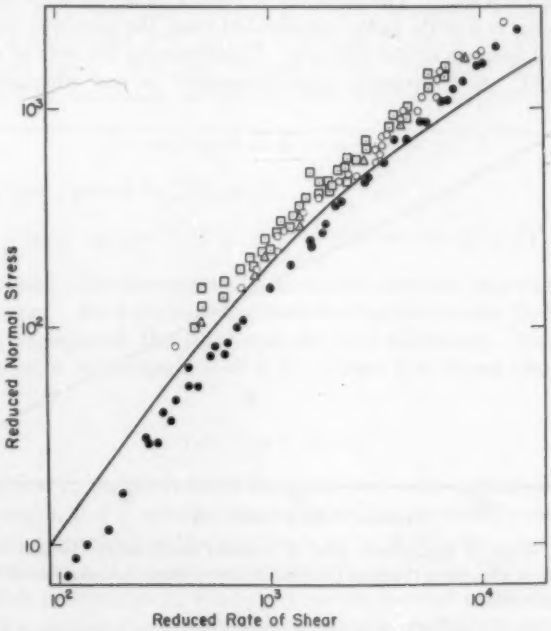

Fig. 2. Reduced plot for normal stress effect in polyisobutylene solutions obtained by torsional shearing between circular discs. Greensmith and Rivlin:[23] (●) B-120 in Tetralin. Markovitz and Williamson:[1] (△)B-100 in Decalin. Sensenbaugh *et al.*:[22] (○) B-140 in Tetralin, (⊡) B-80 in Tetralin. The line is a plot of G'_r against $1.4\omega^*_r$ for solutions of Vistanex B-100 in Decalin.[19]

interest. In view of the amount of scatter, the approximation of assuming the bracket equal to unity is good enough. Once the value of k is determined, equation (20) can be used to apply a small correction in obtaining ν_1. It is thus seen that, for these solutions in this range of variable, measurements on cylindrical torsion are not a very sensitive method for determining ν_2.

The data on which Figure 3 is based are for the most part those used by Padden and DeWitt[19] for their Figure 9. Incomplete data on dynamic properties at that time had led to the incorrect incorporation of the molecular weight into the reduced variables explicitly.

Coaxial Cylinder. Data obtained by means of this type of apparatus on solutions of polyisobutylene have been presented by Padden and DeWitt.[17] The analysis of results obtained with this type of shearing is a little more complicated than the previous two cases discussed because of the difficulty of determining the rate of shear in the liquid. A Newtonian approximation[17] is not adequate. For

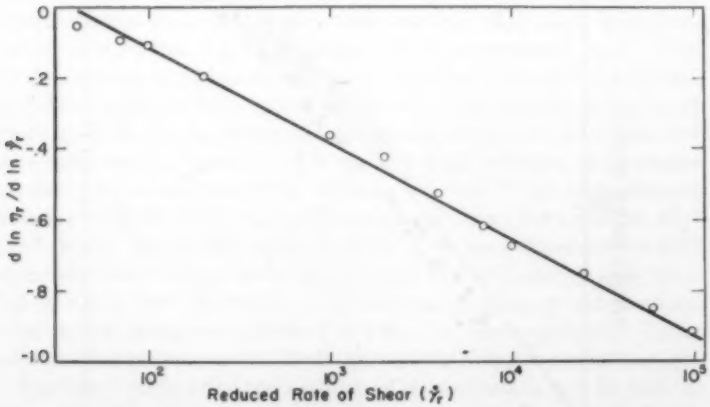

Fig. 3. Slope of logarithmic plot of reduced steady-state viscosity *versus* reduced rate of shear as a function of reduced rate of shear for solutions of Vistanex B-100 in Decalin.

the B-100–Decalin system we are aided by the fact that the functional relationship between viscosity and rate of shear is known.[19] In this type of shearing, the rate of shear, $\dot{\gamma}$, is equal to $r' \, \partial\omega/\partial r'$, where ω is the angular velocity of the liquid at a distance r' from the axis of the cylinders. We therefore can write:

$$d\omega = (\dot{\gamma}/r') \, dr' \tag{23}$$

From the equation of equilibrium we can also find out that $(r')^2\langle r'\theta\rangle$ is a constant throughout the liquid. Since $\langle r'\theta\rangle = \eta\dot{\gamma}$, we also know that

$$\eta\dot{\gamma}(r')^2 = \text{constant} \tag{24}$$

This expression can be differentiated to obtain the connection between $d\dot{\gamma}$ and dr' which can be used in (23) to arrive at the result that:

$$\omega_i - \omega_0 = \frac{1}{2}\int \left(1 + \frac{d \ln \eta}{d \ln \dot{\gamma}}\right) d\dot{\gamma} \tag{25}$$

where the integral is to be taken from the inner cylinder to the outer. It further turns out that $1 + d \ln \eta_r/d \ln \dot{\gamma}_r$ is a linear function of $\ln \dot{\gamma}_r$ over a wide range of $\dot{\gamma}_r$, as can be seen in Figure 3, where the data have been taken from the reduced curves previously published.[19] If a and b are constants, we can therefore write the approximation:

$$1 + d \ln \eta_r/d \ln \dot{\gamma}_r = a + b \ln \dot{\gamma}_r \tag{26}$$

which when inserted in (25) yields:

$$2\omega_i = \dot{\gamma}_o(a + b \ln \dot{\gamma}_o - b) - \dot{\gamma}_i(a + b \ln \dot{\gamma}_i - b) \tag{27}$$

where $\dot{\gamma}_o$ and $\dot{\gamma}_i$ are the rates of shear at the outer and inner cylinders, respectively. We have here also used the fact that in the Padden and DeWitt experiment the outer cylinder was stationary. For the reduced plot, $a = 1.43$ and $b = 0.12$. From (24) it can also be seen that:

$$\dot{\gamma}_o\eta_o/\dot{\gamma}_i\eta_i = (r_i/r_o)^2 \tag{28}$$

where r_i and r_o are the radii of the inner and outer cylinders respectively, and η_i and η_o are the viscosities at the inner and outer walls. From the dimensions of the apparatus ($r_i = 0.36$ and $r_o = 1.26$ cm.) for a given value of $\dot{\gamma}_i$, one can determine η_i, and from (28) a value for $\dot{\gamma}_o\eta_o$ which determines $\dot{\gamma}_o$, which in turn can be used in (27) to obtain a plot of ω_i against $\dot{\gamma}_i$. This graph can then be used for the determination of rate of shear at the rotating cylinder from its speed of rotation.

From Table II it is seen that:

$$\partial\langle R'R'\rangle/\partial r' = -(\nu_1 + 2\nu_2)/r' \tag{29}$$

which can be rearranged to give with the aid of (24):

$$\Delta\langle R'R'\rangle = \frac{1}{2}\int (\nu_1 + 2\nu_2)\left(1 + \frac{d \ln \eta}{d \ln \dot{\gamma}}\right) d \ln \dot{\gamma} \tag{30}$$

where the integral is to be taken from the $\dot{\gamma}_o$ to $\dot{\gamma}_i$ and $\Delta\langle R'R'\rangle = \langle R'R'\rangle_i - \langle R'R'\rangle_o$. Since $\dot{\gamma}_i \gg \dot{\gamma}_o$ for our data ($\dot{\gamma}_o/\dot{\gamma}_i$ is at most 0.05), we can to a good approximation differentiate (30) to obtain:

$$(\nu_1 + 2\nu_2)_i = \frac{2}{(1 + d \ln \eta/d \ln \dot{\gamma})_i} \frac{d\,\Delta\langle R'R'\rangle}{d \ln \dot{\gamma}_i} \tag{31}$$

where the subscript i refers to the value of the quantity at $\dot{\gamma}_i$. The amount of error in this approximation can be estimated if it is assumed

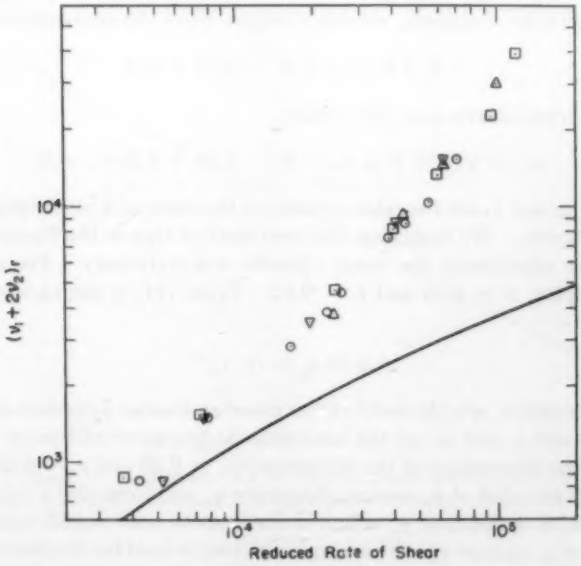

Fig. 4. Reduced plot for normal stress effect in solutions of polyisobutylene (Vistanex B-100) in Decalin as obtained in coaxial cylinder instrument:[17] (⊙) 6%, (△) 8%, (⊡) 10%, (▽) 11%. The line is a plot of G'_r against $1.4\omega^*_r$ for the same system.

that we can write approximately $\nu_1 + 2\nu_2 = k\dot{\gamma}^m$. When this expression is inserted in (30), one finds with the aid of (26) that the percentage error is at most about 10% for these experiments. This technique of estimating the error is similar to the second-order approximation method of Williams and Ferry[24] and could be used to obtain a second-order approximation to $\nu_1 + 2\nu_2$.

Figure 4 shows the coaxial cylinder data of Padden and DeWitt

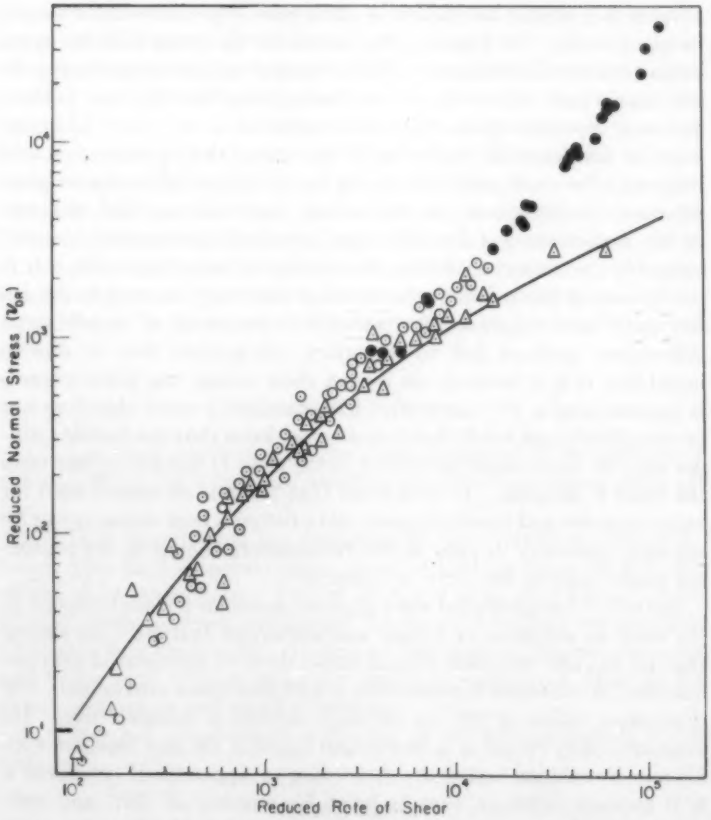

Fig. 5. Reduced plot for normal stress effect in solutions of polyisobutylene as obtained in cone and plate (△), cylindrical torsion (⊙), and coaxial cylinder (●) instruments.

on four solutions of Vistanex B-100 in Decalin in a reduced plot. The ordinate is $-(\nu_1 + 2\nu_2)_r = -(\nu_1 + 2\nu_2)T_0/Tf(c)$, where (31) was used to obtain $\nu_1 + 2\nu_2$. Graphs of much of the original data are given in Figure 7 of reference 17.

It was mentioned above that, of all of the classes of theories listed in Table II, only D and F theories (aside from the general H theories) correctly describe the qualitative behavior for polyisobutylene solutions in the coaxial cylinder case. Class D theories predict that

$-(\nu_1 + 2\nu_2)$ should be equal to ν_1 while class F predicts that it should be equal to $3\nu_1$. In Figure 5, the results for the three different types of instruments are included. For the coaxial cylinder experiments the ordinate is just $-(\nu_1 + 2\nu_2)_r$. It thus appears that the class D theories best represent these data and therefore $\nu_1 = -\nu_2$. Although there is considerable scattering of the data, the agreement is still believed to be quite good considering the variety of molecular weights, solvents, temperatures, concentrations, instruments, and workers. At the highest rates of shear the cone and plate data appear to be considerably lower than that from the coaxial cylinder apparatus. It is not known at the present time whether this truly represents the behavior of these solutions of whether it is the result of experimental difficulties—perhaps due to secondary, nonlaminar flow or due to instability of flow because the rate of shear is near the point where η is approaching a $\dot{\gamma}^{-1}$ behavior. The possibility must therefore not be completely cast aside that it is a coincidence that the coaxial cylinder data fit more nearly according to the class D theories rather than the class F theories. It is obvious that there is an urgent need for more accurate and more extensive data before a final decision can be reached, especially in view of the Weissenberg theory in the preceding paper[1] and on the work of Roberts.[7,8]

Roberts[7,8] has presented some good evidence for a class F theory in his work on solutions of rubber and aluminum laurate. He asserts that he has also obtained normal stress data on solutions of polyisobutylene in *o*-dichlorobenzene with a cone and plate instrument. He determines values of $\langle\Theta\Theta\rangle$ by the same method as reported here. He evaluates $\langle RR\rangle$ by use of a Newtonian liquid in the gap together with his non-Newtonian material. According to Appendix II of reference 8, it appears, however, that he bases his equality of $\langle RR\rangle$ and $\langle\Theta\Theta\rangle$ at the interface on an assumed orientation of that interface. It would seem rather that that orientation would be determined by the normal stresses together with the interfacial tensions. However, there can be no doubt that his experiments were done much more precisely and carefully than almost any other work reported here. Again the need for further experiments is clear.

III. RELATIONSHIP TO DYNAMIC MECHANICAL PROPERTIES

In the previous paper an empirical relationship was noted between the dynamic rigidity and the normal stress as obtained from cone and

plate instruments. In Figures 2, 4, and 5 the curves plotted are those for the reduced dynamic rigidity of Vistanex B-100 solutions in Decalin as published previously.[9] The ordinate is G_r' and the abcissa is $1.4\omega_r^*$ as in the case of Figure 3 of the preceding paper. At the highest rates of shear, the dynamic rigidity data appear to go along with cone and plate data rather than those from coaxial cylinder measurements in Figure 5. More experiments are needed to determine whether $\nu_1(= -\nu_2)$ and G' are simply related over a large range of variables or whether ν_1 and G' are related over a large range of variables while $\nu_2 = -\nu_1$ only over part of the range. In any case, it appears that at least one can use the proposed connection between ν_1, ν_2, and G' as an approximation over much of the range reported here.

IV. CONCLUSIONS

1. A method has been given for classifying some of the rheological theories which have been proposed to describe the normal stress effect.

2. This classification has been used in the evaluation of the published data on polyisobutylene. Some of the classes of theorie are shown to be inadequate. Two of the types of theories appears to be most suitable; however, enough sufficiently good data are not available to reach a firm conclusion. It appears that coaxial cylinder and cone and plate data will be especially useful in reaching a decision for these solutions as well as other systems.

3. Reduced variables are indicated to be valid in normal stress data.

References

1. H. Markovitz and R. B. Williamson, *Trans. Soc. Rheology*, this issue, preceding paper.

2. T. W. DeWitt, *J. Appl. Phys.*, **26**, 889 (1955).

3. R. S. Rivlin, *J. Rational Mech. Anal.*, **5**, 179 (1956).

4. F. H. Garner, A. H. Nissan, and G. F. Wood, *Trans. Roy. Soc.* (*London*), **A243**, 37 (1950).

5. See for example: H. Lamb, *Hydrodynamics*, Dover, New York, 1945.

6. J. G. Oldroyd, *Proc. Roy. Soc.* (*London*), **A200**, 523 (1950).

7. J. E. Roberts, in V. G. W. Harrison, ed., *Proceedings of the Second International Congress on Rheology*, Academic Press, London, 1954, p. 91 ff.

8. J. E. Roberts, "The pressure distribution in liquids in laminar shearing motion and comparison with predictions from various theories," August, 1952. Unpublished British Ministry of Supply Report.

9. N. Pilpel, *Trans. Faraday Soc.*, **50**, 1369 (1954).
10. R. S. Rivlin, *Proc. Roy. Soc.* (*London*), **A193**, 260 (1946).
11. M. Reiner, *Am. J. Math.*, **67**, 350 (1945).
12. I. Braun and M. Reiner, *Quart. J. Mech. and Appl. Math.*, **5**, 42 (1952).
13. M. Mooney, *J. Colloid Sci.*, **6**, 96 (1951).
14. M. Mooney, *J. Appl. Phys.*, **24**, 675 (1953).
15. See for example: A. E. H. Love, *A Treatise on the Mathematical Theory of Elasticity*, 4th ed., Cambridge Univ. Press, London, 1952, p. 90 ff.
16. H. W. Greensmith and R. S. Rivlin, *Trans. Roy. Soc.* (*London*), **A245**, 399 (1953).
17. F. J. Padden and T. W. DeWitt, *J. Appl. Phys.*, **25**, 1086 (1954).
18. J. D. Ferry, *J. Am. Chem. Soc.*, **72**, 3746 (1950).
19. T. W. DeWitt, H. Markovitz, F. J. Padden, Jr., and L. J. Zapas, *J. Colloid Sci.*, **10**, 174 (1955).
20. J. D. Ferry, E. R. Fitzgerald, M. F. Johnson, and L. D. Grandine, Jr., *J. Appl. Phys.*, **22**, 717 (1951).
21. Unpublished data of this laboratory.
22. D. Sensenbaugh, A. Anania, H. Markovitz, and T. W. DeWitt, unpublished data.
23. H. W. Greensmith, Ph.D. Thesis, University of London, 1952.
24. M. L. Williams and J. D. Ferry, *J. Polymer Sci.*, **11**, 169 (1953).

Synopsis

Many rheological theories can be summarized in terms of a dependence on the rate of shear of the deviatoric components of the normal stresses. In such cases two functions of the rate of shear, at most, are needed to characterize the normal stress effect. In some theories these two functions are simply related. A basis for classification of these rheological theories is thus provided. These classes of theories are applied to the cases of shearing between a cone and plate, two parallel circular discs, and coaxial cylinders. Cone and plate data give directly one of the normal stress functions. Coaxial cylinder data are especially useful in obtaining the other function and distinguishing among the theories. The available normal stress data on polyisobutylene solutions are examined and found to favor one of the types of theories. The coaxial cylinder data are analyzed without using a Newtonian approximation with the help of the known flow curve for these solutions. Evidence for a reduced variable treatment of normal stress data is presented. The relationship of normal stress and dynamic rigidity data is discussed.

TRANSACTIONS OF THE SOCIETY OF RHEOLOGY VOL. I, 53–62 (1957)

Stress–Strain Relations in a Suspension of Dumbbells

STEPHEN PRAGER, *Department of Chemistry, University of Minnesota, Minneapolis, Minn.*

INTRODUCTION

As the simplest model for a non-Newtonian system, the dilute suspension of dumbbells has been treated by many authors[1–5] during the past decade. The case of two-dimensional dumbbells in simple, steady shear flow was discussed by Kuhn and Kuhn[1] in 1945. Results on oscillating shear flow were obtained by Kirkwood and Auer[2] in 1951 and have been extended to include both nonlinear terms in the shear rate and the effect of hydrodynamic interaction between the two ends of a dumbbell.[3] Rivlin[4] in 1949 treated irrotational flow fields, and Giesekus[5] has recently discussed the behavior of a suspension of dumbbells in an arbitrary homogeneous velocity gradient.

During the same period stress–strain relationships have been approached[6–10] from a purely phenomenological point of view, without reference to any particular model. In these treatments one seeks to obtain the most general tensor relationship which will be invariant under a rotation of the coordinate axes. The earlier work of this type was restricted to relationships between the stress and the strain rate tensors alone, but Rivlin and Ericksen[9] recently pointed out that there is no reason why such relationships should not also involve the velocity curl and higher derivatives of the velocity.

The object of this paper is to obtain stress–strain relations for a suspension of dumbbells in nonuniform velocity gradient fields. We shall start, however, with a discussion of the homogeneous velocity gradient, since our results here differ somewhat from those of Giesekus.[5] It will be assumed in what follows that there is no hydrodynamic interaction between different dumbbells in the suspension, or between the two ends of a dumbbell.

THE HOMOGENEOUS VELOCITY GRADIENT FIELD

In this section we consider a velocity $\boldsymbol{v} = (v_x, v_y, v_z)$ which can be written as:

$$\boldsymbol{v} = \boldsymbol{s} \cdot \boldsymbol{r} \tag{1}$$

where $\boldsymbol{r} = (x, y, z)$ is the position vector in some fixed Cartesian reference frame, and $\boldsymbol{s}$ is the velocity gradient tensor, assumed for the time being to be independent of position and time. We may split $\boldsymbol{s}$ into a symmetric strain rate tensor $\boldsymbol{\epsilon}$ and a skew symmetric velocity curl tensor $\boldsymbol{\omega}$; if we choose the orientation of our coordinate axes properly, the strain rate tensor becomes diagonal, so that we may write:

$$\boldsymbol{s} = \boldsymbol{\epsilon} + \boldsymbol{\omega} = \begin{vmatrix} \epsilon_x & 0 & 0 \\ 0 & \epsilon_y & 0 \\ 0 & 0 & \epsilon_z \end{vmatrix} + \begin{vmatrix} 0 & -\omega_z & \omega_y \\ \omega_z & 0 & -\omega_x \\ -\omega_y & \omega_x & 0 \end{vmatrix} \tag{2}$$

The angular distribution function $W(\theta, \phi)$ for the orientation of the dumbbells in this flow field is given by the steady-state rotational diffusion equation:

$$D_R \left\{ \frac{1}{\sin\theta} \frac{\partial}{\partial\theta} \left(\sin\theta \frac{\partial W}{\partial\theta} \right) + \frac{1}{\sin^2\theta} \frac{\partial^2 W}{\partial\phi^2} \right\} = \frac{2}{b \sin\theta} \left[\frac{\partial}{\partial\theta} (W v_\theta \sin\theta) + \frac{\partial}{\partial\phi} (W v_\phi) \right] \tag{3}$$

with boundary conditions

$$W(\theta, 0) = W(\theta, 2\pi) \tag{4}$$

and:

$$\int_0^{2\pi} \int_0^{\pi} W(\theta, \phi) \sin\theta \, d\theta \, d\phi = 1 \tag{5}$$

Here θ and ϕ are the usual polar coordinate angles, D_R the rotational diffusion coefficient, and b the length of a dumbbell; v_θ and v_ϕ are the components of $\boldsymbol{v}$ in the θ and ϕ directions at a point in the fluid whose polar coordinates are $\frac{1}{2}b, \theta, \phi$, and may be expressed in terms of the components of $\boldsymbol{\epsilon}$ and $\boldsymbol{\omega}$ by the relations:

$$
\begin{aligned}
v_\theta &= {}^1/_2 b\,(\epsilon_x \cos\theta \sin\theta \cos^2\phi + \epsilon_y \cos\theta \sin\theta \sin^2\phi \\
&\quad - \epsilon_z \cos\theta \sin\theta + \omega_y \cos\phi - \omega_x \sin\phi) \\
v_\phi &= {}^1/_2 b\,((\epsilon_y - \epsilon_x) \sin\theta \cos\phi \sin\phi + \omega_z \sin\theta \\
&\quad - \omega_y \sin\phi \cos\theta - \omega_x \cos\phi \cos\theta) \\
v_r &= {}^1/_2 b\,(\epsilon_x \sin^2\theta \cos^2\phi + \epsilon_y \sin^2\theta \sin^2\phi + \epsilon_z \cos^2\theta),
\end{aligned}
\tag{6}
$$

where the radial component v_r has also been included.

Equations (6) give the velocity of the fluid in the vicinity of one end of a dumbbell whose center is located at the origin. The end itself moves with a velocity $\boldsymbol{v}'$ given by the sum of the tangential component of $\boldsymbol{v}$ and the diffusional velocity introduced by Kuhn and Kuhn[1]:

$$
\begin{aligned}
v_\theta' &= v_\theta - {}^1/_2 b\, D_R \frac{1}{W} \frac{\partial W}{\partial \theta} \\
v_\phi' &= v_\phi - {}^1/_2 b\, D_R \frac{1}{W \sin\theta} \frac{\partial W}{\partial \phi} \\
v_r' &= 0
\end{aligned}
\tag{7}
$$

In doing so it exerts a force

$$
\boldsymbol{F} = \zeta\,(\boldsymbol{v}' - \boldsymbol{v}) \tag{8}
$$

upon the fluid, ζ being a friction factor. The number of dumbbells per unit solid angle oriented in the θ, ϕ direction which penetrate unit area of a plane whose normal is the unit vector $\boldsymbol{\nu}$ is:

$$
bcW|\boldsymbol{\varrho} \cdot \boldsymbol{\nu}| \tag{9}
$$

where c is the total number of dumbbells per unit volume of solution and $\boldsymbol{\varrho} = (\sin\theta\cos\phi, \sin\theta\sin\phi, \cos\theta)$ is the unit vector in the radial direction. The total contribution from dumbbells oriented in all directions to the stress acting across such a plane is therefore:

$$
-\boldsymbol{\nu} \cdot \left[bc \int_0^{2\pi} \int_0^{\pi} \boldsymbol{F}\boldsymbol{\varrho}\, W \sin\theta\, d\theta\, d\phi \right] \tag{10}
$$

so that the stress tensor $\boldsymbol{\sigma}$ is given by:

$$
\boldsymbol{\sigma} = \boldsymbol{\sigma}_0 - bc\,\langle \boldsymbol{F}\boldsymbol{\varrho} \rangle \tag{11}
$$

where $\boldsymbol{\sigma}_0 = -p\boldsymbol{I} + 2\eta_0\boldsymbol{\epsilon}$ is the stress tensor in the absence of any solute (η_0 is the viscosity of the solvent, p the pressure), and the

angular brackets denote an average taken over θ and ϕ with the weighting function W.

The Cartesian components of $\boldsymbol{F}$ are easily found to be:

$$F_x = -\frac{\zeta b}{2}\left[D_R\frac{1}{W}\frac{\partial W}{\partial\theta}\cos\theta\cos\phi - D_R\frac{1}{W}\frac{\partial W}{\partial\phi}\frac{\sin\phi}{\sin\theta} + \sin\theta\cos\phi\,(\epsilon_x\sin^2\theta\cos^2\phi + \epsilon_y\sin^2\theta\sin^2\phi + \epsilon_z\cos^2\theta)\right]$$

$$F_y = -\frac{\zeta b}{2}\left[D_R\frac{1}{W}\frac{\partial W}{\partial\theta}\cos\theta\sin\phi + D_R\frac{1}{W}\frac{\partial W}{\partial\phi}\frac{\cos\phi}{\sin\theta} + \sin\theta\sin\phi(\epsilon_x\sin^2\theta\cos^2\phi + \epsilon_y\sin^2\theta\sin^2\phi + \epsilon_z\cos^2\theta)\right] \quad (12)$$

$$F_z = -\frac{\zeta b}{2}\left[-D_R\frac{1}{W}\frac{\partial W}{\partial\theta}\sin\theta + \cos\theta\,(\epsilon_x\sin^2\theta\cos^2\phi + \epsilon_y\sin^2\theta\sin^2\phi + \epsilon_z\cos^2\theta)\right]$$

Inserting these into (11) and performing the indicated average we obtain, with the aid of an integration by parts, the result:

$$\mathfrak{d} - \mathfrak{d}_0 = (\zeta b^2 c/2)\,[D_R(3\langle\varrho\varrho\rangle - \boldsymbol{I}) + \mathfrak{e}:\langle\varrho\varrho\varrho\varrho\rangle] \quad (13)$$

To evaluate completely the averages appearing in (13) we must, of course, solve equation (3) to obtain $W(\theta, \phi)$. It is, however, possible to simplify (13) considerably without any explicit knowledge of the angular distribution function. If we multiply both sides of (3) by a well-behaved periodic function $g(\theta, \phi)$ and average over θ and ϕ, the result is the identity:

$$D_R\left\langle\frac{\partial g}{\partial\theta}\cot\theta + \frac{\partial^2 g}{\partial\theta^2} + \frac{1}{\sin^2\theta}\frac{\partial^2 g}{\partial\phi^2}\right\rangle = -\frac{2}{b}\left\langle v_\theta\frac{\partial g}{\partial\theta} + \frac{1}{\sin\theta}v_\phi\frac{\partial g}{\partial\phi}\right\rangle \quad (14)$$

Substituting for v_θ and v_ϕ from (6), and setting g successively equal to the different components of the tensor $\varrho\varrho$, we obtain a relationship between the tensors $\langle\varrho\varrho\varrho\varrho\rangle$ and $\langle\varrho\varrho\rangle$ which when inserted into (13) transforms that equation to:

$$\mathfrak{d} - \mathfrak{d}_0 = (\zeta b^2 c/4)\,[(\mathfrak{e} + \omega)\,\langle\varrho\varrho\rangle + \langle\varrho\varrho\rangle\,(\mathfrak{e} - \omega)] \quad (15)$$

Equation (15) depends only on $\langle \varrho\varrho \rangle$ and not on any higher moments, and has the further advantage over (13) that all the terms are clearly of the same order in the components of the velocity gradient.

Let us now apply (15) to the case of a flow field in which one of the velocity components, v_z for example, is everywhere zero. This will include the cases of rectilinear and torsional flow discussed by Rivlin,[10] as well as the flow in a Couette viscometer. For such a flow the velocity gradient tensor has the form:

$$\mathbf{s} = \begin{vmatrix} s_{xx} & s_{xy} & s_{xz} \\ s_{yx} & s_{yy} & s_{yz} \\ 0 & 0 & 0 \end{vmatrix} \tag{16}$$

and when this is inserted into (15) we find that the zz component of $(\dot{\boldsymbol{\sigma}} - \dot{\boldsymbol{\sigma}}_0)$ vanishes identically, so that apart from the hydrostatic pressure there is no normal stress on a surface parallel to the plane of flow, at least if the effects of variations in $\mathbf{s}$ from point to point are ignored. In other words, the Weissenberg effect is absent in a suspension of noninteracting dumbbells. In view of this result, it seems not unreasonable to suggest that the Weissenberg effect cannot be obtained in a solution which is so dilute that the solute particles are completely independent of each other. Further calculations are necessary, of course, to confirm this statement in complete generality.

In order to solve the rotational diffusion equation (3) we resort to the customary device of expanding W into a power series in $1/D_R$:

$$W = (1/4\pi)\left(Q_0 + \frac{1}{D_R} Q_1 + \frac{1}{D_R^2} Q_2 + \ldots\right) \tag{17}$$

where the Q's are finite sums of spherical harmonics satisfying the differential equations:

$$LQ_n = \Omega Q_{n-1} \qquad (Q_0 = 1) \tag{18}$$

In (18) L and Ω represent the operators

$$\frac{1}{\sin\theta}\frac{\partial}{\partial\theta}\left(\sin\theta\,\frac{\partial}{\partial\theta}\right) + \frac{1}{\sin^2\theta}\frac{\partial^2}{\partial\phi^2} \tag{19}$$

and:

$$\frac{2}{b\sin\theta}\left[\frac{\partial}{\partial\theta}(v_\theta \sin\theta) + \frac{\partial}{\partial\phi}(v_\phi)\right] \tag{20}$$

which appear in equation (3). The ensuing calculations are tedious but straightforward, giving as the final result for $\langle \rho\rho \rangle$, up to terms in D_R^{-2}:

$$\langle \varrho\varrho \rangle = \frac{1}{3} \boldsymbol{I} + \frac{1}{15D_R} \boldsymbol{\varepsilon} + \frac{1}{105D_R^2} \left[\boldsymbol{\varepsilon}^2 - \frac{1}{3} S_2 \boldsymbol{I} + \frac{7}{6} (\boldsymbol{\omega\varepsilon} - \boldsymbol{\varepsilon\omega}) \right] + \dots \tag{21}$$

Insertion of (21) into (15) yields:

$$\begin{aligned} \boldsymbol{\mathfrak{d}} - \boldsymbol{\mathfrak{d}}_0 = 2[\eta]_0 w \Big\{ & \boldsymbol{\varepsilon} + \frac{1}{5D_R} \left[\boldsymbol{\varepsilon}^2 + \frac{1}{2} (\boldsymbol{\omega\varepsilon} - \boldsymbol{\varepsilon\omega}) \right] \\ & + \frac{1}{70D_R^2} \left[\frac{1}{3} (S_2 + 7\omega^2)\boldsymbol{\varepsilon} + 2 \left(S_3 - \frac{7}{6} J_1 \right) \boldsymbol{I} \right. \\ & \left. + \frac{13}{6} (\boldsymbol{\omega\varepsilon}^2 - \boldsymbol{\varepsilon}^2\boldsymbol{\omega}) + \frac{7}{2} (\boldsymbol{\omega}^2\boldsymbol{\varepsilon} + \boldsymbol{\varepsilon\omega}^2) \right] + \dots \Big\} \end{aligned} \tag{22}$$

where $[\eta]_0$ is the intrinsic viscosity in the limit of zero strain rate, and w the concentration of solute in terms of weight per cent; S_2, S_3, ω, and J_1 are invariants defined by the relations:

$$\begin{aligned} S_2 &= \epsilon_x^2 + \epsilon_y^2 + \epsilon_z^2 \\ S_3 &= \epsilon_x\epsilon_y\epsilon_z \\ \omega &= (\omega_x^2 + \omega_y^2 + \omega_z^2)^{1/2} \\ J_1 &= \omega_x^2\epsilon_x + \omega_y^2\epsilon_y + \omega_z^2\epsilon_z \end{aligned} \tag{23}$$

In writing (22) we have used relations obtained from the Hamilton-Cayley theorem and the extensions of that theorem recently made by Rivlin:[11]

$$\begin{aligned} \boldsymbol{\varepsilon}^3 &= S_3\boldsymbol{I} + \frac{1}{2} S_2\boldsymbol{\varepsilon} \\ \boldsymbol{\omega}^3 &= -\omega^2\boldsymbol{\omega} \\ \boldsymbol{\omega\varepsilon\omega} &= -(\boldsymbol{\varepsilon\omega}^2 + \boldsymbol{\omega}^2\boldsymbol{\varepsilon}) - \omega^2\boldsymbol{\varepsilon} + J_1\boldsymbol{I} \end{aligned} \tag{24}$$

Equation (22) is equivalent to the corresponding result of Giesekus.[5] Giesekus, however, carried his series one term further, and in so doing obtained a nonvanishing Weissenberg effect, the normal stress in rectilinear flow being proportional to the fourth power of the shear rate. This, of course, contradicts our conclusion from equation (15),

according to which the Weissenberg effect must vanish for all terms of the series.

THE INHOMOGENEOUS VELOCITY GRADIENT FIELD

If the velocity gradient varies with position or with time, the preceding analysis must be somewhat modified. Equation (13) for the stress tensor remains valid, but in evaluating the averages $\langle \varrho\varrho \rangle$ and $\langle \varrho\varrho\varrho\varrho \rangle$ the steady-state angular distribution function can no longer be used. Instead we must use a time-dependent distribution function satisfying, in place of equation (3), the equation:

$$D_R L W = \Omega W + (\partial W/\partial t) \tag{25}$$

where the components of ε and ω appearing in the operator Ω vary with time as the particle in question is carried along with the fluid through regions of different velocity gradients.

Let us assume that ε changes sufficiently slowly with time so that $\partial W/\partial t$ is small compared to the other terms in (25). We may then obtain a series of successively better approximations W_0, W_1, W_2, etc. through the recursion relations:

$$D_R L\, W_n = \Omega W_n + (\partial W_{n-1}/\partial t) \tag{26}$$

where W_0 is the steady state distribution function, given to within terms of first order in D_R^{-1} by:

$$W_0 = \frac{1}{4\pi}\left(1 + \frac{1}{2D_R}\, \varepsilon{:}\varrho\varrho + \dots\right) \tag{27}$$

In carrying out this iteration procedure we lose one of the boundary conditions of the original problem, for we may no longer specify the initial angular distribution of the dumbbells. This is in accord with our expectation that the angular distribution at time t is not appreciably affected by the angular distribution at an earlier time t_0, if $(t - t_0)$ is large compared to the rotational relaxation time.

Insertion of (27) into (26), with $n = 1$, yields:

$$D_R L\, W_1 = \Omega W_1 + \frac{1}{8\pi D_R}\frac{d\varepsilon}{dt}\,{:}\varrho\varrho + \dots \tag{28}$$

The total derivative $d\varepsilon/dt$ appearing in (28) is in general a function of both the time and the position dependence of ε:

$$\frac{d\boldsymbol{\varepsilon}}{dt} = \frac{\partial \boldsymbol{\varepsilon}}{\partial t} + \frac{\partial \boldsymbol{\varepsilon}}{\partial \boldsymbol{r}} \cdot \boldsymbol{v} \tag{29}$$

To find W_1, we can use the same expansion procedure which was employed in obtaining W_0, the first three terms of the resulting series being:

$$W_1 = \frac{1}{4\pi}\left(1 + \frac{1}{2D_R}\,\boldsymbol{\varepsilon}:\boldsymbol{\rho\rho} - \frac{1}{12D_R^2}\frac{d\boldsymbol{\varepsilon}}{dt}:\boldsymbol{\rho\rho} + \ldots\right) \tag{30}$$

so that $<\rho\rho>$ becomes:

$$\langle \boldsymbol{\rho\rho} \rangle = \frac{1}{3}\boldsymbol{I} + \frac{1}{15D_R}\,\boldsymbol{\varepsilon} - \frac{1}{90D_R^2}\frac{d\boldsymbol{\varepsilon}}{dt} + \ldots \tag{31}$$

Since the angular distribution is time-dependent, (15) must be replaced by the relation:

$$\dot{\boldsymbol{\sigma}} - \dot{\boldsymbol{\sigma}}_0 = \frac{\zeta b^2 c}{4}\left[(\boldsymbol{\varepsilon} + \boldsymbol{\omega})\langle \boldsymbol{\rho\rho} \rangle + \langle \boldsymbol{\rho\rho} \rangle\,(\boldsymbol{\varepsilon} - \boldsymbol{\omega}) - \frac{d}{dt}\langle \boldsymbol{\rho\rho} \rangle\right] \tag{32}$$

which can be derived from equation (25) in an entirely analogous manner. On substituting (31) into (32), we obtain the result

$$\begin{aligned}\dot{\boldsymbol{\sigma}} - \dot{\boldsymbol{\sigma}}_0 &= 2[\eta]_0 w\left[\boldsymbol{\varepsilon} - \frac{1}{10D_R}\frac{d\boldsymbol{\varepsilon}}{dt} + \ldots\right] \\ &= 2[\eta]_0 w\left[\boldsymbol{\varepsilon} - \frac{1}{10D_R}\left(\frac{d\boldsymbol{\varepsilon}}{\partial t} + \frac{d\boldsymbol{\varepsilon}}{\partial \boldsymbol{r}}\cdot\boldsymbol{v}\right) + \ldots\right]\end{aligned} \tag{33}$$

where only terms linear in $\boldsymbol{\varepsilon}$ and $d\boldsymbol{\varepsilon}/dt$ have been explicitly included. For steady rectilinear flow equation (33) predicts no new effects, since $d\boldsymbol{\varepsilon}/dt$ and $d\boldsymbol{\omega}/dt$ vanish in this case; it is only in dealing with more complex flows, such as take place, for example, in a divergent channel, that the new terms must be taken into account.

THE EFFECT OF TRANSLATIONAL DIFFUSION

The preceding treatment of inhomogeneous velocity gradients is actually somewhat incomplete, for we have assumed that a suspended particle is simply carried along by the motion of the suspending medium, thus ignoring the translational diffusion of the dumbbells. Stress–strain relations in which translational diffusion is taken into

account have been obtained for a suspension of dumbbells in a rectilinear flow field with a velocity gradient:

$$s = \begin{vmatrix} 0 & \alpha & 0 \\ 0 & 0 & 0 \\ 0 & 0 & 0 \end{vmatrix} \tag{34}$$

where the shear rate α is an arbitrary function of the y coordinate. The differential equation for W appropriate to this case is:

$$D_R L W = \Omega W - D(\partial^2 W/\partial y^2) \tag{35}$$

D being the translational diffusion coefficient. To solve (35) we may again resort to an iterative process, the recursion relations for which are:

$$D_R L W_n = \Omega W_n - D(\partial^2 W_{n-1}/\partial y^2) \tag{36}$$

with W_0 still given by equation (27). As before, we forfeit a boundary condition in this process, for we may no longer specify W or its derivatives on some bounding surface; this is to be expected, for the angular distribution function at a given point should be affected only by conditions in the immediate vicinity of that point.

To obtain the stress tensor once W is known, equation (15) must be modified to read:

$$\mathfrak{d} - \mathfrak{d}_0 = \frac{\xi b^2 c}{4}\left[(\mathfrak{e} + \omega)\langle \varrho\varrho \rangle + \langle \varrho\varrho \rangle (\mathfrak{e} - \omega) + D\frac{\partial^2}{\partial y^2}\langle \varrho\varrho \rangle\right] \tag{37}$$

The resulting stress components are:

$$\sigma_{xy} - (\sigma_{xy})_0 = [\eta]_0 w\left(\alpha + \frac{1}{10}\frac{D}{D_R}\frac{d^2\alpha}{dy^2} - \frac{1}{70D_R^2}\alpha^3 - \frac{1}{210}\frac{D}{D_R^3}\left(\frac{3}{2}\alpha^2\frac{d^2\alpha}{dy^2} + \alpha\left(\frac{d\alpha}{dy}\right)^2\right) + \ldots.\right)$$

$$\sigma_{xx} - (\sigma_{xx})_0 = [\eta]_0 w\left(\frac{1}{5D_R}\alpha^2 + \frac{D}{D_R^2}\left(\frac{1}{14}\alpha\frac{d^2\alpha}{dy^2} + \frac{4}{105}\left(\frac{d\alpha}{dy}\right)^2\right) + \ldots\right)$$

$$\sigma_{yy} - (\sigma_{yy})_0 = -\frac{1}{35}[\eta]_0 w\frac{D}{D_R^2}\left(\alpha\frac{d^2\alpha}{dy^2} + \left(\frac{d\alpha}{dy}\right)^2\right) + \ldots$$

$$\sigma_{yz} = \sigma_{xz} = \sigma_{zz} - (\sigma_{zz})_0 = 0 \tag{38}$$

The Weissenberg effect is represented by $(\sigma_{yy} - (\sigma_{yy})_0)$, and we see that it no longer vanishes, although its magnitude is rather small.

Strictly speaking, if we consider translational diffusion we should, to be consistent, also take into account the variation of the velocity gradient from one end of a dumbbell to the other. The two effects should be of comparable importance, for the ratio D/D_R appearing in equation (38) is of the same order of magnitude as b^2. The manner in which the finite size of the suspended particles modifies the stress–strain relations has been discussed recently by Lifson[12] for a suspension of rigid spheres in a rectilinear flow field.

References

1. W. Kuhn and H. Kuhn, *Helv. chim. acta*, **28**, 97 (1945).
2. J. G. Kirkwood and P. L. Auer, *J. Chem. Phys.*, **19**, 281 (1951).
3. J. G. Kirkwood and R. J. Plock, *J. Chem. Phys.*, **24**, 665 (1956).
4. R. S. Rivlin, *Trans. Faraday Soc.*, **45**, 739 (1949).
5. H. Giesekus, *Kolloid-Z.*, **147**, 29 (1956).
6. M. Reiner, *Am. J. Math.*, **67**, 350 (1945).
7. W. Prager, *J. Appl. Phys.*, **16**, 837 (1945).
8. R. S. Rivlin, *Proc. Roy. Soc.* (*London*), **A193**, 260 (1948).
9. R. S. Rivlin and J. L. Ericksen, *J. Rational Mech. Anal.*, **4**, 323 (1955).
10. R. S. Rivlin, *J. Rational Mech. Anal.*, **5**, 179 (1956).
11. R. S. Rivlin, *J. Rational Mech. Anal.*, **4**, 681 (1955).
12. S. Lifson, *J. Polymer Sci.*, **20**, 1 (1956).

Synopsis

Stress–strain relations are obtained for a dilute suspension of dumbbells, for both uniform and nonuniform velocity gradients. It is shown that such a fluid will not produce a Weissenberg effect in uniform, rectilinear shear flow, but that a small effect of this kind can be obtained if the shear rate is allowed to vary from point to point, as in parabolic flow between two fixed and parallel plates. The normal stress in the latter case is a result of the translational diffusion of the dumbbells.

TRANSACTIONS OF THE SOCIETY OF RHEOLOGY VOL. I, 63–94 (1957)

A Theory of the Viscosity of a Maxwellian Elastic Liquid*

M. MOONEY, *United States Rubber Co. General Laboratories, Passaic, N. J.*

INTRODUCTION

In the Eyring[1] picture of the local molecular movements which constitute a quantum of liquid flow, it is postulated that first a small hole is created in the liquid by a favorable combination of thermal vibrations of the liquid molecules. If a molecule next to the hole has sufficient thermal energy to overcome the molecular binding forces acting on it, it may break away and jump into the hole. The chance that this will happen is favored by the shearing stress acting on the molecule; and, if the jump occurs, this movement contributes to the macroscopic flow. The energy and entropy relationships involved in this process are the basic elements of the Eyring theory of flow as a thermally activated process.

However, the geometry and mechanics of this pictured mechanism are not sound. This point has been discussed by Alfrey,[2] who points out that the jumping of an individual molecule in a particular direction could be favored by a force field, but not by any stress field. Consider for example the situation pictured in Figure 1, where there is at the moment a hole in the liquid between molecules 1 and 2. If the liquid is undergoing a positive shear parallel to the x-axis and is subjected to the shearing stresses indicated by the vectors τ, then the molecule 1, according to the Eyring analysis, is subjected to a positive x force by the molecules above it, and the probability that it will jump into the hole is thereby increased. However, this argument overlooks the fact that an equal and opposite force acts on the bottom of the molecule. The resultant force is zero; and the shearing stress field actually will neither favor nor oppose the jumping of either molecule 1 or 2 into the hole.

* Contribution No. 159 from the General Laboratories.

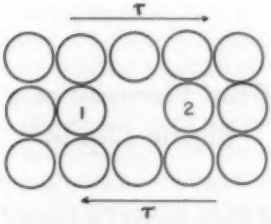

Fig. 1. The Eyring flow mechanism. With positive simple shear parallel to the x axis, molecule 1 is supposed to be forced by the shear stress τ toward the hole. Actually, the shear stress on the top of the molecule is balanced by an equal and opposite shear stress on the bottom, and the resultant force is zero.

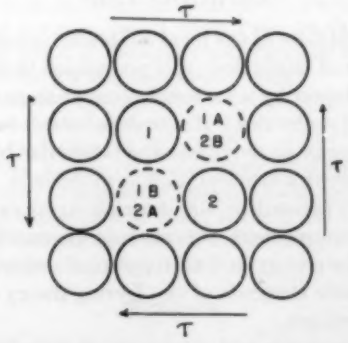

Fig. 2. The Alfrey flow mechanism. The shear stresses τ on the top and bottom of the molecular pair 1,2 constitute a couple which is supposed to cause the pair to rotate to the 1A,2A configuration. Actually, this couple is balanced by an equal and opposite couple consisting of the shear stresses on the two sides of the molecular pair, and the resultant couple is zero.

Alfrey[2] sugests an alternative mechanism of flow, pictured in Figure 2, in which a pair of contiguous molecules have at the moment a little free space on either side so located as to permit rotation of the pair from position 1,2 to position 1A,2A. However, this argument is faulty in the same way; for an x,y shear stress necessarily includes not only the x shearing forces, tending to produce clockwise rotation, but also the equal y shearing forces, tending to produce counterclockwise rotation. The resultant couple is zero and would favor neither of the possible rotations of the molecular pair, to the 1A,2A position or to the 1B,2B position.

While the errors in these pictures of liquid flow are perhaps clear, it is not too easy to see how the errors should be corrected. However, if the mathematical analysis deals with an intermolecular force which favors a shearing movement, if the force is assumed to act throughout the movement, and if the particular molecular movement is molecular in magnitude or greater, then the analysis must assume also that the primary molecular movement is accompanied by some simultaneous secondary movement of those nearby molecules that are exerting this moving force.

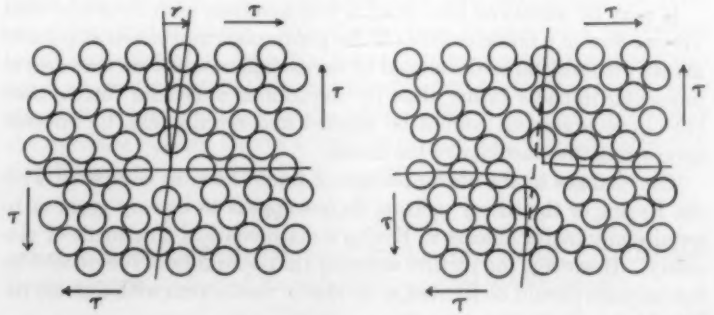

Fig. 3A. Molecular configuration before stress release. The τ's are the shearing stresses and γ is the instantaneous elastic shear.

Fig. 3B. Molecular configuration after stress release in the central area. Immediately after this release of stress there will be an increase in shearing strain sufficient to restore the mean value of the shear stress in the total area.

It can be argued, furthermore, that both the primary movements and the secondary movements of the next-neighbor molecules must take place with a speed determined by the frequency of very high-frequency sound waves in the liquid. This fact becomes apparent when we recognize that the duration of a "hole," or region of low density in the liquid, will be limited by the accelerated movement towards the center of the region which must result from the associated pressure gradient. Such a central movement constitutes a radial sound wave. Therefore the local shearing movements must occur in the time required for a sound wave to travel the diameter of the region of low density. The final and important conclusion from this discussion is that the liquid must act like an elastic solid not only toward a pressure but also toward a shear stress. The conclusion supports the sugges-

tion, first made by Maxwell,[3] that a liquid consists of an elastic body which has a very high rate of stress relaxation. Experimental confirmation of rigidity in glycerine is reported by Raman and Venkateswaran.[4]

We can now draw a more complete and more valid picture of the flow mechanism in a liquid. Figures 3A and 3B show a conceivable two-dimensional change in molecular configuration resulting from a temporary local expansion and loss of rigidity. The strain and stress release originating in the local movements indicated in Figure 3B travels with the velocity of sound out to the boundaries of the liquid.

It may be remarked here that, if it is assumed with Andrade[5] that viscous flow in a liquid consists of the continuous movement of parallel sheets with resistance developed by occasional momentum transfers in molecular impacts rather than by continuous molecular forces, then the above argument cannot be applied and nothing can be inferred concerning the elasticity of the liquid.

The changes in the above picture of liquid flow, as compared with the Eyring or the Alfrey picture, do not appear to be very great or to require any major change in Eyring's mathematical treatment of viscosity. However, the picture suggests that a liquid not only could be but perhaps should be treated as an elastic continuum with a stress relaxation mechanism.

It has been found possible to do this. A postulate of the new theory is that, whenever the local expansion in any region exceeds a certain critical value, the structure in the region loses its rigidity and the subsequent molecular rearrangements are such that the deforming stresses over the boundary of the region are temporarily reduced to zero. The associated movements are therefore proportional to the local stress before the release. When the local expansion is reduced to its normal value the normal rigidity is reestablished in the new configuration and the local stress quickly builds up again to the value imposed by the external shearing stress.

There is a significant difference here from the Eyring theory, according to which the local molecular movements are uniform in magnitude and occur with a frequency which is proportional to the shear stress. In the present theory the local movements are proportional to the stress and occur with a frequency independent of the stress. According to a theory recently published by S. Peter[6] the viscosity of a Newtonian liquid is equal to the product of the velocity of sound, an

exponential function of the activation energy, and some other terms. Such an equation will predict correctly the effect of pressure on viscosity only if the activation energy is allowed to vary with the pressure. Such a variation is not inconsistent with the theory, but the theory in its published form offers no way to predict the required variation.

THEORY OF THE ELASTIC LIQUID

In order to develop a theory of viscosity on the assumptions indicated above, it is necessary to establish a quantitative relationship between the volume of a region of temporary zero rigidity and the stress relaxation that it causes. For this purpose we can use a theoretical formula developed by Jane M. Dewey[7] for the mean modulus of rigidity of an elastic material loaded with spherical particles of elastic constants different from those of the matrix. When the shear modulus of the particles is zero, Dewey's formula for the mean rigidity modulus, μ, reduces to:

$$\mu = \mu_0(1 - hV_s) \tag{1}$$

where μ_0 is the rigidity modulus of the matrix material, V_s is the fractional volume loading of the spherical particles of zero rigidity:

$$h = 15(1 - \rho)/(7 - 5\rho) \tag{2}$$

and ρ is Poisson's ratio of the matrix material.

Suppose now we subject to shear stress τ a liquid of shear modulus μ_0 in which in time interval dt there is created a volume fraction dV_s of small spherical regions of low density, or concentrated free volume. As has been stated, within each such spherical region a complete release of shear stress is assumed to occur. Let γ_1 be the elastic shear before creation of the concentrated free volume and γ_2 the subsequent shear. Then:

$$\begin{aligned} \gamma_1 &= \tau/\mu_0 \\ \gamma_2 &= \tau(1 + h dV_s)/\mu_0 \end{aligned} \tag{3}$$

Taking the difference $\gamma_2 - \gamma_1$ and dividing by dt gives:

$$d\gamma/dt = (\tau h/\mu_0)\ (dV_s/dt) \tag{4}$$

The viscosity, η, is therefore given by:

$$1/\eta = (h/\mu_0)\ (dV_s/dt) \tag{5}$$

The next question is: at what rate does critically expanded material develop within the liquid? To find the answer to this question we follow the method of Debye[8] in the problem of the specific heat of solids and treat the thermal molecular vibrations as the sum of the displacements associated with a large number of elastic waves in the medium. In following Debye, however, we must recognize a difference between the problems of specific heat and viscosity. In the latter problem we are concerned not with all the possible modes of vibration but only with those that cause variations in density. This means that we include longitudinal vibrations but not transverse vibrations.

The Debye analysis gives for the number of waves, W, of longitudinal type in the frequency range $d\nu$:

$$W(\nu)d\nu = 4\pi L^3\nu^2 d\nu/c^3 \tag{6}$$

where L^3 is the volume of the body of liquid and c is the longitudinal wave velocity.

The lower limit of the frequency distribution is zero. In order to establish an upper limit, let it be assumed that the shortest wave length is twice the smallest molecular spacing in the liquid. This assumption is surely approximately correct; and it is doubtful that an elaborate analysis of this point could be made with any certainty. We have then for the minimum wave length, λ_m, and the maximum frequency, ν_m:

$$\lambda_m = 1/\nu_m = 2\delta \tag{7}$$

where δ is the distance between adjacent parallel planes of molecular centers.

It is easily shown that the probability of frequency ν is:

$$P(\nu)d\nu = (3\nu^2/\nu^3)d\nu \tag{8}$$

These thermal elastic waves, as they may be called, are similar to sound waves in a solid; and they differ from sound waves in the liquid in that they are of such high frequency that the period of the wave is too short for appreciable relaxation of the shear stress to occur within one period. The thermal longitudinal wave velocity, c, is therefore:

$$c = \left(\frac{1 + 2(1 - 2\rho)/(1 + \rho)}{\beta D}\right)^{1/2} \tag{9}$$

where β is the adiabatic compressibility, D is the density, and ρ is Poisson's ratio for the liquid in high-frequency stress cycles.

Since the velocity, v, of ordinary sound waves of much lower frequency is $1/(\beta D)^{1/2}$, we have the relationship:

$$c = v\sqrt{1 + 2(1 - 2\rho)/(1 + \rho)} \tag{10}$$

The analysis requires some assumption regarding the pattern of molecular packing in the liquid. Let it be assumed that the pattern resembles most nearly the close-packing of spheres in a face-centered cubic lattice. In this lattice there are 4 molecules per unit cell; and, with a cell dimension of 2δ, the number of molecules, N, per cm.^{3} is:

$$N = 1/2\delta^3 \tag{11}$$

To relate δ to measurable quantities we note that the density is $D = NM/A_n$, M being the molecular weight and A_n Avogadro's number.

Then, from (11):

$$\delta = (M/1.212)^{1/3} \times 10^{-8} \tag{12}$$

For future use an expression will be required for the probability of a given energy density E_ν in a wave of frequency ν. By Boltzmann's principle, this is:

$$P(E_\nu) = \frac{L^3}{kT} \exp\left\{-E_\nu L^3/kT\right\} \tag{13}$$

where k is Boltzmann's constant. In terms of the wave amplitude, A:

$$E_\nu = 2\pi^2 D A^2 \nu^2 \tag{14}$$

Having established these simple relationships, we can proceed with the quantitative analysis of the specific volume fluctuations within the liquid. It may be observed here that the probability of a given departure from the mean density, established by Einstein, is not sufficient for the present problem. What is required here is the frequency of the occurrence of such a departure, whereas Einstein's method gives the product of the frequency by the mean duration.

The x displacement u_i in a compressional wave i traveling in the x direction is:

$$u_i = A_i \sin\left(\omega_i t + 2\pi \frac{x}{\lambda_i} + \theta_i\right) \tag{15}$$

where A_i is the amplitude, θ_i the phase angle, and $\omega_i = 2\pi\nu_i$.

The mean expansion over the range $\pm\xi/2$ from the origin is:

$$\begin{aligned} e_i &= [\mu_i(\xi/2) - \mu_i(-\xi/2)]/\xi \\ &= \frac{2A_i}{\xi} \sin\frac{\pi\xi}{\lambda_i} \cos(\omega_i t + \theta_i) \end{aligned} \tag{16}$$

The total mean expansion, e, within the sphere of diameter ξ will be the sum of all such linear expansions as (16), or:

$$e = \sum_{\lambda_i=\lambda_m}^{\infty} \frac{2A_i}{\xi} \sin\frac{\pi\xi}{\lambda_i} \cos(\omega_i t + \theta_i) \tag{17}$$

For a sphere of a given size the terms in the above sum for which $\lambda_i \gg \xi$ will be relatively unimportant because, as shown by equation (8) or (6), there are relatively few waves of the longer λ, or lower ν. The terms for which $\lambda_i \ll \xi$, if any exist, will produce density fluctuations which have both a maximum and a minimum within the sphere, and hence their effects must be treated in spheres of smaller diameter. Consequently we are justified in dividing the total spectrum of frequencies covered by (17) into groups of waves, each group having wave lengths from $2n\delta$ to $2(n+1)\delta$, these lengths being the diameters of the related nth sphere and the next larger sphere. Thus for the smallest sphere, of diameter $\xi = 2\delta$, the chosen λ limits are 2δ to 4δ. The lower limit, 2δ, gives $\lambda = \lambda_m$, the shortest possible wave length. The sphere of diameter 2δ is just large enough to encompass the smallest group of molecules, roughly spherical in shape, that are contiguous. For the next larger sphere, of diameter $\xi = 4\delta$, the chosen λ limits are $\lambda = 4\delta$ to 6δ. The general relationships are:

$$\begin{aligned} \xi_n &= 2n\delta \\ \lambda &= 2n\delta \text{ to } 2(n+1)\delta \\ \nu &= c/2(n+1)\delta + c/2n\delta \end{aligned} \tag{18}$$

By means of equation (8) it can be shown that the average frequency for a wave group is:

$$\bar{\nu}_n = \frac{3c(4n^3 + 6n^2 + 4n + 1)}{8\delta n(n+1)(3n^2 + 3n + 1)} \tag{19}$$

This gives

$$\bar{\nu}_1 = \frac{45c}{112\delta} = 0.4018c/\delta$$

$$\bar{\nu}_2 = \frac{65c}{304\delta} = 0.2158c/\delta \tag{20}$$

Returning now to equation (17), we see that for the nth wave group we can write:

$$e_n = \sum_{\lambda = 2n\delta}^{2(n+1)\delta} \frac{2A_t}{\xi_n} \sin \frac{\pi \xi_n}{\lambda_{nt}} \cos[(\bar{\omega}_n + \Delta_{nt})t + \theta_t] \tag{21}$$

We can limit t in this equation to sufficiently small values that only two or three cycles of the mean frequency $\bar{\nu}_n$ are covered. Then we may ignore the term $\Delta_{nt}t$ in the argument of the cos; and in this simplified approximate form the fluctuation of the expansion e_n is a sinusoidal function of time of circular frequency $\bar{\omega}_n$. The amplitude of the fluctuation is the vector sum in the complex plane of the vectors:

$$\frac{2A_t}{\xi_n} \sin \frac{\pi \xi_n}{\lambda_{nt}} e^{j\theta_{nt}}$$

With random distribution of the θ_{nt} this is the problem of the random walk in a plane. For such a walk the distribution of the distance from the origin after m_n steps is given by:[9]

$$P(e_n) = \frac{2e_n}{m_n < e_n^2>} \exp\left\{-\frac{e_n^2}{m_n < e_n^2 >}\right\} \tag{22}$$

where $P(e_n)$ is the probability of the distance e_n and m_n is the number of steps, that is, the number of frequencies in the frequency group from:

$$\nu = \frac{c}{2(n+1)\delta} \text{ to } \frac{c}{2n\delta}$$

Now let ϵ be the critical value of the volume expansion at which the rigidity vanishes and molecular rearrangements become possible. We require the probability, Q that $e_n \gtrless \epsilon$. This is:

$$Q_n(\epsilon) = \int_{\epsilon}^{\infty} P(e_n) de_n \tag{23}$$

By equations (22) and (23):

$$Q_n(\epsilon) = \exp\left\{-\frac{\epsilon^2}{m_n < e_n^2 >}\right\} \tag{24}$$

The value of m_n is, from equation (6):

$$m_n = \int_{c/2(n+1)\delta}^{c/2n\delta} W(\nu)d\nu = \frac{\pi L^3}{6\delta^3} F_1(n) \tag{25}$$

$$F_1 = \frac{1}{n^3} - \frac{1}{(n+1)^3}$$

$$\begin{aligned} F_1(1) &= 0.875 \\ F_1(2) &= 0.0888 \end{aligned} \tag{26}$$

For $<e_n^2>$ we have:

$$<e_n^2> = \iint P(A)\, P(\lambda)\, \frac{A^2}{\xi_n^2} \sin\frac{2\pi\xi_n}{\lambda}\, dA d\lambda \tag{27}$$

After transforming to the variables E_ν and ν by equations (7) and (14) the integration can be carried through. The limits are $E_\nu = 0$ to ∞, and $\nu = c/2(n+1)\delta$ to $c/2n\delta$; and the result of the integration is:

$$< e_n^2 > = \frac{3kTc}{\pi^3 D \bar{\nu}_n^3 L^3 \xi_n^3} \Big| x - \sin x \cos x \Big|_{\pi\xi_n/\lambda_f}^{\pi\xi_n/\lambda_i} \tag{28}$$

Here the λ limits are as given by equation (18). This equation reduces to

$$<e_n^2> = \frac{24kT}{\pi^3 D L^3 C^2} F_2(n) \tag{29}$$

$$F_2(n) = \frac{1}{n^3}\left[\frac{\pi}{2(n+1)} + \sin\frac{n\pi}{2(n+1)} \cos\frac{n\pi}{2(n+1)}\right]$$

$$\begin{aligned} F_2(1) &= 1.285 \\ F_2(2) &= 0.1195 \end{aligned} \tag{30}$$

Now from (24) and (26):

$$Q_n(\epsilon) = \exp\left\{-\frac{\pi^2 Dc^2\delta^3\epsilon^2}{4kT\ F_1(n)F_2(n)}\right\} \tag{31}$$

We are now in a position to state the value of dV_e/dt occurring in equation (4). For any chosen point in the liquid there is a probability, given by equation (24), that the mean expansion within the sphere of diameter ξ_n is undergoing periodic fluctuations of amplitude $\geqq \epsilon$ and with the frequency $\bar{\nu}_n$ given by (19). The rate at which, on the average, critically expanded volume is attained at the point is:

$$(\pi\xi_n^3/6)\ \bar{\nu}_n Q_n(\epsilon)$$

However the number of points in unit volume where we have to consider this possible expansion—if we are to consider the possibility for all the material in unit volume— is the reciprocal of the spherical volume $\pi\xi_n^3/6$. This just cancels the volume factor $\pi\xi_n^3/6$; and the rate at which critically expanded volume in parcels of volume $\pi\xi_n^3/6$ is created per unit volume of liquid is just $\bar{\nu}_m Q_n(\epsilon)$. The rate of creation of expanded volume in parcels of all sizes is therefore the sum of terms of the form $\bar{\nu}_m Q_n(\epsilon)$. That is:

$$dV_e/dt = \sum_{n=1}^{\infty} \bar{\nu}_n Q_n(\epsilon) \tag{32}$$

From equation (31) and the numerical values of F_1 and F_2 given above, it is clear that:

$$Q_2/Q_1 \ll 1 \tag{33}$$

except when the argument in the exponential function of equation (31) approaches zero, which would rarely be a case of interest. The same inequalities would apply to all other ratios Q_n/Q_1. We see therefore that in the summation in equation (32) we can almost always ignore all but the first term.

Finally, then, the theoretical equation (5) for fluidity, ϕ, or reciprocal viscosity, η, takes the form:

$$\varphi = \frac{1}{\eta} = \frac{4.018(1-\rho^2)\beta c}{(1-2\rho)\ (7-5\rho)\delta} \exp\left\{-\frac{\pi^2 Dc^2\delta^3\epsilon^2}{4.096\pi kT}\right\} \tag{34}$$

For purposes of computation the equation can be written, by using equation (9):

$$\eta = \frac{A}{G_1} \exp \{BG_2\epsilon^2\}$$

$$A = \frac{2.30 \times 10^{-9} M^{1/3} D^{2/3}}{(\beta D)^{1/2}}$$

$$B = \frac{1.322 \times 10^{-6} M}{T\beta D} \tag{35}$$

$$G_1 = \frac{(1 - \rho^2) G_2^{1/3}}{(1 - 2\rho)(7 - 5\rho)}$$

$$G_2 = 1 + \frac{2(1 - 2\rho)}{1 + \rho}$$

Table I gives some numerical values of G_1 and G_2.

TABLE I

ρ	−0.2	0	0.1	0.15	0.2	0.25
G_1	0.1972	0.2476	0.2984	0.3328	0.3768	0.4375
G_2	4.5	3.0	2.455	2.217	2.0	1.8
ρ	0.3	0.35	0.4	0.43	0.45	5
G_1	0.526	0.670	0.953	1.314	1.792	∞
G_2	1.615	1.445	1.286	1.196	1.138	1.0

COMPARISON WITH EXPERIMENTAL DATA

While the scientific literature abounds with viscosity data at atmospheric pressure, there are relatively few liquids for which there are also data for the compressibility or for the velocity of sound; and even fewer liquids for which such data exist over a range of temperature and pressure. The suitable data that could be found are employed in this section to test the above theory of viscosity.

With regard to the procedure that is used, it is to be noted, first, that the two parameters in the final equation, ρ and ϵ, are known as to order of magnitude and are therefore not adjustable without limits. As the major test of the theory, therefore, we investigate whether the experimental data can be fitted by values of the parameters in the expected ranges.

The values of ρ for most solids lie between 0.2 and 0.4, and the value 0.5 is the upper possible limit. According to the data reported

by Raman and Venkateswaran,[4] the value for glycerin is 0.28. This is the only value known for liquids. The values of ϵ probably should lie somewhere between a few per cent and 2. The former estimate comes from considerations of the expansion required to permit close-packed spheres to move. The latter estimate comes from the ratio of the critical volume to the volume near the melting point, which is approximately 3 for many materials.

In most of the published viscosity equations T occurs only as $1/T$ in an exponential term, and all parameters in the equations are assumed to be independent of temperature. The observed logarithmic derivative of viscosity with respect to reciprocal temperature therefore determines directly the coefficient of $1/T$ in the exponential. In the present theory the temperature coefficient of viscosity cannot be used in this simple manner, because β, which enters into the equation, varies considerably with both temperature and pressure. Conceivably, β at constant volume might be constant. However, according to Bridgman's data on mercury, this is not quite true either, although it is true that the variation of β with T at constant volume is much less than its variation with T at constant pressure. Furthermore, we cannot assume that either ρ or ϵ will be a constant for any chosen liquid. It is known that ρ in solids varies with temperature and pressure. The only reasonable assumption with regard to ϵ is that $(1 + \epsilon)/D$ is constant; but experimental data in most cases examined fail to support this assumption. In the following analyses of experimental data it will be assumed that ρ or ϵ is constant only when the data indicate or permit it. Unless otherwise stated the data used in the analyses below are to be found either in Landoldt-Börnstein or in *International Critical Tables.*

Molten metals, particularly those that crystallize in the cubic system, are perhaps the simplest of monatomic liquids and the liquids most likely to behave in accordance with the preceding theory. There are four molten metals in which the velocity of sound has been measured, at the melting point in three out of the four cases. Compressibilities were computed by equation (9).

Since these are single point data, with no variation in temperature or pressure, it is impossible to determine both ρ and ϵ; but, if a reasonable value is assumed for one of the parameters, the other can then be computed. If the value 0.25 is assumed for ρ, reasonable values are then found for ϵ for the two metals sodium and potassium. The values are shown in Table II.

However, there is difficulty with tin and mercury. For these two metals $G_1\eta/A$ turns out to be less than 1: and the computed values of

TABLE II

Metals at Melting Point

Metal	T, °C.	$10^3 \times \eta$, poise	$10^{12} \times \beta$, cm.²/dyne	D, g./cm.³	ϵ $\rho = 0.25$	ϵ $\rho = 0.40$
Sodium.....	97.5	0.695	18.7	0.97	0.093	—
Potassium.....	62.3	0.537	36.2	0.83	0.082	—
Tin.....	232	1.97	2.79	7.2		0.059
Mercury (not at m.p.).....	20	1.55	3.73	13.55		0.037

ϵ are therefore imaginary. It is found that real values of ϵ are obtained if we choose $\rho = 0.40$. The values of ϵ are then 0.06 for tin and 0.04 for mercury, which seem a little low but not impossible. Before trying to justify the high values of 0.40 for ρ, it is preferable to examine Bridgman's[10] data for mercury over a range of pressures.

The data are presented in Table III. The pressure–volume–temperature data reported by Bridgman permit the computation of the isothermal compressibilities, β_t. To convert to adiabatic compressibility, β, use is made of the thermodynamic equation:

$$\beta = \beta_t - (\alpha^2 T/Dc_p) \tag{36}$$

where α is the temperature coefficient of volume expansion and c_p is the specific heat at constant pressure.

TABLE III

Mercury at Two Temperatures and Four Pressures with $\epsilon = 0.05$

	$10^3 \times \eta$, poise		$10^{12} \times \beta$, cm.²/dyne		D, g./cm.		ρ	
T, °C.	30°	75°	30°	75°	30°	75°	30°	75°
P, atm.								
1.....	1.516	1.340	3.606	3.904	13.48	13.37	0.436	0.448
4000..	1.666	1.466	3.156	3.230	13.69	13.58	0.438	0.450
8000..	1.829	1.604	2.716	2.776	13.87	13.78	0.448	0.453
12000..	2.018	1.769	2.164	2.258	13.92	13.93	0.450	0.462

In analyzing the data of Table III it was found again that ϵ is imaginary if $\rho = 0.25$; but the data were successfully fitted by the theory by setting $\epsilon = 0.05$ and solving for ρ at each temperature and pressure combination. The values of ρ are again high, from 0.436 to 0.462. The significance of a high ρ is that the ratio of shear modulus of rigidity to bulk modulus is low, the ratio being zero for $\rho = 0.5$.

If we examine the data on the elastic constants of crystalline Hg obtained by Grüneisen and Sckell,[11] we find that this metal is highly anisotropic in its elastic moduli. The principal elastic compliances at −190°C. are as follows (the value of s_{11} reported in Landoldt-Börnstein is off by a factor of 10):

$10^{12} \times$	s_{11}	s_{22}	s_{33}	s_{44}	s_{55}	s_{66}	s_{12}	s_{13}	s_{23}
cm.²/dyne	1.5	(1.4)	4.5	15.1	(15.1)	(54.6)	−11.9	−2.1	(−2.1)

The values in parentheses were added to the reported principal values on the basis that the crystal is rhombohedral. From these values it is possible to compute an average value for the compressibility β, the shear compliance γ, and Poisson's ratio ρ:[12]

$$\begin{aligned} \beta &= s_{11} + s_{22} + s_{33} + 2(s_{12} + s_{13} + s_{23}) = 3.1 \times 10^{-12}, \text{ cm.}^2/\text{dyne} \\ \gamma &= (s_{44} + s_{55} + s_{66})/3 = 28.3 \times 10^{-12}, \text{ cm.}^2/\text{dyne} \\ \rho &= (3\gamma - 2\beta)/2(3\gamma + \beta) = 0.45 \end{aligned} \tag{37}$$

Thus it is found that the mean value of ρ computed from the measured properties of crystalline mercury agrees closely with the values deduced from the viscosity theory.

Similar elasticity data on crystalline tin are lacking, but tin crystallizes in the rhombic or the tetragonal forms, and its elastic anisotropy may be similar to that of mercury.

It is observed in Table III that ρ increases slowly but regularly with increasing pressure. This also is in agreement with observation on solids; for Bridgman[13] reports that ρ in metals and glasses increases with pressure.

We turn our attention now to organic liquids. *International Critical Tables* reports measurements of the adiabatic compressibility of a number of liquids at various temperatures, made by Gay and by Tyrer, by a method in which the volume expansion was observed when pressure on the sample was suddenly reduced to atmospheric. Landoldt-Börnstein report measurements of the velocity of sound in organic liquids at various temperatures made by Freyer, Hubbard, and Andrews. When the adiabatic compressibility is computed from the measured velocity, compressibilities are obtained which are in good agreement with the directly measured compressibilities, for those liquids which were measured by both methods.

Before testing equations (35) with these data, it is desirable to examine the expected effect of temperature variations, as indicated by the

TABLE IV

Nonassociated Organic Liquids at Atmospheric Pressure and Several Temperatures

Liquid	T, °C	$10^2 \times \eta$	$10^{12} \times \beta$	$\log(\eta/A)$	B	ρ	ϵ
Ether	0	0.289	124.1	0.527	45.0	0.220	0.055
	20	0.233	138.7	0.482	33.4		
	30	0.213	158.1	0.470	29.1		
Octane	0	0.706	78.6	0.798	90.0	0.232	0.075
	20	0.542	100.3	0.714	73.1		
	40	0.433	118.3	0.654	59.3		
Heptane	0	0.518	93.7	0.698	73.8	0.239	0.074
	20	0.413	109.7	0.637	60.3		
	40	0.332	131.1	0.583	47.4		
Bromoform	15	2.15	39.4	0.882	102.4	0.253	0.081
	30	1.74	42.9	0.821	90.8		
Chloroform	0	0.706	57.7	0.645	65.7	0.261	0.077
	20	0.563	66.9	0.581	54.0		
	30	0.514	73.0	0.561	48.3		
	40	0.464	79.3	0.536	43.9		
Carbon tetrachloride	0	1.340	61.1	0.889	74.6		
	20	0.968	71.8	0.789	60.7	0.271	0.100
	30	0.843	78.0	0.738	54.85		
	50	0.653	91.8	0.673	44.7		
	60	0.585	100.0	0.638	40.9		
Ethylene chloride	0	1.077	48	0.828	76.2	0.277	0.095
	40	0.652	64	0.676	53.4		
	70	0.479	81	0.593	41.15		
Benzene	0	0.912	55.0	0.848	76.8	0.280	0.096
	10	0.900	59.5	0.783	68.9		
	30	0.564	70.7	0.695	55.9		
	50	0.442	84.1	0.626	44.9		
	60	0.392	92	0.596	40.3		
Chlorobenzene	20	0.799	55.0	0.720	83.5	0.294	0.085
	40	0.631	63.0	0.648	69.5		
	80	0.431	82.0	0.544	49.3		
m-Xylene	0	0.806	57.0	0.758	102.2	0.304	0.083
	20	0.620	65.0	0.671	85.2		
	40	0.497	74.5	0.608	70.9		
Carbon disulfide	0	0.420	51.6	0.481	55.2	0.311	0.077
	20	0.367	58.9	0.444	46.1		
	40	0.318	67.8	0.415	38.4		
Acetone	0	0.395	75.9	0.505	45.6		
	20	0.322	89.3	0.546	37.1		
	40	0.267	107.3	0.521	29.7		
Ethyl acetate	0	0.578	69	0.681	66.7		
	20	0.413	82	0.612	53.8		
	50	0.324	108	0.556	38.6		

equations. The compressibility, β, increases considerably with temperature. Therefore the parameter combinations A and B will both decrease rather rapidly with increasing temperature. The parameters ρ and ϵ and the parameter functions $G_1(\rho)$ and $G_2(\rho)$ may conceivably change only slowly with temperature, perhaps at about the same (relative) rate as does the density.

Suppose now that ρ and ϵ for any liquid are constant or nearly so within the temperature range covered in the experiments. Then in the logarithmic form of equation (35.1):

$$2.303 \log (\eta/A) = 2.303 \log (1/G_1) + \epsilon^2 G_2 B \tag{38}$$

we see that $\log (\eta/A)$ is linear or almost linear in B.

Table IV gives values of the viscosity, η, the adiabatic compressibility, β, and $\log (\eta/A)$ and B at various temperatures. For the first eleven liquids, terminating with carbon disulfide, a plot of $\log (\eta/A)$ against B gives graphs which seem to be rectilinear. Typical graphs are shown in Figure 4, curve 4 excepted. The last two liquids in Table IV, acetone and ethyl acetate, give nonlinear graphs, as shown by curve 4 which is for ethyl acetate.

Clearly the $\log (\eta/A)$ intercept of a linear graph determines the value of G_1, by the equation:

$$G_1 = (A/\eta)_0 \tag{39}$$

ρ and G_2 are therefore determined; and ϵ can be computed from:

$$\epsilon^2 = -\frac{2.303}{G_2} \frac{d \log (\eta/A)}{dB} \tag{40}$$

Values of ρ and ϵ are given in the last two columns of Table IV.

The liquids have been arranged in the order of increasing ρ. With this sequence the first three liquids are short chains in molecular form, with 5, 8, and 7 atoms, respectively, in the chain. All the other liquids in the table are more nearly spherical in molecular shape. This indicated relationship between ρ and molecular shape can be understood if we recognize two facts: first, that the entanglements which the chain molecules undergo will increase the shear modulus more than the compression modulus; second, that ρ decreases as the ratio of shear modulus to compression modulus increases.

The curvature of the graphs for ethyl acetate and acetone indicates

an appreciable variation of ρ or ϵ or both with temperature. Why this should be the case for these two liquids is not at present clear.

It should be mentioned that the linear relationship between log (η/A) and B does not prove that ρ and ϵ are constant. ρ and ϵ could vary with temperature if they both varied simultaneously in such a way that the slope of the log (η/A), B curve remained constant; but such a coordinated variation seems highly improbable.

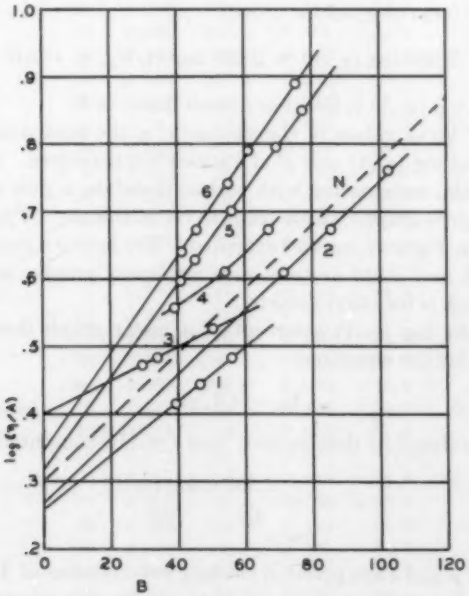

Fig. 4. Nonassociated organic liquids at various temperatures and atmospheric pressure: (1) Carbon disulfide. (2) *m*-Xylene. (3) Ether. (4) Ethyl acetate. (5) Benzene. (6) Chloroform. (N) "Normal" curve for nonassociated liquids.

Data for some additional organic liquids are given in Table V. These liquids all exhibit molecular association, the association being indicated by their dielectric and other physico-chemical properties. Association is indicated also by the high viscosity of any one of these liquids compared with that of another liquid of approximately the same molecular size and cohesive energy.

TABLE V

Associated Organic Liquids at Atmospheric Pressure and Several Temperatures

Liquid	T, °C	$10^3 \times \eta$, poise	$10^3 \times \beta$, cm.²/dyne	log (η/A)	B	n
Aniline	0	10.2	32.1	1.741	135	2.17
	20	4.4	35.6	1.400	115	
	40	2.37	40.0	1.138	98.0	
	50	1.51	42.3	0.975	90.3	
	80	1.09	50.0	0.743	72.0	1.24
Acetic acid	20	1.275	80.5	1.100	32.1	4.06
	40	1.007	93.0	1.031	26.6	
	70	0.600	115	0.855	20.3	3.84
Methyl alcohol	0	0.820	87.7	1.037	21.8	5.01
	20	0.597	100.6	0.934	18.1	
	50	0.403	125.2	0.798	13.7	4.44
Ethyl alcohol	0	1.77	80.4	1.297	32.2	5.12
	20	1.20	92.5	1.164	28.4	
	50	0.70	116.8	0.981	19.5	5.08
Glycerin	0	12,100	20.5	4.740	170.7	5.33
	30	629	21.9	3.439	152.9	4.17

The relationship between molecular association and high viscosity has been emphasized by Bingham,[14] and is revealed by any empirical or theoretical equation relating viscosity to molecular properties. In the present case the points representing the data of Table V would lie for the most part well above the curves drawn in Figure 4, representing nonassociated liquids.

The effect of association can be included in the present theory simply by multiplying M, the molecular weight, by n, the average degree of association, wherever M occurs in equations (35). Unfortunately, when this is done the resulting equations contain one more unknown parameter n. With our present limited knowledge of the liquid properties postulated in this theory of viscosity, the best procedure for evaluating n is probably to assume reasonable or "normal" values for ρ and ϵ. The broken curve in Figure 4 is taken to be the normal, or approximately correct, curve for a simple nonassociated liquid. The corresponding parameter values are $\epsilon = 0.08$, $\rho = 0.288$, $G_1 = 0.5$, $G_2 = 1.655$.

If we now make the additional large assumption that these parameters are not altered by molecular association, equation (35.1) can be solved for n:

TABLE VI

Nonassociated Organic Liquids at Several Temperatures and Pressures

	T, °C	*n*-Pentane			Isopentane		*n*-Hexane			*n*-Octane	
$10^{-8} \times P$, kg./cm.^{2}		0	4	8	0	4	0	4	8	0	4
$10^2 \times \eta$, poise	0°	0.318	2.160	8.07	0.2812	2.202	0.435	3.68	17.93	0.700	11.17
	50°	0.178	1.334	3.84	0.1618	1.267	0.235	1.91	6.76	0.390	4.10
	95°	0.121	0.902	2.86	0.1127	0.833	0.159	1.242	3.58	0.266	2.13
$10^{12} \times \beta$, cm.^{2}/dyne	0°	103.0	20.83	13.52	937	24.0	88.9	18.8	—	71.8	
	50°	113.2	24.92	14.56	122.9	25.1	99.0	23.8	13.3	90.9	22.9
	95°	127.7	27.13	14.15	131.9	27.3	100.5	28.0	13.4	119.9	23.1
$\log (\eta/A)$	0°	0.559	1.029	1.502	0.486	1.048	0.635	1.212	—	0.750	—
	50°	0.334	0.860	1.196	0.311	0.818	0.372	0.980	1.344	0.552	1.261
	95°	0.199	0.711	1.064	0.175	0.702	0.236	0.830	1.124	0.450	0.977
B, numerical	0°	52.6	208	296	57.7	180	69.3	270.0	—	107.4	—
	50°	43.9	150	236	40.3	149	55.4	185.4	306	75.8	246
	95°	37.3	124	193	36.1	123	52.5	140.6	270	53.5	218

T, °C		*n*-Decane		Chlorobenzene		Bromobenzene	
$10^{-3} \times P$, kg./cm.^{2}		0	4	0	4	0	4
$10^2 \times \eta$, poise	0°	1.282		1.023	9.48	1.453	15.08
	50°	0.603		0.576	3.71	0.797	5.30
	95°	0.475		0.390	2.01	0.526	2.07
$10^{12} \times \beta$, cm.^{2}/dyne	0°	—		42.9	—	34.7	—
	50°	91.3		52.2	16.78	46.5	14.84
	95°	112.0		62.0	17.20	71.7	14.42
log (η/A)	0°	—		0.772	—	0.814	—
	50°	0.706		0.570	1.120	0.614	1.180
	95°	0.652		0.447	0.902	0.532	1.029
B, numerical	0°	—		112.7	—	143.6	—
	50°	90.3		82.0	221	95.0	258
	95°	67.8		63.5	194	56.6	229

Liquid	$10^{-3} \times P$, kg./cm.^{2}	$10^2 \times \eta$, poise 20°	80°	$10^{12} \times \beta$, cm.^{2}/dyne 20°	80°	log (η/A) 20°	80°	*B*, numerical 20°	80°
Ether	0	0.228	0.156	83.9	—	0.361	—	55.7	—
	1	0.497	0.287	—	94.3	—	0.482	—	39.6
	4	1.474	0.811	25.06	34.2	0.892	0.701	150	93
	12	12.33	4.01	11.72	13.91	1.642	1.190	280	200
Acetone	0	0.304	0.218	62.1	—	0.447	—	53.4	—
	1	0.513	0.360	—	58.7	—	0.507	—	46.1
	4	1.263	0.766	22.15	25.32	0.830	0.728	124.4	93.2
Carbon disulfide	0	0.391	0.228	45.7	70.0	0.412	0.282	59.5	35.2
	4	1.241	0.804	20.15	23.18	0.730	0.573	114.7	84.6
	12	6.02	2.96	7.56	10.37	1.192	0.956	269.4	160.3

$$2.303\,\frac{\left(\log\frac{\eta}{A}-\log\frac{1}{G_1'}\,\frac{1}{3}\log n\right)}{B\epsilon^2 G_2}=\frac{2.174\times 10^2}{B}\left(\log\frac{\eta}{A}+0.301-\frac{1}{3}\log n\right) \quad (41)$$

Values of n computed by equation (41) for the extreme temperatures of each liquid in Table V are shown in the last column of the table.

Bridgman[11] has made measurements of the viscosity and relative volume of a number of organic liquids at two or three temperatures and over a range of pressures. These data have been analyzed, some of the results being shown in Table VI. Since the viscosity and the volume data are not given for the same temperatures, interpolations were necessary. The viscosity data were interpolated or extrapolated to the temperatures of the volume data, a linear relationship between $\log \eta$ and $1/T$ being assumed.

The computations of the isothermal compressibilities and from them the adiabatic compressibilities by equation (36) are involved and full of uncertainties. It is doubtful that Bridgman's volume data are spaced closely to give a reliable value of the compressibility at atmospheric pressure; and accurate values of α and c_p are lacking for many of the computations involving equation (36). Consequently the adiabatic compressibilities given in Table VI must be considered to be of low accuracy.

In spite of this necessary reservation, Bridgman's data lead to some interesting and informative results. Referring again to equation (38), we note that if ρ and ϵ are constant, $\log(\eta/A)$ is still linear in B regardless of whether variations in A and B are induced by variations in temperature or pressure or both.

Figure 5 shows a few isothermal curves of $\log(\eta/A)$ *versus* B. For the eleven liquids listed in Table VI, such curves show that the isothermals are in most cases closely linear, and that the isothermals for a given liquid nearly coincide. Furthermore, the curves of Figure 5 are in approximate agreement with the "normal" curve for nonassociated liquids in Table III. All of the plotted points for the liquids in Table VI lie within the roughly trapezoidal envelope drawn in Figure 5. Thus the predictions of the theory for constant ρ and ϵ seem to be roughly correct. The statistical record is as follows: For seven out of

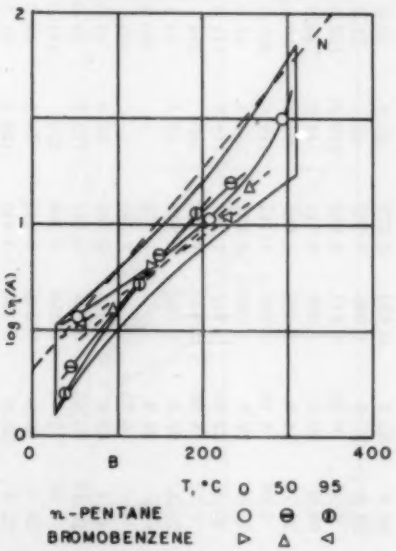

Fig. 5. Nonassociated organic liquids at various temperatures and pressures. N is the "normal" nonassociated liquid.

the eleven liquids, the different isothermals are slightly but distinctly different. Of the isothermals with three experimental points, corresponding to three different pressures, six show no significant curvature, three show slight curvature toward the B axis, and one shows slight curvature away from the B axis. It is uncertain at present whether these variations are due to variations in ρ and ϵ or to errors in the computed compressibilities. Where comparisons are possible, the adiabatic compressibilities computed from Bridgman's data are consistently lower than those in Tables IV and V.

Associated organic liquids measured by Bridgman are shown in Table VII; and some of the corresponding log (η/A) curves are plotted in Figures 6 and 7. Most of these isothermals lie far above the normal curve for nonassociated liquids. These curves exhibit the expected temperature spread in that the higher the temperature of a given liquid, the lower is the isothermal curve, corresponding to a lower degree of molecular association. It is observed also that with

TABLE VII

Associated Organic Liquids at Several Temperatures and Pressures

Liquid	$10^3 \times P$, kg./cm.^{2}	$10^3 \times \eta$, poise		$10^{12} \times \beta$, cm.^{2}/dyne		$\log (\eta/A)$		B	
		20°	80°	20°	80°	20°	80°	20°	80°
Methyl alcohol.....	0	0.601	0.290	66.6	82.4	0.854	0.578	26.4	19.6
	4	1.815	0.791	23.5	25.6	1.086	0.739	65.1	51.0
	12	6.425	2.180	6.15	6.68	1.343	0.883	219.21	172.0
Ethyl alcohol.....	0	1.246	0.422	60.0	90.6	1.086	0.711	44.0	25.9
	4	5.065	1.90	23.7	24.8	1.485	1.065	93.3	76.2
	12	32.8	7.50	9.06	8.16	2.068	1.412	218.6	201.6
n-Propyl alcohol....	0	2.14	0.83	77.0	79.3	1.328	0.932	44.4	37.6
	4	16.20	3.74	19.41	22.09	1.871	1.291	148.3	111.9
	12	222.6	25.54	7.75	8.96	2.834	1.924	330	244
Isobutyl alcohol....	0	4.02	0.701	79.5	87.6	1.604	0.854	52.4	44.1
	4	70.6	7.53	—	22.9	—	1.579	—	130.8
	12	456	124.1	—	8.75	—	2.583	—	304
Ethyl chloride.....	1	0.373	0.264	49.4	62.8	0.454	0.362	59.9	41.5
	4	0.967	0.634	23.15	26.63	0.704	0.544	113.7	84.3
	12	4.78	2.464	9.02	10.74	1.169	0.798	279	181
Ethyl bromide.....	1	0.671	0.419	38.3	60.3	0.545	0.443	79.3	44.3
	4	1.733	1.053	22.6	25.6	0.846	0.648	120.2	91.5
	12	10.93	4.59	7.21	8.44	1.390	1.038	335	242
Ethyl iodide.....	0	0.596	0.358	56.5	65.5	0.510	0.324	64.1	49.4
	4	2.74	1.518	21.30	24.44	0.950	0.726	143.0	106.0
	12	24.6	7.88	7.65	7.70	1.672	1.180	352	297

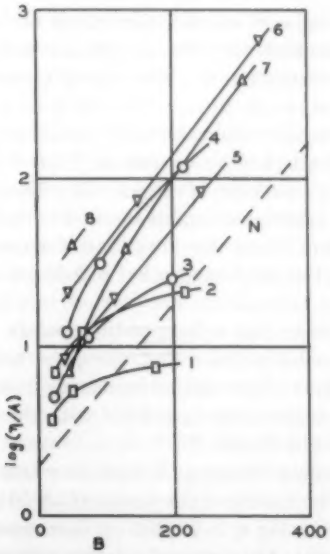

Fig. 6. Alcohols at two temperatures and atmospheric pressure: (1) Methyl alcohol, 80°C., (2) 20°C. (3) Ethyl alcohol, 80°C., (4) 20°C. (5) *n*-Propyl alcohol, 80°C., (6) 20°C. (7) Isobutyl alcohol, 80°C., (8) 20°C. (N) "Normal" nonassociated liquid.

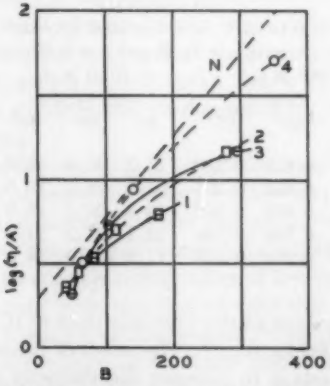

Fig. 7. Ethyl halides at two temperatures and atmospheric pressure: (1) Ethyl chloride, 80°C., (2) 20°C. (3) Ethyl iodide, 80°C., (4) 20°C. (N) "Normal" nonassociated liquid.

the exception of isobutyl alcohol the curves all bend toward the B-axis. This signifies that, with the exception noted, pressure, like temperature, depresses association. The regular increase in viscosity with the number of carbons in the alcohol indicates a regular increase in association or in the effect of association on viscosity.

The data for the last three liquids in Table VII all fall within or nearly within the envelope of Figure 5. Nevertheless, they are grouped with the associated liquids because they exhibit a consistent pattern of departure from the linear law for nonassociated liquids. The data for ethyl chloride and ethyl iodide are shown in Figure 7. The data for ethyl bromide are not plotted, but they fall in positions intermediate between the corresponding points for the other two liquids. These curves indicate that the ethyl halides are somewhat associated, the degree of association increasing from the chloride to the iodide. This conclusion is in agreement with the dielectric constants in solution reported by Smyth.[15]

Table VIII presents Bridgman's data on water at pressures up to 4000 kg./cm.^{2}. The values of the viscosity at 50 and 95° were interpolated linearly on a log η, $1/T$ plot. β is computed by the method previously described. The values of relative volume are given directly by Bridgman at the same values of T and P in the table and hence are not reproduced here.

TABLE VIII

Water at 0 to 95°C. and 0 to 4000 kg./cm.^{2} Pressure with $\rho = 0.25$ and $\epsilon = 0.07$

$10^3 \times P$, kg./cm.^{2}	$10^3 \times \eta$, poise			$10^{-12} \times \beta$, cm.^{2}/dyne			n degree of association		
	0°	50°	95°	0°	50°	95°	0°	50°	95°
0.....	1.792	0.612	0.288	51.3	41.5	42.0	9.06	3.89	1.64
1.....	1.649	0.639	0.335	37.9	33.2	33.5	6.40	3.19	1.51
2.....	1.714	0.676	0.360	28.4	26.1	26.9	4.40	2.57	1.35
3.....	1.835	0.732	0.394	22.1	21.2	21.8	4.05	2.16	1.20
4.....	1.990	0.794	0.436	17.9	17.9	18.6	3.32	1.99	1.15

A remarkable feature of the viscosity data at 0°C. is the minimum at a pressure of 1000 kg./cm.^{2}. The effect of pressure at all temperatures in other liquids is to increase the viscosity continuously. Another peculiar relationship shown in the table is that the compressi-

bility at $T = 0°C., P = 0$, is higher than at $T = 50$ or $95°$, $P = 0$. It is well known that the viscosity at atmospheric pressure is not an exponential function of $1/T$, and that the computed activation energy is not a constant.

These peculiar properties of water undoubtedly result from its high molecular association by hydrogen bonds and from the fact that ice, which is water in a completely associated state, has a lower density than has liquid water at 0°C. The facts reviewed here indicate that the degree of association in liquid water is strongly variable and should be a monotonically decreasing function of both temperature and pressure.

The values of n, degree of association computed by equation (41), are shown in the last three columns of Table VIII. It is seen that n behaves as expected, decreasing steadily with the increasing pressure and increasing temperature. This property of n is not altered by changes in the parameter values within the range indicated above.

It should be pointed out here and perhaps emphasized that we have succeeded in explaining the anomalous viscosity properties of water, including the minimum at $P = 1000$ kg./cm.^{2} and $T = 0°C.$, with constant, normal values of ρ and ϵ and a variable n of the expected properties, with no minimum. With no independent method for determining any of these parameters, this is as far as we can go in testing the theory with these data.

The final set of data to be examined are those for liquid CO_2. The reported measurements were made with the liquid and the gas not far from the critical temperature; and all the viscosity data, when plotted against density, give a smooth curve, nearly the same for all temperatures, a curve which shows no discontinuity between the liquid and the gaseous state.

Using a theory of the viscosity of liquids to interpret these data may therefore be trying to apply the theory beyond its proper field; but it is perhaps interesting to make the test and see the results.

Two values of the density are chosen for analysis, $D = 0.75$ and $D = 0.65$ g./cm.^{2}. The corresponding values of the viscosity for $T = 30$, 35, and 40°C. are read from the plotted viscosity data, the value at $T = 40°$, $D = 0.75$ being an extrapolation. The required isothermal compressibilities were computed from the slopes of the volume–pressure isotherms; and the adiabatic compressibilities were computed therefrom with the value of the specific heat at constant volume as

given by Dieterici (reported correctly in Landoldt-Börnstein, incorrectly in *ICT*).

In order to avoid imaginary ϵ values it was again necessary to depart from the normal values of ρ; and even when this was done quite large values of ϵ were found. It was then decided in this case to assume a constant ϵ for each density, the value chosen being such that $(1 + \epsilon)V = V_c$, where V is the specific volume at the chosen density (that is, $V = 1/D$), and V_c is the critical specific volume, which is 2.15 cm.³/g.

Table IX gives the resulting values of ρ found necessary to agree with the experimental data. If we accept a considerable variation of ρ with temperature at constant volume, the results of the analysis for $D = 0.75$ g./cm.³ appear reasonable. On the other hand, the zero and negative values of ρ at $D = 0.65$ may be characterized as startling, if true. However, some reasons can be advanced for believing that they may actually be true. The points at $D = 0.65$ are all on the shoulders of the P, D curves, just before the density takes a sudden large drop as the pressure is decreased. In other words, the liquid is on the verge of losing its cohesion and expanding into a gas. In this condition it is

TABLE IX

Carbon Dioxide at Three Temperatures and Two Densities

	$10^2 \times \eta$			$10^{10} \times \beta$		
D, g./cm.³	30°	35°	40°	30°	35°	40°
0.75	0.066	0.067	(0.065)	10.0	13.5	26.2
0.65	0.047	0.050	0.050	100.9	60.0	61.5

	ρ			
D, g./cm.³	30°	35°	40°	ϵ
0.75	0.42	0.37	0.26	0.60
0.65	−0.23	0.00	−0.01	0.40

conceivable that, if a column of the elastic liquid is quickly pulled and extended longitudinally, the cohesion forces may be so weakened that the column, instead of contracting laterally, expands laterally due to thermal molecular vibrations. Such behavior is described by a negative value of ρ. Another and perhaps equivalent interpretation is to suppose that at the critical point the shear modulus remains nonzero while the bulk modulus becomes zero.

DISCUSSION

The preceding tables show that the proposed theory of the viscosity of elastic liquids gives satisfactory agreement with the measured viscosities of a number of simple liquids and some associated liquids. The required values of the parameters fall in the expected ranges for the most part; and, when the values are outside of these ranges, there are special reasons which can be suggested to explain the exceptional values.

The theoretical approach in this viscosity theory can probably be extended to yield a theory of self-diffusion. When this is done some cross-checks on some of the parameters should be possible, when the required data are available.

The mathematical treatment of n, the degree of association, is perhaps reasonable if $n = 2$. However, when n is much greater than 2, some unresolved questions become important. Are the associated groups flexible chain structures or rigid spherical clusters? Are all groups approximately of the same size? If the average degree of association is large, does the flow take place principally within regions of low degree of association, acting as a lubricant for the large associated groups? How do these possible variable factors affect the values of ρ and ϵ? Obviously we have much to learn before we can develop an accurate measure of association based on viscosity data.

With the mechanism of flow in the present theory the concept of activation energy has become complicated; and it is not clear how any reasonable concept of it is related to the temperature coefficient of viscosity. The simplest approach is to assume, as an approximation, that the compressibility is independent of the volume, and that ρ and ϵ also are constant. The activation energy at constant volume, E_v, can then be computed by the usual procedure. This has been done for benzene and the results compared with the experimental measurements of viscosity at constant volume by Jobling and Lawrence.[16] The computed values show the same trend with density as do the experimental data, but are slightly lower. Thus at a density of 0.868 the computed value of E_v is 0.59 kcal./mole whereas the measured value, as read from the published graph, is 0.70 kcal./mole. The discrepancy is presumably due to the failure of the assumption of constant compressibility at constant volume. It is to be observed that the computation of E_v is here made by an application of the theory to the data in Table III, showing measurements at constant pressure only.

When we consider the activation energy at constant pressure and the related problem of the temperature variation of viscosity at constant pressure, we encounter the difficulty that the compressibility at constant pressure varies rapidly with temperature and cannot be considered even approximately constant. Therefore, even if Poisson's ratio and the critical expansion were constant, the present theory could not predict the variation of viscosity with temperature at constant pressure without some theoretical or general empirical equation for the compressibility as a function of temperature and volume. These possibilities have not yet been explored; and the linear relationship between $\log \eta$ and $1/T$ found for most liquids therefore remains unexplained for the time being. It is to be noted however that this linear relationship has been observed to fail in some cases near the melting point[17] and it will perhaps be sufficient to predict it as a limited approximation, not as a general, rigorous law.

With regard to the concept of activation energy as applied to liquid flow, the present theory indicates that the basic process involved is not nearly so simple as a chemical reaction depending upon the supply of a certain amount of thermal energy to a simple complex relatively uninfluenced in its reaction by its environment. The critical local expansion required for liquid flow can be thought of as a two-step process. The second step is the one analyzed in the present theory of viscosity. It consists in concentrating free volume in one region, but this happens only at the expense of producing a higher density in other regions. The thermal elastic waves produce no change in the mean density. The total activation process therefore involves a pattern of energy distribution that extends throughout the liquid. But this second step in the process must be preceded by a first step in which the average specific volume is increased enough to give an adequate supply of free space to be favorably distributed in the second step. The first step can therefore logically be considered as melting the crystal and then further expanding the liquid by adding more heat. The compressibility also is increased thereby. The higher the specific volume and the higher the compressibility the more easily is the second step accomplished.

The complexity of the activation process indicated by this discussion explains, perhaps, why disagreement has arisen over what the activation energy of liquid flow really is, and whether it should be

measured by the temperature variation of viscosity at constant pressure or at constant volume.[16] Perhaps it is legitimate to postulate two different activation energies, depending upon what is chosen as the ground state for the system to be activated. Two possible choices of the ground state are, first, the crystal at the melting point and, second, the liquid at any temperature but with a uniform density and uniform distribution of free space. The first choice is probably closely related to the measured activation energy at constant pressure and the second choice, to the measured activation energy at constant volume. The precise details of these relationships are not yet clear.

This work was supported in its initial and important stage by funds from contract W44-109-QM-2030 with the Office of the Quartermaster General of the U. S. Army.

References

1. Glasstone, Laidler, and Eyring, *The Theory of Rate Processes*, McGraw-Hill, New York, 1941.

2. T. Alfrey, Jr., *The Mechanical Behavior of High Polymers*, Interscience, New York-London, 1948.

3. C. Maxwell, *Scientific Papers*, Vol. 2, *Dynamical Theory of Cases*, p. 31.

4. C. V. Raman and C. S. Venkateswaran, *Nature*, Supplement **143**, 978 (1949).

5. E. N. da C. Andrade, *Phil. Mag.*, **17**, 497, 698 (1934).

6. S. Peter, *Naturforsch*, **9a**, 98 (1954).

7. J. M. Dewey, *J. Appl. Phys.*, **18**, 578 (1947).

8. R. C. Tolman, *The Principles of Statistical Mechanics*, Oxford Univ. Press, Oxford, 1938, p. 585.

9. S. Chandrasekhar, *Rev. Mod. Phys.*, **15**, 1 (1943).

10. P. W. Bridgman, *The Physics of High Pressure*, Bell, London, 1949.

11. E. Grüneisen and O. Sckell, *Ann. Physik*, **19**, 387 (1934).

12. D. H. Menzel, *Fundamental Formulas of Physics*, Prentice-Hall, New York, 1955, p. 584. Also A. E. H. Love, *The Mathematical Theory of Elasticity*, Dover, New York, 1944.

13. P. W. Bridgman, *Proc. Am. Acad. Arts Sci.*, **63**, 401 (1929).

14. E. C. Bingham, *Fluidity and Plasticity*, McGraw-Hill, New York, 1922.

15. C. P. Smyth, *Dielectric Constant and Molecular Structure*, Chemical Catalog Co., New York, 1931.

16. A. Jobling and A. S. C. Lawrence, *Proc. Roy. Soc. London*, **A206**, 257 (1951).

17. A. K. Doolittle, *J. Appl. Phys.*, **22**, 1031 (1951). G. Sears, *J. Chem. Phys.*, **23**, 604 (1955). A. A. K. Al-Mahdi and A. R. Ubbelohde, *Trans. Faraday Soc.*, **51**, 361 (1955).

Synopsis

Simple Newtonian liquids are assumed to have elastic rigidity and a high rate of stress relaxation, as suggested by Maxwell. It is postulated that in the basic mechanism of flow thermal energy produces a critical volume expansion in a region enclosing several molecules, and as a result the local rigidity and the shear stress are temporarily reduced to zero. The associated local molecular movements constitute a nucleus of stress release and of strain which are transmitted throughout the liquid with the velocity of sound. Many such events, in the aggregate, constitute the viscous flow. The theory, following Debye, treats the molecular thermal vibrations as the sum of elastic ultrahigh-frequency vibrations; and it makes use of Dewey's formula for the mean elastic moduli of an elastic continuum containing small spheres of different elastic moduli. The resulting formula for viscosity involves the adiabatic compressibility, the critical expansion necessary for loss of rigidity, Poisson's ratio, and the degree of molecular association if there is any. Agreement with published experimental data can be obtained with expected or understandable values of the adjustable parameters.

TRANSACTIONS OF THE SOCIETY OF RHEOLOGY VOL. I, 95–107 (1957)

On Normal Stresses, Flow Curves, Flow Birefringence, and Normal Stresses of Polyisobutylene Solutions. Part I. Fundamental Principles*

W. PHILIPPOFF, *The Franklin Institute Laboratories for Research and Development, Philadelphia 3, Pa.*

The question of normal stresses in steady flow has been discussed at length in the literature since 1946. Comparatively few measurements have been made in a large range of variables, especially in conjunction with other measurements of the flow properties of the materials. In the paper of Roberts,[1] the then existing theories of normal stresses were compared and it was concluded that the theory of Weissenberg[2] was the only one which satisfactorily describes the phenomena involved. We had the opportunity of improving both points: experimental facilities for measuring the flow birefringence, the flow curves, and the normal stresses were available; and the mathematical analysis of the existing theories of normal stresses was made in view of obtaining their *basic similarity* instead of their differences as emphasized by Roberts.

The theories investigated in greater detail were those of Weissenberg[2] and of Mooney.[3] The derivation of Rivlin[4] was discussed subsequently and it could be proved that it essentially gives the same results. All these theories are "continuum-mechanical" ones; the possible correlation with molecular phenomena have been obtained in the previous paper.[5]

The main principle involved in deriving a theory of normal stresses is the assumption of Weissenberg and Herzog (1928) that flowing solutions (of high polymers) have *elastic properties*.[6] With this basic assumption, the deformational mechanics of *elastic solids* can be ap-

* Presented at the Annual Meeting of the Society of Rheology, November 7, 1956, in Pittsburgh, Pa.

plied to flowing solutions. This assumption has been tested and proved by Eisenschitz and Philippoff[7] in 1933, as well as by Philippoff[8] in 1934, and the extensive subsequent dynamic investigation of polymer solutions. The assumption of Mooney (1951) is the statement: "In a flowing solution, a state of elastic stress is reached by an equilibrium of the stressing in laminar flow and the stress relaxation of the solution." Both assumptions lead to a quantity termed "elastic recoverable shear, s," that was emphasized as an important parameter, similar to the Reynolds number by Weissenberg in 1946 and 1948 and introduced by Mooney[9] in 1951. Both assumptions reduce the elastic effects in flowing materials to an "elastostatic" problem. In a recent paper[5] it was possible to show that the optically measured extinction or orientation angle, χ, can be identified with the direction of the principal tensile stress in laminar flow. This leads to the definition of s from deformational mechanics which correlates this angle χ with s[9]:

$$s = 2 \cot 2\chi \tag{1}$$

Having through this relation s independently experimentally measurable, we have rechecked both the theories of Weissenberg and Mooney using as independent variable s or χ. We have, further, found that the emphasis on *plane shear* is important in order to obtain simple experimentally accessible relations between the variables involved.

We will review Weissenberg's theory in an abridged form as it has been treated fairly extensively in previous literature.

Weissenberg considers the stress tensor (which, it must be emphasized, is valid in the form discussed only for isotropic bodies in plane shear) as a "deviator" (directions, see Fig. 2):

$$\begin{vmatrix} P_{11} - P_{22} & P_{12} & 0 \\ P_{12} & 0 & 0 \\ 0 & 0 & P_{33} - P_{22} \end{vmatrix} \tag{2}$$

This means that the stress condition in laminar flow is determined by three independent stresses: the shearing stress P_{12} and the "normal stresses" ($P_{11} - P_{22}$ and $P_{22} - P_{33}$).

In discussing the stress tensor, use is extensively made of the relation:

$$P_{ij} = P_{ji}$$

for $i \neq j$. Only Kolsky[10] has given, as far as could be ascertained, a clear reason for this. Considering the equilibrium in a unit cube, the sum of the shearing stress of two opposite faces must be zero to eliminate any translational motion. Equally, the sum of the shearing stress on two neighboring faces must be equal to 0 in order for the moments to cancel, or else a permanent rotation results. This means that the mentioned relation is valid for any material, not only in the case of Hooke's law. In plane shear $P_{23} = P_{13} = 0$, then only the one shear stress $P_{12} = P_{21}$ remains.

The relationship (2) is combined with the completely general statement of equilibrium of forces in a "volume element" or "unit cube" in *spherical* coordinates:

$$\partial P_{33}/(\partial \ln r) = P_{11} + P_{22} - 2P_{33} \tag{3}$$

and further, with the assumption of Weissenberg that due to its importance is quoted verbatim:

"Let a material move from its virginal groundstate to some loaded state, and consider at any point in the material any two planes of different orientation, each marked initially by a circle of unit area. We then find at every instant throughout the whole movement that the two planes will exhibit across the marked areas the same normal components of traction forces, provided the material was isotropic in the groundstate, and the planes suffered throughout the movement the same changes in their respective normal distances from parallel neighbouring planes.

"There are many applications of the formulation given above. Consider for instance a material which in its virginal groundstate has isotropic symmetry. Let this material then be subjected to a movement in the form of a laminar shearing displacement with arbitrarily chosen experimental conditions concerning the form of the boundaries, the speed, the amount of displacement etc. We concentrate our attention in the immediate neighbourhood of every point on the series of meridian planes, *i.e.*, on the series of planes of different orientation which all contain the direction of shear, and note that all members of this series retain unchanged throughout the movement any circle of

unit area marked on the surface, and suffer the same changes (of zero amount) in the normal distances from their respective parallel neighbouring planes. We then conclude from principle (*c*)* that any two meridian planes must exhibit the same normal component of traction force across a unit area at every point in the material, and every instant throughout the whole laminar shearing displacement, irrespective of the mechanical properties of the material, and of the arbitrary choice of the experimental conditions."

This leads in the well-known *cone and plate* arrangement used to the equality $P_{22} = P_{33}$ and in the above-mentioned stress tensor to $P_{22} - P_{33} = 0$. Outside the statement quoted verbatim, the other equations are well-known ones from deformational mechanics for the force equilibrium in elastic bodies to be found in such textbooks as Ibbetson's[11] or Love's.[9] These general statements are supplemented by the calculation of $(P_{11} - P_{22})$ from the total thrust F in the cone and plate arrangement of radius R according to a formula quoted in Jobling's[12] thesis (integration of the normal stress over the area):

$$P_{11} - P_{22} = 2F/\pi R^2 \tag{4}$$

We see that Weissenberg's development is based on the principle of equilibrium of forces in the volume element in a completely direct manner, but it does not give explicitly, the connections between the rate of shear and shearing stress: "the equation of state"[2] of the material.

In his first papers (as well as in the articles of Roberts), Weissenberg did not mention quantitative relationships between the recoverable shear and the normal stresses, except stating that they should be proportional. Mooney, as much as could be ascertained, in 1951 published a quantitative relationship between normal stresses and the recoverable shear s. In 1954, Pilpel[13] referred to a private communication from Weissenberg giving the calculation of "a modu us of rigidity γ," "a relaxation time τ," "$C = (P_{11} - P_{22})/P_{12}$, a dimensionless quantity that has been termed recoverable shear." In his last paper, Pilpel[14] stated "C to be in certain cases, a measure of network strain." Jobling[15] introduced cot $2\alpha = 2/C$, where "α† is the angle between the major axis of stress and strain velocity." In

* The equation of state.

† See last paragraph of this paper.

the derivation that has just been given, "Hooke's law in shear" (*i.e.*, the proportionality of the shear stress P_{12} to the recoverable shear C) has been *assumed*. The equations above tacitly assume that the properties of the material depend only on the viscosity, η, and the shear modulus, G. The other quantities are derived from them, and the imposed shear stress P_{12}.

We will base the review of the theories of normal stresses on the theory of Mooney,[3] modifying it as we go according to the points outlined above. The first derivation of Mooney has been modified in using a geometric construction adopted from Love (a "kinematic"

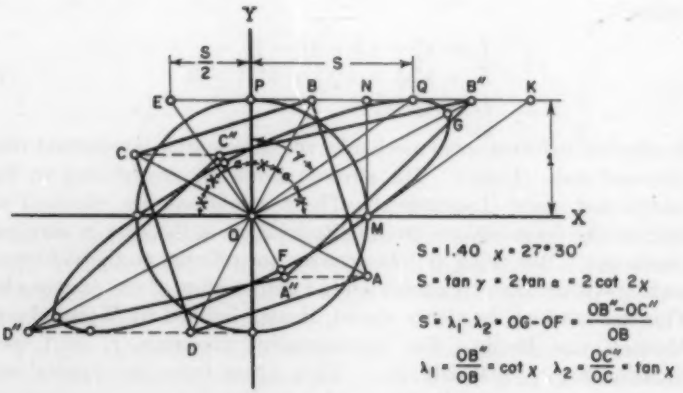

Fig. 1. Deformation in simple shear.

picture of plane shear) correlating the principal strains λ_i = deformed length/initial length (Cauchy measure) with shear strain s and the angle χ *for any amount of shear* of a square in plane shear. This geometric construction is shown in Figure 1 for an arbitrarily chosen $s = 1.4$ or 140% shear deformation. The relation mentioned in equation (1) above follows directly from this construction. We have also drawn the unit circle that is deformed by the same shear into an ellipse whose main axis is inclined toward the direction of shear under the angle χ; this is exactly the same as Weissenberg[16] has been using since 1935 and serves only to demonstrate that these relationships are all identical.

Mooney uses the relations he described in his theory of "superelasticity"[17] (1940). We can, however, modify this slightly to incorporate the discussion of Rivlin.[4] The strain energy function (Green, 1839) depends in tensor notation on three invariants of the strain tensor in the following way:

$$W = C_1 I_1 + C_2 I_2 + C_3 I_3 \tag{5}$$

The principal stresses are:

$$\sigma_1 = \frac{1}{\lambda_2\lambda_3}\frac{\partial W}{\partial \lambda_1}; \quad \sigma_2 = \frac{1}{\lambda_3\lambda_1}\frac{\partial W}{\partial \lambda_2}; \quad \sigma_3 = \frac{1}{\lambda_1\lambda_2}\frac{\partial W}{\partial \lambda_3} \tag{6}$$

where:

$$\begin{aligned} I_1 &= \lambda_1^2 + \lambda_2^2 + \lambda_3^2 - 3 \\ I_2 &= \lambda_2^2\lambda_3^2 + \lambda_3^2\lambda_1^2 + \lambda_1^2\lambda_2^2 - 3 \\ I_3 &= \lambda_1^2\lambda_2^2\lambda_3^2 \end{aligned} \tag{7}$$

In classical deformational mechanics the deformation is referred to the *deformed* state (Euler). The stresses, however, are referred to the *undeformed* state (Lagrange).[18] These conditions are identical as long as the deformations are infinitesimal, as is the case in classical mechanics. But using W, the stresses are referred to the deformed state and so are directly connected to a deformation of any magnitude. This has not been explicitly stated, though implied by Weissenberg, Mooney, and Rivlin. For incompressible materials, $I_3 = 1$ (see equation 8), $\sigma_i = \lambda_i \cdot \partial W/\partial \lambda_i$. This differs from the classical expression by the multiplication with λ_i. However, for infinitesimal deformation ($\lambda_i \backsimeq 1$) $\sigma_i = \partial W/\partial \lambda_i$, which is the classical expression.

The simplest case (assumption) possible is that C_1, C_2, C_3 are *constants; i.e.*, the strain energy function is a *linear relation* of the invariants of the strain tensor. For "soft" plastics, the incompressibility relation holds (assumption which, however, can be experimentally verified):

$$I_3 = 1 \tag{8}$$

then:

$$I_2 = 1/\lambda_1^2 + 1/\lambda_2^2 + 1/\lambda_3^2 - 3 \tag{8a}$$

According to Weissenberg,[2] I_1 can be compared with the "strain density ellipsoid" and I_2 above with the "reciprocal strain density ellipsoid."

One obtains the principal stresses σ_i as a function of the principal strains λ_i, depending only on the constants C_1 and C_2 [$C_1 = (G + H)/2$, $C_2 = (G - H)/2$]:

$$\sigma_i = \frac{G+H}{2}\lambda_i^2 - \frac{G-H}{2}\frac{1}{\lambda_i^2} - p \tag{9}$$

For $G = H$, these relations become: $\sigma_i = G\lambda_i^2 - p$, quoted in Treloar's book[19] and used by Weissenberg (1946). Introducing the relationship between the principal strains for the plane shear of incompressible materials, this becomes:

$$\begin{aligned}
&\lambda_1 = \lambda; \quad \lambda_2 = {}^1/\lambda; \quad \lambda_3 = 1 \\
&\sigma_1 = -p + \frac{G.s}{\sin 2\chi} + \frac{H}{6}s^2 = -p + \frac{\tau}{\sin 2\chi} + \frac{H}{6}s^2 \\
&\sigma_2 = -p - \frac{G\cdot s}{\sin 2\chi} + \frac{H}{6}s^2 = -p - \frac{\tau}{\sin 2\chi} + \frac{H}{6}s^2 \\
&\sigma_3 = -p - \frac{H}{3}s^2
\end{aligned} \tag{10}$$

These equations show that beyond the first-order term with Gs, we have a "second-order" term $H\cdot s^2$ in all three directions of space. The term $\sigma_1 - \sigma_2 = 2\tau/(\sin 2\chi)$ is the one used in the construction of "Mohr's circle."

Further, according to Mooney, we transform these equations[20] which are referred to the *principal* axis of strain to x, the *direction of shear*, y perpendicular to the plane of shear, and z perpendicular to them both:

$$\begin{aligned}
\sigma_x &= -p + \frac{G}{2}s^2 + \frac{H}{6}s^2 \\
\sigma_y &= -p - \frac{G}{2}s^2 + \frac{H}{6}s^2 \\
\sigma_z &= -p - \frac{H}{3}s^2 \\
\tau_{xy} &= G\cdot s
\end{aligned} \tag{11}$$

These equations are identical to Mooney's equation (8). p is an arbitrary hydrostatic pressure which obviously does not cause any deformation in incompressible bodies. "Hooke's law in shear,"

the last equation, *results* from the assumption of the linear relation between the strain energy function and the two strain invariants and does not depend on the constant H, G being the shear modulus. It is not introduced directly here as an assumption; however, the assumption is put into the linear relations of the strain energy function.

Up to here, we have used two constants as Mooney did in his theory, but it seems possible to introduce a new assumption: $G = H$. This *not only requires* Hooke's law in shear but the possibility of describing the elastic properties of the material by one constant only, G, which is identical with the aforementioned assumption of Weissenberg or Rivlin's "neo-Hookean body." A decision on how many constants are necessary is only to be obtained experimentally. Introducing $G = H$ into equation (11), we obtain:

$$\begin{aligned} \sigma_x &= -p + {}^2/_3 G\delta^2 \\ \sigma_y &= -p - {}^1/_3 G\delta^2 \\ \sigma_z &= -p - {}^1/_3 G\delta^2 \\ \tau_{xy} &= G\delta \end{aligned} \tag{12}$$

or by using the same notation as Weissenberg and assuming with Rivlin that the isotropic pressure, $p' = 0$ (that is, considering the deviatoric stress alone):

$$\begin{aligned} p' &= p + {}^1/_3 G\delta^2 = 0 \\ P_{11} &= \sigma_x = G\delta^2 = \tau\delta \\ P_{22} &= P_{33} = \sigma_y = \sigma_z = 0 \\ P_{12} &= \tau_{xy} = G\delta \end{aligned} \tag{13}$$

Thus, we have reduced the observable quantities in shear to only 2: the normal stress $\sigma_x = P_{11}$ and the shear stress $\tau_{xy} = P_{12}$. This is exactly equivalent to the formulation of Weissenberg.

The above derivation for isotropic materials is based beyond the equations of classical mechanics on three assumptions that have been used, but not emphasized as such, by Weissenberg:

1. Linear relation of W and I_1 or the "Hooke's law in shear."
2. Incompressibility.
3. $G = H$ or $C_2 = 0$, or description of the properties by one single constant G.
4. Plane simple shear (laminar flow).

These are Mooney's "postulates" in 1940.[17]

To reduce these relations derived for a volume element to measurable conditions, we introduce similarly as Weissenberg did the force equilibrium conditions, not in *spherical* but in *cylindrical* coordinates (the formulas are standard ones[21]). We obtain the relation for rotational symmetry $\partial/\partial\theta \equiv 0$ and the experimentally imposed symmetry $\partial/\partial Z \equiv 0$ as follows: ("body forces" are disregarded):

$$\begin{aligned} \partial\sigma_r/(\partial \ln r) &= \sigma_\theta - \sigma_r \\ \partial\tau_{r\theta}/(\partial \ln r) &= -2\tau_{r\theta} \\ \partial\tau_{rz}/(\partial \ln r) &= -\tau_{rz} \end{aligned} \tag{14}$$

The notations in cylindrical coordinates are visualized in Figure 2.

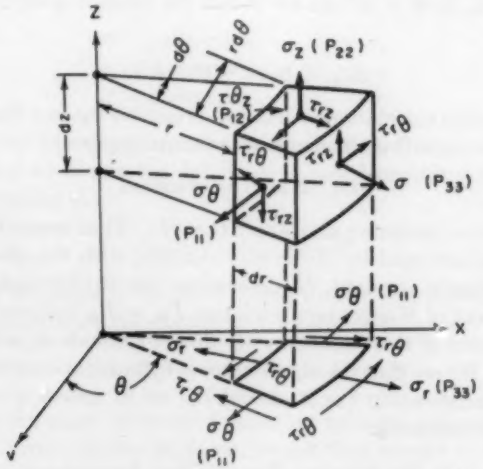

Fig. 2. Notation of forces in cylindrical coordinates.

According to the different geometric arrangements now reviewed, the stress σ_z and shear stress, τ_{zy} are correlated with the different stresses σ and τ as will be seen presently.

(1) *The Cone and Plate Arrangement*

For the cone and plate arrangement with a thin slit (as used in the Weissenberg rheogoniometer):

θ is the x direction, $\sigma_\theta = \sigma_x$
Z is the y direction, $\sigma_Z = \sigma_y$
r is the z direction, $\sigma_r = \sigma_z$

This leads to:

$$\frac{\partial \sigma_r}{\partial \ln r} = \sigma_x - \sigma_z = \frac{G + H}{2} s^2$$

and:

$$\sigma_r - \sigma_Z = \frac{G - H}{2} s^2$$

The experimentally measurable quantity is σ_Z. Only with $P_{33} = P_{22}$ ($\sigma_r = \sigma_Z$ or $G = H$) do we obtain the relation used by Weissenberg:

$$\partial \sigma_Z / (\partial \ln r) = G s^2 = \tau \cdot s \tag{15}$$

If we make this calculation in detail and consider the fact that Roberts[1] found ($\sigma_r = \sigma_Z = 0$ at rim exposed to the atmosphere):

$$\partial \sigma_Z / (\partial \ln r) = \text{constant} \tag{16}$$

for each rate of shear, we also obtain $G = H$. That means the validity of the relation found by Roberts is identical with the assertion that only one elastic constant, G, determines the equilibrium. This, in itself, is proof of Weissenberg's relation $P_{22} = P_{33}$ independent of the measurements of this equality with different liquids as performed by Roberts. We see that the equilibrium in cylindrical coordinates gives the same relationship (as it should be) as in spherical coordinates used by Weissenberg.

(2) *The Rotating Parallel Plate Arrangement*

The notations in this case are identical with the one for the cone and plate arrangement. Using Hooke's law in shear, we find the distribution of the Z component:

$$\sigma_Z = -\frac{\varphi^2}{L^2}\left[\frac{G + H}{4} R^2 + \frac{G - 3H}{4} r^2\right] \tag{17}$$

where φ is the angle of twist. This equation was derived by Rivlin[22] in 1948. For the case $G = H$, we obtain:

$$\sigma_Z = -(1/2)(\varphi^2/L^2) \cdot G(R^2 - r^2) = \sigma_r \tag{18}$$

This is derived, assuming the validity of Hooke's law in shear; however, for a flowing solution, the torsional angle is proportional not to the shear stress but to the rate of shear. Under these conditions the shearing stress at each radius is determined by the properties (viscosity) of the material and the distribution of shear stress over the radius, which causes the normal stress σ_z to become roughly a *linear* function of the radius instead of the quadratic dependence as shown in the preceding equation.[23]

(3) *The Concentric Cylinder Arrangement*

For this case:

$$\begin{aligned} \theta &= z \text{ direction}, & \sigma_\theta &= \sigma_z \\ r &= y \text{ direction}, & \sigma_r &= \sigma_y \\ Z &= z \text{ direction}, & \sigma_Z &= \sigma_z \end{aligned}$$

Using the well-known expressions for the shearing stress in the Couette arrangement we obtain the difference in radial pressures at the outer and inner radius to:

$$\Delta\sigma_r = {}^1/_4 G s_i^2 \cdot (1 - c^4) \tag{19}$$

Where s_i is the shear at the inner cylinder and c = inner radius/outer radius. Introducing the expression for s_i, we obtain $\Delta\sigma_r$:

$$\Delta\sigma_r = G\varphi^2 \cdot (1 + c^2)/(1 - c^2) \tag{20}$$

where φ is the angle of twist of the inner cylinder against the outer cylinder. From the first equation, we see that, when $c < 1$, the value of $\Delta\sigma_r$ quickly reaches a constant value equal to ${}^1/_4$ of the one measured in the cone and plate arrangement; however, for large values of c (thin slit), for s_i = constant, $\Delta\sigma_r$ approaches 0. This probably explains the results of Garner, Nissan, and Wood,[24] as well as Mooney,[25] who did not obtain any normal stresses in the Couette arrangement with thin slits. For small values of c, Padden and DeWitt[26] have measured normal stresses, as have Ward and Lord[27] successfully. This equation (20) is equivalent to the statement[24] that "normal stresses" are observable only for a stress gradient; however, this statement is valid only for the concentric cylinder symmetry ($c < 1$ but not too large!)

(4) *The Capillary*

For this case:

$$Z = x \text{ direction}, \quad \sigma_z = \sigma_x$$
$$r = y \text{ direction}, \quad \sigma_r = \sigma_y$$
$$\theta = z \text{ direction}, \quad \sigma_\theta = \sigma_z$$

For the capillary, as is well known, the shearing stress, τ, is equal to:

$$\tau = rp/2L$$

$$\tau = \tau_r \cdot r/R$$

The equation for the normal stress is:

$$\frac{\partial \sigma_r}{\partial \ln r} = \sigma_z - \sigma_y = \frac{G - H}{2} s^2 \tag{21}$$

In the case of $G = H$, we obtain $\sigma_z = \sigma_y = -p' + \tau s$, and σ_r = constant. Integrating the equation for σ_z over the area of the capillary, we obtain the relationship for the mean tensile stress in the capillary $\sigma_L = {}^1/_2 \tau_R s_R$, where τ_R is the maximum shearing stress at the wall and s_R is the maximum shear strain at the wall, or introducing the extinction angle χ_R at the wall:

$$\sigma_L = \tau_R \cot 2\chi_R \tag{22}$$

This derivation shows that, in laminar flow in a capillary, the "normal stresses" cause an axial tension. This has been known since 1893,[28] and has been called, by Houwink, the "Barus effect."[29]

The foregoing discussion has shown that the normal stresses can be measured in a variety of geometric arrangements. The experimental correlation of the results with different geometries has not yet been done. However, we have enough information to draw the following conclusions about the nature of the normal stresses.

1. Normal stresses occur in elastic bodies—either elastomers (vulcanized rubber) or solutions.

2. They are the result of a "finite shear" that justifies their being called "secondary stresses."

3. They are a manifestation of a reversible elastic energy in a flowing material per unit volume, $E = {}^1/_2 Gs^2$.[24]

4. The "recoverable shear s," which causes them in steady flow, is the result of an equilibrium between stress buildup and relaxation.

5. They can be described in the simplest way for an incompressible material which has one shear modulus G: for the "neo-Hookean body."

6. They can be measured in suitable geometric arrangements, preferably in plane shear.

7. In plane shear with $G = H$ the action of the "normal stresses" is a "pull" in the direction of shear.[2]

8. No other constants but G and s, which are dependent on the experimental conditions, material, concentration, solvent, and temperature are necessary to describe the normal stresses.

9. Weissenberg assumes $P_{22} = P_{33}$ for *any* material, whereas Mooney, and therefore the described derivation, shows, that only for $G = H$ is this valid. The general experimental proof of this relation is still to be given. (Weissenberg[2,16] introduced the "effective angle 2α" between the direction of the principal axis of the stress tensor and the one of the strain velocity tensor. This last one, according to him, is oriented always under 45° to the direction of shear. Thus, as is easily seen from Figure 1, $2\chi = 90 - 2\alpha$ and this angle α is no new parameter, but is another expression, through equation (1), of the "recoverable shear s.")

See pages 117–118 for the References and Synopsis of this article.

TRANSACTIONS OF THE SOCIETY OF RHEOLOGY VOL. I, 109–118 (1957)

On Normal Stresses, Flow Curves, Flow Birefringence, and Normal Stresses of Polyisobutylene Solutions. Part II. Experimental

JOHN G. BRODNYAN, F. H. GASKINS, and W. PHILIPPOFF,
The Franklin Institute Laboratories for Research and Development, Philadelphia 3, Pa.

PROCEDURES

Having described the theory of the effect in the preceding paper, we now proceed to test the conclusions. Experimentally, we used the same equipment that was described in the previous publication.[5] We supplemented the Weissenberg rheogoniometer by using rigid "top plates," eliminating the possibility of measuring shear stresses with the Weissenberg rheogoniometer, as the operation of the instrument became much more stable. By changing the diameter of the top plate, we could verify the equation for the normal stresses used by Jobling.[12] The material tested was P-100, polyisobutylene, obtained from Esso Research & Engineering Co., Linden, New Jersey, in chemically pure Decalin. The concentration was varied in as large a range as possible, the practical limits being 9 to 0.1%.

Results

In Figure 3, the results of the normal stress experiments are plotted: the normal stress $P_{11} - P_{22}$ as functions of the rate of shear D.

In Figure 3, we also have the flow curves: the dependence of the rate of shear D on the shearing stress τ, measured in the lower part with a rotational viscometer, in the top portion in the capillary viscometer. Both experimental arrangements gave an exact overlapping of results.

In Figure 4, we have the birefringence measurements: the degree of birefringence Δn and the orientation angle χ are plotted as func-

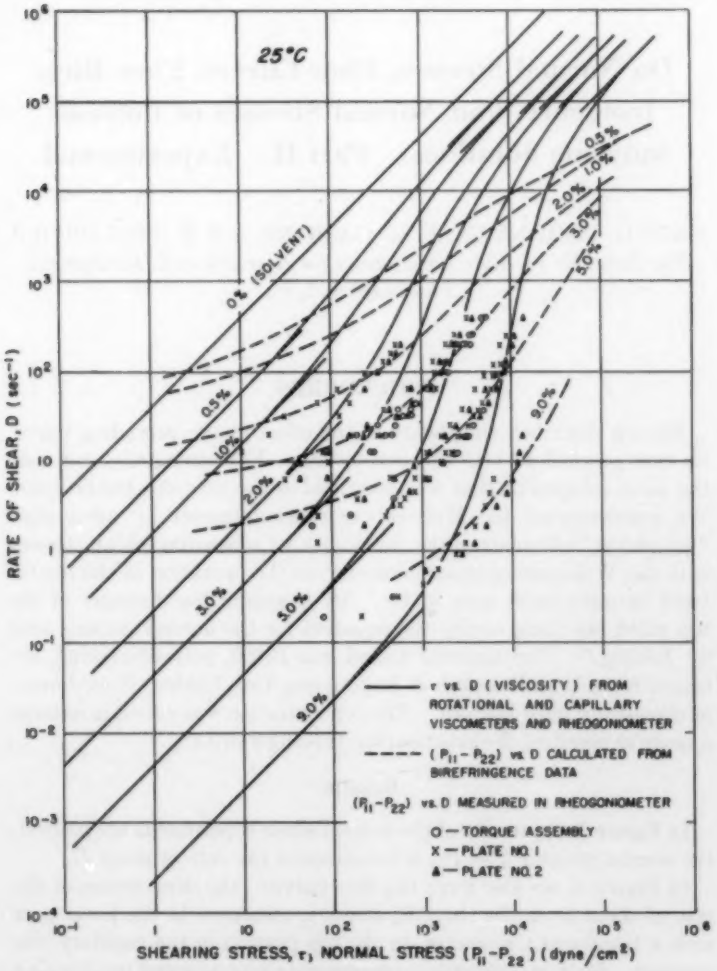

Fig. 3. Shearing stress τ and normal stress $P_{11}-P_{22}$ as functions of rate of shear D (composite for polyisobutylene in Decalin solutions).

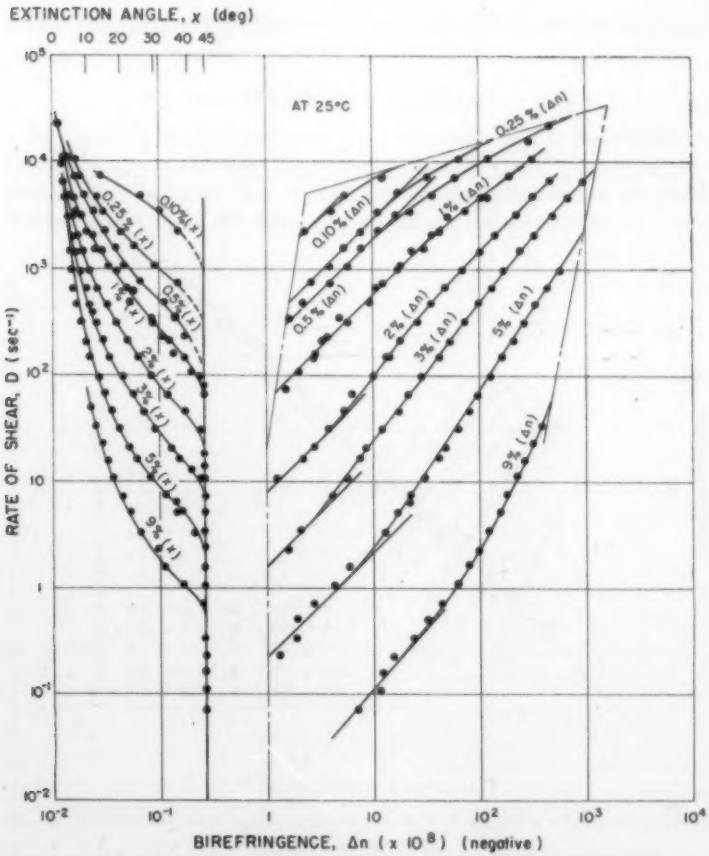

Fig. 4. Birefringence Δn and extinction angle χ *vs.* rate of shear D (composite for polyisobutylene in Decalin solutions).

tions of the rate of shear D. The dotted lines give the limits of measurement: on top the limit of turbulence, at left the sensitivity, and at right the range of the optical compensator, or the heating of the solution in flow.

We see that the range of variables used in these investigations is well above anything reported until now. Especially, the flow curves

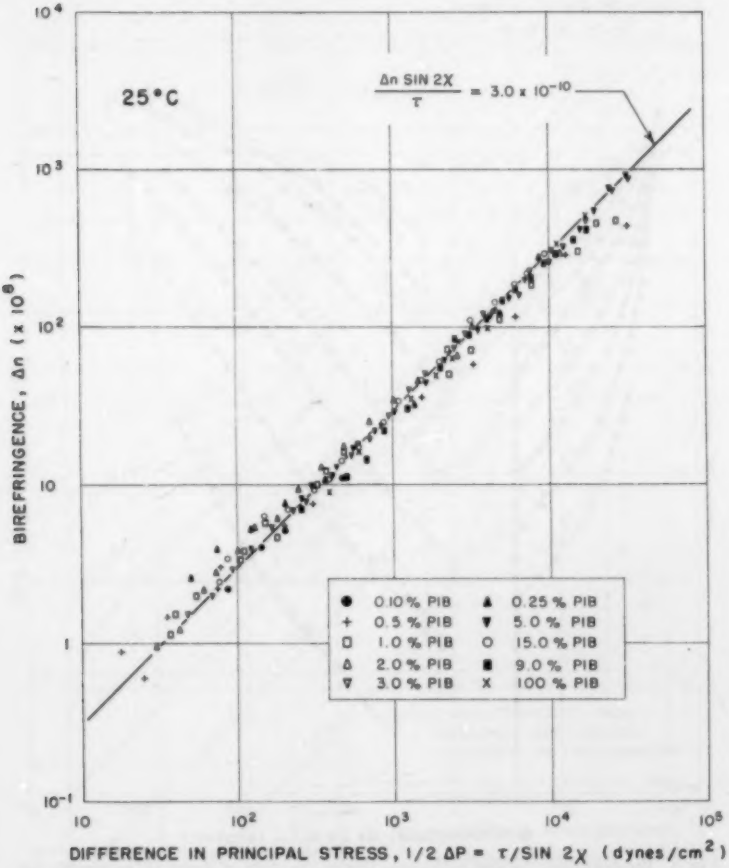

Fig. 5. Birefringence Δn as function of one-half the difference in principal stress, $(1/2)\Delta P = \tau/\sin 2\chi$ (polyisobutylene in Decalin solutions).

have a very distinct S shape and at high rates of shear the limiting viscosity, η_∞, could be reached experimentally in each separate case, sometimes in a region of nearly one decade in the rate of shear.

The measurements of the normal stresses have the greatest experimental errors; however, they are not less precise, and are prob-

ably better, than the measurements of Jobling[12] on similar solutions in a far smaller range of variables.

Discussion of Results

In Figure 5 we have plotted the evaluation of the birefringence measurements in the way suggested by Lodge:[30] plotting Δn, the degree of birefringence, as a function of $^1/_2$ the difference of principal stresses $\tau/(\sin 2\chi)$. We have plotted *all* our values without any cor-

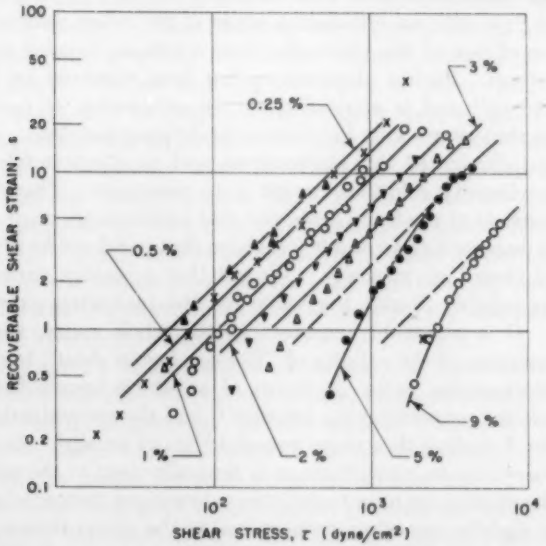

Fig. 6. Recoverable shear strain s as a function of shear stress τ (polyisobutylene in Decalin solutions).

rections between 9% polyisobutylene and 0.1% polyisobutylene in Decalin. In all cases, the points lie with some scatter on a straight line in the whole range of around three decades in both principal stresses and birefringence. This would mean the "stress optical law" valid for solids has been proved for polyisobutylene and its solutions in the experimentally investigated range. Therefore, the investigation of the degree of birefringence does not give any more information than a measurement of the difference in principal stresses.

In Figure 6, we have plotted the recoverable shear s as a function of the shear stress τ calculated according to eq. (1) (p. 96) for the whole range of concentrations for polyisobutylene. We see that the values are definitely dependent on the concentration, as can be also seen from the direct measurements reported in Figure 4. However, the dependence of s on τ is essentially linear. In some of our measurements, the angle measurements at low Δn were seriously affected by the presence of some impurity (either cellulose fibers or zinc stearate) from the polyisobutylene that caused a strong birefringence even without flow with an orientation angle of 90° when referred to the direction of flow of the polyisobutylene solutions, causing small s to be too small. Such a phenomenon has been observed by Zvetkov and Petrova[31] and is attributed to the orientation of microscopic particles that have a very low rotational diffusion constant. Waiting overnight eliminated this phenomenon and an effective filtration of the low viscosity solutions caused it to disappear. Therefore, the measurements of the 3 and lower per cent solutions are more accurate than the ones with the 5 and 9% solution that could not be filtered because of their high viscosity. We see that s reaches values of 20, which is roughly double the value for the maximum extension of rubber. G is reasonably constant in the whole range, supporting the assumption of the validity of "Hooke's law in shear" to considerable deformations, much in excess of anything known heretofore. However, the proportionality between G and the concentration as required by Peterlin's theoretical equation[32] is not present. In order to bring the values to coincidence as is generally used in the method of reduced variables, we have to shift the values along the c axis by values that are slightly more than proportional to the concentration. Similar behavior has been observed in dynamic tests on polyisobutylene by Padden and DeWitt.[26] These experiments, therefore, prove that Lodge's assumption[30] is valid in the whole range available for investigation and that the concentration-dependence of the flow birefringence experiments is confined to the orientation angle χ. It is not astonishing that quantitative relationships derived for dilute solutions should be only qualitatively true for the ones investigated, which cannot possibly be considered dilute.

In Figure 3, we have plotted, besides the direct measurements of the normal stresses with the Weissenberg rheogoniometer, the values calculated from the shear stress τ and s, as determined by the flow

birefringence measurements. We see that both the curves essentially coincide in the whole range measured.

At high shearing stresses, about 1000 dynes/cm.^{2}, the measurements in the Weissenberg rheogoniometer, which has no effective temperature control, deviate from the measurements in the capillary viscometer in the rate of shear (Fig. 3) as well as in the normal stress calculated from birefringence. This deviation is probably caused by heating of the solution under these high rates of shear. This fact is further proved as we can calculate χ from the measurement, with the Weissenberg rheogoniometer and they check with χ measured in flow birefringence much closer than the normal stresses or shear stresses alone. We see that at low rates of shear the normal stresses disappear, the slope being roughly proportional to D^2. This relationship was proposed by Padden and DeWitt,[26] Mooney,[3] and Rivlin[23]; however, at high rates of shear, the normal stresses become nearly proportional to the rate of shear, as has been observed by numerous investigations including Rivlin and Greensmith.[23] From the flow curves in Figure 3 and the normal stress measurements in Figure 3 we see that, as a general rule, the normal stresses become unobservable as soon as the viscosity reaches a constant value: the initial viscosity η_0.

The very exactly measured flow curves reach at high rates of shear the final viscosity η_∞. We have plotted η_∞ against the concentration and have found, as previous measurements by Philippoff[23] in 1936 have shown, that it is proportional to the concentration. The slope (η_{sp}/c with c in weight per cent) gives the value of 3.3. The plot of the initial viscosity η_0 *vs.* concentration gives an exceedingly steep curve which, however, merges into the zero point, with a slope of 5.1. In this particular case, we have shown that the non-Newtonian behavior of polyisobutylene is caused mainly by interaction of the molecules in solution, for this diminishes considerably at highly dilute solutions. The disappearance of the non-Newtonian viscosity is the requirement of both Zimm[24] and Lodge[25] for the behavior of coiled molecules in laminar flow. Whereas the non-Newtonian viscosity, as has just been said, essentially disappears, the flow birefringence and the flow orientation continue. The residual non-Newtonian viscosity is probably caused by the incomplete free rotation in the isobutylene monomer molecule.

Furthermore, it has been stated by Peterlin and Signer[26] that the

shear stress to be correlated with properties in flow birefringence is the increase in shearing stress at a certain rate of shear above the one for the solvent. However, in Figure 5 we have plotted the stress-optical coefficient using the *whole* shearing stress and obtained coincidence between the dilute and concentrated solutions. We must, therefore, conclude that the *whole shearing stress* has to be used in discussing the mechanical properties of high polymer solutions. The difference in the values for the 0.1% solution would be about 1 to 3 if we took the whole shearing stress or only the increment above the one for the solvent, which is far above the experimental error.

The mathematical analysis presented, together with the experimental results, tend to support the assertion that "normal stresses" are a necessary phenomenon complementing the more usual shear relation in laminar flow. Especially the investigations of Ward and Lord[27] have shown that, even with considerable normal stresses, the relationships used for a concentric cylinder geometry remain valid. Greensmith and Rivlin[23] have shown with a very high precision that the normal stresses depend only on the rate of shear, as they changed the geometry considerably and could well correlate their experimental results in this way.

However, the correlation of D and $P_{11} - P_{22}$ is still incomplete except for the comparatively trivial case of small s. The same pertains to the correlation of dynamic tests with the steady flow experiments. Both correlations involve the "equation of state."

From the developments shown, one sees that the correlations are more easily made for "the equilibrium of forces" than for ones involving rate of shear D. Therefore the measurement of the flow birefringence as a function of D, without the simultaneous determination of the flow curve, is incomplete. All this emphasizes the necessity of using a variety of methods simultaneously in a large range of variables to obtain a satisfactory description of the mechanical properties of polymer solutions. This is a somewhat complicated and costly procedure, but in the present stage of development of this field it is not to be ignored.

This work was carried out as part of a Contract with the Army Chemical Center, Edgewood, Maryland. The assistance of this agency is gratefully acknowledged, especially the assistance for obtaining the costly equipment necessary. The measurement of the flow curves was performed by G. K. McConnell, for whose competent help the authors express sincere thanks.

References

1. J. E. Roberts, Ministry of Supply Report No. ADE 13/52 (1952), *Proc. 2nd Intern. Congr. Rheology, New York, 1953*, 91 (1954).

2. K. Weissenberg, Conference British Rheologist's Club 1946, *Proc. 1st Intern. Congr. Rheology, Amsterdam, 1948*, **3**, 36–45 (1949).

3. M. Mooney, *J. Colloid Sci.*, **6**, 96 (1951).

4. R. S. Rivlin, "Large Elastic Deformations," in F. Eirich, ed., *Rheology* N. Y., 1956 and Ch. XIII in Ref. 19 (since 1947 and 1948).

5. W. Philippoff, *J. Appl. Phys.*, **27**, 984 (1956); *Nature*, **178**, 811 (1956).

6. K. Weissenberg and R. O. Herzog, *Kolloids-Z.*, **46**, 277 (1928).

7. R. Eisenschitz and W. Philippoff, *Naturwissenschaften*, **21**, 527 (1933).

8. W. Philippoff, *Physik. Z.*, **35**, 883, 900 (1934).

9. A. E. H. Love, *On the Mathematical Theory of Elasticity*, 4th ed., Dover, New York, 1944, Chap. I, #3.

10. H. Kolsky, *Stress Waves in Solids*, Oxford Univ. Press, Oxford, 1953, Chap. II, p. 5.

11. W. T. Ibbetson, *An Elementary Treatise on the Mathematical Theory of Perfectly Elastic Solids*, London, 1887.

12. A. Jobling, Thesis, Cambridge, 1955.

13. N. Pilpel, *Trans. Faraday Soc.*, **50**, 1369 (1954).

14. N. Pilpel, *Trans. Faraday Soc.*, **51**, 1307 (1955).

15. A. Jobling, *J. Oil Colour Chem.*, **38**, 739 (1955).

16. K. Weissenberg, *Arch. Génève*, **17**, 1 (1935).

17. M. Mooney, *J. Chem. Phys.*, **11**, 582 (1940).

18. I. S. Sokolnikoff, *Mathematical Theory of Elasticity*, New York, 1956, Chap. 1, par. 11, p. 29.

19. L. R. G. Treloar, *The Physics of Rubber Elasticity*, Oxford Univ. Press, Oxford, 1949.

20. A. E. H. Love, reference 9 above, #33, p. 68.

21. A. E. H. Love, reference 9 above, #59, p. 90.

22. R. S. Rivlin, *Phil. Trans. Roy. Soc.*, **A240**, 459 (1948); *Proc. Cambridge Phil. Soc.*, **45**, 485 (1947).

23. H. W. Greensmith and R. S. Rivlin, *Phil. Trans. Roy. Soc.*, **A245**, 399 (1953).

24. F. H. Garner, A. H. Nissan, and G. F. Wood, *Phil. Trans. Roy. Soc.*, **A241**, 379 (1950).

25. M. Mooney, *J. Appl. Phys.*, **24**, 675 (1953).

26. F. J. Padden and T. W. DeWitt, *J. Appl. Phys.*, **25**, 1086 (1954).

27. A. F. H. Ward and P. Lord, *Proc. 2nd Intern. Congr. Rheology, New York, 1953*, 214 (1954).

28. C. Barus, *Am. J. Med. Sci.*, **45**, 87 (1893).

29. R. Houwink, *Elasticity, Plasticity and Structure of Matter*, p. 229, London, 1937.

30. A. S. Lodge, *Nature*, **176**, 838 (1955).

31. V. Zvetkov and A. Petrova, *J. Tech. Phys. U.S.S.R.*, **14**, 289 (1944).

32. A. Peterlin, *Proc. 2nd Intern. Congr. Rheology, New York, 1953*, 343 (1954).

33. W. Philippoff and K. Hess, *Z. physik. Chem.*, **B31**, 237 (1936); *Kautschuk*, **12**, 124 (1936).
34. B. Zimm, *J. Chem. Phys.*, **24**, 269 (1956).
35. A. S. Lodge, *Trans. Faraday Soc.*, **52**, 120 (1956).
36. A. Peterlin and R. Signer, *Helv. Chim. Acta*, **36**, 1575 (1953).

Synopsis

A mathematical analysis of the existing theories of normal stresses is made. It can be shown that they all give identical results and are based on the same three basic assumptions when one discusses large elastic deformations. Experiments in a wide range of variables showed that the normal stresses disappear as soon as the viscosity becomes constant at low rates of shear. The proportionality between the degree of birefringence and the difference of the principal stresses could be confirmed in three decades of variables. "Hooke's law in shear" could be proved up to about a shear of 20.

TRANSACTIONS OF THE SOCIETY OF RHEOLOGY VOL. I, 119–151 (1957)

Strain Aging Hydrogen Embrittlement in Alpha-Beta Titanium Alloys

HARRIS M. BURTE, *Materials Laboratory, Directorate of Research, Wright Air Development Center, Wright-Patterson Air Force Base, Ohio*

I. INTRODUCTION

The effects of hydrogen in titanium-base materials depend upon the type of alloy being considered. The early work of Jaffee and co-workers [1–3] on unalloyed titanium showed that hydrogen is relatively soluble in the beta, body-centered cubic, elevated temperature phase of titanium, but at room temperature is quite insoluble in the alpha, hexagonal close-packed, low temperature phase. In unalloyed titanium or alloys with low contents of alpha stabilizing elements, which at room temperature are predominantly alpha phase, hydrogen in excess of the solubility limit is precipitated as hydride needles or platelets, and this increases the classical ductile to brittle transition temperature. Thus the effects of hydrogen contamination on the ductility of these all-alpha materials is greatest at high strain rates, in the presence of a notch, and at low test temperatures. Hydrogen contamination in the range 0–500 parts per million by weight (p.p.m.) has little effect on properties measured in normal room temperature tensile tests, but has a pronounced effect on the energy absorption measured in a notch-bend impact test.

In alloys with beta stabilizing elements such as iron or manganese, both alpha and beta phases may be present at room temperature, and the effects of hydrogen on mechanical properties are quite different from those for the all-alpha alloys.[4–7] Jaffee *et al.*[4–7] and Kotfila and Erbin[5] showed that in several alpha-beta alloys hydrogen content does not cause a hydride precipitate but does induce a strain rate sensitivity leading to low ductility in tensile tests at slow testing speeds. This is exactly opposite from the effect of strain rate on the

ductility of all-alpha alloys. It was suggested that in alpha-beta alloys hydrogen contributes to a strain aging type of embrittlement. Work at Pratt and Whitney Aircraft Corporation and at Wright Air Development Center[6] showed that hydrogen could cause premature brittle fracture under conditions of sustained loading. Other work on alpha-beta alloys has been reported.[8–10] This paper is concerned with the effects of hydrogen on the room temperature mechanical properties of these alpha-beta titanium alloys, and the mechanism of strain aging hydrogen embrittlement.

II. EXPERIMENTAL METHODS

The materials for which mechanical property test data are reported are described in Table I. They are all commercial or semicommercial

TABLE I
Analyses of Titanium Alloys (As-Received Analysis[a])

Alloy	Heat	Al	Fe	Cr	Mo	Mn	C	N	O	H (p.p.m.)
Ti-140A	M1170		2.1	2.5	1.6		0.09	0.03	0.13	250
C-130AM	B5038	3.2				3.2	0.04	0.05	0.15	60
C-130AM	B3371	3.0				2.8	0.03	0.05	0.08	60
Ti-150A	R68		1.2	3.0			0.10	0.09	0.28	250
Ti-140A	M1192		2.0	2.2	1.7		0.09	0.02	0.10	210
Ti-155AX	Unknown	5.1	1.3	1.3	1.0		0.04	0.03	0.13	260

[a] Balance titanium.

alpha-beta alloys supplied in the form of barstock. Experiments were also performed on sheet material, and on specimens from forged articles, but since these gave results similar to those for barstock they will be discussed in a qualitative manner only. The preparatory procedures described in Table II were performed on the as-received stock in order to obtain different levels of hydrogen contamination in specimens from one heat of a given material. Hydrogen content was decreased below that of as-received material by vacuum annealing; the pressure, measured in a room temperature zone, in the vacuum annealing system was usually below 0.1 micron, and sometimes was as low as 0.01 micron. The hydrogen content was increased over that in the as-received material by heating in a hydrogen atmosphere. In order to isolate the effects of hydrogen contamination from those of other metallurgical variables, the materials of different hydrogen levels prepared from one heat were brought to similar thermal

TABLE II

Preparatory Treatments tc Adjust Hydrogen Content and Thermal History

Alloy and heat	As-received hydrogen level (p.p.m.)	Hydrogen level tested (p.p.m.)	Treatment applied to as-received material
Ti-140A Ht. M1170	250	20	Vacuum anneal, 1200°F., 24 hrs. + furnace cool.
		170	Vacuum anneal, 1200°F., 2 hrs. + air cool + heat in argon, 1200°F., 22 hrs. + furnace cool.
		250	Heat in helium 1200°F., 24 hrs. + furnace cool.
C-130AM Ht. B5038	60	10	Vacuum anneal, 1300°F., 25 hrs. + furnace cool.
		320	Hydrogenate, 1300°F., 21 hrs. + air cool + heat in air, 1300°F., 4 hrs. + furnace cool.
C-130AM Ht. B3371	60	60	Heat in air, 1300°F., 3 hrs. + furnace cool.
		150	Hydrogenate, 1300°F., 21 hrs. + air cool + heat in helium, 1300°F., 5 hrs. + furnace cool.
		190	Hydrogenate, 1300°F., 21 hrs. + air cool + heat in helium, 1300°F., 5 hrs. + furnace cool.
		280	Hydrogenate, 1300°F., 21 hrs. + air cool + heat in helium, 1300°F., 5 hrs. + furnace cool.
Ti-150A Ht. R68	250	10	Vacuum anneal, 1300°F., 25 hrs. + furnace cool.
		250	Heat in air, 1300°F., 24 hrs. + furnace cool.
Ti-140A Ht. M1192	210	210	Heat in air 1200°F., 24 hrs. + furnace cool.
		210	Heat in air 1200°F., 24 hrs. + furnace cool + heat in air 1350°F., 22 hrs. + air cool.
Ti-155AX	260	5	Heat in air, 1250°F., 0.5 hr. + furnace cool + vacuum anneal, 1300°F., 24 hrs. + furnace cool.
		260	Heat in air, 1250°F., 0.5 hr. + furnace cool + thermal treat in air, 1300°F., 24 hrs. + furnace cool.

histories before test specimens were machined. Thermal history adjustment and homogenization of hydrogen content across specimen cross-section were accomplished by heating in air or inert gas. No differences could be attributed to the use of air *vs.* an inert gas since the contaminated surface resulting from heating in air was removed during the machining of test specimens.

Hydrogen analyses were by the vacuum fusion method. Annealing in air or inert gas, or mechanical property testing had no discernible effect upon the hydrogen content. Hydrogen contents are expressed as parts per million by weight (p.p.m.).

Room temperature mechanical property test data are reported for notched and unnotched cylindrical specimens machined from the barstock. Tensile tests were performed at various strain rates corresponding to the testing speeds indicated. Rupture (sustained loading) tests were performed on standard lever-arm creep-rupture frames. In many cases several specimens were loaded in tandem on a single frame. When one specimen broke a new one or a dummy was inserted, and the stress was reapplied. Room temperature for rupture testing was controlled between 72 to 74°F.; room temperature for tensile testing was not controlled and may have varied between 70 to 90°F.

The unnotched cylindrical specimens had a gage length of 1 inch and a gage diameter of 0.187 inch. The notched cylindrical specimen was a 0.294-inch bar with a circumferential 60° V-notch that reduced the load-carrying area to a circle 0.187 inch diameter. Radius at root of notch was 0.01 inch. Specimen ends for both types were $^3/_8$ inch diameter with 16 threads per inch. The majority of the unnotched specimens were tested with as-machined, or as-machined and rough polished, surfaces. The effect of specimen surface preparation was also investigated.

Metallographic specimens were mechanically polished and were etched with one of the following mixtures:

48% HF = 2% (by vol.)	2%	20%
conc. HNO_3 = 10%	—	20%
H_2O = 88%	98%	—
glycerin = —	—	60%

III. STRAIN AGING EMBRITTLEMENT

Tensile and rupture test data for two titanium alloys are presented in Figures 1, 2A, and 2C and Tables III and IV. Considering first

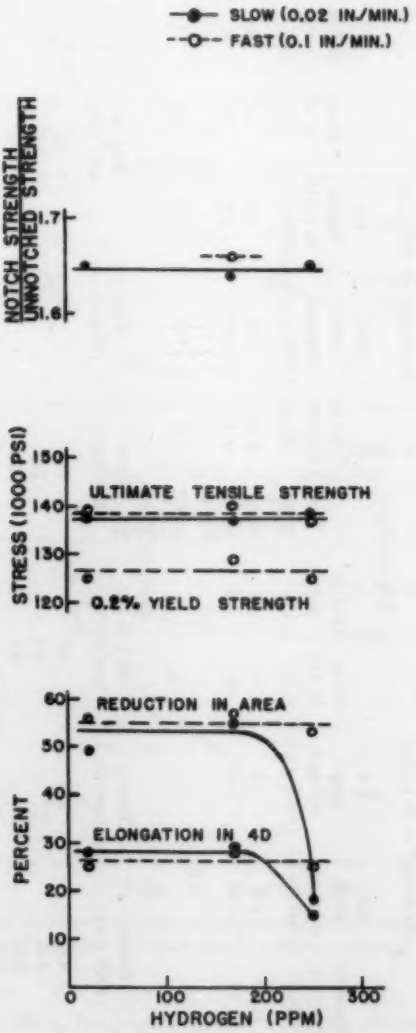

Fig. 1. Effects of hydrogen on room temperature tensile properties of Ti-140A, Ht. M1170. Unnotched specimens except where indicated.

TABLE III

Effects of Hydrogen Contamination on Room Temperature Tensile and Rupture Behavior of C-130AM, Ht. B5038 (Unnotched Specimens)

Tensile Tests

Hydrogen = 10 p.p.m.						Hydrogen = 320 p.p.m.					
Test speed	Time to fracture (hr.)	0.2% yield strength (1000 p.s.i.)	Ult. tensile strength (1000 p.s.i.)	Elong. in 4D (%)	Red. in area (%)	Test speed	Time to fracture (hr.)	0.2% yield strength (1000 p.s.i.)	Ult. tensile strength (1000 p.s.i.)	Elong. in 4D (%)	Red. in area (%)
Fast	0.03	131	143	18	46	Fast	0.03	126	145	17	39
Slow	0.17	N.M.	138	20	43	Slow	0.17	N.M.	146	17	37
						Very slow	1.8	127	149	10	17

Rupture Tests

Stress (1000 p.s.i.)	Time to fracture (hr.)	Red. in area (%)	Stress (1000 p.s.i.)	Time to fracture (hr.)	Red. in area (%)
137	2.3	46	144	0.04	33
135	27	40	143	1.3	12
133	62	43	136	9.0	9
129	Did not fracture in 1200 hrs.		129	22	5
			123	442	3

N.M. = not measured.

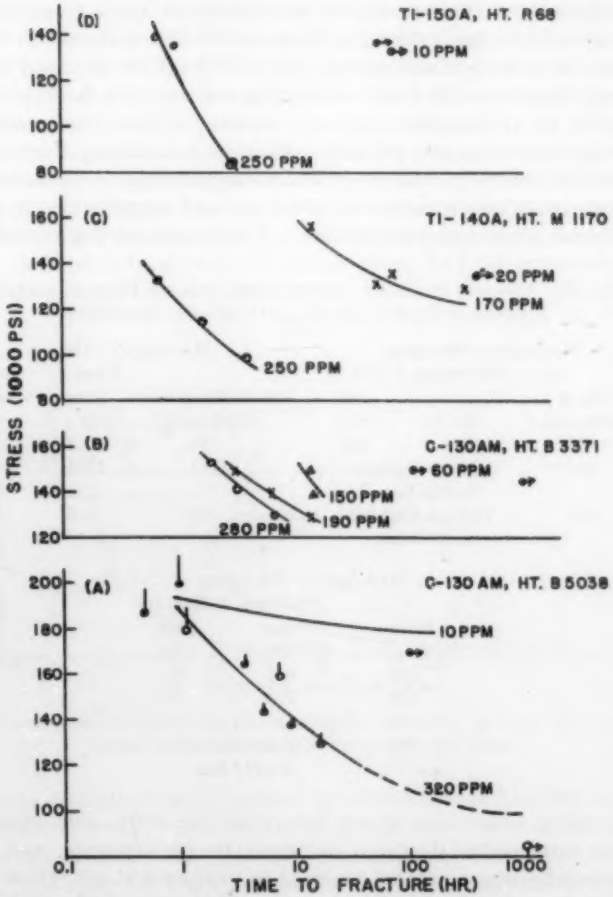

Fig. 2. Effects of hydrogen on room temperature rupture behavior of notched specimens. In (A) the height of a line extending above a point is proportional to the reduction in area at fracture.

the tensile test data, hydrogen content between 10 and 400 p.p.m. has little effect on the ultimate tensile strength, the yield strength, or the ratio of notched strength to unnotched strength. Ductility, as measured by elongation or reduction in area, is reduced by hydro-

gen content, but the amount of the reduction is not a single valued function of hydrogen content. It depends on the strain rate at which the test is performed and other factors which will be discussed below. At high strain rates hydrogen-containing material may show the same ductility as hydrogen-free material, whereas at low strain rates the ductility may be greatly reduced. This strain rate dependence of the tensile test ductility of hydrogen-containing material is characteristic of the embrittlement under consideration, and suggests that it arises from some strain aging mechanism. Two important features of this

TABLE IV. Effects of Hydrogen Contamination on Room Temperature Rupture Behavior of Ti-140A, Ht. M1170 (Unnotched Specimens)

Hydrogen = 10 p.p.m.			Hydrogen = 170 p.p.m.		
Stress (1000 p.s.i.)	Fracture time (hr.)	Red. in area (%)	Stress (1000 p.s.i.)	Fracture time (hr.)	Red. in area (%)
137	0.4	52	136	0.3	16
118	Did not fracture in 803 hrs.		131	13.1	13
102	Did not fracture in 1244 hrs.		129	2.5	13

Hydrogen = 250 p.p.m.		
Stress (1000 p.s.i.)	Fracture time (hr.)	Red. area (%)
138	0.1	19
119	2.4	3
101	Did not fracture in 1244 hrs.	

strain aging embrittlement are how slow the strain rate must be for an appreciable ductility reduction to be apparent, and the minimum hydrogen content required to produce it at any strain rate.

Consider now the rupture test data for unnotched specimens. For both hydrogen-free and hydrogen-containing materials, as the stress level is decreased the time to fracture is increased. The rate of increase of fracture time with decrease of stress is much greater for hydrogen-free than for hydrogen-containing material. Furthermore, the ductility of hydrogen-free specimens is relatively independent of stress level or time to fracture, whereas that of hydrogen-containing specimens decreases markedly as time to fracture increases. Very

high stress levels and short fracture times correspond to rapid rates of plastic deformation and this is analogous to fast strain rates in the tensile test. In Figure 3, ductility measured as reduction in area is plotted against time to fracture for both tensile test and rupture test specimens. It is recognized that such a comparison can be only approximately valid, but the data do indicate the importance of time to fracture in determining the extent of embrittlement developed in either tensile or rupture tests. Time to fracture in the tensile test is controlled by the strain rate, and in the rupture test by the stress level. If time to fracture is sufficiently short the hydrogen-contaminated material tends to act in a ductile manner.

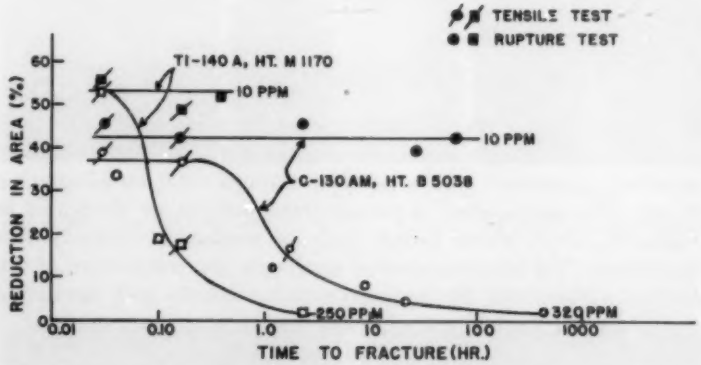

Fig. 3. Influence of time to fracture on ductility measured in room temperature tensile and rupture tests. Unnotched specimens.

It was difficult to make accurate measurements of ductility for the notched specimens; however, the data that are presented in Figure 2A include an indication of the reduction in area at fracture. Qualitatively, the behavior of notched specimens is quite comparable to that of unnotched specimens. At very high stresses and short fracture times the hydrogen-free and hydrogen-containing specimens fracture in comparable times, both in a ductile manner. At lower stress levels where the hydrogen-free specimens fracture in long times still in a ductile manner, or do not fracture, the hydrogen-containing specimens show premature brittle fracture. The data in Figure 2C are all in the range in which the hydrogen-containing specimens fracture in a premature brittle manner.

In rupture tests as in tensile tests there are two important features of the strain aging embrittlement; a minimum rupture time which is necessary for embrittlement to be observed, and a minimum hydrogen content for premature brittle fracture even at very long rupture times. It is evident that a strain aging mechanism for the hydrogen embrittlement must explain premature and low stress fracture in sustained loading as well as the strain rate sensitivity of the ductility.

The characteristic qualitative features of the strain aging hydrogen embrittlement are as described above; the influence of factors such as specimen surface condition, specimen type, hydrogen content, alloy composition, and microstructure will be discussed below. All these factors affect quantitative rather than qualitative aspects of the embrittlement.

IV. SPECIMEN SURFACE CONDITION

The unnotched cylindrical specimens that were tested had one of the following surface conditions: as-machined; machined + rough polished; machined + fine polished through 0000 metallographic paper. The appearances of the specimen surfaces are illustrated in Figure 4, which shows broken ends of mechanical property test specimens. For the as-machined specimens, the intersection of the fracture surface with the specimen surface coincides with machining marks around most if not all of the specimen circumference. For rough polished specimens part of the intersection of the fracture surface with the specimen surface coincides with polishing scratches. For the fine polished specimens there was no apparent influence of specimen surface marks. These observations are general for both hydrogen-free or hydrogen-containing specimens tested in tensile or rupture tests.

The appearances of the fracture surfaces of unnotched specimens are shown in Figure 5, and will be discussed more fully in Section VIII. Two types of fracture surface are observed, one for specimens which fracture in a ductile manner, and one for specimens which fracture due to strain aging hydrogen embrittlement. For either ductile or hydrogen embrittled specimens, the appearance of the fracture surface is similar for all three types of specimen surface.

The ductile fracture specimens show a classical "cup and cone," and it is generally agreed that fracture is initiated in the interior of

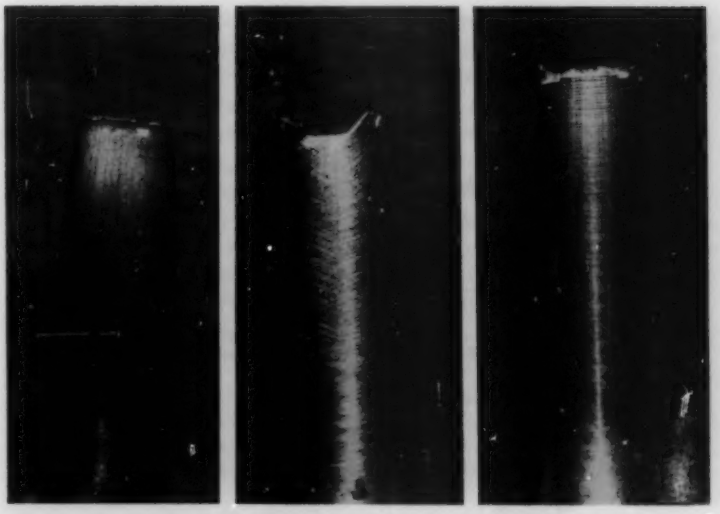

(a) (b) (c)

Fig. 4. Effects of specimen surface condition: (a) fine polished, (b) rough polished, (c) as-machined.

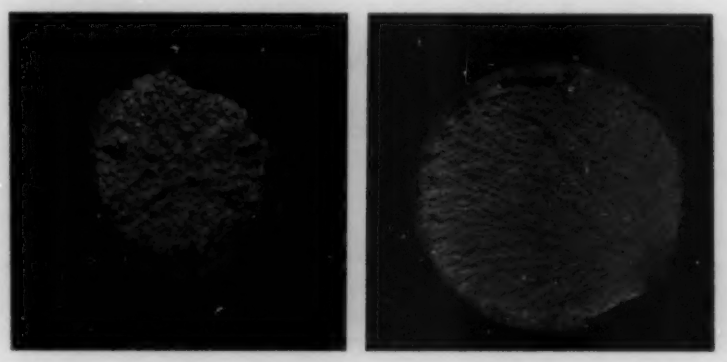

(a) (b)

Fig. 5. Appearances of fracture surfaces for unnotched specimens: (a) ductile fracture, (b) brittle fracture due to strain aging hydrogen embrittlement.

such a specimen. The effects of surface condition on tensile or rupture properties should be minor for specimens with this type of fracture. For the brittle fracture specimens with as-machined or rough polished surfaces, the fracture nucleus can usually be associated

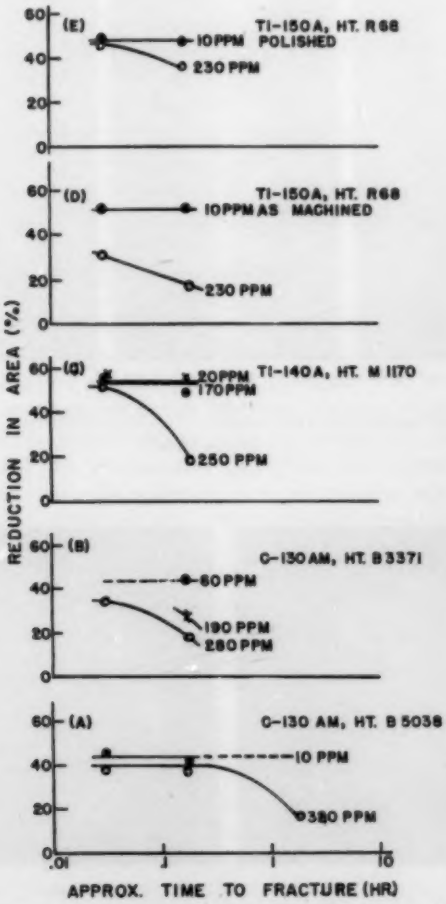

Fig. 6. Effects of various factors on ductility measured in room temperature tensile tests. Unnotched specimens.

with a scratch on the surface. For the fine polished, brittle fracture specimens no association of the fracture nucleus with visible surface scratches is apparent.

Data on the effects of specimen surface condition on mechanical properties are presented in Table V and Figures 6d and 6e for tensile tests, and in Table VI for rupture tests. As expected, specimen surface condition has no significant effect upon the mechanical properties of ductile, hydrogen-free material. For hydrogen-containing material specimen surface condition does not affect qualitative features of the strain aging embrittlement, but it does have quantitative effects. In rupture tests at a given stress level, the polished specimens require a longer time for premature brittle fracture. In tensile tests there is an indication that polished specimens may require slower strain rates for an appreciable ductility reduction to be apparent. An alternate explanation of the tensile test data in Figures 6D and 6E is that in some alpha-beta alloys hydrogen can cause a notch sensitivity type of embrittlement at fast strain rates in addition to the strain aging embrittlement being considered here.

TABLE V

Effects of Specimen Surface Condition on Room Temperature Tensile Behavior of Low Hydrogen Material

Surface condition	Testing speed (in./min.)	Ult. tensile strength (1000 p.s.i.)	Red. in area (%)
C-130AM, Ht. B5038, 10 p.p.m.			
Rough polished	0.02	138	43
Fine polished	0.02	142	44
Ti-150A, Ht. R68, 10 p.p.m.			
As-machined	0.1	142	52
Fine polished	0.1	143	49
As-machined	0.02	143	52
Fine polished	0.02	141	46

With the exception of the fine polished specimens of Ti-150A, and the specimens of Ti-140A, Ht. M1170, 250 p.p.m., the unnotched hydrogen-containing (above 100 p.p.m.) specimens for which data are reported in Tables III and IV and Figures 1, 3, and 6 had as-machined surfaces. The specimens of Ti-140A, Ht. M1170, 250 p.p.m. had as-machined + rough polished surfaces.

TABLE VI
Effects of Specimen Surface Condition on Room Temperature Rupture Behavior of C-130AM, Ht. B5038

Surface condition	Stress (1000 p.s.i.)	Time to fracture (hrs.)	Red. in area (%)
	10 p.p.m.		
Rough polished.....	135	27	40
Fine polished.....	135	9.3	39
	320 p.p.m.		
As-machined.....	130	6.0	8.1
As-machined.....	130	6.7	9.4
Fine polished.....	130	203	9.1
Fine polished.....	130	47	10.6

Any conclusions in this paper which rest upon quantitative aspects of the tensile or rupture data have been evaluated for the possibility that variations in specimen surface condition are producing spurious results. Quantitative comparisons are presented only when such a possibility is very remote.

The V-notched cylindrical specimens tested were all machined in the same way. Inspection of fractured specimens indicates no evidence for any effects of machining marks at the root of the notch.

V. SPECIMEN TYPE

A variety of notched and unnotched tensile and rupture test specimens have been used (Fig. 7). These have included cylindrical specimens from barstock and forgings and flat specimens from various gages of sheet. The effects of hydrogen on tensile and rupture test behavior are qualitatively the same for all of these specimen types.

Rupture data for unnotched and V-notched cylindrical specimens are compared in Figure 8. The extrapolation of the curve for notched specimens to cross that for unnotched specimens is justified by the general experience that these notched specimens can show premature brittle fracture at lower nominal stresses than unnotched specimens (*e.g.*, see data for Ti-140A, Ht. M1170). Premature brittle fracture in notched specimens can occur at nominal stresses as low as 40% of the short time notched tensile strength. The qualitative features of strain aging hydrogen embrittlement are the same for both types of specimens. For each there is a stress above which fracture will be ductile due to short fracture time,

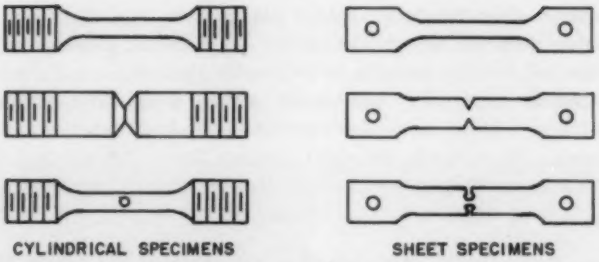

Fig. 7. Mechanical property specimens that have been tested. Not drawn to scale. Mechanical property data are reported only for the unnotched and V-notched cylindrical specimens.

and naturally there is a stress below which fracture will not occur in time periods of practical interest. In each case there is an intermediate range of stress over which hydrogen-contaminated specimens fracture prematurely, in a brittle manner. However, for this V-notched specimen, the range of stress (nominal stress based on original cross-sectional area) over which premature brittle fracture can occur is much greater than for unnotched specimens. Two factors must be considered to understand the effect of this type of notch: the triaxial

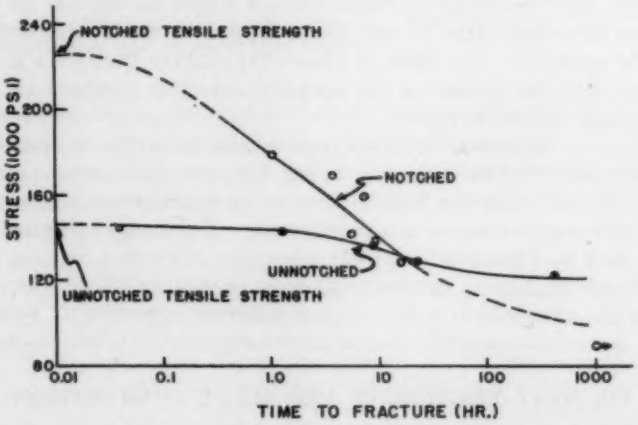

Fig. 8. Comparison of room temperature rupture data for unnotched and V-notched cylindrical specimens. C-130AM, hydrogen = 320 p.p.m.

stress state which tends to restrict plastic flow, and the stress concentration near the root of the notch. The former causes the short time notched tensile strength to be greater than the unnotched ultimate tensile strength. The latter allows long time premature brittle fracture to occur at lower stresses in notched than in unnotched specimens. As a result, for short rupture times the notched specimens require a higher stress than the unnotched specimens; for relatively long times to rupture the reverse is true.

VI. HYDROGEN CONTENT

At the low hydrogen contents of the vacuum annealed "hydrogen-free" material none of the alloys tested exhibit any tendency toward strain aging embrittlement. There must, therefore, be some minimum hydrogen content below which embrittlement will not occur no matter how slow the strain rate is in a tensile or rupture test.

The influence of hydrogen content above this minimum, on tensile test ductility, is illustrated by the data in Figures 6C and 6D. At a hydrogen content of 170 p.p.m. the alloy Ti-140A, Ht. M1170 will show premature brittle fracture in rupture tests and it can therefore be assumed that there would be a reduction in tensile test ductility if slower strain rate tensile tests were performed. It may be concluded that increasing hydrogen content allows an increase in the strain rate which must be used for an appreciable ductility reduction to be apparent. The data in Figure 6D indicate that for a given strain rate the amount of the ductility reduction increases as the hydrogen content increases.

Since the dependence on strain rate or time to fracture is similar in tensile and rupture tests, increasing the hydrogen content must decrease the minimum time to fracture at which premature brittle fracture can be observed in a rupture test. The times to fracture for the data in Figures 6C and 6D are above this minimum, and the hydrogen containing specimens all show premature brittle fracture. At a given stress level in this range of behavior, increasing the hydrogen content decreases the time required for premature brittle fracture.

VII. HEAT TREATMENT AND ALLOY COMPOSITION

Rupture test data on two heat treated conditions of a hydrogen containing material are presented in Table VII. One set of otherwise

identical specimen blanks was furnace cooled from a temperature low in the alpha-beta range for this alloy, the other was air cooled from a temperature higher in the alpha-beta range. Microstructures obtained are shown in Figures 9a and 9b. The rupture data indicate

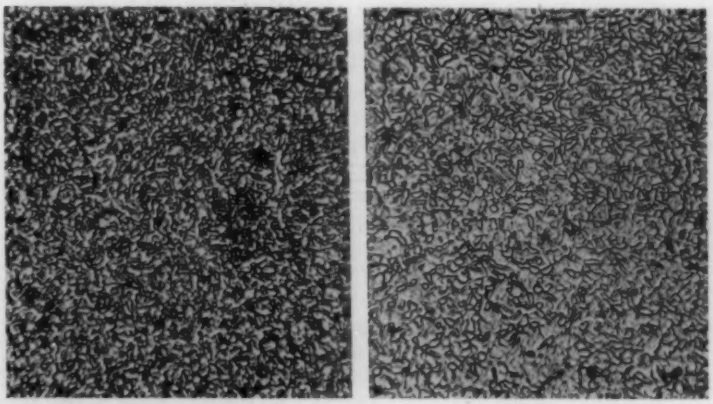

(a) (b)

Fig. 9. Photomicrographs of Ti-140A, Ht. M1192, 210 p.p.m. Unstrained material. Perpendicular to rolling direction. Mag. 500×. (a) Furnace cooled from 1200°F. (b) Air cooled from 1350°F.

that heat treatment alone can cause profound differences in the susceptibility of a given alloy to hydrogen embrittlement.

At appropriate hydrogen levels or heat treatments strain aging hydrogen embrittlement has been observed in alpha-beta alloys with the following nominal compositions:

Ti-8Mn
Ti-4Al-4-Mn
Ti-6Al-4V
Ti-1.5Fe-2.7Cr
Ti-2Fe-2Cr-2Mo
Ti-3Mn-1Fe-11V-Cr-1Mo

Note that embrittlement can occur whether or not a eutectoid reaction is possible.

As a consequence of the vacuum annealing, hydrogenation, and homogenization treatments described previously, the materials now to be discussed were in: annealed low in the alpha-beta region + furnace-cooled conditions. Microstructures before mechanical property testing are shown in Figures 13, 14b, 15, and 17a. Variations in prior mill processing caused a variety of microstructures even though the final thermal treatments for these materials were similar. Tensile and rupture data pertinent to this discussion are contained in Figures 2, 3, and 6 and Table VIII. It is evident that, although heat treatment can have an effect, susceptibility to hydrogen embrittlement is not peculiar to one particular type of microstructure.

TABLE VII

Effect of Heat Treatment on Susceptibility to Hydrogen Embrittlement (Room Temperature Rupture Tests on Notched Specimens of Ti-140A, Ht. M1192)

Heat treated condition	Stress (1000 p.s.i.)	Time to fracture (hrs.)
Furnace cooled from 1200°F....	168	1.0
	146	4.0
Air cooled from 1350°F.....	169	Did not fracture in 93 hrs.
	143	Did not fracture in 1300 hrs.

The tensile test data in Figures 6A and 6B are for two heats of nominally the same alloy, both given final thermal treatments of furnace cool from 1300°F., and both with very similar microstructures. Due to slight differences in composition or mill processing a much lower strain rate (longer time to fracture) must be used in order to observe embrittlement in Ht. B5038 than in Ht. B3371 even though the former has a higher hydrogen content. The notched rupture test data in Figures 2A and 2B show a similar difference in the time to rupture at a given stress level. Other comparisons are possible from the data in Figures 2, 3, and 6 to show that alloy composition or microstructure or an interaction between these two can affect quantitative features of the embrittlement such as minimum time to fracture for embrittlement to be produced in either tensile or rupture tests, or time to premature brittle fracture at a given stress level in the rupture tests. For example, even polished specimens of Ti-150A, Ht. R68 at 250 p.p.m. require a shorter minimum time to fracture in tensile tests than as-machined specimens of C-130AM, Ht. B5038 at 320 p.p.m.

TABLE VIII. Room Temperature Mechanical Properties of a Material Which Does Not Exhibit Strain Aging Embrittlement at a Hydrogen Content of 260 p.p.m. (Ti-155AX)

Hydrogen = 5 p.p.m.				Hydrogen = 260 p.p.m.			
Tensile Tests							
Testing speed (in./min.)	Unnotched ult. tensile strength (1000 p.s.i.)	Unnotched red. in area (%)	Notch tensile strength (1000 p.s.i.)	Testing speed (in./min.)	Unnotched ult. tensile strength (1000 p.s.i.)	Unnotched red. in area (%)	Notch tensile strength (1000 p.s.i.)
0.1	159	44	—	0.1	165	40	—
0.02	161	45	253	0.02	164	37	252
Unnotched Rupture							
Stress (1000 p.s.i.)	Time to fracture (hrs.)	Red. in area (%)		Stress (1000 p.s.i.)	Time to fracture (hrs.)	Red. in area (%)	
158	1.2	43		157	106	43	
154	Did not fracture in 1200 hrs.			156	Did not fracture in 1200 hrs.		
Notched Rupture							
Stress (1000 p.s.i.)	Time to fracture (hrs.)			Stress (1000 p.s.i.)	Time to fracture (hrs.)		
200	64			200	122		
176	Did not fracture in 650 hrs.			176	Did not fracture in 652 hrs.		

Table VIII and Figure 18 present data for an alpha-beta alloy, in an annealed condition, at a hydrogen level which does cause embrittlement in many other alpha-beta alloys. However, this alpha-beta alloy does not show any evidence for strain aging hydrogen embrittlement. It is evident that composition or microstructure or an interaction between these two can also affect the minimum hydrogen content which can cause embrittlement even at very slow strain rates.

Although these data do not provide an unequivocal demonstration of the effect of composition as separated from the possible effects of heat treatment or an interaction between composition and heat treatment, it is felt that composition must be an important primary variable contributing to the susceptibility of a given material to strain aging hydrogen embrittlement.

VIII. MACROSCOPIC EXAMINATION OF FRACTURED SPECIMENS

The appearances of the fracture surfaces of unnotched cylindrical specimens are presented in Figure 5 and have been partially discussed. Ductile fracture, whether for hydrogen free material, or for hydrogen-containing material tested at high strain rates, results in a characteristic "cup and cone" appearance around the entire circumference of the specimen. For brittle fracture the cup and cone characteristics are greatly reduced and do not extend entirely around the specimen circumference. The portion of the fracture surface which is perpendicular to the specimen axis has a relatively smooth area adjacent to the portion of the specimen circumference where the cup and cone appearance is absent, and a rougher area radially opposite to this. It should be mentioned that similar fracture surfaces have been observed to result from brittle behavior in titanium alloys due to causes other than strain aging hydrogen embrittlement.

The appearance of ductile and premature brittle fractures in notched sheet specimens is presented in Figure 10. Premature brittle fractures contain a smooth area, perpendicular to the specimen axis, extending from the root of the notch. Note that the extent of this smooth area is greater, the smaller the stress level which caused fracture.

Fig. 10. Appearances of fractures in notched specimens of Ti-6Al-4V Sheet. *Top:* Ductile fracture. Hydrogen = 50 p.p.m. Short time tensile test. *Middle:* Brittle fracture. Hydrogen = 800 p.p.m. Rupture test at 130,000 p.s.i. Rupture time = 9 hrs. *Bottom:* Brittle fracture. Hydrogen = 800 p.p.m. Rupture test at 60,000 p.s.i. Rupture time = 91 hrs.

The appearance of these hydrogen embrittled fracture surfaces suggests that the nucleus of fracture is in the smooth area at or near the specimen surface. Premature brittle fracture consists of growth of this nucleus into a crack which propagates across the specimen until the residual cross-sectional area can no longer support the applied load, followed by ductile fracture in this residual cross section.

The appearance of the fracture surface of a hydrogen containing V-notched cylindrical specimen is shown in Figure 11. With these specimens it was not possible to establish clear-cut differences between the general appearances of ductile and premature brittle fractures, but it was noted that hydrogen-contaminated specimens contain cracks running more or less parallel to the specimen axis. The intersection of such cracks with the fracture surface can be seen in Figure 11. A section taken parallel to the specimen axis is shown in Figure 12, and further illustrates the nature of these cracks. A few tensile test specimens were examined immediately after fracture and thereafter. In this case, visible cracks could not be detected immediately

Fig. 11. Appearance of the fracture surface for notched specimens of high hydrogen material. Both ends of one specimen. Note the postfracture cracks.

after fracture but were present 1 week later. Examination of all other specimens was at least several weeks after fracture. In general, the crack traces in the fracture surfaces of the two broken ends of the specimen do not coincide if the fracture surfaces are brought together; this is another indication that most of the cracks tend to form over a period of time after fracture. Such postfracture cracks are found in the broken ends of almost all cylindrical V-notched specimens where the hydrogen content is such as to render the particular material under test susceptible to strain aging embrittlement. They occur irrespective of whether high or low strain rates leading to ductile or brittle original fractures are used. Postfracture cracks are also prevalent in unnotched cylindrical specimens if high strain rates

Fig. 12. Postfracture cracking. Longitudinal section through fractured end of notched, high hydrogen specimen.

leading to ductile fractures preceded by necking are employed. Unnotched specimens which fail in a brittle manner, with little or no necking, exhibit little or no postfracture cracking.

It is evident that this postfracture cracking is due to the same strain aging hydrogen embrittlement that leads to premature brittle fracture in rupture tests, and is caused by residual radial stresses in the 2 halves of the fractured specimen. The radial stresses are set up by the triaxial stress state induced in cylindrical specimens by a notch or necked region.

IX. MICROSCOPIC EXAMINATION

Representative microstructures of unstrained material, and of material near the fracture surfaces of test specimens, are shown in

Figures 13 to 19. Sections have been taken both perpendicular to and parallel to the rolling direction of the barstock. The hydrogen-free and hydrogen-containing materials, in an unstrained condition, have essentially the same microstructure. Examination of the region near fracture in mechanical property test specimens shows that testing does not affect the microstructure of hydrogen-free material. Similarly, for many of the materials tested, fracture due to strain aging hydrogen embrittlement is not accompanied by visible microstructural changes. There are occasionally some indications of a precipitate near the ends of postfracture cracks, but this evidence is not at all clear-cut. For Ti-150A, Ht. R68 a dark etching precipitate *does*

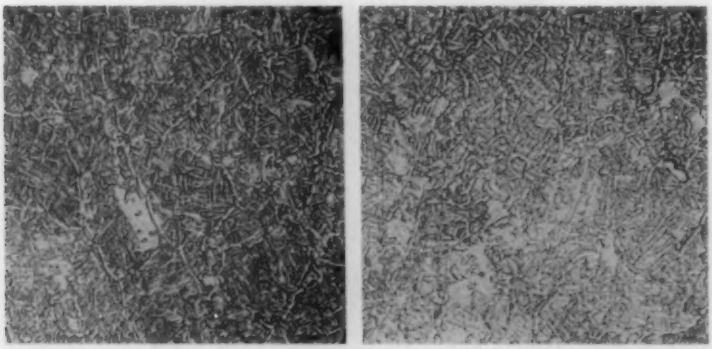

(a) (b)

Fig. 13. Photomicrographs of Ti-140A, Ht. M1170. Unstrained material. Perpendicular to rolling direction. Mag. 500×. (a) 20 p.p.m. (b) 170 p.p.m.

appear in strained regions of the hydrogen-containing fractured test specimens. It is most prevalent near the original fracture surface and around the ends of postfracture cracks. This precipitate can be redissolved to yield a microstructure comparable to that in unstrained material by heating in air or inert gas. Most of the precipitate disappears after 45 hours at 800°F.; after 7 hours at 1200°F. it has been completely redissolved. Figure 17d shows a partially redissolved precipitate at the end of a postfracture crack.

The postfracture cracks present in Figures 14c, 16b, 17c, and 18c tend to follow an intergranular path. From this it may be concluded that strain aging hydrogen embrittlement leads to intergranular fracture.

X. DISCUSSION

There is a marked similarity between the qualitative aspects of hydrogen embrittlement in steel[11–14] and strain aging hydrogen

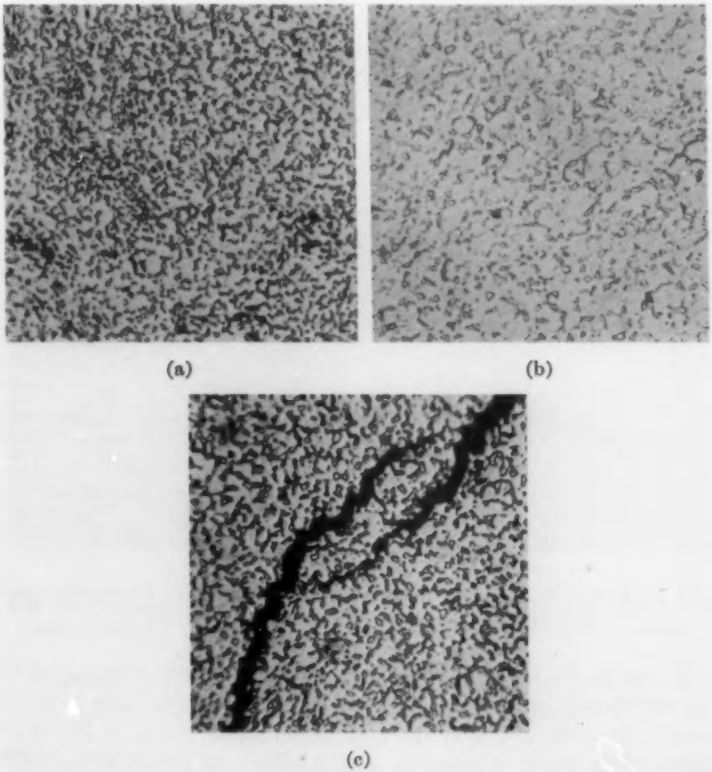

Fig. 14. Photomicrographs of C-130AM, Ht. B3371, perpendicular to rolling direction. Mag. 500×. (a) 60 p.p.m., near fracture. (b) 280 p.p.m., unstrained material. (c) 280 p.p.m., near fracture.

embrittlement in alpha-beta titanium alloys. It is quite possible that the mechanisms of embrittlement are also very similar.

The following is proposed as the framework for a mechanism of strain aging hydrogen embrittlement in alpha-beta titanium alloys.

Initially, in unstrained materials, the hydrogen is in interstitial solid solution. Plastic deformation provides microscopic regions toward which there is a tendency for the hydrogen to segregate. The net result of such microsegregation is to provide regions where microcracks can be initiated and propagate, thus providing a low stress route to brittle fracture.

The similarity between the microstructures of unstrained hydrogen free and hydrogen containing alpha-beta alloys suggests that initially the hydrogen is in interstitial solid solution. The titanium-hydrogen phase diagram[3] indicates that hydrogen is a beta phase stabilizer, and has very little room temperature solid solubility in unalloyed alpha phase. It is conceivable that alloying the alpha or beta phases

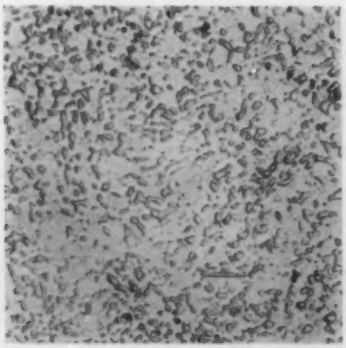

Fig. 15. Photomicrograph of C-130AM, Ht. B5038, 320 p.p.m. Unstrained material. Perpendicular to rolling direction. Mag. 500×.

can change the solid solubilities of hydrogen in these phases, but in alpha-beta alloys such as Ti-1.5Fe-2.5Cr in which the alpha phase is relatively pure, the hydrogen, at room temperature, is probably partitioned to the beta phase. Even within unstrained beta phase there will be a tendency for the interstitial hydrogen atoms to segregate to lattice defects such as dislocations, vacancies, or grain boundaries. The intercrystalline nature of hydrogen embrittlement fractures suggests that plastic deformation affects the structure in some manner as to establish more sites for such segregation at the grain boundaries. The hydrogen atoms will tend to diffuse toward such sites. The extent of such microsegregation will depend upon the extent of the deformation, the partition function between the new

sites and the remainder of the beta phase, the initial concentration of hydrogen in the beta phase, and the rate at which the necessary diffusion can occur. It is suggested that if this microsegregation causes a high enough local concentration of hydrogen atoms, a microcrack can be formed. The exact manner of formation of the intercrystalline microcrack cannot yet be described; in at least one of the materials tested there is evidence that it involves formation of a third, possibly hydride, phase. Another possibility involves condensation of molecular hydrogen in lattice vacancies. Growth of the microcrack may involve a continuation of this embrittlement process in the strained material around the periphery of the crack.

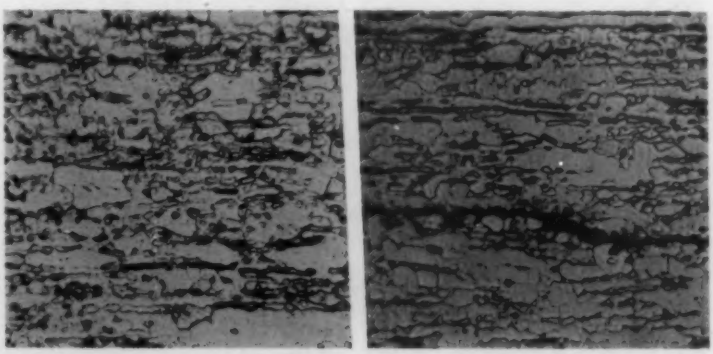

(a) (b)

Fig. 16. Photomicrographs of C-130AM, Ht. B5038, 320 p.p.m. Parallel to rolling direction. Mag. 500×. (a) Unstrained material. (b) Near fracture.

Application of this mechanism to the mechanical property data must consider both the tendency toward microsegregation and the rate at which microsegregation and consequent embrittlement can occur. The tendency toward microsegregation is provided by the initial hydrogen concentration, and plastic deformation which may be quite localized. The rate of microsegregation, involving diffusion of the hydrogen, may be relatively slow. Ductility measured in a tensile test will depend upon the rate at which this microsegregation can occur relative to the rate of straining imposed on the material. At high strain rates the material fails in a ductile manner by plastic deformation before appreciable microsegregation and consequent embrittlement can occur. At very slow strain rates a localized region

of the specimen is sufficiently deformed to induce microsegregation, and this takes place with consequent fracture before total deformation of the specimen is very great. Similarly, in rupture tests at very

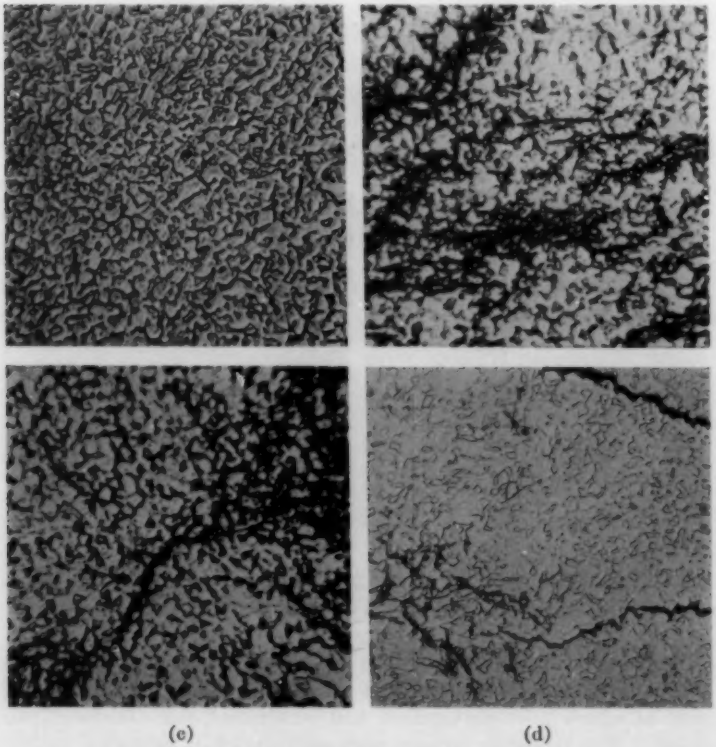

Fig. 17. Photomicrographs of Ti-150A, Ht. R68, 250 p.p.m. Perpendicular to rolling direction. Mag. 500×. (a) Unstrained material. (b) Near fracture, third phase. (c) Near fracture, postfracture crack and third phase. (d) Postfracture crack plus partially redissolved third phase.

high stress levels the rate of straining due to creep is so great that ductile fracture occurs before microsegregation is appreciable. At low stresses, where creep is slow, a critical amount of deformation in a localized section leads to microsegregation and fracture before

much creep can occur. This can happen even at stress levels where the creep is so slow that normal ductile fracture would not occur in time periods of practical interest. The time for premature brittle fracture in a rupture test at a given stress level will depend upon the time required for sufficient plastic deformation to initiate the embrittlement, the rate at which microsegregation occurs, and the rate of propagation of the microcrack which is formed.

A stress concentration such as exists at a notch or a surface scratch can lower the stress, or at a given stress can decrease the time required

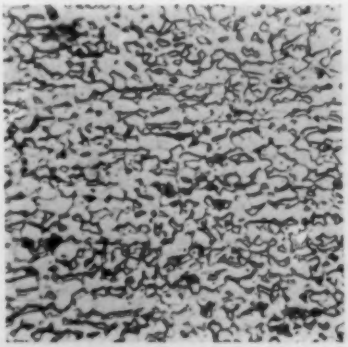

(a)

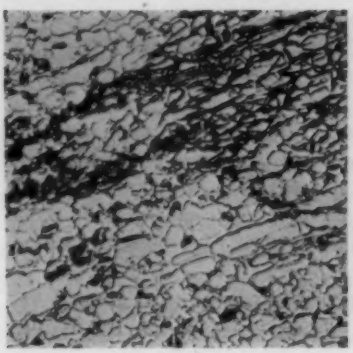

(b)

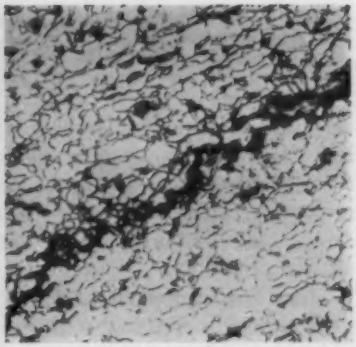

(c)

Fig. 18. Photomicrographs of Ti-150A, Ht. R68, 250 p.p.m. Parallel to rolling direction. Mag. 500×. (a) Unstrained material. (b) Near fracture, third phase at end of postfracture crack. (c) Near fracture, postfracture crack.

for sufficient localized plastic deformation to initiate the embrittlement. In some notched specimens the complicating influences of triaxial stress states must be considered.

At this stage in the discussion the information available[5–7,9] on the effects of test temperature on strain aging hydrogen embrittlement should be considered. If tensile tests at a constant slow strain rate are performed over a range of temperatures the ductility reduction due to hydrogen is zero at high temperatures, goes through a maximum as temperature is decreased, and again approaches zero at very low temperatures. The temperature of the maximum ductility reduction

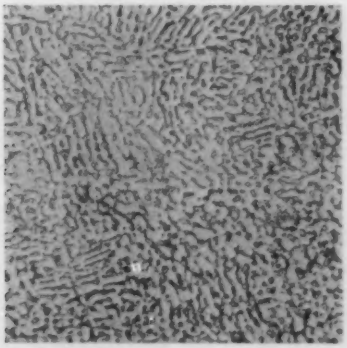

Fig. 19. Photomicrograph of Ti-155AX, 260 p.p.m. Unstrained material. Perpendicular to rolling direction. Mag. 500×. This material not susceptible to strain aging hydrogen embrittlement.

depends upon the alloy, hydrogen content, and strain rate, and may be below room temperature. Rupture tests performed at room and elevated temperatures indicate that a hydrogen content that leads to premature brittle fracture at room temperature, may not do so at elevated temperatures. Rupture tests at subzero temperatures have not been reported.

These data suggest that temperature affects both the susceptibility toward embrittlement at a given hydrogen content, and the rate at which embrittlement can occur. Increasing test temperature might be expected to affect the tendency for hydrogen to partition between general interstitial solid solution and microsegregation to deformation

induced sites in favor of the former. Therefore, increasing test temperature decreases the tendency toward embrittlement. Decreasing the temperature decreases the rate at which hydrogen can diffuse, and therefore decreases the rate at which embrittlement can occur even though the tendency toward embrittlement is increased. In tensile tests at a constant strain rate there will be no ductility reduction at elevated temperatures because there is no tendency toward embrittlement. At very low temperatures there is no ductility reduction because the rate of embrittlement is slow with respect to the strain rate. Between these two temperature extremes the ductility reduction goes through a maximum.

The effects of composition and microstructure on susceptibility to strain aging hydrogen embrittlement have been demonstrated, and may be due to many causes. Composition can be expected to affect the solubilities of hydrogen in the alpha and beta phases, and the partition between general interstitial solution and microsegregation. Heat treatment can affect the ratio of alpha phase to beta phase present at room temperature, and the compositions of these phases. Heat treatment and differences in content of other interstitial elements can affect the nature of the alpha-beta grain interfaces, which, since fracture is intergranular, should influence the strain aging embrittlement.

Attention in this report has been focused on strain aging hydrogen embrittlement; it must be pointed out, however, that hydrogen can have additional effects on the properties of alpha-beta alloys. With some alpha-beta alloys suitable combination of hydrogen content and heat treatment may result in material which, at room temperature, has a hydride phase in its microstructure.[15] This might be expected to produce the greatest reduction in ductility when the material is tested at fast strain rates and in itself should not cause the premature brittle fracture in rupture tests which is characteristic of strain aging embrittlement. At elevated temperatures where strain aging embrittlement does not occur, a different type of embrittlement frequently takes place.[6] Here, specimens which have been exposed to elevated temperature creep conditions are found to have lowered ductility when tested in subsequent room temperature, fast rate tensile tests. When strain aging embrittlement can occur in conjunction with these other types of embrittlement, the effects of hydrogen on the mechanical properties may be quite complex.

XI. SUMMARY

Hydrogen contamination can cause more than one type of embrittlement in alpha-beta titanium alloys. In this report attention is focused upon strain aging embrittlement which occurs at room temperature. Only alpha-beta alloys are considered.

Strain aging embrittlement has its greatest effect on properties measured at slow strain rates. It can cause low ductility in room temperature tensile tests, and premature brittle fracture in room temperature rupture tests. The presence of stress concentrations lowers the applied load at which premature brittle fracture can occur.

Susceptibility to strain aging embrittlement is a function of alloy composition and microstructure. Both the minimum hydrogen content required to produce embrittlement and how slow the strain rate must be for embrittlement to be perceptible may be affected.

Strain aging embrittlement can occur whether or not the alloy composition is such that a eutectoid reaction is possible.

Examination of fracture surfaces suggests that premature brittle fracture consists of propagation of a crack until the residual cross-sectional area can no longer support the applied load, followed by ductile fracture in this residual cross-section.

In many of the alpha-beta alloys tested, metallographic examination of hydrogen contaminated specimens shows no evidence for a third phase either before or after fracture. In at least one alloy a third phase was visible after fracture.

Many of the broken ends of hydrogen contaminated mechanical property test specimens develop cracks which are parallel to the long axis of the specimen. This occurs after the specimen is broken in a mechanical property test which causes a triaxial state of stress. These cracks are presumably hydrogen embrittlement fractures due to residual radial stresses, and they tend to be intergranular.

Increasing test temperature seems to decrease the tendency toward hydrogen embrittlement but increase the rate at which it can occur.

A mechanism of strain aging embrittlement is suggested which involves microsegregation of hydrogen to the grain boundaries in plastically deformed material. This microsegregation involves diffusion of the hydrogen and proceeds at a finite rate. Properties measured in a mechanical property test depend upon whether the rate of deformation is fast or slow relative to the rate of microsegregation and consequent embrittlement.

References

1. R. I. Jaffee and I. E. Campbell, *Trans. AIME*, **185**, 646–655 (1949); *J. Metals* (September, 1949).

2. C. M. Craighead, G. A. Lenning, and R. I. Jaffee, *Trans. AIME*, **194**, 1317–1319 (1952); *J. Metals* (December, 1952).

3. G. A. Lenning, C. M. Craighead, and R. I. Jaffee, *Trans. AIME*, **200**, 367–376 (1954); *J. Metals* (March, 1954).

4. F. C. Holden, H. R. Ogden, and R. I. Jaffee, *Trans. AIME*, **200**, 169–184 (1954); *J. Metals* (February, 1954).

5. R. J. Kotfila and E. F. Erbin, *Metal Progress*, **66**, 128–131 (October, 1954).

6. H. M. Burte, E. F. Erbin, G. T. Hahn, R. J. Kotfila, J. W. Seeger, and D. A. Wruck, *Metal Progress*, **67**, 115–120 (May, 1955).

7. R. I. Jaffee, G. A. Lenning, and C. M. Craighead, paper presented at AIME meeting, New York (February, 1956).

8. C. M. Craighead, G. A. Lenning, and R. I. Jaffee, paper presented at AIME meeting, New York (February 1956).

9. Ripling, E. J., *Trans. AIME*, **206**, 502–503 (1956); *J. Metals* (May, 1956).

10. H. A. Kessler, R. G. Sherman, and J. F. Sullivan, *J. Metals*, **7**, 242–246 (February, 1955).

11. E. R. Slaughter, *J. Metals*, **8**, 430–431 (April, 1956).

12. J. T. Brown and W. M. Baldwin, *Trans. AIME*, **200**, 298–303 (1954).

13. C. A. Zapffee and C. E. Sims, *Trans. AIME*, **145**, 225–271 (1941).

14. N. J. Petch and P. Stables, *Nature*, **169**, 842–843 (1952).

15. C. W. Phillips, "The Effect of Heat Treatment on the Structure of a Commercial Titanium-Rich Alloy," Ph.D. Thesis, University of Michigan, 1954.

Synopsis

Hydrogen contamination in the alpha-beta class of titanium alloys leads to a very pronounced strain rate sensitivity of the ductility of these materials, and to low stress, premature fracture under sustained tensile loading (creep). The effects of strain rate, hydrogen concentration, temperature, stress concentrations, alloy composition, and microstructure are described. A mechanism for this strain aging embrittlement is suggested which involves plastic deformation inducing microsegregation of interstitially dissolved hydrogen to the grain boundaries of these two-phase polycrystalline materials. This microsegregation involves diffusion of the hydrogen and proceeds at a finite rate. Properties measured under various conditions of loading depend upon whether the rate of deformation is fast or slow relative to the rate of microsegregation and consequent embrittlement.

TRANSACTIONS OF THE SOCIETY OF RHEOLOGY VOL. I, 153–168 (1957)

A Stochastic Process Model for Mechanical Breakdown

BERNARD D. COLEMAN, *E. I. du Pont de Nemours and Company, Carothers Research Laboratory, Wilmington, Del.*

I. INTRODUCTION

The purpose of this article is to present the development of an abstract model for discussing the kinetic events occurring in the failure of a load-bearing fiber. The essential feature of this model is that it regards mechanical failure as being a stochastic process whose primary event is the breaking of a localized chemical bond. It turns out that this assumption is sufficient, even when crudely developed, to account qualitatively for the size-dependence, the time-dependence, and the extreme autocatalytic nature of mechanical breakdown phenomena.

Most of the present discussion is confined to a "perfect" fiber of uniform cross-section which contains no defects or Griffith flaws.[1–4] Recognition is taken, however, of the fact that the time of occurrence of microscopic events, such as the breaking of chemical bonds, cannot be exactly predicted, even if the applied stress is exactly known.

Tensile strength measurements have the distinctive characteristic that they measure a property of the *weakest cross-section*, and not a *volume-average* quantity. As a consequence of this, we cannot say that it is *obvious* that a long perfect fiber, free from flaws, and containing, say, 10^9 molecules per cross-section, possesses fluctuations in tensile strength too small to be measured. In the present treatment, however, it is proved that such is the case, and it is also shown that, though the tensile strength of a perfect test sample depends on its length, the dependence is slight. This result confirms an assumption commonly made,[3,4] namely, that the relatively large variance and "size effects" encountered in real fibers must be due to the presence

of flaws. Toward the end of this article a route is suggested for extending the theory to discussions of imperfect systems when the distribution of flaws is known.

The tensile strength of many materials, including the oriented polymeric fibers of textile importance, increases somewhat as the speed of measurement increases[5–8] (or the time interval allowed for failure decreases). For example, the early work of Peirce[5,6] has shown that the tensile stress supported by cotton yarns and filaments increases about 10% for every tenfold increase in the speed of measurement over a range of breaking times of about seven decades. The model of the present theory apparently accounts for such observations quite satisfactorily, in contrast to the static statistical models which, in the classical theories,[2,4,10,11] have been treated by the methods of extreme value statistics.

The stochastic process model also presupposes a point of view markedly different from that taken by R. Fürth[9] in the development of a thermodynamic theory of breaking strength. In order to be able to emphasize the *time-dependence* of fracture phenomena, this discussion is limited to systems for which the applied forces are large enough so that the minimum energetic requirements for the creation of a new surface need not be considered. In other words, it is assumed here that the test sample is bearing a load sufficiently large so that it is known that fracture will eventually occur. The question to be answered is: "How long must we wait?" On the other hand, it is also assumed that the lifetime of the sample is long enough to allow the neglect of impulsive loading and wave effects.

II. THEORY

1. Description of the Model

Let us consider a fiber of uniform cross-section and of length, l, which is bearing a uniaxial tensile stress, f. The present discussion is limited to cases in which f is a constant. Our problem is to calculate the probability, $q_f(t_B)dt_B$, that the fiber will break in a time interval at t_B, or the associated cumulative distribution function:

$$Q_f(t_B) = \int_0^{t_B} q_f(t)dt \tag{1}$$

Denoting by z the distance along the fiber axis, we shall consider the fiber to be divided into a set of thin slabs of thickness, Δz, whose

planar boundaries perpendicularly intersect the fiber axis at the points $z_1, z_2, \ldots z_i, z_{i+1}, \ldots$ etc. The symbol S_i shall refer to the region bounded by the planes at z_i and z_{i+1}. It will be assumed that, when the fiber breaks, the fracture will be completely contained in a particular slab, S_B. Let $t = 0$ be the time at which the fiber is loaded with f. We shall say that at this time the region S_i contains N_i chemical bonds, all of which must eventually be broken if the fiber is to break at S_i. After the load is applied, the number of unbroken bonds in each slab will start to decrease. Let $n_i(t)$ be the number of unbroken bonds in S_i at a time t. The time required for $n_i(t)$ to decrease to zero shall be called the lifetime of S_i. The lifetime of S_B is t_B, and S_B is that slab for which $n(t)$ first reaches zero.

The present discussion will be simplified by assuming that the fiber is uniform to the extent that all of the slabs contain the same number of bonds, N, at $t = 0$. We shall say that a given slab, S_i, is in the state $\varepsilon_{N,n}$ at time, t, if it contains n bonds at that time.

The basic statistical assumptions of the present theory may be stated as follows:

(*1*) The only allowed transitions for a given slab are $\varepsilon_{N,N} \rightarrow \varepsilon_{N,N-1} \rightarrow \varepsilon_{N,N-2}$ and so on up to $\varepsilon_{N,0}$.

(*2*) If the stress is held constant in time, the probability of the occurrence of a transition $\varepsilon_{N,n} \rightarrow \varepsilon_{N,n-1}$ remains unchanged as long as S_i is in the state $\varepsilon_{N,n}$, regardless of the status of the nearby slabs, S_{i+1}, S_{i-1}, S_{i+2}, etc.

(*3*) If it were possible to maintain the force per bond constant in time, then it would be found that the bonds in S_i break according to first-order chemical kinetics, and the probability of the transition $\varepsilon_{N,n} \rightarrow \varepsilon_{N,n-1}$ taking place in a small time interval dt would be $nkdt + \mathbf{o}(dt)$, where k is a function of f alone. Since, however, the force per bond in S_i must increase as n_i decreases, we would in general expect k to actually increase with decreasing n_i. If we assume that the load released by a broken bond is equally shared by the remaining unbroken bonds in its slab, then k will be a function of fN/n. In practice, it may happen that the rupture of several bonds may affect the local geometry in a particular slab so as to concentrate the stress on some of the bonds in such a manner that they bear a load considerably greater than fN/n. For present purposes, we shall neglect such effects and assume that $k = k(fN/n)$.

The theory of absolute reaction rates[12] may be used to obtain a reasonable postulate for the functional form of $k(fN/n)$. Arguments

first presented by Tobolsky and Eyring[13] in a discussion of the creep failure of polymeric filaments may be interpreted as indicating that:

$$k(fN/n) = \alpha \exp\{\beta fN/n\} \tag{2}$$

where α and β are functions of the temperature, but not of the stress.

The probability that S_t is in a state $\mathcal{E}_{N,n}$ at a time, t, when it is *known* that the stress is f, will be denoted by $P_{N,n}(t|f)$ and the transition probability, $nk(fN/n)dt$, will be written as $\lambda_{N,n}dt$.

The statistical assumptions (*1*), (*2*), and (*3*) are equivalent to stating that the behavior of S_t in time constitutes a stochastic process[14] obeying the following system of differential equations (the symbols $P^{(1)}$ and $P^{(m)}$ will indicate the first and mth partial derivatives of P with time):

$$\begin{aligned} P^{(1)}_{N,N} &= -\lambda_{N,N}P_{N,N} \\ &\vdots \\ P^{(1)}_{N,n} &= -\lambda_{N,n}P_{N,n} + \lambda_{N,n+1}P_{N,n+1} \\ &\vdots \\ P^{(1)}_{N,0} &= \lambda_{N,1}P_{N,1} \end{aligned} \tag{3}$$

subject to the conditions that for all values of n and t:

$$0 \leq P_{N,n}(t|f) \leq 1 \tag{4a}$$

for all $n \neq N$:

$$P_{N,n}(0|f) = 0 \tag{4b}$$

and:

$$P_{N,N}(0|f) = 1 \tag{4c}$$

In this paper we shall not discuss systems for which the broken bonds can reform. This means that we neglect the possibility of transitions of the type $\mathcal{E}_{N,n} \rightarrow \mathcal{E}_{N,n+1}$. If such transitions do occur, they may be accounted for by adding a term $\mu_{N,n-1}P_{N,n-1}$ to the expression for $P^{(1)}_{N,n}$ in equations (3). The theory of Tobolsky and Eyring suggests that:

$$\mu_{N,n-1} = (n-1)\alpha \exp\{-\beta fN/(n-1)\} \tag{5}$$

For most of the strong textile fibers, one must apply a load such that $Bf \gg 1$ if fracture is to occur in a reasonably short time interval. For such systems, $\lambda_{N,n} \gg \mu_{N,n-1}$, and the neglect of the healing of broken bonds is justified.

The quantity, $1 - P_{N,0}(t|f)$, is the probability that S_t has a lifetime greater than t when the stress is f. Let $M = l/\Delta z$ be the number of slabs in the fiber. It is apparent that our assumption (2) above implies that the probability, $1 - Q_f(t_B)$, that the fiber has a lifetime greater than t_B, is equal to the probability of occurrence of M independent events each of probability, $1 - P_{N,0}(t_B|f)$:

$$1 - Q_f(t_B) = [1 - P_{N,0}(t_B|f)]^M \tag{6}$$

To obtain a precise knowledge of the distribution of t_B for arbitrary M, one must solve equations (3) and (4), which describe a single slab, and then use the "weakest link" hypothesis of equation (6) to calculate the behavior of the fiber. For most real systems, however, M will be extremely large, and equation (6) indicates that in such cases only those values of t_B for which $P_{N,0}(t_B|f)$ is small will yield an appreciable value for $1 - Q_f(t_B)$. Therefore, in the limit as $M \to \infty$, we need only to know the behavior of $P_{N,0}(t_B|f)$ for t_B close to zero. For long perfect fibers, it shall suffice to have the following result:

LEMMA: Equations (3) and (4) imply that for all $m < N$:

$$P_{N,0}^{(m)}(0|f) = 0 \tag{7a}$$

and:

$$P_{N,0}^{(N)}(0|f) = N!\Lambda_N \tag{7b}$$

where:

$$\Lambda_N \equiv (N!)^{-1} \prod_{i=1}^{N} \lambda_{N,i} \tag{7c}$$

To show this we successively differentiate the last of equations (3) and use the others to eliminate the derivatives of $P_{N,1}$, $P_{N,2}$, etc.:

$$\begin{aligned} P_{N,0}^{(1)} &= \lambda_{N,1}P_{N,1} \\ P_{N,0}^{(2)} &= -\lambda_{N,1}^2 P_{N,1} + \lambda_{N,1}\lambda_{N,2}P_{N,2} \\ P_{N,0}^{(3)} &= \lambda_{N,1}^3 P_{N,1} - \lambda_{N,1}^2\lambda_{N,2}P_{N,2} - \lambda_{N,1}\lambda_{N,2}P_{N,2} \\ &\quad + \lambda_{N,1}\lambda_{N,2}\lambda_{N,3}P_{N,3} \\ &\vdots \end{aligned} \tag{8}$$

By virtue of (4b), all of the terms on the right in equations (8) will vanish at $t = 0$ until we reach the Nth derivative of $P_{N,0}$, which is the first to contain a term with $P_{N,N}$ as a factor. The term in $P_{N,N}$ will be $N!\ \Lambda_N P_{N,N}$ and the use of (4c) will yield (7b).

Although equations (6) and (7) supply the necessary apparatus for a discussion of long perfect fibers, it is instructive to first examine in detail the behavior of a single slab.

2. The Rate of Breakdown in a Single Slab

When the stress f is a constant, $\lambda_{N,n}$ is not an explicit function of t, and the solution of equations (3) and (4) is:

$$P_{N,n}(t|f) = \lambda_{N,n}^{-1} \sum_{j=N}^{n} \phi_{N,n,j} \lambda_{N,j} e^{-\lambda_{N,j} t} \tag{9a}$$

$$\phi_{N,n,j} = \prod_{\substack{i=N \\ i \neq j}}^{n} (1 - \lambda_{N,j}/\lambda_{N,i})^{-1} \tag{9b}$$

This is most readily verified by direct substitution.

The probability, $p_{N,n}(t|f)dt$, that the transition $\varepsilon_{N,n} \to \varepsilon_{N,n-1}$ occurs in a small time interval at t is simply $\lambda_{N,n} P_{N,n}(t|f)dt$:

$$p_{N,n}(t|f)dt = \sum_{j=N}^{n} \phi_{N,n,j} \lambda_{N,j} e^{-\lambda_{N,j} t} \tag{10}$$

Equation (10) yields the following expressions for the average time, $E_{N,n}\{t\}$, at which the transition $\varepsilon_{N,n} \to \varepsilon_{N,n-1}$ occurs, and the variance, $\sigma_{N,n}^2$, in this time:

$$E_{N,n}\{t\} = \sum_{j=N}^{n} \lambda_{N,j}^{-1} \phi_{N,n,j} \tag{11}$$

$$\sigma_{N,n}^2 = 2 \sum_{j=N}^{n} \phi_{N,n,j} \lambda_{N,j}^{-2} - \left\{ \sum_{j=N}^{n} \phi_{N,n,j} \lambda_{N,j}^{-1} \right\}^2 \tag{12}$$

These expressions for $E_{N,n}\{t\}$ and $\sigma_{N,n}^2$ are too complicated to be of immediate use. Simpler expressions may be obtained by computing the characteristic function,[15] $E_{N,n}\{e^{i\psi t}\}$, ($i = \sqrt{-1}$, ψ real):

$$E_{N,n}\{e^{i\psi t}\} = \int_0^\infty e^{i\psi t} p_{N,n}(t|f)dt \tag{13}$$

$$= \sum_{j=N}^{n} \phi_{N,n,j} (1 - i\psi/\lambda_{N,j})^{-1} \tag{14}$$

and noting that the right side of equation (14) is the partial fraction expansion of the following:

$$E_{N,n}\{e^{i\psi t}\} = \prod_{j=N}^{n} (1 - i\psi/\lambda_{N,j})^{-1} \tag{15}$$

The mth moment, $E_{N,n}\{t^m\}$, and the mth semiinvarient $\chi_{N,n,m}$, may be calculated from the general properties of characteristic functions:

$$i^m E_{N,n}\{t^m\} = \left.\frac{\partial^m E_{N,n}\{e^{i\psi t}\}}{\partial \psi^m}\right|_{\psi=0} \tag{16}$$

$$i^m \chi_{N,n,m} = \left.\frac{\partial^m \ln E_{N,n}\{e^{i\psi t}\}}{\partial \psi^m}\right|_{\psi=0} \tag{17}$$

According to (15), the Maclaurin series expansion of $\ln E_{N,n}\{e^{i\psi t}\}$ is:

$$\ln E_{N,n}\{e^{i\psi t}\} = \sum_{r=1}^{\infty} \left\{ \frac{(i\psi)^r}{r} \sum_{j=N}^{n} \lambda_{N,j}^{-r} \right\} \tag{18}$$

Thus we obtain the following remarkably simple expressions for $E_{N,n}\{t\}$, $\sigma^2_{N,n}$, and the third moment about the mean, $\mu^3_{N,n}$:

$$E_{N,n}\{t\} \equiv \chi_{N,n,1} = \sum_{j=N}^{n} \lambda_{N,j}^{-1} \tag{19a}$$

$$\sigma^2_{N,n} \equiv \chi_{N,n,2} = \sum_{j=N}^{n} \lambda_{N,j}^{-2} \tag{19b}$$

$$\mu^3_{N,n} \equiv \chi_{N,n,3} = 2 \sum_{j=N}^{n} \lambda_{N,j}^{-3} \tag{19c}$$

When $\lambda_{N,j} = jk(fN/j)$, and N is very large, the summations in equations (19), can be made into Reimann integrals by putting $y = j/N$, and noting that when j increases by 1, $\Delta y = N^{-1}$:

$$\lim_{N\to\infty} E_{N,n}\{t\} = \int_{n/N}^{1} \frac{dy}{yk(f/y)} \tag{20a}$$

$$\lim_{N\to\infty} \sigma^2_{N,n} = N^{-1} \int_{n/N}^{1} \frac{dy}{y^2 k^2(f/y)} \tag{20b}$$

$$\lim_{N\to\infty} \mu^3_{N,n} = 2N^{-2} \int_{n/N}^{1} \frac{dy}{y^3 k^3(f/y)} \tag{20c}$$

These results for large N justify the intuitive notion that in the limit, as $N \to \infty$, $n(t)$ should obey the "deterministic" equation:

$$-dn/dt = nk(fN/n) \tag{21}$$

with negligible fluctuations, for equation (20a) is a solution of (21).

For a slab of size N, the probability density function for the distribution of lifetimes is given by $p_{N,1}(t|f)dt$. Thus, the mean lifetime, its

variance, and third moment about the mean for a nearly infinite slab are

$$\lim_{N \to \infty} E_{N,1}\{t\} = \int_0^1 \frac{dy}{yk(f/y)} \tag{22a}$$

$$\lim_{N \to \infty} \sigma^2_{N,1} = N^{-1} \int_0^1 \frac{dy}{y^2k^2(f/y)} \tag{22b}$$

$$\lim_{N \to \infty} \mu^3_{N,1} = 2N^{-2} \int_0 \frac{dy}{y^3k^3(f/y)} \tag{22c}$$

It should be noted that the integrals of equations (22) are finite for a very general class of functions, $k(fN/n)$, of which equation (2) gives only a special case. In fact, we need only to postulate that $k(fN/n)$ is always greater than zero, monotonic in f, and that:

$$\lim_{y \to 0} k(f/y) \to \infty \tag{23}$$

at least as fast as some positive (yet arbitrarily small) power of f/y to guarantee that the following statements are true: (*a*) The average lifetime of the slab is finite for all N, finite or infinite. (*b*) As N approaches infinity, the lifetime distribution becomes perfectly sharp with a coefficient of variation, $\sigma_{N,1}/E_{N,1}\{t\}$ that is proportional, in the limit, to $N^{-1/2}$. (*c*) As N increases, $\mu^3_{N,1}$ becomes negligible when compared to $\sigma^3_{N,1}$.

Furthermore, if we let Δt_n be the time the slab spends in the state $\mathcal{E}_{N,n}$, it is now evident that the quantities $\Delta t_n (n = N, N-1, \ldots 1)$ constitute a set of independent random variables drawn from different populations. The lifetime of the slab is just the sum of these random variables. Thus, items (*a*), (*b*), and (*c*) above are more than sufficient for us to state that Liapounoff's form of the central limit theorem[16] applies to the lifetime distribution. We can, therefore, conclude that as N approaches infinity the lifetime distribution for an isolated slab is *asymptotically normal*, with a mean and variance given by equations (22a) and (22b), respectively.

The "autocatalysis" condition of equation (23) obviously applies to systems which obey equation (2). For such systems:

$$\lim_{N \to \infty} E_{N,1}\{t\} = \alpha^{-1} \int_{\beta f}^{\infty} \frac{e^{-x}}{x}\, dx = -\alpha^{-1} Ei(-\beta f) \tag{24}$$

Here, we have put $x = \beta f y^{-1}$. The function $-Ei(-\beta f)$ is tabulated.[17,18] From equations (2) and (22b) we obtain:

$$\lim_{N \to \infty} \sigma_{N,1}^2 = (2N\alpha^2\beta f)^{-1} e^{-2\beta f} \tag{25}$$

Thus, for large slabs the coefficient of variation in the lifetime distribution is:

$$\lim_{N \to \infty} \sigma_{N,1}/E_{N,1}\{t\} = \frac{1}{H}\left(\frac{\beta f}{2N}\right)^{1/2} \tag{26}$$

where H is defined by:

$$H \equiv -\beta f e^{\beta f} Ei(-\beta f) \tag{27}$$

For large βf:

$$H \simeq 1 - (\beta f)^{-1} + 2!(\beta f)^{-2} - 3!(\beta f)^{-3} + \ldots \tag{28}$$

3. Behavior of a Long Fiber

We consider a long perfect fiber with $M \gg 1$. For such a fiber we may expand $P_{N,0}$ in equation (6) about $t = 0$, and use (7) to write, for (6):

$$1 - Q_f(t_B) = [1 - \Lambda_N t_B^N + \ldots]^M \tag{29}$$

For large M, this becomes:

$$1 - Q_f(t_B) = \exp\{-M\Lambda_N t_B^N\} \tag{30}$$

and, recalling equation (1):

$$q_f(t_B) = NM\Lambda_N t_B^{N-1} \exp\{-M\Lambda_N t_B^N\} \tag{31}$$

The most probable value of t_B is:

$$\lim_{M \to \infty} \langle t_B \rangle_{mode} = (1 - 1/N)^{1/N}(M\Lambda_N)^{-1/N} \tag{32}$$

The mth moment of this distribution is:

$$\lim_{M \to \infty} E\{t_B^m\} = (M\Lambda_N)^{-m/N}\Gamma(1 + m/N) \tag{33}$$

where Γ denotes the gamma function. It is seen that such dimensionless quantities as the coefficient of variation, $\sigma_B/E\{t_B\}$, and the coefficient of skewness, μ_B^3/σ_B^3, for t_B are independent of both the length

of the bundle and the functional form of $k(fN/n)$ when M is very large:

$$\lim_{M \to \infty} \sigma_B / E\{t_B\} = \left\{ \frac{\Gamma(1 + 2/N)}{\Gamma^2(1 + 1/N)} - 1 \right\}^{1/2} \tag{34}$$

and:

$$\lim_{M \to \infty} \mu_B^3 / \sigma_B^3 = \frac{\Gamma(1 + 3/N) - 3\Gamma(1 + 1/N)\Gamma(1 + 2/N) + 2\Gamma^3(1 + 1/N)}{\{\Gamma(1 + 2/N) - \Gamma^2(1 + 1/N)\}^{3/2}} \tag{35}$$

In the limit as both M and N become large, the distribution of t_B sharpens. The following expansion for the gamma function:

$$\Gamma(1 + x) = 1 - \gamma x + (\pi^2/6 + \gamma^2) \frac{x^2}{2!} - (b_3 + 3\gamma\pi^2/6 + \gamma^3) \frac{x^3}{3!} + O(x^4) \tag{36a}$$

where:

$$\gamma = 0.577215665\ldots \tag{36b}$$

$$b_3 = 2 \sum_{r=1}^{\infty} r^{-3} = 2.40411381\ldots$$

may be used to show that:

$$\lim_{\substack{M \to \infty \\ N \to \infty}} E\{t_B\} = (M\Lambda_N)^{-1/N} \tag{37}$$

$$\lim_{\substack{M \to \infty \\ N \to \infty}} \sigma_B / E\{t_B\} = \pi 6^{-1/2} N^{-1} \tag{38}$$

and:

$$\lim_{\substack{M \to \infty \\ N \to \infty}} \mu_B^3 / \sigma_B^3 = -b_3 6^{3/2} \pi^{-3} \tag{39}$$

Apparently, for a long fiber with many bonds per cross-section, the coefficient of variation in the lifetime decreases as N^{-1}. A comparison of this result with that of equation (26) indicates that for large N a long fiber has a much sharper lifetime distribution than a single slab. It will also be noticed that, although the lifetime distribution of a long fiber sharpens rapidly as N increases, it is never normal, because the coefficient of skewness approaches a constant value.

For the special case in which the individual slabs obey equation (2), equation (33) yields:

$$\lim_{M \to \infty} E\{t_B\} = \Gamma(1 + 1/N) M^{-1/N} \alpha^{-1} \exp\left\{-\beta f \sum_{n=1}^{N} \frac{1}{n}\right\} \quad (40)$$

For large N, this may be simplified by using the following expression[19] for γ:

$$\gamma = \lim_{N \to \infty} \left\{\sum_{n=1}^{N} \frac{1}{n} - \ln N\right\} \quad (41)$$

thus:

$$\lim_{\substack{M \to \infty \\ N \to \infty}} E\{t_B\} = M^{-1/N} \alpha^{-1} N^{-\beta f} e^{-\gamma \beta f} \quad (42)$$

Equations (40) and (42) imply that, for a long fiber with given M and N, the logarithm of t_B should be a linear function of the applied force. This relation is in agreement with experiment over a wide range of t_B for a large class of substances including cotton, rayon, and drawn polyamide and polyester fibers.[5-8]

Let us now consider an experiment in which the breaking strengths of fibers are measured by holding them under constant stresses, f^*, and determining whether they break in a time interval, $0 \leq t \leq t^*$, where t^* is the maximum time available. Substitute t^* for t_B and f^* for f in equations (1) and (30). Since $Q_{f^*}(t^*)$ is the probability that a given fiber does not last until t^*, when held under f^*, it represents, in this experiment, the probability that the fiber has a strength less than f^*, that is, the cumulative distribution of breaking strength. If we continue to use equation (2), and put:

$$\Omega \equiv M(t^* \alpha)^N \quad (43a)$$

$$\Upsilon \equiv \beta \sum_{n=1}^{N} (1/n) \quad (43b)$$

in equation (30), we obtain the following expression for the probability density function, $h(f^*|t^*)$, for breaking strengths:

$$h(f^*|t^*) df^* = \frac{\partial Q_{f^*}(t^*)}{\partial f^*} df^* \quad (44a)$$

$$= \Upsilon\Omega \exp\left\{\Upsilon f^* - \Omega e^{\Upsilon f^*}\right\} df^* \quad (44b)$$

The most probable breaking strength is:

$$\lim_{M \to \infty} \langle f^* \rangle_{mode} = \Upsilon^{-1} \ln \Omega^{-1} \tag{45}$$

Equation (41) may be used to evaluate (45) for large N:

$$\lim_{\substack{M \to \infty \\ N \to \infty}} \langle f^* \rangle_{mode} = \beta^{-1}(\gamma + \ln N)^{-1}[-\ln (t^* \alpha) - N^{-1} \ln M] \tag{46}$$

Thus, it is seen that there is a dependence of the tensile strength on fiber length; but, as $N \to \infty$, this dependence very rapidly becomes negligible. It will also be noticed that at constant N and M the strength decreases linearly with increasing $\ln t^*$, and that for very heavy fibers $\langle f^* \rangle_{mode}$ is nearly inversely proportional to $\ln N$.

For real systems, N and $(t^* \alpha)^{-1}$ will be $\gg 1$, and, therefore, Ω will be $\ll 1$. Thus, according to equations (30) and (44), $h(f^* | t^*)$ will be normalized in the sense that:

$$\int_0^\infty h(f^* | t^*) df^* = 1 \tag{47}$$

The average breaking strength, $E\{f^*\}$, is calculated by putting $x = \Omega \exp(\Upsilon f^*)$ and integrating by parts:

$$\lim_{M \to \infty} E\{f^*\} = \int_0^\infty f^* h(f^* | t^*) df^* = \Upsilon^{-1} \int_\Omega^\infty \frac{e^{-x}}{x} dx \tag{48a}$$

For small Ω this becomes:

$$\lim_{\substack{M \to \infty \\ N \to \infty}} E\{f^*\} = \Upsilon^{-1} (\ln \Omega^{-1} - \gamma) \tag{48b}$$

Since the difference between the mean and the mode is a negative quantity, distribution of f^* is skewed to the left. The variance in f^* obtained from equation (44b) is:

$$\lim_{\substack{M \to \infty \\ N \to \infty}} \sigma_{f^*}^2 = \pi/6\Upsilon^2 \tag{49}$$

This quantity decreases faster than N^{-2} with increasing N, but is independent of M and t^*.

4. Systems Containing Flaws

The discussion given above was for systems free from stress-concentrating flaws. We can now get slightly closer to reality by imagining

a fiber which still obeys the three statistical assumptions of Section II-1, but which possesses small impurities and/or cracks which concentrate the stress so that the value of f in a particular slab may be considered a random variable. If we let θ represent the tensile stress measured by a macroscopic observer, it is reasonable to postulate that the cumulative distribution function for f, $G_\theta(f)$, is independent of z and possesses the properties:

$$Pr\{f < \theta\} = 0 \tag{50a}$$

$$Pr\{f \geq \theta\} = 1 - G_\theta(f) \tag{50b}$$

It must, of course, be realized that f is now a fictitious quantity, or rather an "effective stress" which has been averaged over the slab. It will be assumed that the volume occupied by the flaws is small enough so that N is still the same for all the slabs. We shall denote by $Q_\theta(t_B)$ the cumulative distribution of breaking times and by $g_\theta(f)$ the probability density function corresponding to equations (50). Equation (6) now becomes:

$$1 - Q_\theta(t_B) = [1 - P_\theta(t_B)]^M \tag{51}$$

where:

$$P_\theta(t_B) = \int_0^{t_B} p_\theta(t)dt \tag{52}$$

and:

$$p_\theta(t) = \int_\theta^\infty p_{N,1}(t|f)g_\theta(f)df \tag{53}$$

The density function, $p_{N,1}(t|f)$, is still given by equation (10).

For small N, one must use equation (53) to evaluate (51). For heavy fibers, however, we can make use of the fact that $p_{N,1}(t|f)$ becomes a Dirac delta function as N increases without bound:

$$p_{N,1}(t|f) = \delta(t - a) \tag{54a}$$

where:

$$a = a(f) = \lim_{N \to \infty} E_{N,1}\{t\} \tag{54b}$$

Let $a^*(t_B) = f$ represent the inverse function for $a(f)$, that is, the function which gives the value of f for which:

$$\lim_{N \to \infty} E_{N,1}\{t\} = t_B$$

Since $a^*(t_B)$ is a monotonic decreasing function of t_B, we can write:

$$\lim_{N \to \infty} P_\theta(t_B) = 1 - G_\theta[a^*(t_B)] \tag{55}$$

Thus, for large N, equation (51) becomes:

$$\lim_{N \to \infty} [1 - Q_\theta(t_B)] = \{G_\theta[a^*(t_B)]\}^M \tag{56}$$

If a specific functional form for $G_\theta(f)$ is assumed, the classical methods of the theory of extreme value statistics may be used to evaluate equation (56) and thereby to obtain explicit expressions for the distribution of lifetimes under constant loads.

5. Implications

When fibers are broken through the isothermal application of tensile stresses, subsequent examination of the fragments does not always yield evidence of any significant chemical change having taken place throughout the fibers during fracture. This well-known fact appears to conflict with the assumption of the present theory that, immediately upon the application of the stress, chemical bonds start to break in all the slabs comprising a fiber. The following simple calculation, however, resolves this apparent difficulty.

Consider a long perfect fiber test sample, say, 1 mil in diameter and 25 cm. in length. For such a fiber, reasonable values of N and M are 10^9 and 10^4, respectively. Assuming that the fiber obeys equation (2), we shall show that, in the absence of flaws, it is quite likely that at the moment when this fiber breaks no appreciable change will have occurred in any of the S_i, except S_B. If we use the theory of absolute reaction rates,[12] we can expect the parameter β to have the order of magnitude:

$$\beta = v/2kT \tag{57}$$

where T is the absolute temperature, k is Boltzmann's constant, and v is roughly equal to the area per chemical bond times the distance moved when the bond is broken. If a force greater than 10^9 dynes

cm.$^{-2}$ is required to break the fiber in a reasonably short time at room temperature in the absence of flaws, then we can say that $\beta f > 2$. Equations (42) and (38) yield the result that, for this perfect fiber, the fluctuations in t_B are negligible and:

$$\alpha t_B < e^{-42} \tag{58}$$

The quantity N is sufficiently large for us to safely assume that the mean value of n/N, $\langle n/N \rangle_{av}$, averaged over all the slabs in the fiber, is determined by equation (21). Thus, when $t = t_B$:

$$\alpha t_B = -Ei(-\beta f) + Ei(-\beta f \langle n/N \rangle_{av}) \tag{59}$$

A comparison of equations (58) and (59) indicates that, when $t = t_B$, $\langle n/N \rangle_{av}$ is so close to unity that no method of chemical analysis could hope to detect signs of degradation except, perhaps, at the surface created by the fracture. The extremely small value of αt_B indicates that we can vary the assumed values for the molecular parameters over a considerable range and still come out with the same conclusion. This result is a consequence of the extreme autocatalytic nature of mechanical breakdown.

The discussion of this paper rests on the three statistical assumptions listed in Section II-1. It is recognized that the use of assumption (*2*) and the assumption that $k = k(fN/n)$ reduces this treatment to an abstract model with only qualitative implications. It is felt, however, that the predictions of the theory with regard to the magnitude of the variance and skewness to be expected in tensile strength measurements on perfect specimens, the dependence of strength on speed of measurement, and the autocatalytic nature of the breakdown process, are significant. The reader may find it of interest to contrast the methods and results of this study with those of the theory of Daniels[20] for calculating the strength of parallel arrays of filaments for which time effects can be neglected.

Actual fiber specimens show a variance in t_B that is many orders of magnitude greater than that calculated here for perfect fibers.[8] Since the large dispersion in the behavior of real systems is caused by flaws, the following question arises: "How much can one learn about the distribution of flaws from studies of the distribution of t_B in long fibers?" This important question will be discussed in detail in a future publication.

References

1. A. A. Griffith, *Trans. Roy. Soc.* (*London*), **A221**, 163 (1920).
2. A. A. Griffith, *Proc. Intern. Congr. Appl. Mech., Delft*, **1**, 55 (1924).
3. F. T. Peirce, *J. Textile Inst. Trans.*, **17**, 355 (1926).
4. B. Epstein, *J. Appl. Phys.*, **19**, 140 (1948).
5. J. C. Mann and F. T. Peirce, *Shirley Inst. Mem.*, **5**, 7 (1926).
6. E. Midgley and F. T. Peirce, *Shirley Inst. Mem.*, **5**, 102 (1926).
7. W. F. Busse, E. T. Lessig, D. L. Loughborough, and L. Larrick, *J. Appl. Phys.*, **13**, 715 (1942).
8. B. D. Coleman, *J. Appl. Phys.*, **27**, 862 (1956).
9. R. Fürth, *Proc. Roy. Soc.* (*London*), **A177**, 217 (1941).
10. J. I. Frenkel and T. A. Kontorova, *J. Phys.* (*U. S. S. R.*), **7**, 180 (1943).
11. W. Weibull, *Ing. Ventenskaps Akad. Handl.*, No. 151 (1939); *ibid.*, No. 153 (1939).
12. S. Gladstone, K. J. Laidler, and H. Eyring, *The Theory of Rate Processes*, McGraw-Hill, New York, 1941.
13. A. Tobolsky and H. Eyring, *J. Chem. Phys.*, **11**, 125 (1943).
14. W. Feller, *An Introduction to Probability Theory and Its Applications*, Vol. 1, Wiley, New York, 1950, Chap. 17.
15. H. Cramer, *Mathematical Methods of Statistics*, Princeton Univ. Press, Princeton, 1946, pp. 185–187.
16. *Ibid.*, pp. 213–218.
17. E. Jahnke and F. Emde, *Tables of Functions with Formulae and Curves*, Dover, New York, 1945, pp. 1–8.
18. T. Akahira, *Sci. Papers Inst. Phys. Chem. Research* (*Tokyo*), **10**, 181 (1929).
19. P. M. Morse and H. Feshback, *Methods of Theoretical Physics*, McGraw-Hill, New York, 1953, p. 422.
20. H. E. Daniels, *Proc. Roy. Soc.* (*London*), **A183**, 405 (1945).

Synopsis

A model is developed for discussing the time-dependence of mechanical strength measurements. This model is particularly applicable to polymeric fibers which show large time effects that are not accounted for by the classical "weakest link" theories. Most of the discussion is confined to a perfect fiber, free from flaws, that can be divided into a set of noninteracting slabs. Calculations have been made of the distribution of breaking times for isolated slabs and long fibers composed of many slabs. It is found that, under rather general conditions, the single slab lifetime distribution is asymptotically normal as the number of bonds increases without limit, although the corresponding distribution for a long fiber is never normal. It also appears that, as the cross-sectional area increases, the coefficient of variation of breaking times for a long fiber goes to zero much faster than for a single slab. Toward the end of the article a route is suggested for estimating the effect of stress-concentrating flaws on the distribution of breaking times.

TRANSACTIONS OF THE SOCIETY OF RHEOLOGY VOL. I, 169–175 (1957)

On Ideal Locking Materials

WILLIAM PRAGER, *Brown University, Providence, R. I.*

I. INTRODUCTION

Stress analyses in engineering are most frequently based on the linear theory of elasticity, though deviations from the linear stress–strain law are observed for practically all engineering materials.

Depending on the character of these deviations, materials may be classified as *soft* or *hard*. For a soft material, the stress increment required to produce a specified strain increment diminishes with progressing deformation; for a hard material, on the other hand, this stress increment grows as the deformation proceeds. Examples of these two types of mechanical behavior are provided by the structural metals (steel or aluminum) and the materials used for package cushioning[1] (excelsior or foam rubber).

The perfectly plastic solid[2] exhibits an extreme type of soft behavior: once a certain stress level (called the yield limit) has been reached, deformation may proceed under a constant state of stress. Since the theory of perfectly plastic solids has proved useful in establishing a qualitative understanding of the mechanical behavior of soft materials, the corresponding theory for hard materials will be developed in this paper.

For simple compression, the extreme type of hard behavior considered here is indicated by the stress–strain diagram OAB in Figure 1: the stress response to a sufficiently small strain is governed by Hooke's law; when the strain reaches a certain limiting value, there is *locking* in the sense that any further increase in stress will not cause any changes in strain.

In the theory of perfectly plastic solids, useful results are obtained from a simplified analysis that neglects all elastic strains. The corresponding analysis for the solids considered here would neglect the elastic stresses in comparison to the much larger stresses that can be

supported in the locked state. This simplification will be adopted in the following; it amounts to replacing the stress–strain diagram OAB in Figure 1 by OA*B.

One obviously has a good deal of latitude in specifying the corresponding behavior for more general states of stress. In the absence of experimental evidence, it seems best to use the analogy with perfectly plastic solids as a guide to sufficiently general stress–strain laws that promise to be adaptable to a wide range of experimental results once these become available. In plasticity, theoretical speculations about the structure of the yield condition or stress–strain law repeatedly pointed the way to unexpected experimental results, and the same may be expected to happen in the new field investigated in this paper.

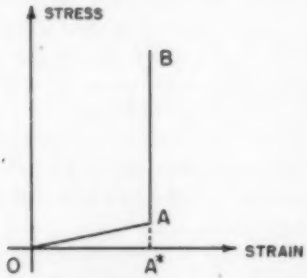

Fig. 1. Ideal locking material in simple compression.

II. STRESS–STRAIN LAW

In the following discussion of the relation between locking strains and stresses, it will be assumed that the principal axes of stress at a generic point coincide with the principal axes of strain at this point. Since the orientation of these coincident axes must be immaterial in an isotropic solid, the stress–strain law reduces to a relation between the principal stresses $\sigma_1, \sigma_2, \sigma_3$ and the principal strains $\epsilon_1, \epsilon_2, \epsilon_3$.

It will be useful to represent the state of strain by the point (strain point) in strain space that has the rectangular Cartesian coordinates $\epsilon_1, \epsilon_2, \epsilon_3$. The radius vector of the strain point will be denoted by ϵ. Similarly, the state of stress will be represented by the vector σ that has the components $\sigma_1, \sigma_2, \sigma_3$ with respect to the coordinate axes of strain space.

States of strain that can occur in the considered material will either produce a negligible elastic stress or cause locking. It will be assumed that the points representing these *admissible* states of strain form a *convex* region of strain space, whose interior or boundary points respectively correspond to purely elastic or locking states of strain. A plane through a boundary point of this *admissible region* of strain space is called a *supporting plane*, if it bounds a half-space that contains the admissible region.

As in the case of simple compression, we assume that each locking state of strain is associated with a one-parameter family of states of stress. Considering a locking state of strain, let P be the correspond-

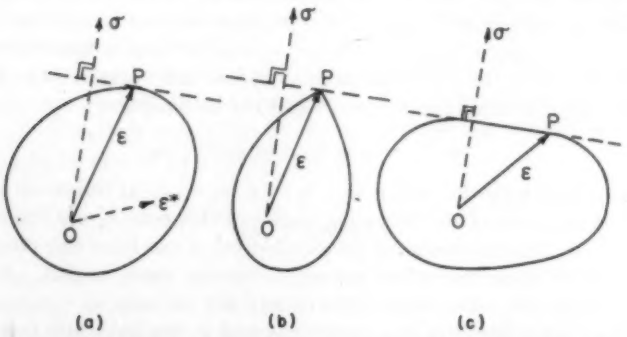

Fig. 2. Typical admissible regions in strain space and associated stress vectors.

ing boundary point of the admissible region, ϵ its radius vector, and σ the vector representing an associated state of stress. In analogy to Koiter's[3] theory of the generalized plastic potential, we assume that σ is normal to a supporting plane of the admissible region at P and directed from the origin O of strain space toward this plane. Figures 2a to 2c indicate various situations. The point P in Figure 2a is *regular* because the supporting plane through P is uniquely determined and contains no other points of the admissible region. The points P in Figures 2b and 2c are *singular*. In Figure 2b an infinity of supporting planes exists through P, but none of these contains any other points of the admissible region. In Figure 2c the supporting plane through P is unique but contains an infinity of boundary points of the admissible region.

In the situations shown in Figures 2a and 2b, the state of stress σ uniquely specifies the locking state of strain ϵ by which it is caused. In the situation indicated in Figure 2c, the state of stress σ may be caused by any one of an infinity of locking states of strain. In all three cases, however, the scalar $I = \sigma \cdot \epsilon$ is uniquely determined by the state of stress:

$$I = I(\sigma) = I(\sigma_1, \sigma_2, \sigma_3) \tag{1}$$

For brevity, the term *ideal locking material* will be used in the following to refer to any material that has the mechanical properties specified in this section.

As an example consider the ideal locking material defined by the following statements: none of the principal strains ϵ_1, ϵ_2, and ϵ_3 can fall below a given negative value $-\epsilon_0$, and locking occurs whenever at least one of the principal strains reaches this value. The admissible region in strain space, specified by the inequalities:

$$\epsilon_1 \geq -\epsilon_0, \epsilon_2 \geq -\epsilon_0, \epsilon_3 \geq -\epsilon_0$$

is an octant with the vertex $\epsilon_1 = \epsilon_2 = \epsilon_3 = -\epsilon_0$. If the strain point lies on only one of the bounding planes of this octant, say the plane $\epsilon_1 = -\epsilon_0$, the corresponding principal stress σ_1 can have any nonpositive value while the other principal stresses must vanish. If the strain point lies on an edge of the octant, say the edge $\epsilon_1 = \epsilon_2 = -\epsilon_0$, the corresponding principal stresses σ_1 and σ_2 can have any nonpositive values, but $\sigma_3 = 0$. Finally, if the strain point coincides with the vertex, all three principal stresses are nonpositive. In all cases the invariant I is given by:

$$I = -\epsilon_0 (\sigma_1 + \sigma_2 + \sigma_3) \tag{2}$$

III. THE PROBLEM

Considering a body made of an ideal locking material, let the part S_T of its surface S be free from surface tractions while the (infinitesimal) surface displacements are prescribed on the remainder S_U of S. Can the body accommodate itself to these boundary conditions or will the attainment of the prescribed surface displacements be prevented by locking?

The discussion of this problem is facilitated by the introduction of the following concepts.

1. A displacement field that is defined throughout the volume V of the considered body is called *kinematically admissible*, if it satisfies

the boundary conditions on S_U. Such a field is called *free*, if the corresponding strains do not imply locking at any point of V.

2. A stress field defined throughout V is called *statically admissible* if it satisfies the condition of equilibrium in V and the boundary condition of vanishing surface tractions on S_T. Such a stress field is called *locking*, if the work of its surface tractions on the prescribed surface displacements on S_U exceeds the volume integral of the scalar I introduced in connection with equation (1).

We are now ready to state two theorems, which are useful in solving the problem formulated at the beginning of this section.

Theorem 1. Locking will not occur if a free, kinematically admissible displacement field can be found.

Theorem 2. Locking must occur, if a locking, statically admissible stress field can be found.

The analogy between ideal locking materials and perfectly plastic solids has already been pointed out. The theorems stated above obviously correspond to the fundamental theorems of limit analysis[4] and can be proved in a similar manner.

IV. EXAMPLE

Consider a hollow sphere of the interior radius a and the exterior radius b, made of an ideal locking material and containing a rigid sphere of the radius a. All points of the exterior surface of the hollow sphere are to be given the purely radial displacement u_0 directed toward the center of the sphere. Assuming that the material of the hollow sphere locks whenever at least one of the principal strains reaches a given negative value $-\epsilon_0$, determine the magnitude of u_0 which causes locking.

Using spherical coordinates r, θ, φ, consider first the kinematically admissible displacement field determined by the purely radial displacement:

$$u = -u_0 \frac{r-a}{b-a} \tag{3}$$

which satisfies the boundary conditions at $r = a$ and $r = b$. The corresponding principal strains are:

$$\epsilon_r = \frac{du}{dr} = -\frac{u_0}{b-a}, \qquad \epsilon_\theta = \epsilon_\varphi = \frac{u}{r} = -\frac{u_0}{b-a}\left(1 - \frac{a}{r}\right) \tag{4}$$

For $a \leq r \leq b$, the constant strain ϵ_r has the largest absolute value. The considered kinematically admissible displacement field is therefore free if $u_0/(b-a) < \epsilon_0$. It follows then from *Theorem 1* that *locking cannot occur* if:

$$u_0 < \epsilon_0 b[1 - (a/b)] \tag{5}$$

In a similar manner any free, kinematically admissible displacement field furnishes a lower bound for the surface displacements that cause locking.

Consider next the statically admissible stress field with the principal stresses:

$$\sigma_r = \sigma_\theta = \sigma_\varphi = -p = \text{constant} \tag{6}$$

which corresponds to a state of uniform hydrostatic pressure p. For the ideal locking material considered in the present problem, the invariant (2) is:

$$I = -\epsilon_0(\sigma_r + \sigma_\theta + \sigma_\varphi) \tag{7}$$

where σ_r, σ_θ, and σ_φ are the principal stresses on account of the spherical symmetry. The statically admissible stress field (6) will therefore be locking whenever

$$4\pi b^2 p u_0 > {}^4/_3\,\pi(b^3 - a^3)3p\epsilon_0 \tag{8}$$

It follows then from *Theorem 2* that *locking must occur* if:

$$u_0 > \epsilon_0 b[1 - (a^3/b^3)] \tag{9}$$

In a similar manner any locking, statically admissible stress field furnishes an upper bound for the surface displacements that cause locking.

When the ratio a/b does not differ too much from unity, the bounds (5) and (9) may be sufficiently close to each other for practical purposes. If closer bounds are desired, the particularly simple stress field (6) must be replaced by a more realistic one. The strain field (4) suggests that in the limiting case only the strain ϵ_r assumes the critical absolute value ϵ_0. It therefore seems appropriate to consider a stress field for which only the stress σ_r differs from zero. The condition of equilibrium:

$$(d/dr)(r^2\sigma_r) = 0 \tag{10}$$

then requires that the stress field be of the form:

$$\sigma_r = -c/r^2, \ \sigma_\theta = \sigma_\varphi = 0 \tag{11}$$

where c is a positive constant. This statically admissible stress field will be locking if

$$4\pi b^2 \frac{c}{b^2} u_0 > 4\pi \frac{b}{a} \frac{c}{r^2} \epsilon_0 r^2 dr = 4\pi c \epsilon_0 (b-a) \tag{12}$$

Theorem *2* shows then that locking must occur if:

$$u_0 > \epsilon_0 b \, [1 - (a/b)] \tag{13}$$

The inequalities (5) and (13) establish $u_0 = \epsilon_0(b-a)$ as the critical value of the surface displacement.

The results presented in this paper were obtained in the course of research sponsored by the Office of Naval Research under Contract N7onr 562(10).

References

1. See R. D. Mindlin, *Bell System Tech. J.*, **24**, 353–461 (1945).
2. See, for instance, P. G. Hodge, Jr., and W. Prager, *Theory of Perfectly Plastic Solids*, John Wiley & Sons, New York, 1951, Chap. 1.
3. W. T. Koiter, *Quart. Appl. Math.*, **11**, 350–354 (1953).
4. See, for instance, W. Prager, *Probleme der Plastizitäts theorie*, Birkhäuser, Basel, 1955, Chap. 3.

Synopsis

The paper is concerned with the mechanics of ideal locking materials. Such a material deforms freely under negligible stresses until a certain strain invariant reaches a limiting value when locking occurs in the sense that, depending on the locking strain, certain kinds of stress increase will not cause any change in strain. The following boundary value problem is discussed. A body made of an ideal locking material is subjected to prescribed surface displacements over part of its surface, while the surface tractions are required to vanish over the remainder of the surface; can the body accommodate itself to these boundary conditions or will the attainment of the prescribed surface displacements be prevented by locking? Theorems are given which furnish bounds for the surface displacements that cause locking. A simple example is discussed in some detail.

TRANSACTIONS OF THE SOCIETY OF RHEOLOGY VOL. I, 177–190 (1957)

Heat Generation and Conduction in the Flow of a Viscous Compressible Liquid

H. L. TOOR, *Chemical Engineering Department, Carnegie Institute of Technology, Pittsburgh 13, Pa.*

The flow of a fluid under a large pressure gradient is characterized by a significant amount of frictional heat generation. High polymers at elevated temperatures are an important class of viscous fluids which are commonly transported under very large pressure gradients. Attempts to determine the isothermal stress rate of strain curves under these conditions are complicated by the temperature gradients which arise due to the frictional heat generation.

It was shown recently[1] that, under the conditions in which frictional heat generation is large, real liquids cannot be considered as incompressible—for, even though volume changes are small, thermal energy changes caused by liquid expansion are appreciable. The limiting temperature profiles obtained in long, nonadiabatic conduits were shown to be considerably different from those obtained for incompressible liquids.

In flow through a conduit there are at least three thermal states. Immediately after the flow starts there will be an unsteady-state period in which the temperature will vary with θ, x, and r which will be succeeded by a steady-state period in which the temperature will vary only with x and r. Finally, for large enough values of x the temperature will vary only with r.

Temperature profiles in the inlet region where the temperature is a function of x and r have been determined for incompressible liquids, both Newtonian[2] and non-Newtonian[3] and profiles for compressible and incompressible liquids have been determined for the large values of x.

In this paper, temperature profiles for compressible liquids will be determined for the inlet region where the temperarure varies with x

and r, and the distance necessary to reach the steady profile will be determined.

The energy equation is:[1]

$$\rho c_p \frac{dT}{d\theta} = \epsilon' \frac{dp}{d\theta} + k\nabla^2 T + \Phi \tag{1}$$

where ϵ' is T times the thermal expansion coefficient.

In applying this equation to steady flow through a tube, a number of assumptions are made[1]—the most important being that the velocity profile is constant along the tube. With a stress–rate of strain curve given by:

$$\partial u/\partial r = -A\tau^{n-1} \tag{2}$$

the following equations may be obtained:[1]

$$\frac{u}{u_m} = \frac{n+2}{n}\left[1 - \left(\frac{r}{R}\right)^n\right] \tag{3}$$

$$u_m = \frac{AR^n}{n+2}\left(-\frac{dp}{2dx}\right)^{n-1} \tag{4}$$

$$\Phi = \frac{n+2}{2} W \left(\frac{r}{R}\right)^n \tag{5}$$

$$W = -u_m(dp/dx) \tag{6}$$

If the last five equations are combined with equation (1):

$$\frac{n+2}{n} u_m\left[1 - \left(\frac{r}{R}\right)^n\right]\frac{\partial T}{\partial x} = \frac{k}{\rho c_p}\left(\frac{\partial^2 T}{\partial r^2} + \frac{1}{r}\frac{\partial T}{\partial r} + \frac{\partial^2 T}{\partial x^2}\right) + \frac{n+2}{n}\frac{W}{\rho c_p}\left[\frac{n}{2}\left(\frac{r}{R}\right)^n - \epsilon'\left(1 - \left[\frac{r}{R}\right]^n\right)\right] \tag{7}$$

It has been shown[1] that for flow in a long tube, after a sufficient time and distance have elapsed, the temperature profile becomes independent of x and is given by:

$$\frac{T - T_w}{(T_c - T_w)_0} = \frac{2(n+2)^2}{n}\left[\frac{n + 2\epsilon'}{2(n+2)^2}\left(1 - \left[\frac{r}{R}\right]^{n+2}\right) - \frac{\epsilon'}{4}\left(1 - \left[\frac{r}{R}\right]^2\right)\right] \tag{8}$$

$(T_c - T_w)_0$ is the difference between the center line temperature and the wall temperature when x is large and $\epsilon' = 0$. It is given by:

$$(T_c - T_w)_0 = \frac{1}{2(n+2)} \frac{R^2 W}{k} \tag{9}$$

Equation (7) can be put in dimensionless form by the following transformations:

$$\Theta = (T - T_w)/(T_c - T_w)_0 \tag{10}$$

$$Z = r/R \tag{11}$$

$$X = \frac{2n}{n+2} \frac{x}{R} (N_{Pe})^{-1} = \frac{n\pi}{n+2} (N_{Gr})^{-1} \tag{12}$$

where:

$$N_{Pe} = \frac{2RU_m}{\alpha}, \qquad N_{Gr} = \frac{\pi R^2 u_m}{\alpha x} \tag{13}$$

If conduction in the axial direction is neglected, equation (7) in reduced coordinates is

$$(1 - Z^n) \frac{\partial \Theta}{\partial X} = \frac{1}{Z} \frac{\partial}{\partial Z} \left(Z \frac{\partial \Theta}{\partial Z} \right) + (n+2)^2 Z^n - 2 \frac{(n+2)^2}{n} \epsilon' (1 - Z^n) \tag{14}$$

and equation (8) is:

$$\Theta_s = \frac{2(n+2)^2}{n} \left[\frac{n + 2\epsilon'}{2(n+2)^2} (1 - Z^{n+2}) - \frac{\epsilon'}{4} (1 - Z^2) \right] \tag{15}$$

Complete Adiabatic Flow: $k = 0$

In the complete absence of conduction, the temperature in reduced coordinates is, from equation (14):

$$\Theta = (n+2)^2 \left[\frac{Z^n}{1 - Z^n} - 2 \frac{\epsilon'}{n} \right] X \tag{16}$$

or:

$$T - T_w = \frac{\Delta p}{\rho c_p}\left[\frac{n}{2}\frac{Z^n}{1 - Z^n} - \epsilon'\right] \tag{17}$$

At the center line $Z = 0$ and:

$$\Theta_c = -2\frac{(n+2)^2}{n}\epsilon' X \tag{18}$$

or:

$$T_c - T_w = -\epsilon'(\Delta p/\rho c_p) \tag{19}$$

where Δp is the pressure drop from the inlet to the point in question. This may be compared with the equation for the mean temperature in an adiabatic tube, obtained by an over-all energy balance:

$$T_m - T_w = (1 - \epsilon')(\Delta p/\rho c_p) \tag{20}$$

The group $(1 - \epsilon')/\rho$ was assumed constant in the derivative of this equation. If the Spencer and Gilmore[4] equation of state for high polymers is used this assumption is correct.[5]

Equation (18) or (19) predicts a decrease in temperature in the center of the tube and the results given below show that even when conduction is taken into account this conclusion is correct for small values of X. The equations give the maximum decrease in temperature which can be obtained. The maximum increase in temperature from equation (16) or (17) is infinite.

INLET REGION—ISOTHERMAL WALL

In the real case where conduction is important, equation (14) must be solved with the appropriate boundary conditions. If we consider a fluid entering a tube whose wall temperature is constant and equal to the entering fluid temperature we have:

$$\begin{aligned} X &= 0, \quad \Theta = 0 \\ Z &= 1, \quad \Theta = 0 \\ Z &= 0, \quad \partial\Theta/\partial Z = 0 \end{aligned} \tag{21}$$

The method of solution is similar to Bird's[3] for an incompressible liquid in which the complete solution is assumed to be given by:

$$\Theta = \Theta_s + \Theta_1 \tag{22}$$

and Θ_s is the solution for $X = \infty$, equation (15). The reduced temperature used here is four times the value used by Bird and following his procedure we substitute equation (22) into (14) and remove the heat generation and expansion terms. The resulting equation for Θ_1 is then identical with that obtained in the incompressible case and both solutions are of the same form:

$$\Theta_1 = -\sum_{i=1}^{\infty} B_i \varphi_i(Z) e^{-a_i X} \tag{23}$$

where $\varphi_i(Z)$ and a_i have the same values as in the incompressible case and the B_i are now given by:

$$B_i = \frac{\dfrac{n+2\epsilon'}{n}\int_0^1 (1-Z^n)(1-Z^{n+2})Z\varphi_i(Z)dZ - \dfrac{(n+2)^2}{2n}\epsilon'\int_0^1 (1-Z^n)(1-Z^2)Z\varphi_i(Z)dZ}{\int_0^1 \varphi_i^2(Z)Z(1-Z^n)dZ} \tag{24}$$

The complete solution obtained by adding Θ_s and Θ_1 is:

$$\Theta = \frac{n+2\epsilon'}{n}(1-Z^{n+2}) - \frac{(n+2)^2}{2n}\epsilon'(1-Z^2) - \sum_{i=1}^{\infty} B_i \varphi_i(Z) e^{-a_i X} \tag{25}$$

The first three values of B_i, obtained from equation (24) for $n = 3$, and Bird's values for a_i are given in Table I. The φ_i for this case are tabulated by Bird.[3]

TABLE I

i	a_i	B_i	B_i'
1	6.582	$1.396 - 3.776\epsilon'$	3.776
2	39.09	$0.588 + 0.368\epsilon'$	−0.368
3	99.50	$0.316 - 0.156\epsilon'$	0.156

The effect of expansion can be seen more clearly by separating the effect of expansion from that of heat generation:

$$\Theta = \Theta' - \epsilon' \left[\frac{(n+2)^2}{2n} (1 - Z^2) - \frac{2}{n} (1 - Z^{n+2}) - \sum_{I=1}^{\infty} B_i' \varphi_i(Z) e^{-a_i X} \right] \quad (26)$$

where Θ' is the value of Θ for an incompressible liquid and the B_i' are shown in Table I. The term in brackets is always positive and it rises from zero at $X = 0$ to its maximum value at $X = \infty$. The magnitude of the expansion term is directly proportional to ϵ'.

Figures 1, 2, and 3 show the reduced temperature profiles for ϵ' of 0, 0.2, and 0.3, respectively, calculated from equation (25) with $n = 3$.

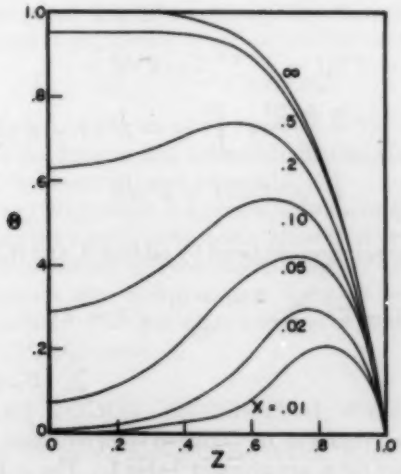

Fig. 1. Reduced temperature profiles, $\epsilon' = 0$, $n = 3$.

The center line temperature is given as a function of X in Figure 4 with ϵ' as a parameter, and Figure 5 shows on an expanded scale the variation of temperature with X for various values of Z when $\epsilon' = 0.3$.

DISCUSSION

The curves show that initially even for small values of ϵ' the fluid in the center of the tube cools since the expansion term is a maximum at this point while the heat generation term is zero. This decrease in the center line temperature approximately follows the adiabatic equa-

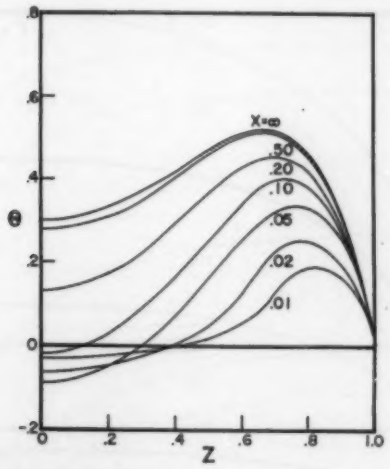

Fig. 2. Reduced temperature profiles, $\epsilon' = 0.2$, $n = 3$.

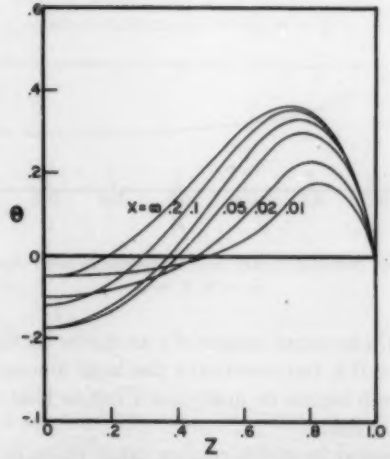

Fig. 3. Reduced temperature profiles, $\epsilon' = 0.3$, $n = 3$.

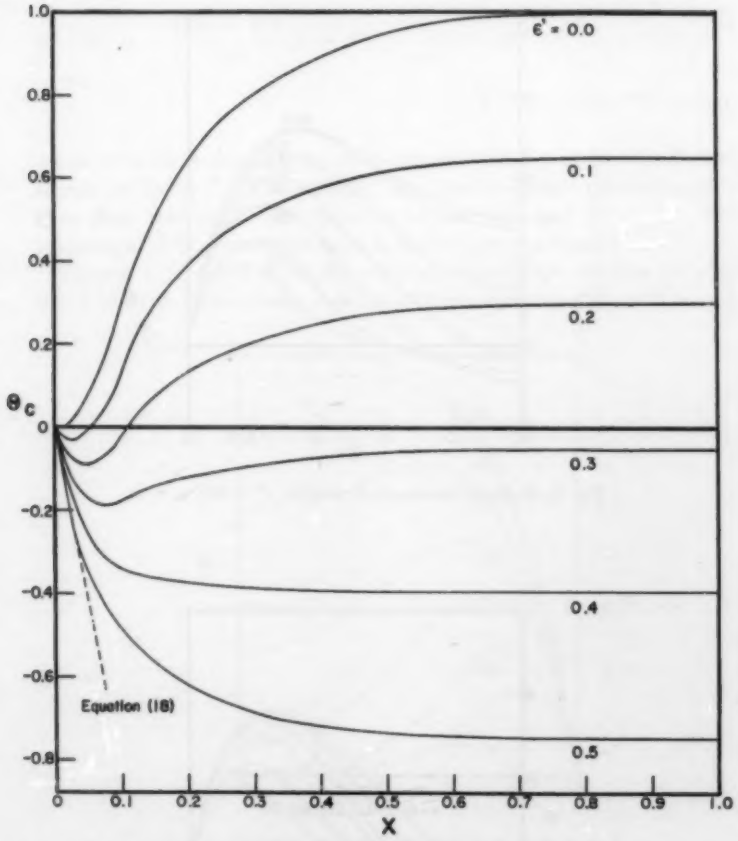

Fig. 4. Variation of reduced center line temperature with distance along tube, $n = 3$, $Z = 0$.

tion (equation 18) for small values of x as shown by the broken line in Figure 4 for $\epsilon' = 0.5$, but eventually the large amount of heat generated near the wall begins to make itself felt as heat is conducted in toward the center line.

During the period in which cooling takes place in the center, the temperature out near the walls is only slightly affected by expansion since the expansion term is small and conduction inward is still small.

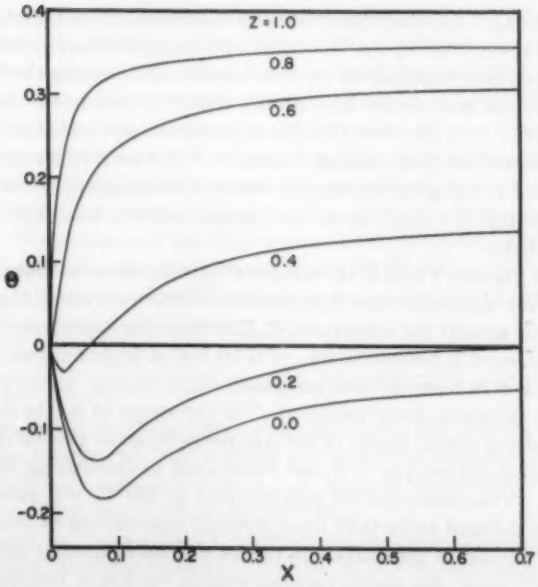

Fig. 5. Change of reduced temperature with distance along tube at varying radical distances, $\epsilon' = 0.3$, $n = 3$.

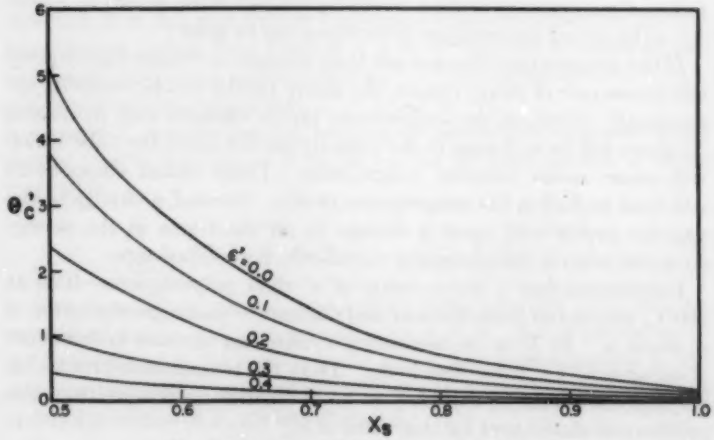

Fig. 6. Unaccomplished temperature change.

However, as X increases heat flows by conduction from the region near the wall toward the center line, causing the center line temperature to fall less rapidly than before or even to rise, and causing the temperature near the wall to rise less rapidly than it would in the absence of expansion. As ϵ' increases the temperature at any value of Z and X decreases and for large enough values of ϵ' the conduction toward the center line is not great enough to return the temperature to its original value and the final center line temperature is less than the inlet temperature.

When Figures 1 and 3 are compared at the same values of X it is found that the maximum temperature difference across the tube is somewhat greater for compressible flow than for incompressible flow up to values of X between 0.05 and 0.10, but at higher values of X the difference is reduced by the expansion.

Many polymers have values of ϵ' in the range of 0.1 to 0.3. The stress–rate of strain curve of certain polyethylenes can be described by equation (2) with $n = 3$, the value used in calculating the above profiles. The value of ϵ' for polyethylene at 200°C. and atmospheric pressure is found to be 0.33 from Spencer and Gilmore's equation of state.[4] At higher pressures the values will be somewhat lower than this. Although the above number cannot be taken too literally it would appear from Figure 4 that the reduced center line temperature for this polymer would lie close to the inlet temperature, and that the reduced temperature profiles would be close to those shown in Figure 3. (The actual temperature differences can be large.)

If the temperature changes are large enough to change significantly the stress–rate of strain curves, the above results can be modified appreciably. First, as the temperature profile changes with increasing X, there will be a change in the velocity profile along the tube which will cause radial velocity components. These radial components will tend to flatten the temperature profile. Second, a change in the velocity profile will cause a change in all the terms in the energy equation, even in the absence of radial velocity components.

Polystyrene has a lower value of ϵ' than polyethylene—0.20 at 200°C. calculated from Spencer and Gilmore[4]—and a greater value of n, about 5. At $X = \infty$, increasing n causes an increase in the effect of expansion,[1] *i.e.*, a decrease in Θ_s. Thus, the temperature profiles for polystyrene would be expected to be of smaller magnitude than the profiles calculated here for this value of ϵ'.

Bird[3] has compared his temperature calculations for an incompressible liquid to experimental flow curves for polyethylene by calculating the flow which would result if the polymer had traveled through the entire tube with the final temperature profile. This procedure, which should overemphasize the temperature effect, appeared to yield too small an effect. If expansion is taken into account the temperature effect is decreased whether the wall is isothermal, as assumed above, or adiabatic, as may have been the case in the flow curves used by Bird. In either case the discrepancy between theory and experiment is apparently increased when expansion is taken into account. However, no positive conclusions can be drawn because of the lack of accurate physical property data.

DISTANCE REQUIRED TO REACH STEADY PROFILE

If a steady temperature profile can be reached and held for a major part of the tube length, the analysis of flow curves would be considerably simplified. Consequently, it is of interest to determine the distance required to reach the steady profile.

Figures 1 to 3 show that the difference between the temperature at any value of X and the steady profile at $X = \infty$ is a maximum at the center line. Consequently, the center line temperatures in Figure 4 can be used as a criterion for the distance needed to approach the steady profile. Most of the temperature change has taken place by the time $X = 0.5$, and Figure 6 gives the unaccomplished center line temperature change for values of X greater than 0.5 in terms of per cent of the maximum possible change, *i.e.*, the change in Θ_c for an incompressible liquid going from $X = 0$ to $X = \infty$.

Thus, if X_s is the value of X which gives the desired approach to the steady profile, equation (12) yields for the distance needed to reach this value:

$$\left(\frac{x}{R}\right)_s = \frac{n+2}{2n} X_s N_{Ps} = \frac{n+2}{2n} X_s \left(\frac{2 R u_m}{\alpha}\right) \tag{27}$$

Equation (27) is general, and follows from equation (14), but the calculated values of X_s are true only for $n = 3$. For other values of n, the values of X_s for $n = 3$ should give a first approximation to the distance required to reach the steady profile, since the profile changes slowly for values of X_s greater than 0.5.

It is interesting to compare equation (27) with the equation for the distance required to reach a steady velocity profile for an isothermal, Newtonian fluid entering a tube with a flat velocity profile. The equation is:

$$(x/R)_s = CN_{Re} \tag{28}$$

and the constant is approximately 0.015 for an approach to within 2% of the steady profile.[6]

Thus, the distance required to reach a steady temperature profile is given by an equation very similiar in form to that which gives the distance required to reach a steady velocity profile, and the Peclet number serves the same function in the temperature case as the Reynolds number does in the velocity case. Since:

$$N_{Pe} = N_{Re}N_{Pr} \tag{29}$$

and since for very viscous liquids N_{Re} is usually small and N_{Pr} is very large, the distance required to reach the steady velocity profile will be much less than the distance needed to reach the steady temperature profile (neglecting the effect of the changing temperature profile on the velocity profile). The ratio of the two distances, in fact, is merely a constant times the Prandtl number.

EFFECT OF TUBE DIMENSIONS

For rheological measurements the shear stress at the wall may be considered to be the major independent variable. If equation (27) is combined with (4) and the force balance:

$$\tau_w = -(dp/dx)(R/2) \tag{30}$$

then

$$x_s = \left(\frac{A}{n}\frac{X_s}{\alpha}\right) R^3\tau_w^{n-1} \tag{31}$$

so for any desired value of τ_w the distance required to reach the steady temperature profile is a minimum when R is a minimum.

As the tube radius and length are varied, the pressure required to attain the desired shear stress also varies. If the actual length is Bx_s, equations (30) and (31) give for the pressure drop:

$$\Delta P = (2BAX_s/n\alpha)R^2\tau_w^n \tag{32}$$

So again the inlet pressure required is minimized when R is minimized.

The third point to be considered is the effect of R on the steady temperature. If we consider the center line temperature given by equation (8) with $Z = 0$ it can be shown that:

$$T_c - T_w = \left[\frac{A\left(1 - \epsilon' \frac{n+4}{2}\right)}{(n+2)^2 k}\right] R^2 \tau_w^n \tag{33}$$

so that the steady temperature is also reduced by reducing the tube radius.

The above calculations indicate that, for a fixed value of the shear stress, the smallest possible tube radius gives the minimum length to reach the steady profile, the minimum inlet pressure, and the minimum temperature gradient. Unfortunately, for a high shear stress the radius required to make this technique practical would be extremely small, but for moderate shear stresses it appears to have possibilities.

Another approach would be to attempt to minimize the temperature gradients at distances less than X_s. To do this simply we approximate the maximum reduced temperature by:

$$\Theta_{max} = 0.274 X^{1/3} \tag{34}$$

Θ_{max} is the maximum reduced temperature, obtained from Figure 2, where $\epsilon' = 0.2$. The above equation is a rough approximation for values of X from 0 to about 0.5. From equation (34) we obtain:

$$T_{max} - T_w = \frac{0.274(\alpha A^2)^{1/3}}{(n+2)^2 k} x^{1/3} R \tau_w^{(2n+1)/3} \tag{35}$$

Now the temperature gradients are minimized by decreasing R and x, but the effect of changing x is small and the effect of changing R is less than in the previous case. For high values of τ_w, operating at a minimum R and x is the only possibility, so that rheological data have to be interpreted for a system in which the temperature is varying in both the radial and the axial directions.

References

1. H. L. Toor, *Ind. Eng. Chem.*, **48**, 922 (1956).
2. H. C. Brinkman, *Appl. Sci. Res.*, **A2**, 120 (1951).
3. R. B. Bird, *Society of Plastics Engineers Journal*, **1**, September (1955).
4. R. S. Spencer and G. P. Gilmore, *J. Appl. Phys.*, **21**, 523 (1950)
5. H. L. Toor and S. D. Eagleton, *J. Appl. Chem.*, **3**, 354 (1953).
6. S. Goldstein, *Modern Developments in Fluid Dynamics*, Vol. I, Oxford Univ. Press, Oxford, 1938.

Synopsis

The energy equation has been solved for the case of a compressible non-Newtonian liquid entering a tube at temperature equal to the wall temperature. It is shown that the temperature in the center of the tube initially decreases with distance due to expansion of the liquid while away from the center it increases with distance due to frictional heat generation. For most polymers the heat generation eventually predominates and at some distance along the tube the center line temperature begins to rise. The increase continues until the steady temperature profile is reached. A simple equation is presented which gives the distance required to closely approach the steady profile, and two different methods for obtaining rheological data are considered.

TRANSACTIONS OF THE SOCIETY OF RHEOLOGY VOL. I, 191–202 (1957)

The Thermal Incline: A Means of Measuring Viscosities of Plastisols at Elevated Temperatures

E. T. SEVERS* and J. M. AUSTIN,
Bakelite Fellowship, Mellon Institute, Pittsburgh, Pa.

INTRODUCTION

Change in viscosity with temperature is an important factor in the formulation and application of many engineering materials. Usually, a rise in temperature produces a decrease in viscosity of the material. In the case of plastisols, which are fluid dispersions of a vinyl chloride resin in a plasticizer, raising the temperature decreases the viscosity of the plasticizer. However, this simultaneously increases the solvation of the resin by the plasticizer and, therefore, the viscosity of the mixture is increased. This makes possible the application of plastisols by dipping, slush molding, rotational casting, and roller and knife coating. In addition, plastisols may be foamed in the fluid state and gelled or fused by heat to preserve the applied shape.

Although heating results in tremendous viscosity changes in plastisols, most flow data are based on room temperature measurements. The lack of data at elevated temperatures is a result of the experimental difficulties involved in obtaining them.

Conventional methods of viscosity determination, such as rotational viscometers or extrusion rheometers at elevated temperatures, are difficult to use since the material often changes viscosity faster than measurements can be made. Furthermore, the viscosity is a first-order function of: the speed of rotation, or torque, of a rotational viscometer; and the applied pressure, or efflux rate, of the extrusion rheometer. This means that, for large viscosity changes, a series of bobs or orifices must be used to obtain satisfactory measurements.

* Present address: Natvar Corporation, Woodbridge, N. J.

There is a need for some device that will rapidly measure the viscosity of heat-sensitive materials, such as plastisols, and at the same time have the measured variable of a higher ordered function of viscosity so that large viscosity ranges may be accommodated.

APPARATUS

Thermal gradient bars designed for melting point measurements have been used for determining the gel point of plastisols, and inclined planes have been used to determine the fluidity of plastisols at a single temperature. Combination of these two instruments results in a

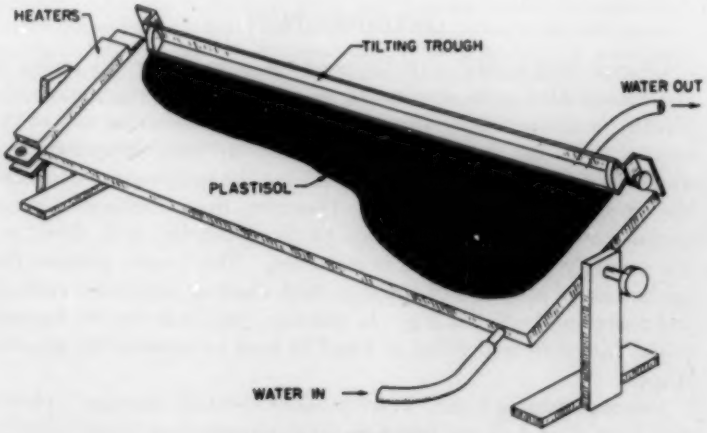

Fig. 1. Thermal incline.

thermal gradient inclined plane or thermal incline. The main part of the instrument is a plane plate of aluminum 30 inches long, 6 inches wide, and 0.5 inch thick as shown in Figure 1. Pivots support the plate at the center of each end, and one of the pivots is spring-loaded and retractable to provide for thermal expansion and removal of the bar from the frame. The small contact area of the pivot mounting also minimizes heat losses by conduction to the frame. The plate is heated at one end by two 150-watt strip heaters and cooled at the other end by the passage of water through a channel parallel to the end.

A 25 inch long tilting trough, made of aluminum angle bar with $^5/_8$ by $^5/_8$ inch inside dimensions, is supported by pivots at the upper side of the plate. One of the pivots is spring-loaded and retracts for removal of the trough, and the supports attaching the trough to the plate are insulated from the plate by Transite wallboard.

The plate has scribed lines at 5-centimeter intervals along its length to facilitate the location of temperature determinations by means of a surface pyrometer. Temperature of the hot end is controlled by a variable transformer which supplies power to the strip heaters.

PROCEDURE

Operation of the thermal incline is illustrated by a test on a plastisol. The attainment of constant temperature is indicated by spot measurements of temperature at intervals of time and requires about 30 to 40 minutes when starting with a cold plate. Once constant temperature has been obtained, subsequent runs may be made immediately. Aluminum foil, 1 mil thick, is placed on the upper surface of the plate using a dioctyl phthalate plasticizer as an undercoat to facilitate smoothing and eliminate an air film between the foil and plate. An extremely thin coating of plasticizer applied to the top of the foil by means of a cloth reduces surface tension effects which cause irregular profiles of flow. Temperatures at 10-centimeter intervals along the center line of the plate are recorded just prior to application of the plastisol and are later plotted *versus* distance, so that the temperature at any point along the plate may be obtained. The trough is not attached until use to prevent its heating by radiation. The trough is filled level full with plastisol, placed in position on its pivots, and tilted to discharge plastisol onto the plate. The plate may be at any desired angle but best results with plastisols have been obtained by keeping the plate horizontal for 120 seconds and then inclining at 15 degrees from horizontal for 10 seconds. The horizontal position allows time for heating the plastisol prior to flow. At the end of the 10-second period, the plate is quickly returned to a horizontal position, the foil supporting the plastisol is removed, and the plastisol is gelled with a heat lamp. The flow down various lines of the inclined plane is measured from the point of contact of the trough with the plate to the leading edge of the plastisol. The flow

in centimeters is plotted *versus* temperature of the surface of the plate at the line of flow.

RESULTS USING PLASTISOLS

The results of this procedure applied to a series of plastisols are shown in Figure 2. This indicates the effect on flow of various plasti-

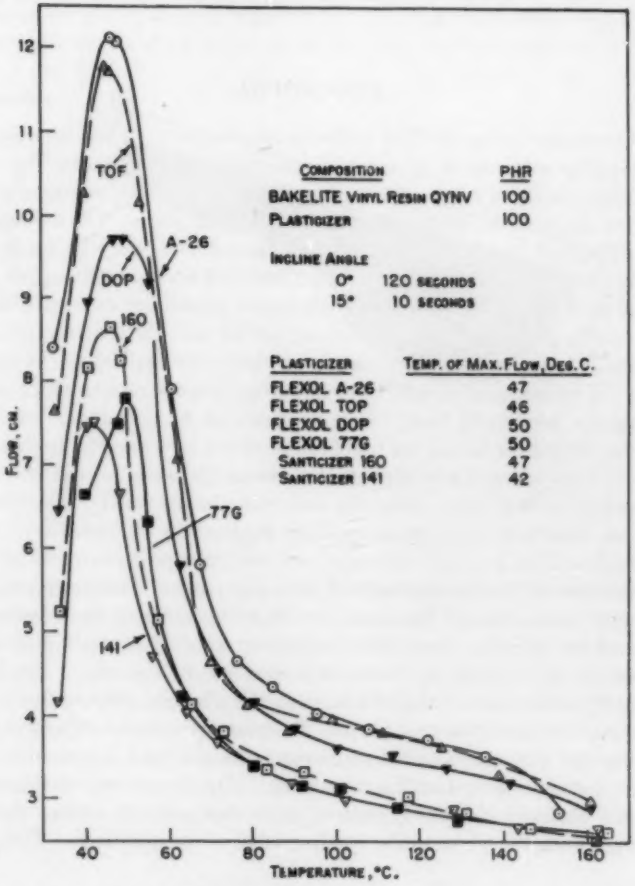

Fig. 2. Effect of plasticizer on flow of plastisols.

cizers with 50% Bakelite vinyl resin QYNV present. At lower temperatures, the flow increases with temperature because the fluidity of the plasticizer is increased. However, solvation of the resin, which decreases the fluidity, soon overcomes the increase in fluidity of the plasticizer, and causes a maximum in the distance of flow. At higher temperatures, the plastisol is quickly gelled and little flow occurs.

The temperature of maximum flow for the various plastisols did not vary as much as one might expect, and ranged from 42°C. for

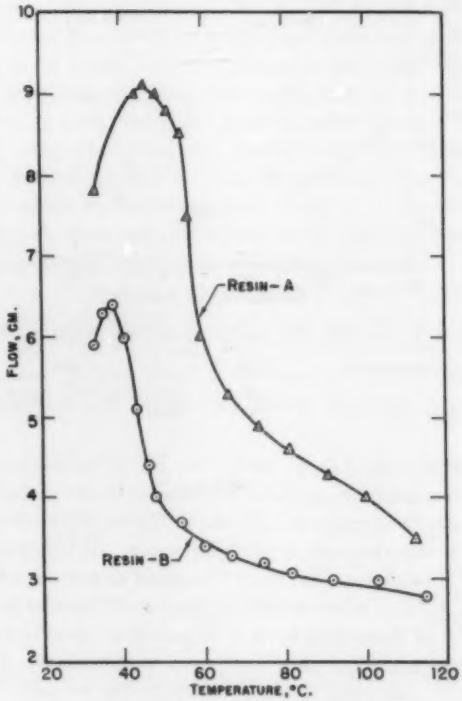

Fig. 3. Effect of resin on flow of plastisols:

Composition	PHR
Resin	100
Santicizer 141	100

Incline angle 0° for 120 seconds and 15° for 10 seconds.

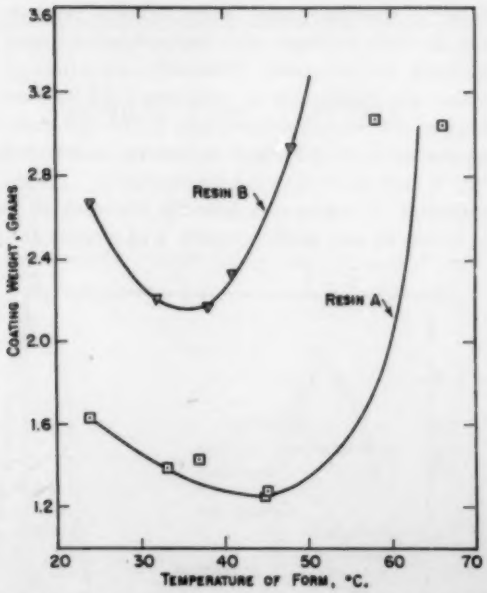

Fig. 4. Effect of form temperature on coating weight of plastisols:

Composition	PHR	Form
Resin.....	100	1-inch diam. test tubes, water-filled
Santicizer 141	100	

Santicizer plasticizer 141 to 50°C. for Flexol plasticizers DOP and 77G. There were more marked differences in the distance of flow at the maximum temperature. Most of these differences are due to differences in the viscosity of the plasticizer. If the height of all the curves were changed so that they coincided at a lower temperature—for instance, 40°C.—there would be smaller differences in the maxima.

The utility of these flow tests is apparent in several ways. Plasticizers producing low maxima and lower temperatures of gelation are desirable for reducing tearing during dip-coating. Conversely, plasticizers with high maxima and high temperatures of gelation promote viscosity stability at slightly elevated temperatures and increase flow-out after application. Plastisols requiring a change in formulation and maintenance of flow properties through a range of

temperature should not have substitution of plasticizers on a weight-for-weight basis but on the basis of contribution to flow properties. For example, substitution of Flexol plasticizer TOF for DOP could be accompanied by the addition of some Flexol plasticizer 77G to offset the increased fluidity of the TOF. If film properties are not critical, the amount of TOF could be reduced when replacing DOP.

The effect of using different vinyl chloride resins on the flow of plastisols is shown by Figure 3. Two experimental resins are compared in a plastisol formulation containing Santicizer plasticizer 141. The resin A plastisol has greater flow and a higher temperature of maximum flow.

These data were compared with dipping properties by the following experiment. Test tubes 1 inch in diameter were filled with water to increase the heat capacity, and were preheated at various temperatures to simulate the procedure used in dipcoating. These tubes were dipped into the plastisol, slowly withdrawn, and plunged into a glycerin bath at 350°F. until the coating was fused. After cooling, the coating was removed and weighed. Temperatures were obtained with a thermometer immersed in the test tube during dipping and are shown plotted *versus* coating weight in Figure 4.

Comparison of these dipping tests with the data of Figure 3 indicates that the coating weight decreased as the fluidity increased to a maximum. After the maximum fluidity was exceeded, the coating weight increased as the fluidity decreased. The location of the maximum fluidities and minimum coating weights are compared in Table I.

TABLE I

Resin	Min. coating wt.	Max. flow
A	45°C.	45°C.
B	36°C.	37°C.

The temperature of maximum flow determined by the thermal incline predicted the temperature at which minimum coating weight occurred in dipping. Furthermore, there was qualitative agreement between the distance of flow-out and the coating weight. The resin A plastisol, having the greater flow, produced the lesser coating weight.

These results demonstrate the importance of selecting the proper preheat temperature in dipping operation. Too low a preheat temperature will allow a temporary increase in fluidity during the fusion cycle as the plastisol is heated through its maximum fluidity, and the increased flow will result in tears. However, in some cases a small amount of increased flow may be desirable to improve gloss by flow-out.

The data obtained by using the foregoing method are useful as formulating and control testing, but it is often desirable to obtain flow information in a more fundamental form. It is also important, even when obtaining empirical data, to know the fundamentals underlying the procedure.

THEORETICAL CONSIDERATIONS

Consider the flow of a unit width of liquid down an inclined plane.

Let z be the axis normal to the plane and x be the axis down the plane in the direction of flow. Then, according to Lamb,[1]

$$\eta \, (\partial^2 u/\partial z^2) = -\rho g \sin \alpha \tag{1}$$

where η = viscosity, u = velocity, z = distance on axis normal to plane, ρ = density, g = acceleration of gravity, and α = angle between plane and horizontal.

When $z = 0$, $u = 0$ and when $z = h$, $u = U$, where h is the depth of liquid normal to the plane and U is the maximum velocity. Solving equation (1) for u, determining U by setting $du/dz = 0$, integrating equation (1) between the boundaries, and substituting for U, we obtain:

$$\int_0^h u dz = \frac{h^2 \rho g \sin \alpha}{3\eta} \tag{2}$$

The left-hand side is the volumetric flow rate per unit width and equals $\bar{u}h$ where $\bar{u}$ is the average velocity in the profile of flow.

Substituting and rearranging.

$$\bar{u} = d\bar{x}/dt = (h^2 \rho g \sin \alpha)/3\eta \tag{3}$$

where $\bar{x}$ = average distance down plane and t = time.

If the assume that the thickness of the liquid at any given time is uniform down the plane, then the volume per unit width:

$$V = h\bar{x} \tag{4}$$

Substituting (4) into (3) we obtain:

$$\eta = (V^2 \rho\, g \sin \alpha\, dt)/3\eta\bar{x}^2 d\bar{x} \tag{5}$$

which for small differences is:

$$\eta = \frac{V^2 \rho g \sin \alpha\, (t_2 - t)}{3\eta \left[\frac{(\bar{x}_2^2 + \bar{x}_2^2)\ (\bar{x}_2 - \bar{x}_1)}{2} \right]} \tag{6}$$

If we integrate (5) we obtain:

$$\eta = [V^2 \rho g \sin \alpha\, (t_2 - t_1)]/(\bar{x}_2^3 - \bar{x}_1^3) \tag{7}$$

Equations (6) and (7) produce equivalent results when $\bar{x}_2 - \bar{x}_1$ is small compared to $\bar{x}_1$. For instance, when $\bar{x}_2 - \bar{x}_1$ is 20% of $\bar{x}_1$ the viscosities calculated by the two equations differ only by 1.6%.

Examination of (7) indicates that the viscosity of the liquid is inversely proportional to the cube of the velocity of flow down the plane. This means that liquids having a wide range of viscosities may be studied under the same set of experimental conditions without flowing beyond the edge of the incline.

Results Using Newtonian Liquid

The equations for flow down the incline were tested as follows: The procedure was similar to that employed previously for plastisols except that photography was used to record the distance of flow down the incline and at the same time record the time by a stopwatch in the field of view. Multiple exposures were made on the same film which was parallel to the plane of the incline. The test liquid was UCON Brand 50HB44,500 (Experimental), a viscous, polyalkylene glycol, Newtonian liquid of good thermal stability. Viscosity determinations were made on this lubricant using a modified Ostwald viscometer of the Cannon-Fenske type. The data are shown in Table II.

TABLE II
Thermal Incline Data—Ucon Lubricant

Temp., °C.	Density, g./cm.³	Distance of flow, cm. 23.1 sec.	47.0 sec.
32	1.062	4.12	4.85
38	1.057	4.40	5.26
44	1.053	4.45	5.48
51	1.043	4.66	6.04
58	1.038	5.21	6.46
66	1.032	5.61	7.07
74	1.027	6.48	8.16
82	1.020	7.29	9.15
91	1.013	8.29	10.50
100	1.006	9.70	12.12

Volume of material discharged per unit width of trough = 1.015 cm.³/cm. Sin α = 0.282.

TABLE III
Capillary Viscometer Data

Temp., °C.	Viscosity, poises
37.8	101.1
54.4	50.8
98.9	14.24

Using these data in equation (6), viscosities were calculated at various temperatures and are shown by Figure 5. Calculation by equation (5) gave almost identical results since the differences in flow distance were small compared to total flow distance. Viscosities were obtained using the capillary viscometer and plotted in Figure 5 for comparison.

The lines obtained by the two methods are skewed, with the thermal incline data producing lower viscosities at high temperature and higher viscosities at low temperatures. The point of intersection is at 60°C., which was at the center line of the liquid flowing down the incline. As the liquid flows, the height decreases, with the hotter and more fluid liquid at one end of the incline decreasing in height faster than the more viscous liquid on the cold end of the incline. This creates a difference in height between the cold and hot ends and it is possible for liquid to flow to the hot end at the expense of the cold end.

This could increase the apparent viscosity at the cold end and decrease the apparent viscosity at the hot end since the equations used assume no flow across the incline. The skewing of the lines could be caused by such a flow.

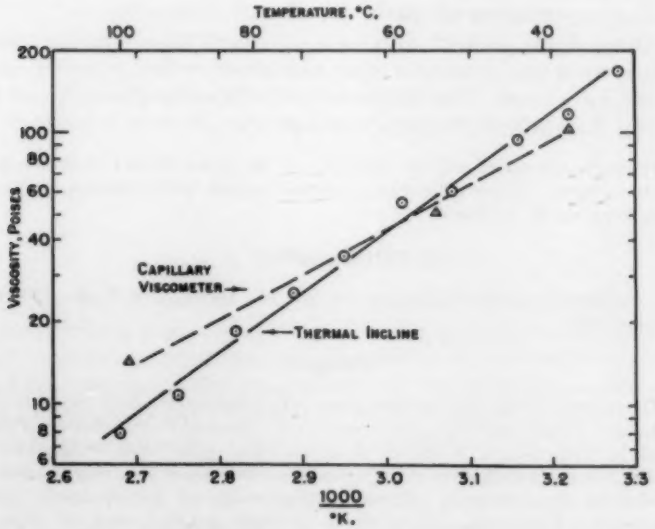

Fig. 5. Viscosity of Ucon lubricant.

Considering the assumption of a rectangular profile down the incline, the agreement between the two methods of viscosity determination is considered good and justifies the statement that the viscosity is at least roughly inversely proportional to the cube of the distance of flow.

CONCLUSIONS

These experiments have demonstrated that the two things sought for in an instrument for measuring the viscosity of plastisols over a wide range of temperatures have been achieved. First, use of the thermal incline is rapid, requiring less than three minutes from the dumping of the trough to the end of flow. Second, the measured

variable, distance, is a higher order function of the viscosity which permits a wide range of viscosities to be measured at one time. If the limits of the incline are exceeded, it is simple to change the angle or decrease the volume of liquid applied. One other advantage in the case of plastisols is that the flow pattern may be preserved by gelation to form a permanent record.

Although the thermal incline was developed for evaluating plastisols, it could also be used for other heat-sensitive fluid polymers, such as polyester resins. An improved version is being manufactured by Castor Engineering Company, Carnegie, Pa.

Mathematical advice and the assistance of Mr. Louis Zapas is acknowledged by the author. The experiments on coating weight determinations were performed by Mr. R. D. Swain.

Reference

1. Sir Horace Lamb, *Hydrodynamics*, 6th ed., Dover, New York, 1945, pp. 577 and 582.

Synopsis

The thermal incline is an inclined plane with a thermal gradient perpendicular to the line of flow, enabling a continuous measurement of fluidity through a wide range of temperatures. Data are presented showing the effect of formulation on the flow of vinyl chloride resin plastisols and how these data may be used to predict the temperature of minimum coating weight of dipped objects. Viscosities of a Ucon (polyalkylene glycol) lubricant obtained using the thermal incline agree reasonably well with viscosities obtained from capillary viscometer data.

TRANSACTIONS OF THE SOCIETY OF RHEOLOGY VOL. I, 203–212 (1957)

Capillary Flow of Molten Polyethylene—A Photographic Study of Melt Fracture

J. P. TORDELLA, *Polychemicals Department, E. I. du Pont de Nemours & Company, Inc., du Pont Experimental Station, Wilmington, Del.*

I. INTRODUCTION

In the flow of amorphous or molten polymers through capillaries, a rather striking phenomenon occurs.[1–3] At and above a critical flow rate or pressure, the surface and cross-section of the extruded polymer become irregular. The cross-section of the extruded polymer no longer resembles the cross-section of the capillary or die through which it was extruded. The lower four specimens in Figure 1 illustrate the effect. The magnitude of the nominal shear rate at which this phenomenon occurs varies with the polymer, its molecular weight, the extrusion temperature, and the shape of the inlet to the capillary.

The cause of the irregularly shaped extrudates has been the subject of previous studies. In one of these,[1] it was concluded that the cause of the irregularity was fracture or rupture of the molten polymer in the vicinity of the capillary inlet. This conclusion was based largely on the flow behavior of several unusual specimens. The pertinent observations were (*a*) clearly audible tearing noise during flow, (*b*) specimens whose surfaces were irregular to the extent of being jagged and even discontinuous, (*c*) indications that flow in the capillary inlets was not axially symmetric.

In this study, flow of polyethylene in the inlet regions of capillaries was observed directly in glass apparatus. The purpose of the work was to provide a basis for judging the validity of the hypothesis that fracture or rupture occurring in capillary inlets may cause irregularly shaped extrudates.

II. EXPERIMENTAL

(a) Apparatus

The experiments were carried out using a capillary viscometer designed for study of molten polymers. This instrument, described in greater detail elsewhere,[1] consisted of a heated metal cylinder to which metal capillaries could be attached and within which a piston was driven by a pneumatic cylinder. For the experiments described

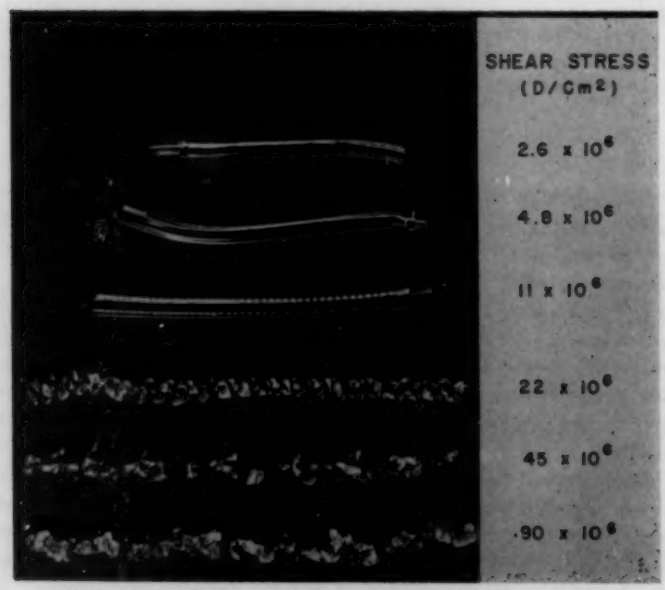

Fig. 1. Polymethyl methacrylate specimens extruded at 170°C.

herein, the steel capillary was replaced by a 1 in. diameter, commercial, glass to metal seal. The arrangement is shown schematically in Figure 2. The glass to metal seal (D) was essentially an extension of the rheometer cylinder. At the bottom of the glass section, which was about $^1/_2$ in. I.D., a capillary about $^1/_{16}$ in. in diameter was formed. The sleeve or bushing (B), hard soldered to the glass to metal seal, and the lock nut (C) provided mechanical connections to the rheometer cylinder (A). An air thermostat (E), constructed of glass tubing, was used to maintain the glass to metal cylinder and capillary at the

temperature of the rheometer cylinder. This arrangement provided a means of observing flow of the molten polyethylene in the inlet region of a capillary. (The glass to metal seals were capable of sustaining pressures as large as 1,000 p.s.i. repeatedly for times at least as long as $^1/_2$ minute.) For convenience, the glass tube will be referred to as the cylinder, and the region of this cylinder just above the capillary, as the capillary inlet or inlet. The contour of the inlets was quite flat, approximately as indicated in Figure 2.

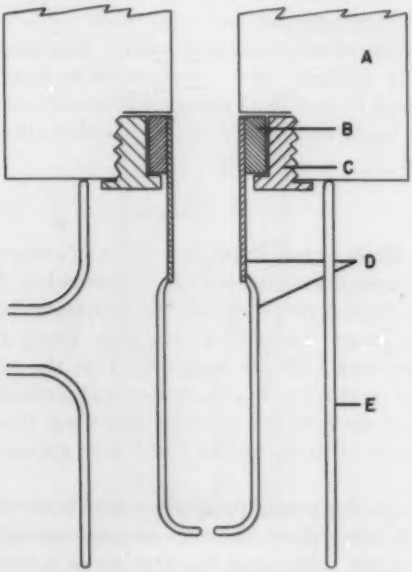

Fig. 2. Diagram of capillary rheometer assembly.

The polymer used was a commercial, high pressure, polyethylene characterized by a density of 0.914 d_4^{25} (specimen annealed $^1/_2$ hr. at 100°C. prior to density determination) and a melt index (ASTM D-1238–52T) of 1.7. The particle size of the sample was in the range 10 to 100 mesh. The temperature of the molten polymer was 125°C. except as noted.

Molten polyethylene is clear and colorless. Its refractive index is not much different from that of glass. As a result, the polymer–glass interface was not readily apparent. Likewise, flow of the poly-

mer was not visible except from the velocity of the extrudate. To provide an indication of flow, small particles of carbon filled polyethylene were added. The particles, which were about 25–50 mesh in size, constituted about $^1/_{20}\%$ of the volume of the sample. Two carbon black filled compositions were used. Of these, one was "hard"; it contained about 25% carbon and its viscosity was about eightfold larger than that of the matrix of natural polyethylene. The other black composition was "soft" by comparison; it contained about 1% carbon and its flow properties were almost identical to those of the matrix polymer.

Results were recorded photographically. The glass apparatus was back-lighted by diffused light. A standard motion picture camera capable of speeds from 8 to 64 frames per second was used except for one sequence, which was made with a high speed camera at about 600 frames/second.

(b) Results

With Hard Black Tracer Particles. Flow of compositions containing the hard black tracer particles was observed at flow rates below and above the critical rate at which the extrudates became irregular. At flow rates below the critical rate, the black particles moved smoothly down the cylinder, accelerated in the inlet region, and flowed out the capillary. The flow appeared laminar; the particles near the axis of the cylinder moved faster than those near the periphery. Flow in both the cylinder and inlet appeared axially symmetric.

There were two features of possible interest in the flow at rates below the critical rate. First, the net change in size of the hard black particles was small. Although the amount of deformation of these particles in the inlet region was 100 to 300%, the particles substantially recovered to their initial size after emerging from the capillary.

The second additional feature was the formation of a gradual streamlined inlet of molten polymer just above the glass inlet. This inlet was indicated by the configuration of the two hard black particles in the inlet region in Figure 3. The polymer in the volume between the streaks and the wall of the glass cylinder appeared to be trapped. This was obvious in another experiment carried out at 250°C. Several black particles occurred in the volume of polymer near the glass

inlet. As shown in Figure 4, these particles (and the matrix polymer as well) circulated but did not flow out. At the interface between the polymer inlet and the flowing stream, the particles and the associated matrix polymer flowed toward the capillary. However, near the capillary the trapped polymer flowed away from the capillary, up the cylinder, and then down again near the interface.

At the onset of the phenomenon of melt fracture when the extrudates became irregular, the flow pattern in the inlet region underwent a marked change. Flow in this region was neither axially symmetric nor stable. The black particles did not move toward the capillary continuously. Rather a given particle (and, presumably,

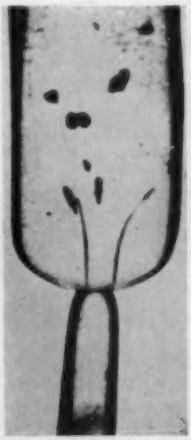

Fig. 3. Elongated black particles which indicate formation of polymer inlet.

the volume of matrix polymer immediately surrounding it) advanced, paused, and then retreated. At the time one particle retreated, another or other particles advanced. The rather unusual case of a "see-saw" mode of flow with a net positive flow toward the capillary is illustrated in Figure 5. These axially unsymmetric and irregular flow effects, which began at the flow rate at which the extrudate became irregular, increased in degree and rate with further increase in flow rate.

Effects similar to those described above were observed at 190 and 250°C. While the net flow was faster, the magnitude of the irregular flow effects did not appear to decrease at the higher temperatures.

With Soft Black Tracer Particles. The flow behavior of the soft black tracer particles was substantially the same as that of the matrix, natural resin. As a result, in the laminar flow region in the cylinder, the soft tracer particles deformed into long black streaks. These streaks provided a more continuous indication of the mode of flow in the inlet region than that provided by the hard tracer particles.

Fig. 4. Sequence showing counterclockwise circulation of black particles trapped in polymer inlet. The numbers on the photographs identify individual particles. The numbers below the photographs refer to the position of the individual photograph in the sequence made at 8 frames per second.

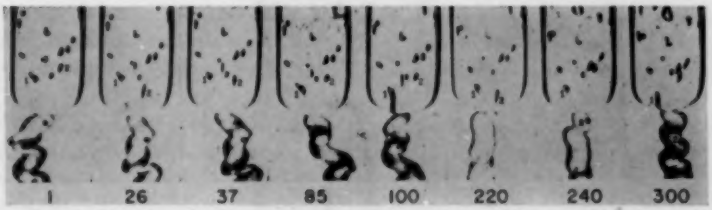

Fig. 5. Sequence showing "see-saw" motion of two black particles toward capillary. The numbers on the photograph identify individual particles; those under the photograph refer to the position in the sequence made at 32 frames per second.

At rates below the critical rate, regular, stable flow occurred. The streaks converged and elongated sharply in the inlet region, but remained continuous and separate in the inlet, in the capillary, and in the extrudate. At rates above the critical rate, flow in the inlet region was neither symmetric nor stable. As a result, the stretched-out black particles were discontinuous in the extrudates.

Characteristic flow behavior in the inlet is illustrated in a sequence of photographs in Figure 6. Cessation of flow into the capillary of one streak is shown. The first photograph illustrates the normal appearance of the streak during its flow into and through the capillary.

In the following three frames, successively $^1/_{600}$ sec. later, that part of the streak in the capillary became successively thinner till, in the fifth frame, it had disappeared. From then on through the twenty-fifth frame, the end of the streak drew up from the capillary. The complete cycle for this streak, flow, cessation, and retraction occurred over several hundred frames.

It appeared from photographs of the type shown in Figure 6 that flow of a given streak into the capillary suddenly ceased. That part

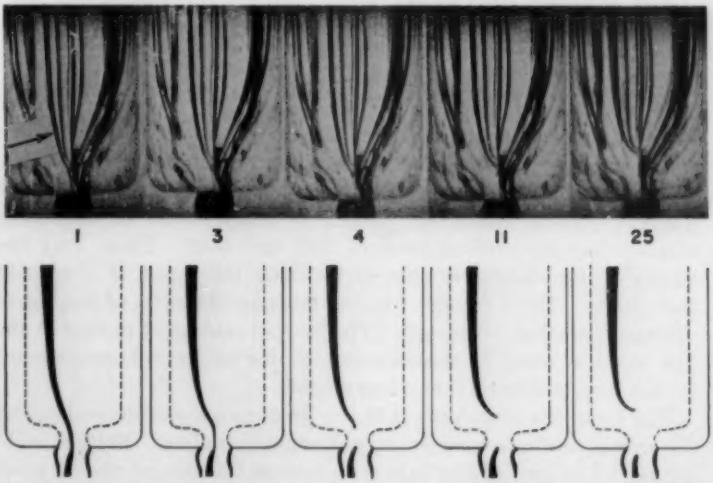

Fig. 6. Photographs of flow of polyethylene containing soft, black particles. Cessation of flow of the marked streak in the first photograph shown schematically. Numbers under photographs indicate position of frame in sequence made at 600 frames per second.

of the streak remaining within the capillary was subsequently carried through by polymer entering from another part of the inlet region. The site of the phenomenon was very close to the beginning of the capillary where the shear stress and shear rates presumably approach the maximum of the system.

III. DISCUSSION

Conclusions of earlier work that the occurrence of extrudates of irregular shape was accompanied by irregular flow in the capillary melt

were clearly demonstrated. The cause of the irregular flow was not visible. It appears appropriate, therefore, to reconsider the hypothesis that the cause is fracture or rupture of the molten polymer.

Onset of Reynolds' turbulence is a possible explanation of the phenomenon. However, this is unlikely since (*a*) the magnitude of the Reynolds numbers at onset of the phenomenon is very small and (*b*) the dependence of the critical flow rate on viscosity and capillary radius predicted by the Reynolds criterion does not obtain.

The Reynolds equation is usually written in terms of the mean velocity of the liquid in the tube. For the present purposes, it is convenient to express the mean velocity in terms of the flow rate:

$$R_e = V\rho R/\eta = (Q/R\eta)(\rho/\pi)$$

where R_e is the Reynolds number, V the mean velocity, ρ the density, R the capillary radius, η the viscosity, and Q the flow rate, which is $V\pi R^2$. Calculated values of the Reynolds number are given in Table I. These values are several to many orders of magnitude smaller than the critical value of 1000 and 1500. These very low values of the Reynolds number preclude the onset of Reynolds' turbulence. The Reynolds number involves the ratio of inertial to viscous dissipation of energy. The inertial storage of energy at the flow rates at onset of the phenomenon for polytetrafluoroethylene, for instance, is so small that it is negligible.

The Reynolds turbulence criterion predicts a linear dependence of the critical flow rate on viscosity and capillary radius. Neither is observed. The critical flow rate is an inverse function of viscosity (*cf.* Table I and references 1 and 2). The critical flow rate varies as the third power of the radius[1-3] rather than as the first power.

The applicability of the melt fracture or rupture hypothesis to the unsteady flow phenomenon appears to depend on whether such a mechanism would require formation of visible voids. Formation of voids is not necessary. While tensile fracture might be expected to result in voids, no such restriction is necessary for the case of shear fracture. The only requirement is that there be a shear surface across which the liquid structure is weakened or ruptured. The stress concentrations at the extremities could easily cause the rupture to propagate to such a size that a macroscopic flow disturbance would result. Void formation is neither necessary in shear failure nor probable in capillary inlets in view of the large hydrostatic pressure in that region.

TABLE I

Reynolds Numbers at Onset of Melt Fracture

Material	Capillary			Data at Onset of Fracture (1)			
	Temp., °C.	Diam., in.	Length, in.	Apparent viscosity,[a] poises	Shear rate, $4Q/\pi R^3$, sec.$^{-1}$	Flow rate, cc./sec.	Reynolds Number
Polytetrafluoroethylene	350	0.170	0.170	10^{10}	2×10^{-4}	1.6×10^{-6}	4.7×10^{-10}
Polyethylene	125	0.062	0.062	1.1×10^{5}	1×10	3.9×10^{-3}	1.4×10^{-7}
Polymethyl methacrylate	200	0.031	0.500	5×10^{4}	1×10^{2}	4.8×10^{-3}	7.7×10^{-7}
66 Nylon	275	0.031	0.050	3.2×10	2.8×10^{5}	1.4×10	3.9

[a] Apparent viscosity $= (PR/2L)/(4Q/\pi R)$, where P is pressure, R and L are capillary radius and length, respectively, and Q is volume rate of flow.

The experiments described herein did not prove that a shear failure mechanism is involved. They did demonstrate that irregular, unsteady flow effects of a type which would be expected to accompany shear failure do occur. Strong support of the rupture or fracture mechanism is to be found in the tearing noises sometimes audible during extrusion and the occurrence of jagged and discontinuous extrudates. In view of the combined evidence, it was concluded that shear fracture of rupture does occur in capillary inlets at and above a critical shear rate, and that irregular, unsteady flow results. Strain recovery at the outlet of the capillary, partially reproduces these irregular flow effects. Extrudates of irregular shape are the result.

References

1. J. P. Tordella, *J. Appl. Phys.*, **27**, 454 (1956).
2. R. S. Spencer and R. E. Dillon, *J. Colloid Sci.*, **4**, 241 (1949).
3. Bagley, *J. Appl. Phys.*, to be published.

TRANSACTIONS OF THE SOCIETY OF RHEOLOGY VOL. I, 213-222 (1957)

Proposed Nomenclature for Linear Viscoelastic Behavior*

HERBERT LEADERMAN, *National Bureau of Standards, Washington 25, D. C.*

I. INTRODUCTION

A systematic standardized nomenclature is very desirable to facilitate communication among physicists working in the same field or in associated fields; such a nomenclature gives names and symbols to measurable related quantities. After the fundamentals of a branch of physics are fairly well established, it is then possible to draw up a logical complete nomenclature system. Unfortunately, by that time the field is usually burdened with several systems which are not generally accepted and which are not completely logical; these systems may or may not be related to nomenclature systems in associated branches of physics.

Ideal nomenclature systems which are prepared subsequent to the understanding of the relationships between measurable quantities in a branch of physics are often proposed. They may represent radical departures from more or less established usage; under these circumstances the proposals do not gain general acceptance. A practical improvement on a haphazard nonstandardized nomenclature can only be gained by adhering as closely as possible to existing usage. In this report an attempt has been made to devise a nomenclature following this principle.

When certain materials are deformed such that the stored elastic energy and the rate of dissipation of mechanical energy are sufficiently small, then the mechanical behavior of these materials approximates to the idealized behavior known as *linear viscoelastic behavior*, which may be defined in general by equations such as (1) and (2) given

* This is the final report of the Committee on Nomenclature of the Society of Rheology.

below. This report deals with a proposed nomenclature for primary measurable quantities and for related quantities applicable to *isotropic* materials manifesting (approximate) linear viscoelastic behavior. While this nomenclature is planned primarily in order to systematize the somewhat extensive literature on the behavior of amorphous polymeric systems, it is also adaptable, perhaps with some modifications, to other materials such as inorganic glasses and metals. The *proposed nomenclature* is given in Table II, which contains *primary measurable quantities*. In Table III are given certain *auxiliary quantities*, namely, limiting values and spectra. No attempt has been made to make this nomenclature consistent with the nomenclature for dielectric behavior, since in practice only one of the four primary methods of presenting data considered in this report is used in the specification of dielectric behavior. Furthermore, no attempt has been made to prepare a *complete* system of nomenclature. For materials manifesting linear viscoelastic behavior, many different methods of specifying behavior are possible; in the present proposed nomenclature a minimum number of measurable and related quantities are defined. The text of this report gives the basis for the nomenclature, and some of the relations between the quantities specified in Tables II and III. For the reasons given above, generally accepted usage has been followed as much as possible.

II. STEP-FUNCTION AND DYNAMIC MODULI AND COMPLIANCES

The linear viscoelastic behavior of a material (at a given temperature) is generally specified by the response of the material in certain types of experiment. While any reasonable type of experiment is theoretically acceptable, in practice four types of experiment are customarily considered for the specification of viscoelastic behavior. Linear viscoelastic behavior may be specified in general by either of the equivalent relations:

$$\epsilon(t) = \int_{-\infty}^{t} \frac{d\sigma(u)}{du}\, k(t-u)\, du \tag{1}$$

$$\sigma(t) = \int_{-\infty}^{t} \frac{d\epsilon(u)}{du}\, m(t-u)\, du \tag{2}$$

where $\epsilon(t)$ is a strain and $\sigma(t)$ is a stress at time t, and $k(t)$ and $m(t)$ are time-dependent functions of the dimensions, respectively, of compliance and modulus; these functions represent the viscoelastic properties of the material. It is seen that, if a *unit stress* is applied instantaneously, that is, *stepwise* (and maintained constant thereafter), then the *strain* at time t is given by $k(t)$. Similarly, if a *unit strain* is applied stepwise at zero time, then the *stress* at time t is $m(t)$. The functions $k(t)$ and $m(t)$ define, respectively, the *creep compliance* and *relaxation modulus* functions.

From equation (1) it can be shown that if the stress is varying sinusoidally with time with circular frequency ω, then in the steady state the strain varies sinusoidally with time, and the amplitude of the strain is proportional to the amplitude of the stress. In general, the strain differs in phase from the stress, so under these conditions the ratio of strain to stress can be represented by a frequency-dependent *complex* compliance $k^*(\omega)$. Thus the complex compliance represents in phase and amplitude the strain response, as a function of frequency, to a sinusoidal stress of unit amplitude. Similarly, if the stress is varying sinusoidally with time, then from equation (2) it can be shown that the ratio of stress to strain can be represented by a frequency-dependent complex modulus $m^*(\omega)$.

TABLE I

Symbols and Terminology for Modulus and Compliance

Type of deformation	Remarks	Modulus, m	Compliance, k
Shear		G	J
Bulk (volume)		K	B
Longitudinal (a)	No transverse stress. Strain measured longitudinally	E	D
Longitudinal (b)	No transverse strain. Stress measured longitudinally	M	(N)
Longitudinal (c)	No transverse stress. Strain measured laterally	—	—
Longitudinal (d)	No transverse strain. Stress measured laterally	(λ)	—

The above time- or frequency-dependent moduli and compliances are related to the moduli and compliances of classical elasticity theory. These are given in Table I. It is seen from the table that there are four cross-measures, involving a transverse strain (or stress) and a longitudinal stress (or strain); one of these is the Lamé con-

stant λ. These four measures seem to be of limited use in representation of viscoelastic behavior, and will not be considered further. The compliance N has not yet been used in viscoelasticity; it is introduced here for completeness.

III. RELATIONS BETWEEN STEP-FUNCTION MODULI AND COMPLIANCES

In this report definitions are proposed for three creep compliances, namely, the *shear creep compliance* $J(t)$, the *bulk* (or *volume*) *creep compliance* $B(t)$, and the longitudinal creep compliance $D(t)$. The corresponding relaxation moduli are denoted by $G(t)$, $K(t)$, and $E(t)$. The relations between the moduli and compliances of classical elasticity theory are analogous to the relations between the Carson transforms of the time-dependent step-function moduli and compliances given above, where the Carson transform of a creep compliance $k(t)$ is given by:

$$p\int_0^\infty e^{-pt}\,k(t)\,dt = p\mathfrak{L}\{k(t)\}$$

and similarly for the Carson transform of a relaxation modulus. Thus, for example, the relation between a creep compliance $k(t)$ and its associated relaxation modulus $m(t)$ is given by:

$$p\mathfrak{L}\{k(t)\} = 1/p\mathfrak{L}\{m(t)\}$$

IV. METHODS OF REPRESENTATION OF DYNAMIC BEHAVIOR

Dynamic behavior refers to the response of a material manifesting linear viscoelasticity when the stress and strain vary sinusoidally with time. The strain can be considered as consisting of two components, one in phase with the stress and the other lagging 90°. The ratio of the amplitude of the former component to the amplitude of the stress is the *storage compliance*, $k'(\omega)$. The ratio of the amplitude of the latter component to the amplitude of the stress is the *loss compliance*, $k''(\omega)$. Alternatively, the stress can be considered as consisting of two components, one in phase with the strain, and the other leading by 90°. The ratio of the amplitude of the former component to the amplitude of the strain is the *storage modulus*, $m'(\omega)$;

the ratio of the amplitude of the latter component to the amplitude of the strain is the *loss modulus*, $m''(\omega)$. Thus in general:

$$k^*(\omega) = k'(\omega) - jk''(\omega) \tag{3}$$

and:

$$m^*(\omega) = m'(\omega) + jk''(\omega) \tag{4}$$

The *absolute modulus*, $|m(\omega)|$, is given by:

$$|m(\omega)| = [m'^2(\omega) + m''^2(\omega)]^{1/2} \tag{5}$$

and the *absolute compliance*, $|k(\omega)|$, is given by:

$$|k(\omega)| = [k'^2(\omega) + k''^2(\omega)]^{1/2} \tag{6}$$

The *loss tangent* or *damping*, $\tan \delta$, is given by:

$$\tan \delta = m''(\omega)/m'(\omega) = k''(\omega)/k'(\omega) \tag{7}$$

The quantity $m''(\omega)/\omega$ has the dimensions of viscosity and is generally called the *dynamic viscosity*, $\eta'(\omega)$.

TABLE II
Primary Measurable Quantities

	Type of deformation			
Quantity	Shear	Bulk	Longitudinal (a) (no lateral stress)	Longitudinal (b) (no lateral strain)
Creep compliance	$J(t)$	$B(t)$	$D(t)$	—
Relaxation modulus	$G(t)$	$K(t)$	$E(t)$	—
Storage compliance	$J'(\omega)$	$B'(\omega)$	$D'(\omega)$	—
Loss compliance	$J''(\omega)$	$B''(\omega)$	$D''(\omega)$	—
Storage modulus	$G'(\omega)$	$K'(\omega)$	$E'(\omega)$	$M'(\omega)$
Loss modulus	$G''(\omega)$	$K''(\omega)$	$E''(\omega)$	$M''(\omega)$
Complex compliance	$J^*(\omega)$	$B^*(\omega)$	$D^*(\omega)$	—
Complex modulus	$G^*(\omega)$	$K^*(\omega)$	$E^*(\omega)$	$M^*(\omega)$
Absolute compliance	$\lvert J(\omega)\rvert$	$\lvert B(\omega)\rvert$	$\lvert D(\omega)\rvert$	—
Absolute modulus	$\lvert G(\omega)\rvert$	$\lvert K(\omega)\rvert$	$\lvert E(\omega)\rvert$	$\lvert M(\omega)\rvert$
Loss tangent (damping)	$\tan \delta_s$	$\tan \delta_v$	$\tan \delta_l$	$\tan \delta_p$
Dynamic viscosity	$\eta_s'(\omega)$	$\eta_v'(\omega)$	$\eta_l'(\omega)$	$\eta_p'(\omega)$

In principle, six moduli and compliances can be defined (compare Table I). In practice, three compliances and four moduli are sufficient. The three complex compliances are thus the *complex shear compliance*, $J^*(\omega)$, the *complex bulk compliance*, $B^*(\omega)$, and the *complex lon-*

gitudinal compliance, $D^*(\omega)$. The four moduli are, respectively, $G^*(\omega)$, $K^*(\omega)$, $E^*(\omega)$, and $M^*(\omega)$. The relations between the complex moduli and compliances are the same as those existing between the corresponding moduli and compliances of classical elasticity theory. *When necessary*, values of tan δ and $\eta'(\omega)$ corresponding to different moduli may be distinguished by subscripts, thus tan δ_s, tan δ_v, tan δ_l, and tan δ_p represent the loss tangents associated, respectively, with $G^*(\omega)$, $K^*(\omega)$, $E^*(\omega)$, and $M^*(\omega)$. Similarly, the corresponding dynamic viscosities may be denoted by $\eta_s'(\omega)$, $\eta_v'(\omega)$, $\eta_l'(\omega)$, and $\eta_p'(\omega)$.

The behavior of a material in step-function or dynamic tests can thus be expressed in terms of the primary measurable quantities given in Table II.

V. LIMITING VALUES

In principle, certain limiting values exist, corresponding to zero and infinite time in step-function experiments, and zero and infinite frequency in dynamic experiments. These limiting values are defined as follows:

$$\left.\begin{aligned} k_g &= \lim_{t \to 0} k(t) = \lim_{\omega \to \infty} k'(\omega) \\ m_g &= \lim_{t \to 0} m(t) = \lim_{\omega \to \infty} m'(\omega) \\ k_g &= 1/m_g \end{aligned}\right\} \tag{8}$$

The quantities k_g and m_g are called, respectively, the *glass compliance* and *glass modulus*. The quantity defined usually by:

$$\left.\begin{aligned} 1/\eta &= \lim_{t \to \infty} \{dk(t)/dt\} \\ \eta &= \lim_{\omega \to 0} \eta'(\omega) \end{aligned}\right\} \tag{9}$$

is called the *viscosity*. Similarly, the quantities k_e and m_e are defined by the relations:

$$\left.\begin{aligned} k_e &= \lim_{t \to \infty} \{k(t) - t/\eta\} = \lim_{\omega \to 0} k'(\omega) \\ m_e &= \lim_{t \to \infty} m(t) = \lim_{\omega \to 0} m'(\omega) \\ k_e &= 1/m_e \quad \text{if } \eta = \infty \end{aligned}\right\} \tag{10}$$

The quantity k_e may be called the *equilibrium compliance* for a crosslinked material, for which the viscosity is infinite; otherwise, it may be called the *steady-state elastic compliance*. The quantity m_e differs from zero only when the viscosity is infinite, in which case it may be called the *equilibrium modulus*. In practice these limiting values may be experimentally inaccessible; or they may not be determinable experimentally.

VI. EQUIVALENT CONTINUOUS SPECTRA

The creep compliances are related to the complex compliances, and the relaxation moduli are related to the complex moduli through retardation and relaxation spectra, respectively. These spectra may be in principle discrete, continuous, or mixed. Molecular theories of viscoelasticity of amorphous polymers lead to discrete spectra. Since it is not possible to obtain these from experimental data, it is customary to obtain from experimental data the equivalent continuous spectra defined below.

The *retardation spectrum* $L(t)$ is defined by the relationships:

$$\left.\begin{aligned} k(t) - k_g - t/\eta &= \int_{-\infty}^{\infty} (1 - e^{-t/\tau}) L(\tau)\, d \ln \tau \\ k'(\omega) - k_g &= \int_{-\infty}^{\infty} \frac{L(\tau)}{1 + \omega^2\tau^2}\, d \ln \tau \\ k''(\omega) - 1/\omega\eta &= \int_{-\infty}^{\infty} \frac{\omega\tau L(\tau)}{1 + \omega^2\tau^2}\, d \ln \tau \end{aligned}\right\} \tag{11}$$

and the *relaxation spectrum* $H(t)$ is defined by the relationships:

$$\left.\begin{aligned} m(t) - m_e &= \int_{-\infty}^{\infty} e^{-t/\tau} H(\tau)\, d \ln \tau \\ m'(\omega) - m_e &= \int_{-\infty}^{\infty} \frac{\omega^2\tau^2 H(\tau)}{1 + \omega^2\tau^2}\, d \ln \tau \\ m''(\omega) &= \int_{-\infty}^{\infty} \frac{\omega\tau H(\tau)}{1 + \omega^2\tau^2}\, d \ln \tau \end{aligned}\right\} \tag{12}$$

When necessary, the retardation and relaxation spectra for shear and for bulk deformation can be distinguished by subscripts, thus we may write $H_s(t)$ and $L_s(t)$ for shear, and $H_v(t)$ and $L_v(t)$ for bulk (volume)

deformation. The terms *relaxation spectrum* and *retardation spectrum* refer to the function over the range of values of t from zero to infinity. The value of $H(t)$ at a specified value of t may be termed the *spectral strength* at time t. The auxiliary quantities, namely, the limiting values and spectra, are listed in Table III. It will be noticed that in this table the viscosity is characterized by a suffix when it is required to distinguish between the longitudinal and shear viscosities; the bulk viscosity of course does not exist.

TABLE III
Auxiliary Quantities

	Type of deformation		
Quantity	Shear	Bulk	Longitudinal (no transverse stress)
Glass compliance	J_g	B_g	D_g
Equilibrium compliance	J_e	B_e	D_e
Steady-state elastic compliance			
Glass modulus	G_g	K_g	E_g
Equilibrium modulus	G_e	K_e	E_e
Viscosity	η_s	—	η_l
Retardation spectrum	$L_s(t)$	$L_b(t)$	$L_l(t)$
Relaxation spectrum	$H_s(t)$	$H_b(t)$	$H_l(t)$

VII. DISCUSSION

In this report a minimum of quantities has been defined. It is observed that time- or frequency-dependent quantities are systematically labeled, while limiting quantities are denoted by suffixes. In the system used in this report, the connection between linear viscoelasticity and classical elasticity theory is apparent. For this reason, the more commonly used symbols for elastic moduli (G, K, E, and M) are adopted here. With regard to compliances, J is a generally used symbol, as is also B. The symbol D has been adopted for longitudinal compliance, replacing the previously used symbol F, to which objection was raised. Similarly, the symbol for the "dummy" compliance k replaces the earlier symbol c.

There are some difficulties with regard to nomenclature for the limiting values k_g, m_g, k_e, and m_e. The suffixes zero and infinity do not give rise to confusion in the analogous but not so complete system of

nomenclature for dielectric behavior; with linear viscoelasticity, however, their use is unjustified. The terms "initial" and "instantaneous" modulus and compliance seem uncertain. For amorphous polymers the appropriate modulus and compliance are often obtained as limiting values when the timescale is short enough at any given temperature, the material behaving under these conditions as an organic glass. On this account the terms glass modulus and glass compliance have been chosen, and these quantities have been denoted by m_g and k_g. For other materials, for example, metals, another term would be preferable. It does not seem likely that a term for these limiting values suitable for all categories of materials can be proposed. For the other limiting values, namely, k_e and m_e, the terms "static" and "ultimate" have been suggested. Here again these do not seem to be an improvement over the terms proposed in this report. The letter suffix for the symbol should of course be related to the name adopted for the limiting value. For papers published in languages other than English, it would be desirable that the letter suffixes adopted be associated with the nomenclature for the limiting values in other languages. This desirable state of affairs would seem to be difficult to accomplish.

In the case of nonlinear behavior, the term "viscosity" is sometimes used to denote the ratio of shear stress to rate of shear in general, while the limiting value at very small values of the parameters is denoted by a term such as "Newtonian" viscosity. Since in this report we are dealing only with linear behavior, it seems that such a modifying term is unnecessary here. Objections have been raised to the term "dynamic viscosity" for $m''(\omega)/\omega$. Since this name is well established for a useful quantity, it has been adopted in this report.

Much of the material of previous preliminary versions of this report has been eliminated in line with the objective of defining a minimum number of quantities in order to promote uniform methods of reporting data. In theoretical treatments it may be convenient to define further functions, for example:

$$\{k(t) - k_g - t/\eta\}/(k_e - k_g)$$

It does not seem either necessary or desirable to standardize a nomenclature for such quantities at this stage.

The Chairman and members of the Committee on Nomenclature gratefully acknowledge the help of the many rheologists whose suggestions and whose comments on earlier versions have been of great assistance in the preparation of this final report:

R. D. Andrews
A. B. Bestul
R. Buchdahl
J. D. Ferry
I. L. Hopkins
R. S. Marvin
A. W. Nolle
A. S. Nowick
W. Philippoff
H. Leaderman (*Chairman*)